Advancement of process control system in ammonia production

Zečević, Nenad

University of Zagreb
FACULTY OF CHEMICAL ENGINEERING AND TECHNOLOGY

Nenad Zečević

ADVANCEMENT OF PROCESS CONTROL SYSTEM IN AMMONIA PRODUCTION

UNAPRJEĐENJE SUSTAVA ZA VOĐENJE U PROIZVODNJI AMONIJAKA

DOCTORAL THESIS

Zagreb, 2021

SVEUČILIŠTE U ZAGREBU
FAKULTET KEMIJSKOG INŽENJERSTVA I TEHNOLOGIJE

Kandidat **Nenad Zečević**
predao je dana: 17. travnja 2021. doktorski rad izrađen pod mentorstvom prof. dr. sc. Nenada Bolfa, Fakultet kemijskog inženjerstva i tehnologije Sveučilišta u Zagrebu.

Povjerenstvo za ocjenu doktorskog rada u sastavu:
Doc. dr. sc. Igor Dejanović, Fakultet kemijskog inženjerstva i tehnologije Sveučilišta u Zagrebu
Prof. dr. sc. Ante Jukić, Fakultet kemijskog inženjerstva i tehnologije Sveučilišta u Zagrebu
Doc. dr. sc. Marko Katinić, Strojarski fakultet u Slavonskom Brodu Sveučilišta u Slavonskom Brodu
pozitivno je ocijenilo doktorski rad doktoranda Nenada Zečevića, a Fakultetsko vijeće Fakulteta kemijskog inženjerstva i tehnologije Sveučilišta u Zagrebu na sjednici održanoj dana 12. srpnja 2021. prihvatilo je ocjenu i odobrilo obranu doktorskoga rada pred povjerenstvom u sastavu:

Prof. dr. sc. Vesna Tomašić, Fakultet kemijskog inženjerstva i tehnologije Sveučilišta u Zagrebu
Prof. dr. sc. Ante Jukić, Fakultet kemijskog inženjerstva i tehnologije Sveučilišta u Zagrebu
Doc. dr. sc. Marko Katinić, Strojarski fakultet u Slavonskom Brodu Sveučilišta u Slavonskom Brodu

Obrana doktorskoga rada održana je dana 19. srpnja 2021.

D e k a n

Prof. dr. sc. Tomislav Bolanča

University of Zagreb
FACULTY OF CHEMICAL ENGINEERING AND TECHNOLOGY

Nenad Zečević

ADVANCEMENT OF PROCESS CONTROL SYSTEM IN AMMONIA PRODUCTION

DOCTORAL THESIS

Supervisor(s):
Prof. Nenad Bolf, Ph. D.

Zagreb, 2021

Sveučilište u Zagrebu
FAKULTET KEMIJSKOG INŽENJERSTAVA I TEHNOLOGIJE

Nenad Zečević

UNAPRJEĐENJE SUSTAVA ZA VOĐENJE U PROIZVODNJI AMONIJAKA

DOKTORSKI RAD

Mentor(i):
Prof. Nenad Bolf, dr.sc.

Zagreb, 2021.

Bibliographic page

- **UDK:** 681.5:661.53(043.3)=111
- **Scientific area:** Technical science
- **Scientific field:** Chemical engineering
- **Scientific branch:** Analysis, synthesis and control of chemical processes
- **Institution:** University of Zagreb, Faculty of Chemical Engineering and Technology, Measurements and Process Control
- **Mentor:** Prof. Nenad Bolf, Ph. D.
- **Page numbers:** 189
- **Figure numbers:** 53
- **Table numbers:** 33
- **Appendix numbers:** 1
- **Reference numbers:**119
- **Dissertation defence date:** 19th July 2021
- **The committee appointed for thesis evaluation:**
  1. Assoc. Prof. Igor Dejanović, Ph. D. - Committee Chairman
  2. Prof. Ante Jukić, Ph. D.
  3. Assoc. Prof. Marko Katinić, Ph. D.

- **The thesis is stored in:**
  Library of Faculty of Chemical Engineering and technology University of Zagreb, Marulićev trg 20

Dissertation thesis is accepted on 235th session of the Council of the Faculty of Chemical Engineering and Technology, held on April 27th 2020, Item 10 on the agenda and approved on 1st session of the Senate of the University of Zagreb, held on October 13th 2020.

Mentor information

Prof. **Nenad Bolf,** Ph. D, full professor
University of Zagreb, Faculty of Chemical Engineering and Technology

B. Sc. in 1996 University of Zagreb, Faculty of Chemical Engineering and Technology
M. Sc. in 1999 University of Zagreb, Faculty of Chemical Engineering and Technology
Ph. D. in 2003 University of Zagreb, Faculty of Chemical Engineering and Technology
Head of Measurements and Process Control, Faculty of Chemical Engineering and Technology, University of Zagreb
All other details available through https://www.fkit.unizg.hr/nenad.bolf#

Acknowledgements

I would like to express my sincere gratitude to my thesis mentor, Prof. Nenad Bolf, Ph. D., for his valuable guidance, close supervision, and constructive criticism during the course of my thesis research. I greatly value the discussions during our meetings that have immensely contributed to the worth of the research work presented in this thesis. My thanks to him for devoting his valuable time providing me intellectual freedom in my work, reading my immature first drafts, and providing the expertise to improve them. This has been impossible without his support and guidance.

Also, I would like to express my heartfelt thanks to Prof. Ante Jukić, Ph. D., Prof. Marko Rogošić, Ph. D., Assoc. Prof. Igor Dejanović, Ph. D., Prof. Vesna Tomašić, Ph. D., and Prof. Elvira Vidović, Ph. D. for the care and kind understanding that they have shown to me during all my exams during the thesis process and all care that they take to review drafts of manuscripts, presentations, and other materials. In fact, I think I have considerably improved my writing and presentation skills with their help.

My warmest gratitude to Tonino DiBella, Ph. D. from Honeywell for providing me essential software for the development of this thesis, namely UniSim Design R470, because without his help this work will be impossible.

Special thanks to my unreserved professional and private colleague Jovica Zorjanović, Ph. D. from Clariant for being patient in ensuring all necessary information related to the catalyst simulation procedure.

My sincere gratitude to Otmar Lorenz, Ph. D. from SIEMENS who conveyed to me elementary knowledge about the simulation of chemical processes from the automation side and reveals to me the beauty of the control matrix as help in defining control problems.

Thanks to all SIEMENS and Petrokemija Plc. employees who believed in me during my quest and gave me all the necessary support to finish this work. I will never forget Dalibor, Ivana, Adriano, Miroslav, Martin, Vesna, Matej, Goran, Snježana and others.

My special thanks to Assoc. Prof. Marko Katinić, Ph. D. my colleague who went Petrokemija Plc. to find a new adventure in the scientific area. Please find out Marko that with your help, I will join with you as soon as possible.

For all special achievements, scientists need the support and comfort of independence to expand horizons beyond the boundaries. This help belongs to Pavo and Damir. So, my friend's special thanks from all my heart to you and your unreserved support from the first day

when we met each other. In the end, I only can say one big THANK YOU – from you I learned what really means friendship, unselfishness, and a positive attitude in any negative situation.

All the love to my daughters Noa and Una, my greatest source of strength. This one is for you. Go inspire and be better than me!

And in the end, I cannot express with words all my feelings to my first love in this journey, my wife Biljana as a partner, as a friend, as the strongest supporter, for every minute, every day, every month and year, for everything, since I met You. Without You, this work will not be possible. In the end, this is your work and you must be proud of yourself!

Thank You Morky for bringing us Daisy!

I did it, and I did it my way! Be Yourself!

Abstract

A model representing the steady–state and dynamic behaviour of a Haber-Bosch ammonia plant was developed based on plant data from Croatian fertilizer company Petrokemija Plc. Kutina. The plant model was developed with the aim to study the performance of advanced control strategy and optimize the economic performance of the plant.

Industrial ammonia plant within fertilizer production asset typically comprises eight highly integrated catalysed process steps with many process units, heat integration, and gas recycles. The intensive nature of the ammonia production process with many nested mass and energy streams makes it a significant challenge to design the appropriate control system. The objective of the research was to design an optimal control strategy based on the plant model. The model takes the main dynamic relationship between the ammonia production rate and other relevant process parameters in downstream and upstream units. As an additional feature, online monitoring of the reforming catalyst and reformer tubes performance in the steam–natural gas reformer as the main energy consumer of an ammonia plant was considered.

In order to design an optimised advanced control system, the plant model was divided into three logical process units to reduce the computational effort needed for the optimal synthesis gas preparation, raw synthesis gas purification, and ammonia synthesis loop.

With respect to achieving scientific contribution and subsequently practical implementation of the proposed control strategy, a custom advanced process control scheme has been developed that uses programmed cascade functions to predict and adjust critical process parameters in ammonia production. Specifically, it was developed an advanced ratio–cascade process control scheme, which provides efficient disturbance rejection. To reach an optimal economic level the ammonia production rate (set point) acts as the primary/master control loop while holding the steam–to–natural gas and air–to–natural gas molar ratios as secondary/slave controllers.

To enhance the profit of the ammonia plant the economic profit objective function is proposed. Feedback from the profit function is used in the advanced process control scheme as an input to bring the ammonia plant operation to the maximum profitability level.

The benefits of the developed process control strategy are more effective disturbances' rejection, simplification of ammonia process control operation, and plantwide optimization of the overall ammonia plant.

The developed model offers the opportunity to operate the plant with higher energy and throughput efficiency with more comprehensive insight into the operation of the catalysts and reformer tubes with the possibility to predict its lifetime.

With the practical implementation of the proposed control scheme, an ammonia plant can increase profitability, availability, improve safety, and handle environmental related issues.

Keywords: advanced process control, ammonia production, optimization, plant model

Sažetak

Na temelju procesnih podataka s postrojenja za proizvodnju amonijaka baziranog na Haber-Boschovom postupku u sastavu kompleksa proizvodnje mineralnih gnojiva Petrokemije d.d. Kutina, razvijeni su statički i dinamički modeli procesa proizvodnje amonijaka. Model postrojenja razvijen je za izvedbu napredne strategije vođenja i analize njezinog utjecaja na ekonomske pokazatelje procesa proizvodnje amonijaka.

Tipično postrojenje za proizvodnju amonijaka integrirano u proizvodnju mineralnih gnojiva karakterizira nekoliko kemijskih reakcija za čije odvijanje je nužno osam različitih katalizatora uz maksimalno učinkovito korištenje toplinske energije i recikliranje sinteznog plina što se postiže različitom stacionarnom i rotacionom procesnom opremom. Kompleksnost procesa proizvodnje amonijaka, koje uključuje međusobnu povezanost materijalnih i energetskih procesnih tokova, predstavlja značajni izazov prilikom projektiranja sustava za vođenje procesa.

Svrha ovog istraživanja bila je unaprijediti sustav za vođenje postrojenja proizvodnje amonijaka na temelju detaljnog modela procesa. Model procesa uzima u obzir sve odnose između proizvodnog kapaciteta i drugih bitnih procesnih parametara u ostalim dijelovima postrojenja.

Modelom procesa prati se i rad katalizatora i katalitičkih cijevi u dijelu parnog reforminga prirodnog plina kao najvećeg potrošača energije u proizvodnji amonijaka.

U cilju optimizacije sustava vođenja, model je podijeljen u tri sekcije kako bi se smanjilo potrebno vrijeme za provedbu izračuna parametara modela. Osnovne sekcije su priprema sinteznog plina, pročišćavanje sinteznog plina i procesna petlja sinteze amonijaka.

Znanstveni doprinos i praktična primjena temelji se na razvoju prilagođene napredne metode kontinuiranog vođenja procesa u kojoj se primjenjuju programirane kaskadne funkcije za predviđanje i podešavanje kritičnih procesnih parametara tijekom proizvodnje amonijaka. Razvijena metoda temelji se na kaskadnoj regulacija omjera temeljenog na prediktivnom vođenju za kompenzaciju poremećaja u procesu.

U cilju smanjenja operativnih troškova proizvodnje predložena je ekonomska funkcija cilja. Rezultat ekonomske funkcije cilja unaprijeđeni je sustav vođenja koji osigurava rad postrojenja za proizvodnju amonijaka uz minimalne operativne troškove.

Doprinos istraživanja na osnovi razvijenog naprednog sustava vođenja su bolja kompenzacija procesnih poremećaja, unaprjeđenje vođenja i optimizacija postrojenja proizvodnje amonijaka. Boljim vođenjem procesa očekuje se veća djelotvornost kemijskih

reakcija i toplinske energije uz mogućnost praćenja i predviđanja rada katalizatora za parni reforming prirodnog plina i katalitičkih cijevi.

Praktičnom primjenom predloženog naprednog sustava vođenja u procesu proizvodnje amonijaka može se smanjiti varijabilni trošak proizvodnje, povećati dostupnost rada postrojenja, poboljšati sigurnost te smanjiti emisija stakleničkih plinova.

Ključne riječi: model postrojenja, napredno vođenje procesa, proizvodnja amonijaka, optimizacija.

Table of contents

Nomenclature

LIST OF SYMBOLS

A	-	pre–exponential factor or area, kmolbar$^{0.5}$/(kg$_{cat}$hr), kmol/(barkg$_{cat}$hr) or m^2
a	-	interfacial area per unit volume or relay amplitude, m^2/m^3
a_i	-	activity
a_p	-	specific area of packing, m^2/m^3
B	-	pre–exponential factor, bar^{-1}
BM_p	-	benchmark for ammonia (expressed in EUAs / unit of product)
C	-	specific heat capacity or molar concentration, kJ/kgK or kmol/L
Cv	-	characteristic value of the valve
c_p	-	specific heat at constant pressure, kJ/m^3·K
c_i	-	molar concentration, kmole/m^3
$CLEF_{p,k}$	-	applicable carbon leakage exposure factor for product p in year k
D	-	denominator or diameter or diffusivity, dimensionless or m or m^2/s
D_a	-	diffusivity, m^2/s
d	-	diameter or radius or disturbance variable, m or dimensionless
D_{KA}	-	Knudsen diffusivity, m^2/s
E	-	activation energy or enhancement factor, kJ/mol or dimensionless
$e(t)$	-	error
$Elec.use$	-	total electricity consumption within the system boundaries of the production of ammonia over the baseline period, MWh
Em_{direct}	-	direct emissions within the system boundaries of the production of ammonia over the baseline period
Em_{inderct}	-	indirect emissions from electricity consumption within the system boundaries of the production of ammonia over the baseline period
$Em_{\text{NetHeatImport}}$	-	emissions from any net measurable heat import from other ETS installations and non-ETS entities over the baseline period by a sub-installation producing ammonia, irrespective of where and how the heat is produced
F	-	flow rate, kg/h or kmol/h
F_r	-	Froude number

$F_{p,k}$	-	annual preliminary allocation for a product benchmark sub-installation producing ammonia in year k, EUAs
f	-	friction factor
f_i^o	-	reference fugacity
G	-	mass velocity, kg/(m^{2}h)
g	-	gravity acceleration, m/s^2
$g(s)$	-	closed–loop transfer function
$g_j(x)$	-	the set of inequality restrictions, which contains upper and lower bounds for mass and heat transfer rates, temperatures, pressures, concentrations as well as limits for the environmental and safety-related issues
h	-	heat transfer coefficient or holdup or relay hysteresis, kJ/kg or dimensionless
$h_i(x)$	-	the set of the equality restrictions, which contains the equations derived from the conservation laws (mass, energy, momentum, cost) and the constitutive equations of the plant model, variable connections, correlations for physical and chemical property
h_i, h_G	-	ion-specific parameter, m^3/kmol
h_T	-	temperature correction, m^3/kmolK
H	-	enthalpy and calorific value, kJ/mol
H_a	-	Hatta number
H_e	-	Henry constant of gas-water system, Pam^3/kmol
HAL_p	-	historical activity level
K	-	chemical equilibrium constant or apparent adsorption constants, bar^{-1}
K_p *or* K_c	-	controller gain
K_u	-	ultimate gain
k	-	kinetic rate constant or mass transfer coefficient or conductance, m^3/kg$_{cat}$h or m^3/kmols or s^{-1} or kmol/m^{2}s
k_0	-	pre–exponential factor
k_H	-	reverse of Henry constant, kmol/m^{3}Pa
l	-	length or load (input) of controller, m
L	-	mass velocity of liquid, kg/m^{2}s
M, m	-	mass flow or molar weight, kg/h or kg/kmol

N	-	molar flux (absorption flux), kmol/m^{2}s
N_i	-	molar amount, kmol
$\dot{n}$	-	molar flow rate, kmol/h
P	-	operational profit function
p	-	pressure and partial pressure, bar
P_u	-	ultimate period
Q	-	absorbed heat, J
q	-	volume flow, m^3/h
r	-	rate of reaction, kmol/(kg$_{cat}$h)
$r(s)$	-	set point change
R	-	universal gas constant, kJ/kgmolK
Re	-	Reynolds number
S	-	specific surface area or section area, m^3/m^2 or m^2
Sc	-	Schmidt number
T	-	thermodynamic temperature, K
T_i	-	controller integral time, s
t	-	time, h
U	-	heat transfer coefficient, kJ/(m^{2}hK)
u	-	superficial velocity or speed or manipulated variable, m/s
V	-	volume and volume flow rate, m^3 or m^3/h
v	-	velocity or molar volume, m/s or m^3/kmol
X	-	conversion rate, %
x	-	the set of the continuous real independent variables corresponding to design and operating parameters of the components of the chemical plant
x_i, y_i	-	mole fraction, mol. %
y	-	the set of the discrete independent variables used in the design optimization
$y(s)$	-	controller output
Y	-	molar ratio
Z	-	empirical coefficient equal to 1.859×10^{-3} atm·Å^{2}cm^2(kg/kmol)$^{1/2}$/(K$^{3/2}$s)
Z_T	-	packing height, m

z	-	length or the set of the integer independent variables used to determine the structure of the optimal flowsheet, m
W	-	weight, kg
w	-	mass flow in kg/h
W_e	-	Weber number

LIST OF GREEK LETTERS

α	-	convective heat transfer coefficient or ratio T_i/T_d, kJ/(m^2hK) or dimensionless
β	-	gain ratio
ϵ	-	porosity or void fraction, m^3_{void}/m^3_{cat}
η	-	efficiency and effectiveness factor, %
μ	-	viscosity, Pas
ρ	-	density, kg/m^3
π	-	cross section, m^2
ν	-	stoichiometric coefficient
φ	-	phase angle
ϕ	-	Thiele module or association factor
ϕ_i	-	fugacity coefficient
σ	-	collision diameter or critical surface tension, Å, N/m
λ	-	thermal conductivity, kJ/(m^2hK)
Ω	-	collision integral
ζ	-	axial position in packed column
τ	-	time constant in PID controller
Δ	-	change and/or difference

LIST OF SUB- AND SUPERSCRIPTS

B	-	bed
cat	-	catalyst
g	-	gas
i	-	component
IN	-	input
j	-	component

k	-	reaction
mix	-	mixture
OUT	-	output
RF	-	reformer furnace
rgo	-	reformed gas outlet
tot	-	total
vk	-	volumetric–kinetic
w	-	weight
wg	-	waste gas
wtt	-	tube wall temperature

LIST OF ABBREVIATIONS

APC	-	advanced process control
ATE	-	temperature approach to equilibrium
ATV	-	auto tuning variation
CFD	-	computational fluid dynamics
COCO	-	Cape–Open–to–Cape–Open
CV	-	controlled variable
DCS	-	distributed control system
DDS	-	dynamic disturbance sensitivity
DEA	-	diethanolamine
DPT	-	deviation from the production target
DV	-	disturbance variable
ETS	-	European Trading Scheme
EUA	-	European Emission Allowances
FC	-	flow controller
FCV	-	fuel calorific value
HRCT	-	heat recovery convection train
HT	-	high temperature
IFSH	-	integrated frame of simulation and heuristics
LHV	-	low heating value
LP	-	low pressure
LPG	-	liquefied petroleum gas

LT	-	low temperature
MCV	-	multivariable control
MP	-	medium pressure
MPC	-	model predictive control/controller
MV	-	manipulated variable
ODE	-	ordinary differential equations
PDE	-	partial differential equation
PEM	-	prediction–error minimization
PFD	-	process flow diagram
PFR	-	plug flow reactor
PI	-	proportional–integral
PID	-	proportional–integral–derivative
PQM	-	product quality manipulator
PV	-	process variable
PWC	-	plantwide control
RC	-	ratio controller
SISO	-	single–input–single–output
SMR	-	steam methane reformer/reforming
S/N.G.	-	steam–to–natural gas
SOC	-	self–optimizing control
SQP	-	sequential quadratic programming
SP	-	set point
SR	-	steam reforming
SRS	-	separation recycle system
TAD	-	adiabatic flame temperature
TPM	-	throughput manipulator
TRE	-	real gas temperature
USD	-	United States Dollar
WGS	-	water gas shift

List of figures

Figure 51. Catalyst outlet temperature readings regarding to equilibrium temperature at outlet methane molar concentrations of 10,.60, 10,40 and 10,20 mol.%.

Figure 52. Tube wall temperature readings before implementation of recommendations from the model.

Figure 53. Tube wall temperature readings after implementation of recommendations from the model.

List of tables

1. INTRODUCTION

1.1.Ammonia production – overview

Ammonia is a basic building block for most nitrogen fertilizers except for some naturally occurring nitrates. In nature, ammonia occurs almost only as different ammonium salts (*e.g.* NH_4Cl, $(NH_4)_2CO_3$, etc.). However, the natural resources of ammonia were limited in quantity, and in parallel, they did not suffice for fertilization. The constant growth of the human population, limited earth's land surface for agricultural activity with related soil productivity and sustainability, imposed the neediness for ammonia production on an industrial scale. The first technological pathway for the production of synthetic nitrogen compounds as fertilizer was the Frank–Caro calcium cyanamide process from 1898 onwards [1].

However, the supply was far from sufficient to increase agricultural yields and prevent future famine. Therefore, the problem of synthetic ammonia production was addressed at the end of the 19^{th} century by Sir William Crooks in his famous presidential speech to the British Association of Advanced Science [1]. Based on all technological developments, in 1904 the ammonia synthesis process was developed primarily by Fritz Haber, and in 1909 he demonstrated the process on a laboratory scale of 80 g of NH_3 per hour [1]. The credit for developing the pilot scale and then commercial–scale ammonia plant belongs to Fritz Haber and Carl Bosch, which used a promoted iron catalyst discovered by Alwin Mittasch [1]. The first commercial scale ammonia production of 30 tonnes per day started in 1913 in Oppau, Germany [1]. The process was based on the catalytic reaction of hydrogen and nitrogen at elevated temperatures and pressure with the recycling of an unconverted synthesis mixture. This basic concept is still extensively used today. The main process steps in the ammonia synthesis section include a reaction between hydrogen and nitrogen in the molar ratio 3 to 1 over an iron catalyst at an elevated temperature between 400 and 500^oC (originally up to 600^oC) and pressures above 100 bars with the recycling of the unconverted part of the synthesis mixture. The last process step is the separation of the ammonia product under high pressure and subsequent liquefaction.

However, Carl Bosch has been well aware that the production of a pure hydrogen–nitrogen mixture is the largest single contributor to the total production cost of ammonia. Besides the synthesis section, dramatic changes happened over the years in the synthesis technology gas generation. Today industrial ammonia processes differ mainly regarding synthesis gas preparation and purification. The main raw materials for ammonia synthesis (nitrogen and

hydrogen) are abundantly available as air and water. Physical methods can separate these raw materials and/or chemical catalysed reactions using different sources of energy, mainly fossil sources (*e.g.* natural gas, liquefied petroleum gas (LPG), naphtha, and higher petroleum fractions like coal or coke). With respect to accomplish successfully the ammonia synthesis on an industrial scale the typical production facility comprises individual process steps such as feedstock purification and pre-treatment (steam reforming), carbon monoxide shift conversion, carbon oxides (CO and CO_2) removal, compression, ammonia synthesis, and ammonia separation. All these process steps in the modern ammonia plants are now only designed according to the integrated single-train concept. Integrated single-train ammonia plant incorporates the essential features of the complex facility, namely many equipment, component inventory, heat integration, and gas recycle.

1.2.Ammonia production – process control

The complex and intensive nature of industrial–scale anhydrous ammonia production in the highly competitive global marketplace requires plant owners and operators to adopt the best available technology to achieve as simple as possible production with the minimum feedstock and fuel input. Nevertheless, conventional control systems typically cannot meet these control and optimization objectives given the many constraints often associated with these objectives. The industrial operators of any ammonia plant would like to have the ability to model and predict the performance of the steam methane reformer and ammonia synthesis units with the related catalyst in its regular operation life in a dynamic mode.

Many models have described steam methane reforming and ammonia synthesis units with varying levels of detail and with different approaches in solving this task [2-8]. Sophisticated simulators have been used to describe the performance of the units with high fidelity [5]. Nevertheless, many of these simulators take a long time to converge, which is impractical for regular industrial use and, at the same time, does not allow for the continuous prediction of process parameters with the possibility for their adjustment and improvement to achieve the optimum performance. Besides that, a series of catalyst beds within ammonia plants need simple and practical online monitoring of their performance regarding activity, selectivity, and lifetime. In an attempt to meet this requirement, ammonia producers are not looking solely for process modifications, but also for utilizing the equipment to its optimum potential.

One area that can be improved is the plant's control system's ability to sustain the optimal process condition. Some benefits can be achieved by the installation of programmable single

loop controllers, but to engage the latest advanced control structures, which include sophisticated mathematical calculations, advanced computer–based control systems are required. Going beyond the better control of the plant, the process parameters must be appropriately selected to accomplish the goals of the production facility. Generally, two objectives are considered – maximum production and/or minimum feedstock and fuel usage per unit of product. The process parameters selected for these two goals can differ significantly. Even within a single objective, the process conditions will change over time with ambient conditions, feedstock and fuel composition, catalyst age, and large increments of production rate.

One way to ensure the whole plant is constantly operating within the best process condition is to implement a continuous optimization control scheme. Moreover, owners of the ammonia facilities have the opportunity either to upgrade or to replace entirely their current distributed control systems (DCS) with commercially available advanced process control (APC) systems to achieve safer and smoother operations, while reaching the plant economic requirements.

However, all the proposed APC solutions mainly focused on individual control schemes of various sections in the ammonia plant. These are control of H_2–to–N_2 molar ratio of the make–up gas, control of steam–to–natural gas molar ratio (S/N.G.), control of primary reformer firing, and control of inert gas molar concentration in the synthesis loop [9-11]. According to the literature findings, the best achievement until now is the solution as an integrated module for the management of interactions and constraint control between different independent modules to control the front–end pressure of the ammonia plant [12].

A couple of control schemes were proposed as APC techniques by implementing proportional–integral (PI) or proportional–integral–derivative (PID) controllers and model predictive controllers (MPC) [5-13]. The use of MPC methods to control such complex systems has not yet been fully explored [5], particularly the control strategies that exhibit higher degrees of performance like the ratio–cascade MPC.

At the top of this, in the last decade, several influencing studies have proposed and discussed the partial or complete control of the ammonia production process based on different control strategies, *e.g*. systematic plantwide control (PWC), heuristics–based methodologies, integration of linear and nonlinear MPC, *etc*. [13-19].

However, as it is stated in the paper of Zhang *et al.* [17] each of the proposed methodologies has certain benefits and drawbacks. The main recognized drawbacks are the lack of an adequate mathematical model which will be able to realistically and effectively simulate the process behavior, and an appropriate level of operational knowledge and insight to apply adequately

heuristics–based methodologies. A theoretical approach based on recommendations of the eight levels of integrated frame of the simulation and heuristics (IFSH) methodology proposed by Konda *et al*. [19] seems like a workable perspective and a good starting point for proofing of the new proposed APC scheme.

1.3.Background – motivation, problem statement, and scope of work

With respect to understand the operation of the process equipment, heat integration, and catalyst behaviour during ammonia production, it is necessary to have a reliable simulation of the entire process based on mathematical models that can identify satisfactorily the process response. Even so, the majority of the currently available models describe the ammonia production process independently and separately, and thus, the model which can adequately handle the integrated ammonia production facility is lacking. Thus, the first motive of this dissertation is to build up a workable steady–state and dynamic model which can identify the operation of the integrated ammonia production process. With respect to the simulation model, aspects such as the individual chemical reaction steps defined by the stoichiometric equations along with the rate equations are necessary to be specified. Additionally, reaction phase equilibrium and thermodynamics expressions are also used to develop the kinetic and thermodynamic model of all independent process steps during ammonia production.

Specifically, the research will be focused on the dynamic relationship between the ammonia production rate, synthesis gas temperatures, and molar concentration of methane at the outlet of reformer tubes. Besides that, the research will investigate the relationship between the manipulated and disturbance variables such as fuel gas flow rate, airflow rate, process gas flow rate, steam mass flow rate, S/N.G., H_2–to–N_2 molar ratios, ambient temperature, and inert gas molar concentration in the synthesis loop (Ar + CH_4). With respect to accomplish this relationship, subsequent monitoring of catalyst and reformer tube performance will be performed, with special emphasis to burner management.

From the discussion in the previous section, it can be recognized that process control of the ammonia plant is an important and active area of research. In order to contribute additionally to this research area, the second motive is the further development of the advanced process control in industrial ammonia production based on operational experience and heuristic methodologies. This part considers the design of advanced process controllers for the dynamic distributed parameter system that regulates the production process using a combination of

feedforward, feedback, ratio, and cascade control techniques with related gain-scheduled process control.

The other important issues considered are the definition of the economic profit objective function, which will bring to industrial users an optimization and decision tool to run the plant under different economic constraints like the influence of the natural gas, energy, and CO_2 emission prices.

All mentioned present the motive, problem statement, and objectives for additional research efforts to deliver a novelty in the advancement of process control in industrial ammonia production with the final solution of the advanced control system which will manipulate the output capacity of the ammonia production unit. Consequently, there is a need for an ammonia plant custom control system that will deliver a simple, reliable, and robust solution to meet all process steps during ammonia production.

1.4.Objectives and hypotheses of thesis

The objectives of the research are:

- To develop a steady–state and dynamic mathematical model that describes the dynamic relationship between the ammonia production rate and controlled, manipulated and disturbance variables;
- To define control matrix with mutual relationships between relevant process parameters such as synthesis gas temperatures, the molar concentration of methane at the exit of the reformer tubes, fuel gas flow rate, airflow rate, process gas flow rate, steam mass flow rate, S/N.G., and H_2–to–N_2 molar ratios, ambient temperature, inert gas molar concentration in the synthesis loop (Ar + CH_4) and burner condition;
- To propose an adequate method for monitoring of catalyst and reformer tube performance;
- To design, advanced process controllers for the dynamic distributed parameter system that regulates the production process using advanced feedforward, feedback, ratio, cascade, and gain-scheduled process control;
- To define the economic profit objective function which will bring to industrial users an optimization and decision tool to run the plant under different economic constraints like the influence of the natural gas, energy, and CO_2 emission prices.

Hypotheses of the research are:

- Developed steady–state and dynamic mathematical model will enable more comprehensive insight into the operation of the catalysts and reformer tubes used in ammonia production with the possibility to prolong its lifetime;
- The developed process control method will deliver plantwide optimization and control of the whole ammonia plant;
- The developed process control method will cause better disturbances' rejection, simplification of ammonia process operation, higher efficiency, better profitability and it will meet environmental and safety–related issues.

1.5. Organization of the dissertation

This thesis comprises six chapters. The following chapter shows a detailed literature review of the various advanced control methodologies applied either in isolated parts of the ammonia plant or in the whole plant. The literature review is primarily based on PWC and the heuristic approach. A critical review of the identified bottlenecks and constraints was recognized and stressed. Regarding the literature survey, it was recognized as an area for further improvement. Chapter 3 describes the method and comprehensive description of the conducted activities, which served for collection, and analysis of process data, model development, identification of control objectives, and design of advanced control structure, and final list of applications used for tuning, testing, and validation of the results. Chapter 4 presents the process description of the reference ammonia plant, methodology for building of the steady–state flowsheet of an ammonia plant, transfer of the steady–state model to a dynamic model, and design of the advanced control system whose main goal is to control the whole ammonia plant. An advanced control structure based on feedforward, feedback, ratio, cascade, and gain-scheduled techniques are suggested and evaluated in Chapter 5. The results were discussed after tuning all functional parameters. The optimization analysis was performed together with the results of the economic objective function. Last, validation and testing results against a real process case are discussed and the principal contribution of the research was highlighted. Finally, the conclusions and recommendations for future work are outlined in Chapter 6. Note that Chapters 3 to 5 are based on published journal papers and/or submitted manuscripts. Nonetheless, care was taken to minimize the repetition. However, some part of the text in these chapters was repeated with the sole intention of making the concerned chapter easier to follow.

2. LITERATURE REVIEW

The complexity of the ammonia production process requires plant operators to apply the best accessible innovations to accomplish as much as simpler production for the minimum feedstock and energy input. In order to achieve these two objectives during the year's researches were concentrated in two directions, namely the practical implementation of the advanced process control at the industrial level and theoretical considerations, which will better explain complex control structures. To address properly, better understand, and recognize possible shortcomings of the already conducted research, the literature review was made in these two directions. First, it is considered a literature survey of practical solutions already implemented in actual cases, and second, it is considered necessary theoretical background which can additionally support successful implementation of the practical solutions.

2.1.Practical applications of advanced process control in the ammonia production

In the following section, an overview of the most influencing case studies and practical examples of the APC control systems implementation in ammonia plants is given. All the cases are published by the American Institute of Chemical Engineers and presented at different conferences under *Safety in Ammonia Plants & Related Facilities Symposium*.

So far, all the practical and already proven APC solutions implemented at the industrial level are mainly concentrated on single control schemes in isolated parts of the ammonia production process.

One of the first works that were related to the application of digital computers in five commercial ammonia plants was given by Daigre and Nieman [20]. They recognized four broad areas for implementation of computer control; closed–loop computer control of key control loops in the ammonia plant, monitoring process variables for potential and existing alarm conditions, calculating critical parameters which do not lend themselves to easy, direct measurement, S/N.G. molar ratio for example, preparation of logs, and management reports. In the first category, closed–loop computer control has been achieved in the following areas;

1. primary reformer control, including feedstick flow determination, catalyst tube temperature control, methane leakage control, waste gas temperature control, and S/N.G. molar ratio control,
2. synthesis H_2–to–N_2 molar ratio,

3. purge gas flow control,
4. synthesis reactor temperature control,
5. optimal loading of the centrifugal compressors,
6. centrifugal compressor trip out response.

After successful implementation in five ammonia plants in the period from 1959 to 1973, they summarized the advantages to placing certain key control loops or functions under the control of the computer. These are consistently in operation, smoother operation, responding to unusual conditions, overcoming problems because of the human errors and increased efficiency of 2 to 3%.

Based on this work, Tijssen [21] proposed for the first – time construction of a mathematical plant model which can be applied in ammonia production. More precisely, he defined a mathematical model which was comprised of a coherent set of formulas, or calculation procedures covering every relevant aspect of plant operation. A set of equations was defined and integrated with the mass balances and other pertinent information into a model of the complete ammonia plant. Mass balances were calculated based on the detailed composition of the natural gas feed. For a fixed composition, a set of simple equations is developed connecting the quantities of process gas, process air, synthesis gas, ammonia, and purge gas. Besides that, in this work for the first time, he has defined a relation for the economic optimization of the ammonia plant based on linear programming. The economic objective function was set up to calculate a set of operating conditions for the plant that obey the model equations, satisfy the constraints, and maximizing the profit. According to the published results, the author claimed that with the application of the mathematical model approach it is possible to increase the output to 25% of the design with feedstock consumption well below design over a five-year operating period.

Friedman [22] in his work explored the influence of statistical control performance measures to the control loops which were in charge for control of H_2–to–N_2 molar ratio, S/N.G. molar ratio, synthesis loop pressure, converter inlet temperature and quench ratios. The test results showed how much control tuning is justified before processing optimization, as described by Tijssen [21]. Besides that, the second conclusion was that slower H_2–to–N_2 molar ratio and ammonia synthesis converter temperature loops will control better if the faster pressure and S/N.G. molar ratio control loops are working properly.

One of the first practical work which addressed the industrial application of the APC system in ammonia plant was conducted by Yost *et al*. [23]. The major goal of this project was to

investigate the possibilities for a more advanced control system in Wycon's nominal 272 metric t/day ammonia plant at Cheyenne, Wyoming. The original requirements for the control system were; control the inlet primary reformer S/N.G. molar ratio automatically, control the synthesis loop H_2–to–N_2 molar ratio consistently and accurately, control the synthesis loop purge gas flow automatically, control the primary reformer outlet temperature automatically. The outcome of this project was to maximize production without increasing total natural gas consumption and to have a minimum predicted 95% on–stream time. The project was successfully executed by Foxboro. The independent advanced control loops increased the ammonia yield greater than original estimates with better process on–stream time, which was expected.

In 1980 Parrish [24] disclosed information on how to use effectively the process data from the DCS system in an appropriately designed model which can give recommendations on what moves must be considered for improving the efficiency of an ammonia plant based on working point. A block processing diagram with the related program was set up with the possibility to write the executive routine as a product from the dialog between the user and the development program routine. The program has been developed for ammonia units that will perform a complete ammonia unit heat and material balance with calculations of approaches to equilibrium for unit catalysts. The programming included all physical properties of the components and be able to predict their behaviour in mixtures, make fugacity corrections for non–ideal behaviour, and have all chemical equilibrium relationships. However, except for the general description, the paper did not disclose any specific details in fulfilling all mentioned in the paper.

Allen [25] described the case study of the successful installation of the M. W. Kellogg Ammonia Optimizer at the two Canadian Fertilizers Limited ammonia plants in Medicine Hat, Alberta, Canada. Advanced control strategies installed at these two ammonia plants have provided demonstrable benefits to the plant operation. The benefits were measured by statistical analysis techniques on data gathered both before and after the commissioning of the control strategies. The variability of the process parameters around the respective set points was measured and a 95% confidence interval (± two standard deviations) was calculated. The paper states that the improved control provides energy savings, but it is not easily directly measured. The included independent control strategies were control of steam–to–carbon molar ratio, methane leakage of the secondary reformer effluent, synthesis loop inert gas purges flow rate, refrigeration purges, H_2–to–N_2 molar ratio, and ammonia synthesis converter temperature control. Besides that, the optimization software performs a detailed heat and material balance

on the synthesis loop and additional calculations for the front–end of the ammonia unit to determine the optimum values for the H_2–to–N_2 molar ratio, inert gas level, and the converter bed inlet temperatures every 3 hours. The objective optimization function was designed to be switched between either maximizing production or minimizing energy consumption. The software can be run in an open–loop or incomplete closed–loop mode with the optimal target values passed directly to the control strategy software. However, the system is semi–automated. The energy savings are not disclosed and cannot be found the influence of the process disturbances on the applied advanced control system.

In the period 1991 to 1992, Rashtriya Chemicals and Fertilizers Ltd. India installed in their 2 x 1350 metric t/day ammonia plant an advanced control system developed by Haldore Topsøe A/S, and the case study was presented by Deshmukh *et al*. [26]. The system can maintain automatically the important key process parameters such as H_2–to–N_2 molar ratio, steam–to–carbon molar ratio, inert gas level in the synthesis loop, and reforming firing at a constant and energy–efficient level. Comparing the operation before and after the commissioning of the system, an energy saving of 2,0% and an increase in production of 0.8% were shown. The task of the advanced system involves three basic steps which are required to be executed on a real–time basis. The first step is to retrieve data from the DCS installed in the plant regarding flow, pressure, temperature, and composition for some selected process streams. The second step is to validate the filter, apply correction to the received raw data, and calculate the optimum set points for the DCS controllers. The third step is to transmit the calculated set points to the single loop controllers. The control system uses feedforward and feedback algorithms to control process parameters with minimum deviation from the operator's set points. This was achieved by transmitting new set points to selected single loop controllers in the DCS once every 15 seconds. For functional utility, the control system was divided into three individual modules and the same cannot operate in parallel:

1. Module 1 – plant load control, make-up gas H_2–to–N_2 molar ratio control, and steam–to–carbon molar ratio for the primary reformer control,
2. Module 2 – primary reformer firing control,
3. Module 3 – inert gas level in the synthesis loop control.

They indicated the possible improvements, and their focus was mainly concentrated on the installation of additional and improved instrumentation equipment (smart transmitters) and analysers. However, again, it gives only a general description with no specific theoretical basis,

and they did not bring up anything about how different process disturbances influencing the advanced control system.

Kharbat *et al*. [27] developed a system for the economic optimization of adaptive technology and advanced process control for a variety of unit operations in an ammonia plant. The major goals were to increase the ammonia production rate and decrease energy consumption. They presented adaptive technologies as a blend of old and new modelling and advanced process control techniques. Specifically, they encompassed neural networks, fuzzy logic, chaotic systems, different algorithms, and other mathematical procedures to predict or learn information about the process from the historical data, which was a completely alternative approach at the industrial level in ammonia plants. Described adaptive technology was applied only to synthesis gas converter and tested in the open and closed–loop regime. All other units of the ammonia plant were not considered because of different reasons which cannot be found in the paper. The result of the advanced control technique was the improvement of the ammonia production rate of 27 metric t/day and energy savings of 0.4 kcal/t. Although this approach was extremely innovative, further implementation of the proposed approach cannot be found in the recent literature survey.

The first application of multivariable control (MCV) technology to the ammonia plant was presented by Grasdal *et al*. [11]. The main objectives of the MCV project and its subsequent implementation were following; to provide smoother plant operation, to reduce operator intervention from the application of closed–loop supervisory control, to minimize constraint violations with better safety guarantees, to reduce energy consumption, to increase throughputs and to provide better process performance information. The MCV system was designed by several individual modules supervised by an overall economic optimization. The goal was to achieve the operating objectives in the following parts of the production process, hydraulic module, primary reformer furnace temperature control module, primary reformer riser temperature balance control module, secondary reformer module, water gas shift (WGS)/methanator module, CO_2 removal module and ammonia converter module. Each module contained a simplified, though rigorous, thermodynamic–kinetic and dynamic model of the unit operation. The overall economic optimization function is stated as a scalar function. The optimization module integrates the individual unit controller modules, and considers the effect of steam generation, compression, feed gas composition variation, and so forth. A plantwide energy and material balance are also included in this module. An additional feature of the MCV optimization technology is that the objective function contains terms that are functions of the key control and manipulated variables. These variables and their nonlinear

relationships are updated for every execution cycle to create a dynamic economic optimization. After the commissioning of the advanced control system, the fuel consumption decreased by 1,5%, and ammonia production increased by 0,6%.

Frahm *et al*. [12] demonstrated the application of an MCV in the ammonia production process. The primary objectives were the improvement of overall plant safety and smoother plant operations while achieving plant economic optimization. The MCV system was designed to control roughly 45 variables throughout most of the process sections of the ammonia plant. The control architecture was set up through modular design, which covered primary reformer furnace exit temperature control, primary reformer riser temperature balance control, secondary reformer, WGS unit, CO_2 removal unit, ammonia converter, and ammonia flow optimization module. Finally, an integrated module was designed for the management of interactions and constraint control between modules to control the front–end pressure of the ammonia plant. Any quantification of the constraints is missing, but it is stated that all the constraints were handled adequately. Also, it is missing any deeper elaboration of the method which was used for the model development.

In the last decade, several influencing studies have proposed and discussed the partial or complete control of the ammonia production process based on different control strategies, *e.g*. systematic plantwide control (PWC), self–optimizing control (SOC), heuristics–based methodologies, integration of linear and non–linear model predictive controllers (MPC). Amongst all of them, which shows the most perspective to address the complete control of the ammonia plant is the systematic PWC technique which achievements in ammonia production will be reconsidered in the next section.

2.2.Theoretical background of advanced process control in the ammonia production

With respect to deliver a reliable, advanced control system in an ammonia plant, in parallel with practical cases, it is necessary to investigate the theoretical background which can explain certain phenomena in control structures. Due to the reason that the concept of this thesis is mainly based on operational experience and heuristic approach, one of the interesting theoretical areas which seems like a feasible perspective and a good starting point for proofing the APC scheme novelty, is a PWC strategy with the related process–oriented approach. Three PWC methodologies are known, namely the integrated framework of heuristics and simulation (IFSH), Luyben's heuristic procedure, and the self–optimizing control (SOC) procedure of Skogestad.

The practical application of PWC in the ammonia industry is still at a relatively early stage of its development and the ammonia plant has received little attention in the PWC perspective However, the progress over the last few years, both in terms of case studies and theoretical work, shows promise for the future. The major problem will probably be to generate process models efficiently, and to provide adequate means for their analysis.

The PWC concept is trying to propose a single optimizing controller, which stabilizes the process while perfectly coordinates all the manipulated variables based on dynamic on-line optimization. One approach, which can achieve this, is the use of cascading feedforward and/or feedback loops through which it will be possible to control large and complex plants such as ammonia plant. The major challenge will be how to design an appropriate cascade control system which will not be complicated and heavily nested. One useful way to reconsider is the development of an appropriate model that will give enough payback in terms of simplicity and/or improved performance. Also, the model will have the possibility to determine the control structure which will apply for such a complex system.

To commence with the literature survey of the PWC concept, it is necessary to mention the first comprehensive discussion on plantwide control which was given by Page Buckley in his book “Techniques of process control” in a chapter on Overall process control [28]. The chapter introduces the main issues, and presents what is still in many ways the industrial approach to plantwide control.

According to Foss [29] the main questions that plantwide control tries to answer are:

1. which variables should be controlled?
2. which variables should be measured?
3. which inputs should be manipulated?
4. which links should be made between them?

One of the most significant features of the ammonia plant is the presence of recycle in the synthesis loop which is under the concept of plantwide control. The most common constituents of recycling process are presence of the reactor and separator units. This kind of process setup was studied by many researchers, *e.g.* Papadourakis *et al*. [30], Wolff *et al*. [31], Price *et al*. [32], Luyben [33], Luyben and Floudas [34], Mizsey and Kalmar [35], Wu and Yu [36], Hansen [37] and Ng and Stephanopoulos [38].

Araújo and Skogestad [16] have discussed the application of the PWC design procedure of Skogestad [39] to the ammonia process. A control system for the ammonia synthesis process was designed by applying the SOC procedure proposed by Skogestad [40]. This work was only

investigated the ammonia synthesis loop and reactor configuration from the work of Morud and Skogestad [41].

However, they claimed that the reactor model did not produce the oscillations found in the work of Morud and Skogestad [41]. Three models of operation were considered; given feedstock rate, maximum and "optimized" throughput. Two control structures were proposed. For the two first modes of operation, they proposed control structure which can keep constant purge gas rate and compressor power. The main conclusion of the first control structure was that there is no bottleneck in the process. In the second mode of operation, they tried to keep the compressors at their maximum capacity and it is proposed adjustment of the feed rate such that the inert gas concentration is constant. The standard objective function was proposed with the primary goal to maximize the profit. For the first time it was introduced the disturbance effect to the manipulated and controlled variables. The flowsheet was first optimized regarding steady – state degrees of freedom for various disturbances to identify the active constraints, and then a local linear analysis was employed to identify remaining controlled variables. They identified eight steady–state degrees of freedom for optimization that is, purge gas flow rate, feedstock and compressor power, the three split ratios into the synthesis reactor beds, and the cooling water flow rate in the two heat exchangers. The regulatory layers comprised controllers that aim to avoid excessive drifts from the nominal operating point. The main tested disturbances in dynamic simulation (Aspen Plus) were the mole fraction of CH_4 in the gas feed, cooling water temperature, compressor power and gas feed rate. The reactor inlet/outlet temperature responses were not shown, but they claimed very smooth performance with a maximum change of about 8^oC. They found that designed control structure is not economically attractive to operate the process beyond the production rate determined by the economic bottleneck corresponding to the maximum gas feed rate. The major conclusion which is important for further research is that they found optimal operation by keeping the constant set point policy for the feed compressor power, recycle compressor power and purge gas flow rate when the gas feed rate is given, which corresponds to the practice currently adopted in the industrial ammonia synthesis plant. However, they did not bring into account the changes of the steam system which is the second important layer in the ammonia production. The variation of the process parameters in the steam system can significantly influence the operation of the syngas compressor, due to reason that the same is driven in almost all the ammonia plants by the steam turbine. Besides that, the front–end of the ammonia plant was not considered and finally their influence on the operation of ammonia synthesis loop. This influence from the practical point of view cannot be disregarded.

Van Wuck [42] gave observation that the ammonia production plant presents a complex arrangement of equipment with an ideal goal to operate such that the production of ammonia is maximized while the consumption of natural gas and energy is minimized. However, he concluded that conventional control systems typically cannot meet these control and optimization objectives given the many constraints often associated with these objectives. In his work, van Wuck encompassed all production units in ammonia plant and proposed control system included at least one processor operable to control production equipment using at least one model. The model is associated with a plurality of controlled variables and a plurality of manipulating variables. For the first time he tried to recognize some controlled, manipulated and disturbance variables in the whole ammonia plant. The minimization strategy and the quadratic optimization were used in order to maximize plant profit. He claimed that developed advanced process control system can support a single robust multivariable predictive control strategy. The main control loops stated in the work are control of the methane slip in the secondary reformer between specified limits, control of the air compressor speed below the operating limit, control of the primary reformer temperature below the heating limits, control of the CO_2 slip in CO_2 wash section, control of the volume flow and temperature of the lean solution in the CO_2 wash section, control of the pressure of a synthesis reactor section, and control of the synthesis gas compressor speed. For all control loops, transfer functions were identified. Despite to extremely exhaustive research, all the identified control loops are mutually independent and it cannot be recognized the master controller which will control all other control loops.

In order to show the application of the IFSH developed by Konda *et al*. [19], a PWC structure for the ammonia synthesis process was developed by Zhang *et al*. [17]. This approach was then compared with developed control structure by Araújo and Skogestad [16] that used the SOC procedure. The primary goal of the research was an assessment of the dynamic performance and steady–state profit. Regarding Konda *et al*. [19] recommendations, they applied eight steps of an IFSH method to ammonia synthesis loop with definition of the throughput manipulator (TPM) location. The main PWC objective was ammonia production rate, while any change in throughput should be accomplished smoothly and rapidly. The number of control degrees of freedom was 14. The main tested disturbances were mass flow rate of ammonia product in amount of ± 5%, mole fraction of CH_4 in the feed by 0,001 from 0,003, cooling water temperature increase for 5^oC, and a feed compressor power increase for + 5%. The settling time was chosen as a measure for performance setting and tuning criteria. The TPM was fresh feed flow. The flash separator pressure control was chosen as product quality manipulator (PQM).

The temperature control of all three reactor beds was chosen as a manipulator for more severe controlled variables such as pressure and temperature in ammonia synthesis convertor. The pressure control at the flash outlet was chosen as a manipulator for less severely controlled variables. Unit operations were controlled by flow, temperature, and pressure controllers. Material component balances were controlled by a simple ratio control between purge gas flow rate and recycle flow rate. Any effects because of integration were not recognized. According to the analysis of remaining control degrees of freedom, no additional loops were not implemented. After results evaluation from the simulation tests, the same were compared with the results got from the work of Araújo and Skogestad [16]. It was found that both control systems (based on IFSH and SOC) gave satisfactory response; while IFSH performs better in terms of control and management of production rate during the transient period, while the SOC gives higher steady–state profit. Regarding this work and identification of the ammonia production rate as the main TPM, it must be further evaluated how the front–end of the ammonia plant units will respond to the ammonia plant overall control. This is also one of the major objectives for future research.

As it is stated in the work of Vasudevan [43] the ammonia process flowsheet incorporates the essential features of a complex test bed for PWC, namely many units, component inventory, heat integration and gas recycle. Besides that, the flowsheet is unique in that the fresh feed is mixed with the product stream from the reaction section instead of the recycle as is generally the case with the other PWC test beds. As it was mentioned, Zhang *et al*. [17] proposed the regulatory control structure of the ammonia synthesis section and in the work of Vasudevan [43] the same was considered as the base case and called Amm–IF control structure. Vasudevan defined in his control structure all important controlled variables (CV) and manipulated variables (MV). The one of the most important CV was ammonia production rate. Zhang proposed in the original structure that the inert gas composition control is achieved by controlling the purge–to–recycle flow ratio to manipulate the purge gas flow rate. However, Vasudevan in his work studied the feasibility of utilizing the purge gas flow rate as a manipulator for direct control of the inert gas composition. Three different locations for methane composition control are investigated, namely the reactor inlet, flash outlet, and purge streams. These locations have been selected based on the control structures and an analysis of the process topology. Using compressor duty to control of inert gas composition was not considered. Dynamic disturbance sensitivity (DDS) showed that the original strategy of controlling the purge–to–recycle ratio performs slightly better than direct control of methane composition. Deviation from the production target (DPT) results generally showed otherwise.

Vasudevan showed that the location for inert gas composition control is not a decisive factor in control performance of the ammonia process as indicated by the similar values of DDS and DPT from the earlier studies. He concluded that the best location for control of inert gas composition of the ammonia plant would be in the purge gas stream, as it is located right after the fresh feed is injected. In the Amm–IF control structure Vasudevan proposed three locations for pressure control, namely outlet pressure is controlled by manipulating the reactor outlet flow, flash pressure is controlled by manipulating the vapor outflow and recycle pressure is controlled using recycled compressor duty. Vasudevan also investigated two aspects of pressure control. First, he investigated whether pressure control is really needed at any other location besides the flash separator (which is needed for maintaining purity of ammonia). According to given results, it can be concluded that without no pressure control, pressure drifts in every section of the plant. This has repercussions on plant production rate and hence profit. On the other hand, he noticed that control of flash pressure suffices to maintain pressure throughout the plant. Second, he investigated the choice of the manipulator for flash pressure control, and subsequently he proposed another control manipulator, namely recycle compressor duty. According to conducted simulation results, the main conclusion was that the control structure with the use of recycling compressor duty to control flash pressure performs better for most disturbances, and is recommended over the original Amm-IF control structure. In this case study, Vasudevan disclosed mainly the information about the ammonia synthesis section and the work was dedicated to the purge gas rate and pressure control in the ammonia synthesis section. However, in his work he did not investigate the overall ammonia plant and the influence of front–end process units to the ammonia synthesis section.

Holter [44] tried to show how feedforward control can be used in stabilizing an unstable ammonia reactor with heat integration. The major goal of research was to prevent the instability by the use of feedforward strategies and design of feedforward controller. The test model was executed in the MATLAB/Simulink application and in parallel it is developed state–space model. The feedforward design was shown in two different cases; with a stable and an unstable disturbance model. The main conclusions of the research were:

- the ammonia converter can be stabilized with the controlling the temperature, which enters the first bed, using the mass flow before the first quench as input,
- if the reactor is influenced by larger disturbances, the controller may not stabilize the reactor,
- the feedforward strategy only applies in a small disturbance range,

- the pressure as the influencing disturbance has more influence on the reactor than temperature feed, and
- PI–controller cannot stabilize the system and instead of that derivative action must be included in order to stabilize the ammonia reactor.

The findings from this work served for further evaluation how indicated shortcomings may be overcome in designing the feedforward control system.

According to work of Zhang *et al*. [17], and Vasudevan [43], in the study made by Chi [45] the ammonia synthesis process was employed as a test bed to develop and to compare the performance of the SOC and IFSH methodologies. The simple–separation–recycle (SRS) system has been used as a test bed in PWC study. In the study it is assumed that hydrogen is supplied from an upstream synthesis gas facility, which can present the shortcoming, due to reason that it is not investigated the influence of the industrial ammonia plant front–end on the overall ammonia production process. The steady–state and dynamic simulation were done using Aspen HYSYS. Peng–Robinson equation of state for the prediction of fluid properties was chosen. Chi achieved the similar results as in the work of Araújo and Skogestad [16] which used Aspen Plus. He concluded that the SOC control system of Araújo and Skogestad [16] can be implemented without redesign. The steady–state model was converted to dynamic model with the help of pressure–flow relations, which were specified in Aspen HYSYS. All eight levels of IFSH method were described. As the TPM was chosen ammonia production rate. The author assumed that the ammonia produced has to undergo further purification to meet industrial grade ammonia purity specifications. The control objectives of the plant were following; production rate to be achieved at nominal conditions, and any change in throughput should be accomplished smoothly and quickly and in parallel to reduce variations in product purity as far as possible. The major operational constraints of the process were following; pressure less than 250 bars because of equipment constraints, and temperature higher than 300^{o}C because of reaction kinetics considerations. Control degrees of freedom were 14. The expected disturbances were the same as in the work of Araújo and Skogestad [16]. The performance measures considered in the work were settling time, dynamic disturbance sensitivity (DDS), deviation from the production target (DPT), and final steady–state profit. According to performed simulations (steady–state and dynamic) both control structures (SOC and IFSH) showed excellent response against disturbances within reasonable time. The major noticed difference between the SOC and IFSH control structures is the pressure regulation, which was noticed through smaller DDS values. It was concluded that pressure fluctuations are regulated better by IFSH. This confirmed that pressure loops improve performance in gas–

phase systems, especially when the pressure is high. The conclusion was that both control systems give satisfactory response; while IFSH performs better in terms of control and management of production rate during the transient period. At the same time SOC gives higher steady–state profit. The recommendation of this work was that there is space for improvement in incorporating mathematical and optimization tools in a heuristic–based method. Vasudevan [43] has developed one such hybrid methodology of heuristics and optimization. However, improvements of heuristics–based method might allow better steady–state profits to be achieved in the presence of disturbances, which interests the ammonia industry.

The paper which does not specifically deals with PWC method, but discloses certain valuable information about steady–state and dynamic regimes of ammonia synthesis converter is given by Vinatoru [46]. In this paper, the author emphasized an advanced control structure using the fresh gas flows between catalyst layers as manipulated variables. The major goal was to present the possibilities of ammonia synthesis converter optimization to get a higher conversion factor using the control of gas flows between the catalyst layers. This was achieved by determination of the optimum cooling flows between the catalyst layers and working temperatures in the converter. In order to optimize the problem, it was proposed advanced control algorithm which determines periodically or on demand optimum process parameters. The program allows the operators from the control room to evaluate permanently the working conditions and compare them with the optimal values, to achieve the permanent control of process parameters and to conduct the simple adaptation to the real optimal working conditions.

In the work of Desai *et al*. [47] it was presented a flowsheet of ammonia synthesis loop for industrial production, which was developed on SciLab (kinetic model), while the simulation was performed using Cape–Open–to–Cape–Open simulator (COCO). COCO simulator is an open-source simulator available to the academic community and it can be an alternative to more sophisticated simulator software such as HYSYS, Aspen Plus, UniSim Design, *etc*. The simulation was used for analysis of various output parameters and corresponding operational profits for different input feed flow rates. The advantage of the model in comparison with previous models is the definition of the catalysts effectiveness factor, according to work of Gunorubon *et al*. [48] and component fugacity coefficients according to Upaka *et al*. [49]. The flowsheet closely represents the industrial unit which was simulated by Araújo and Skogestad [16] using Aspen Plus. The operational profit was calculated according to the proposed formula by Araújo and Skogestad [16]. One of the principal contributions of this work was the conclusion that the profit from the process mainly depends upon the ammonia total production.

In the work of Dastjerd *et al*. [50] it is given steady–state and dynamic simulations of the ammonia unit and system behaviour study versus the feed flow rate change. The simulation included all process units in the ammonia plant. The Aspen Plus simulator was used for simulation cases. The control structure was designed with the help of PI and PID controllers as basic controllers, while the tuning was performed by the Tyreus–Luyben method. The accuracy of the proposed control structure was tested against feed flow disturbance within 5% of the nominal rate. The conclusion was, that 5% increase in unit feed flow rate is well controlled and this shows that the designed control system is suitable and has the ability of feedstock capacity increase.

Recently, Luyben [6] proposed a straightforward control structure that provides effective plantwide control of the whole ammonia production process. In this work the flowsheet for an integrated reformer/ammonia process is developed that produces ammonia from the raw material of methane, water and air using multiple units. The proposed control scheme was tested for disturbances in throughput and feedstock composition. However, a comprehensive control structure, which can control the total ammonia production rate, was not disclosed.

Regarding other achievements, it is worthwhile to be mentioned the researches as follows. Reddy and Husaln [51] simulated the ammonia synthesis loop and investigated the effects of the H_2–to–N_2 molar ratio of the recycle gas, loop pressure, recycle gas flow rate, and the concentration of inert gases on the ammonia production rate. The simulation results showed that the most important process parameter is the H_2–to–N_2 molar ratio and its optimum value are around 2.5. Pedernera *et al*. [52] simulated the ammonia synthesis loop in a steady–state and investigated the effect of the manipulated variables on the reactor stability. Rahimpour and Kashkooli [53] developed a mathematical model for removal of carbon dioxide from the synthesized gas into amine–promoted hot potash solution and investigated the influences of the important parameters of the model, such as amine addition and operating pressure on the absorption performance. The results showed that adding piperazine to the potash solution carbonate increases the CO_2 absorption rate [53]. In order to determine the optimal inlet temperatures of the catalyst beds of an ammonia synthesis reactor, Akpa and Raphael [54] maximized the objective function of the fractional conversion of nitrogen on the four catalyst beds of the reactor subject to variation of the inlet temperature to each catalyst bed. The results showed a 42,38% increase in fractional conversion and 56,48% increase in ammonia concentration at the end of the fourth catalyst bed.

2.3.Summary of literature review

This chapter summarizes the literature in practical and theoretical applications of the advanced process control in the ammonia production process.

However, as it was mentioned, this is only one part of the most influencing case studies, which defined the basis for further implementation of advanced process control system in ammonia production facilities.

Literature review shows that idea of advanced process control exists even before introducing the microprocessor computers at the industrial level. With the progress of powerful computers, the advanced control systems become even more presented in the ammonia production facilities. The increased availability of rigorous process simulators means that it is possible to develop more efficient advanced process control structures based on steady–state and dynamic simulations during control structure development. The primary objectives are to increase production rate and to minimize energy consumption, ensuring smoother operation and increasing process safety.

However, all the conducted research is mainly concentrated to the individual process units in the complex ammonia process trying to interconnect each of them with module–based approach.

It can be also concluded that not much attention has been paid to the systematic advanced control structure of the overall ammonia plant or how to control the overall process with the main (master) controller which will control all other loops relevant for ammonia production.

From the theoretical point of view, the work of Araújo and Skogestad [16] is a case in point.

Finally, a combined approach of the practical experience and PWC methodologies to the actual ammonia plant can be an interesting area for additional investigation to ensure better control and to provide advancement in control systems of industrial ammonia plants.

3. METHODOLOGY OF THE RESEARCH

Specific control problems in ammonia production were adapted and tackled in each level of the procedure regarding already available and published literature data given in the previous chapter and many years of operational experience during operation of the reference ammonia plant.

The research was carried out in cooperation between the fertilizer production complex Petrokemija Plc., Kutina and a group of scientists at the Department of Measurement and Automatic Process Control of the Faculty of Chemical Engineering and Technology, University of Zagreb, Croatia. Advancement in the process control of the ammonia production process was investigated. Based on previous research and application conducted in recent years, the necessary industry experience was gained and several research papers on modelling, inferential measurement and advanced process control have been published, making it the basis for this research.

Development of advanced process control method in the proposed research is based on data from the process history database of the ammonia plant in Petrokemija Plc., Kutina. Regarding this, an advanced process control structure is proposed, which can interconnect all relevant process variables in ammonia production by a combination of feedforward, feedback, ratio, cascade, and gain-scheduled control strategy with accompanying profit objective function.

During the first step, attention was focused on collection, analysis and preprocessing of the historical data from the referenced ammonia plant. The research was continued with the development of a steady–state model based on the literature data adapted to the process data, considering thermodynamic and kinetic parameters of the processes.

After validation of the steady–state model, the flowsheet was transferred to the dynamic hold–up model in which all dynamic features of the process and control equipment were defined according to the reference ammonia plant case.

To enhance economic performance of the ammonia facility feedforward, feedback, ratio, cascade, and gain-scheduled strategy was designed with profit-based function based on quadratic program economics that maximizes plant profit.

An overview of the activities follows:

1. Study of the literature containing the latest theoretical research and practical application of advanced process control in ammonia production;
2. Analysis of ammonia production process based on history data:

a) analysis of dynamical behavior of the key process control loops;
b) analysis of potential control loops to be included in advanced process control strategy;

3. Data collection, selection and preprocessing;
4. Identification of control objectives;
5. Design of an advanced process control scheme and identification of the critical process parameters;
6. Defining of the assumptions for model developing and simulation;
7. Spatial and time dependence analysis (process model equations);
8. Development of steady–state model;
9. Development of dynamic model and simulation of process response to changes in the input variables and process parameters to determine control loops transient response and settling time;
10. Development of advanced process control structure that includes:
    a) classification of controlled and manipulated, disturbance variables and process parameters;
    b) development of the state–space models;
    c) definition of transfer function and system linearization;
    d) determination of control matrix;
11. Tuning the parameters of advanced process controller;
12. Advanced control system simulation, testing and validation;
13. Comparison of the simulation and real–process data;
14. Publication of research results.

4. STEADY–STATE AND DYNAMIC MODELLING

The steady–state and pressure–flow holdup dynamic flowsheets are based on the reference ammonia plant in Kutina, Croatia, owned by Petrokemija Plc. fertilizer company. Produced ammonia is the main raw material for further processing of nitric acid and finished fertilizer products such as urea, ammonium–nitrates and different complex NPK's. The ammonia technology provider was M. W. Kellogg Inc. Ammonia plant comprises a high–pressure catalytic reforming method for producing 1360 metric tons per day of ammonia from primary raw materials; hydrocarbon feedstock (mainly CH_4), steam, and air. For convenience presentation of the complex flowsheet and to test the proposed control structure, the equipment has been grouped into three major parts – synthesis gas generation, synthesis gas purification and ammonia synthesis loop. The simplified flowsheet of all process units is shown in Figure 1.

The steady–state model is developed using UniSim Design R470 (Honeywell) with modular operations, which are combined with a non–sequential algorithm. Information is processed as soon as it is supplied. The results of any calculation are automatically distributed throughout the flowsheet, both forward and backwards. Material, energy and composition balances are considered at the same time. Pressure, flow, temperature and composition specifications are considered equally [56].

The steady–state model is embedded into the lumped dynamic model for all unit operations, followed by basic steps. The basic steps included further identification of material stream which are connected to two–unit operations with no pressure and flow relation and whose flow must be specified in dynamic mode. In parallel, the equipment was additional checked against size by using the actual plant equipment and the same was defined accordingly. Finally, the key control process parameters that exist within the ammonia plant was identified and analysed in dynamic simulation. Ordinary differential equations (ODE) were solved using the implicit Euler method with maximum speed performance. Dynamic calculations are performed at three different frequencies: volume (pressure–flow), energy and composition. Holdup values of all process units (vessel volumes, pump heads, valves, heat exchangers, compressors, reactors, *etc*.) have been specified according to technical documentation of the reference ammonia plant to reflect actual behaviour of the process. Flows exiting from holdup are calculated from a resistance equation in which parameters are defined as per technical documentation. In total, the model comprises 1245 equations.

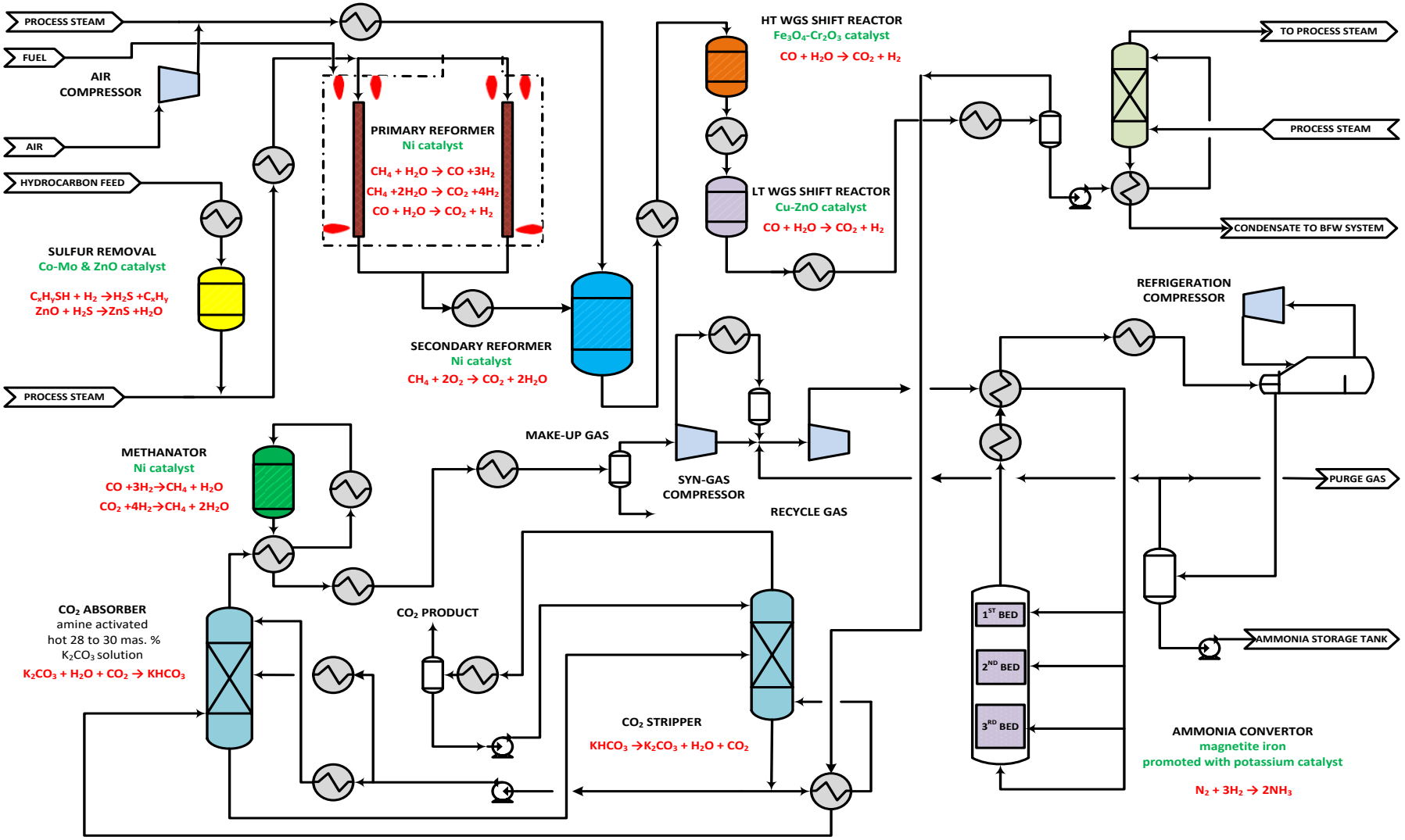

Figure 1. Ammonia plant flowsheet.

Control valves and actuators are modelled in instantaneous mode. That means the actuator moves instantaneously to the desired OP % position from the controller.

In order to develop feedforward, feedback, ratio, cascade, and gain–scheduled advanced control structure, data driven modelling was used. Based on the transient response, transfer functions were determined using the MATLAB System Identification Toolbox [57]. System Identification Toolbox provides MATLAB functions, Simulink blocks, and an application for constructing mathematical models of dynamic systems from measured input–output data. It lets to create and use models of dynamic systems not easily modelled from first principles or specifications. By the usage of time–domain and frequency–domain input–output data, it is possible to identify continuous–time and discrete–time transfer functions, process models, and state–space models. The toolbox also provides algorithms for embedded online parameter estimation. The toolbox provides identification techniques such as maximum likelihood, prediction–error minimization (PEM), and subspace system identification. To represent nonlinear system dynamics, it is possible to estimate Hammerstein–Weiner models and nonlinear ARX models with wavelet network, tree–partition, and sigmoid network nonlinearities. The toolbox performs grey–box system identification for estimating parameters of a user–defined model. The application can be used for identification of the model for system response prediction.

The parameters of the single–input–single–output (SISO) plant model was identified. The plant model was converted to a discrete–time state-space plant model for feedforward, feedback, ratio, cascade, and gain–scheduled control. The model was used for controller parameter tuning by *Auto Tuning Variation* (ATV) technique [56, 57]. Besides that, the application MATLAB System Identification Toolbox was used also for determination of controller poles and zeros and to test controller loop gain.

4.1.Process description – Steady–state modelling

A detailed description of the ammonia production process supported with the accompanying flowsheets built in UniSim Design R470 is given. The flowsheets are prepared according to the relevant process flow diagrams (PFD) of the reference ammonia plant. In parallel, set of kinetic and thermodynamic expressions is given, which ensures to the steady–state model enough reliability to be used in dynamic simulations and validation of the proposed control structure.

4.1.1. Synthesis gas generation model

The steady–state flowsheet of the synthesis gas generation model build in UniSim Design R470 is shown in Figure 2.

Natural gas feed at a pressure of about 32 bar enters the natural gas knock–out drum 120-F for elimination of entrained liquid. The outlet line of 120–F feeds the one–stage centrifugal natural gas feed compressor 102–J driven by steam turbines. The outlet pressure of natural gas is at the level of 42 bar. Hydrogen required for desulphurization of the natural gas is injected into the paralleled natural gas stream entering the natural gas heater 103–B. This stream is controlled by the control valve FV–166. The outlet temperature of the 103–B is 400^{o}C. The heated natural gas stream flows through two reactors in series. The first is the hydrogenator 101–D which contains a single bed of the cobalt–molybdenum (Co–Mo) catalyst. In this reactor, the organic sulphur compounds are converted to hydrogen sulphide (H_2S) in the presence of the H_2 injected upstream of 103–B. The natural gas stream next passes into desulphuriser reactor 102–D, which contains a single bed of zinc–oxide (ZnO) catalyst. In this reactor the H_2S is converted to zinc sulphide (ZnS) which remains in the catalyst.

The desulphurised natural gas, plus residual H_2, leaves 102–D with a sulphur content of 0,25 ppm and at the temperature of 370^{o}C. The natural gas plus residual H_2 stream controlled by control valve FV–108 is joined by process steam in the mixer. The process steam is at a pressure of about 40 bar and a temperature of 392^{o}C and controlled by control valve FV–109. The steam flow is controlled with the steam–to–natural gas (S/N.G.) molar ratio controller.

The steam–natural gas feed gas (mixed feed) flows in the mixed feed coil, which is located in the convection section of the steam reformer furnace. In this coil, the mixed feed is heated to about 510^{o}C. After heating, the mixed feed flows down through ten rows of reformer tubes that are suspended in the radiant box of primary reformer 101–B. Eleven rows of forced draught down fired burners are located in parallel rows to the catalyst tubes – in total 198 burners. They raised the feed temperature to about 790^{o}C at the outlet of the catalyst tubes. In addition, 11 tunnel burners are used for heating the waste gases passing from radiant to convection part of the SMR furnace. 520 catalyst tubes contain 30 m^3 of nickel reforming catalyst. It is modelled as an isothermal plug flow reactor (PFR) with the effluent temperature set at the constant methane outlet molar concentration of 10,35 mol.% per dry basis. To control the methane outlet molar concentration at mentioned level the reformer furnace is modelled with a heat flux specification of 95,2 kW/h and with the total reformer furnace duty of 198,10 MW. This heat

duty is accomplished as it was mentioned with 198 arch, 11 tunnel, and additionaly with 21 superheater burners for steam superheating and 5 auxiliary boiler burners for steam generation.

Process air for the secondary reforming operation is supplied by the air compressor 101–J. The compressor draws in atmospheric air and discharged at a pressure of about 35 bar and a temperature of 174^{o}C. The air compressor 101–J is a four–stage centrifugal compressor driven by steam turbine. In between of each compressor stage it is located the knockout drum (JF–1 to JF–3) for elimination of the water from the air and related heat exchangers for cooling down the air after each compression stage (JC–1 to JC–3). The process air flow to the secondary reformer is controlled by the control valve FV–112. The process air flow is joined by a small flow of 40 bar steam, which is controlled also by the control valve FV–113. The steam flow serves for two functions. During normal operation, the small steam flow helps to prevent backflow of process gas into the air line if the compressor trips. In case of low air flow, the steam flow protects the steam/air coil for overheating. The combined air/steam flow is heated in the steam/air coil, located in the convection section of the primary reformer furnace. The outlet temperature of this coil during normal operation is about 468^{o}C.

The partially reformed gas from the primary reformer transfer line enters the secondary reformer 103–D at the top section and passes in the combustion zone together with the process air. Combustion takes place in the combustion zone and the gases with a temperature of about 1190^{o}C, pass down through a shallow bed of high temperature chromium catalyst and then through a deeper bed of nickel reforming catalyst. The heat provided by the combustion above the catalyst bed gives the energy required to reform residual methane. At the outlet of the secondary reformer, the temperature of the process gas is about 1000^{o}C and the methane content is designed to be 0,28 mol.% on a dry gas basis. The burner is modelled as Gibbs reactor, while the secondary reformer is modelled as a plug flow reactor (PFR).

The quantity of air added to the secondary reforming stage is governed by the nitrogen requirements of the synthesis loop. At the outlet of the secondary reformer the H_2–to–N_2 molar ratio will be about 2,5 to 1. The effluent process gas from the secondary reformer divides and equal streams pass through two primary waste heat boilers 101–CA and CB. This bayonet heat exchangers serves for generation of the 125 bar steam and to cool down the process gas to about 480^{o}C. The effluent gases from the 101–CA and CB combine in the inlet channel of the secondary waste heat boiler 102–C. This is a shell and tube heat exchanger in which the process gas passes through the tubes, generating steam at 125 bar on the shell side. At the outlet of this line temperature controller with TV–124 control valve which controls the inlet temperature to the high temperature shift conversion at 371^{o}C.

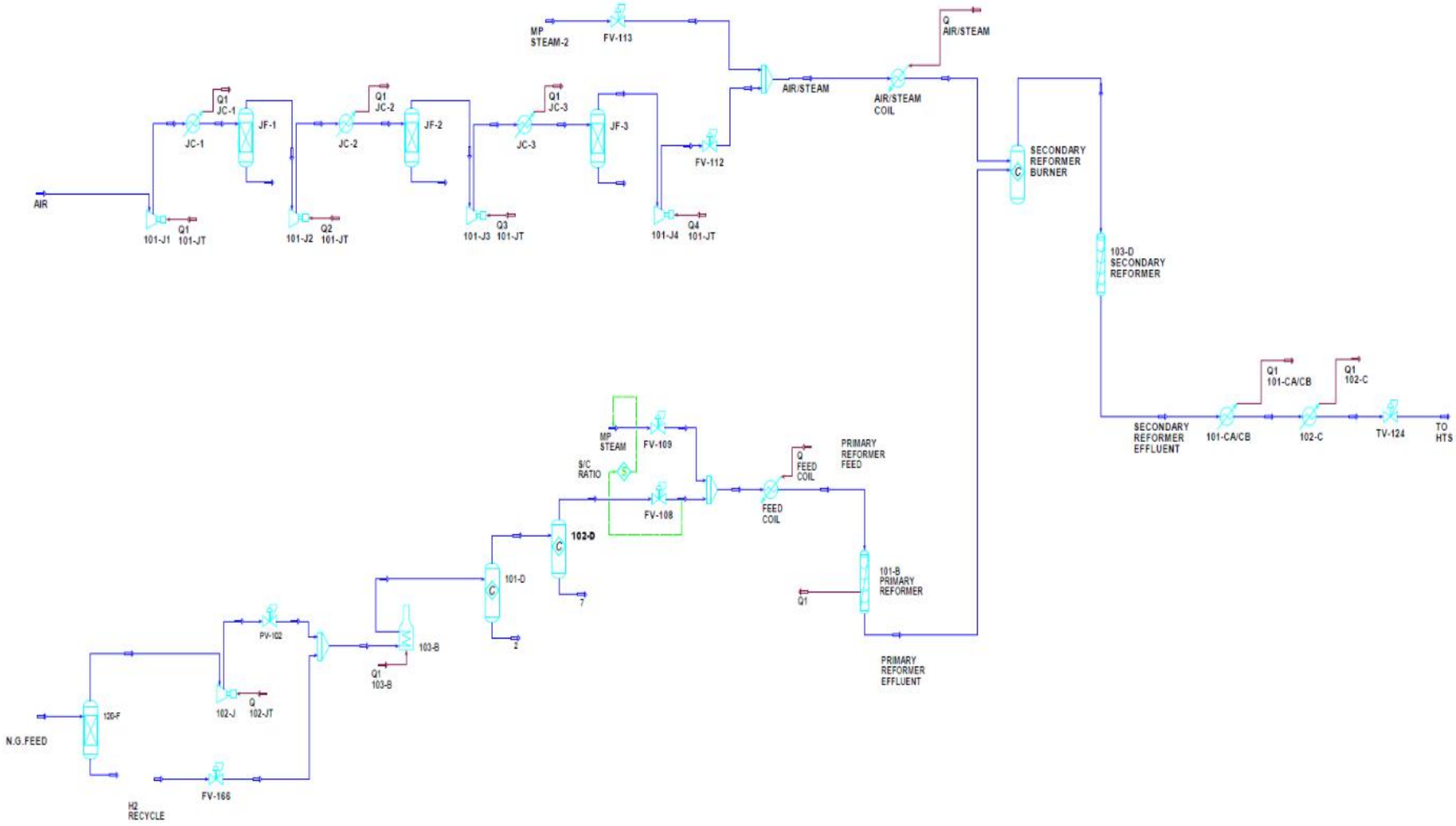

Figure 2. Synthesis gas generation steady–state flowsheet.

4.1.1.1.Desulphurisation unit

The most common poison found in hydrocarbon feedstock is sulphur. Sulphur is a severe poison for the steam reforming catalyst, which contains nickel. It is absorbed on the nickel as a surface sulphide and interferes with the steam reforming reaction. Losing activity can lead to carbon deposition and subsequent overheating of the reformer tubes, which may cause tube failure [60]. Most steam reformers can operate with a sulphur level of up to 0,5 ppm in the hydrocarbon feedstock, however the reference ammonia plant was designed to withstand the level of sulfur up to 0,25 ppm.

The desulphurisation unit comprises two steps, namely hydrogenolysis of organic sulphur with hydrogen and absorption of the H_2S on the ZnO bed. According to this layout, the hydrogenator was modelled as conversion reactor, while the desulphuriser was modelled as the equilibrium reactor. The input value of organic sulphur was 9 ppm as per design, while conversion rate would have given at the outlet of desulphuriser the sulphur content of 0,25 ppm.

The reactions showed in Table 1 were assumed that take place in the hydrogenolysis unit to accomplish the conversion of mentioned sulphur content.

Table 1. A hydrogenolysis reaction scheme [60].

Reaction	ΔH^{o}_{298} [kJ/mol]
$C_2H_5SH + H_2 \leftrightarrow C_2H_6 + H_2S$	-70,2
$C_2H_5SC_2H_5 + 2H_2 \leftrightarrow 2C_2H_6 + H_2S$	-117,2
$C_4H_8S + 2H_2 \leftrightarrow C_4H_{10} + H_2S$	-120,2
$C_4H_4S + 4H_2 \leftrightarrow C_4H_{10} + H_2S$	-280,3

These reactions are exothermic but, because of the very low levels of organic sulphur compounds in the reference feedstock, a temperature rise was neglected.

The hydrogenator contains 27,6 m^3 of Co–Mo catalyst (1,5% of CoO; 5% of MoO_3 and the balance is Al_2O_3) with the size of 2,5 mm and shape of asymmetric quadralobe. The bulk density is 0,40 to 0,45 kg/L, surface area is > 350 m^2/g and porosity is between 0.35 to 0.45 mL/g. The optimum operating temperature range is between 315 to 413^{o}C according to the catalyst provider's technical specification. As per design, inlet feed gas temperature of 399^{o}C was chosen. The vessel dimensions are 2468 mm in diameter and 5770 mm in height.

The ZnO absorption unit removes all the H_2S produced in the hydrogenolysis unit. The active absorbent ZnO reacts almost completely with H_2S to form ZnS as shown by following equation:

$$ZnO + H_2S \rightarrow ZnS + H_2S \quad (1)$$

Kinetic studies of the H_2S with ZnO have shown that the reaction is the first–order regarding the H_2S concentration, with a rate constant given by following equation [60]:

$$k = 9{,}46x10^{-2}\exp\left(-\frac{7{,}236}{RT}\right) \quad (2)$$

where *k* represents the rate constant, *R* denotes universal gas constant in kJ/kgmolK, and *T* is the respective thermodynamic temperature in K.

Under normal conditions, (as it was assumed) the equilibrium is strongly in favour of sulphide formation.

The absorber contains 27,6 m^3 of ZnO catalyst (90% of ZnO; 2.0% of CaO and balance is Al_2O_3) with the size of 3 to 5 mm and shape of extrudates. The bulk density is 1.1 kg/L, surface area is >25 m^2/g and porosity is between 0.10 to 0.15 mL/g. The optimum operating temperature range is between 315 to 413ºC according to the catalyst provider's technical specification. A design inlet temperature of 399ºC was chosen as with hydrogenator. The vessel dimensions are 2468 mm in diameter and 5770 mm in height.

4.1.1.2.Steam–natural gas reforming (SMR) unit

The objective of the catalytic steam reforming process is to extract the maximum quantity of hydrogen held in water and hydrocarbon feedstock (in this case natural gas). The reforming reactions are accompanied by the water–gas–shift reaction (WGS). Although there are eleven possible reactions in steam methane reforming (SMR) process, a simplified SMR scheme presented in Table 2 can be used for approximation of industrial SMR unit [58-60]. According to previous findings, only those reactions are critical in the rate–determining step [58-60].

Industrial steam reformers are usually fixed–bed reactors located in a reformer box in charge of insuring necessary heat flux for strong SMR endothermic reaction. Their performance is strongly affected by the heat transfer from the furnace to the reformer tubes. According to the reactions given in Table 2 it is clear that the reforming reaction is strongly endothermic, so the forward reaction is favored by high temperature as well as by low pressure, while the WGS reaction is exothermic and is favored by low temperature but is largely unaffected by changes in pressure.

Table 2. A simplified steam–methane reforming reaction scheme.

Reaction description	Reaction	ΔH^{o}_{298} [kJ/mol]
Steam-methane reforming 1, SR1	$CH_4 + H_2O \leftrightarrow CO + 3H_2$	206,10
Water-gas shift, WGS	$CO + H_2O \leftrightarrow CO_2 + H_2$	-41,15
Steam-methane reforming 2, SR2	$CH_4 + 2H_2O \leftrightarrow CO_2 + 4H_2$	165,00
Carbon dioxide-methane reforming	$CH_4 + CO_2 \leftrightarrow 2CO + 2H_2$	247,30

It can be seen that with methane the stoichiometric requirement for steam per carbon atom is 1,0 and that the overall reaction is strongly endothermic. However, it has been showed that this is not practicable because all available commercial catalysts promote carbon forming reactions under steam reforming conditions. These reactions can only be suppressed by using an excess of steam, with the minimum ratio of 1,7 [1, 60]. Modern natural gas–based ammonia plants with conventional primary reformer use a steam–to–carbon ratio of around 3,0, compared to values of 3,6 to 4,0 in older installations [1, 60].

Lowering the steam–to–carbon molar ratio means attractive energy savings from one side, but these operating conditions in parallel create severe reaction condition for the reformer tube material, which can exhibit creep with the result of their stress rupture. Continuous operation over the design temperature of the reforming tube can result in a decrease in their lifetime. A prolonged increase of the tube wall temperature of 20°C over the design temperature decreases the reforming tube's lifetime by half [61-63]. By design and industry practice, maximum allowable tube wall temperatures will give an in–service lifetime of 100000 hours when considering the stress–to–rupture properties of the particular alloy used in manufacturing the tube [61]. As noted by Schillmoller *et al*. [61] an increase in temperature of only 38°C above the design with the common HK–40 material (25% chrome, 20% nickel alloy) can shorten the tube lifetime from 10 years to 1,4 years.

The catalyst in all the SMR furnaces is contained in heat resistant alloy tubes that typically have outside diameters from 80 to 180 mm, wall thickness of 9 to 20 mm and the overall length of 10000 to 13000 mm [1, 60]. Fired lengths in commercial SMR furnaces vary from approximately 200 to as much as 3500 mm [1, 60]. Firing is usually controlled such that tube wall temperatures are maintained at values that will give a reasonable tube lifetime. The general SMR furnace classifications according to firing pattern are following: top fired, side fired, and bottom fired [1]. All the SMR furnaces have combustion heat recovery sections used for preheating feed streams, boiler feed water, *etc*.

Catalyst activity has an important effect on the reformer tube wall temperature in all SMR furnaces and is usually monitored by the plant operators by portable measurement devices. The heat transfer through the walls of the reformer tubes influences to the catalyst activity. Of the total heat being transferred, the high activity catalyst uses more for the endothermic reforming reaction and less for raising the gas temperature. Besides that, feed gases can vary in composition from being nearly pure methane to the heavy hydrocarbons such as naphtha. As a result, specific catalyst formulations have been developed so far for different feed gas compositions [1, 60]. Xu and Froment [58, 59] used in their work catalyst which contained 15,2% nickel, supported on magnesium spinel with BET surface area of 58 m^2, nickel surface area of 9,3 m^2/g_{cat} and with the void fraction of 0,528. The catalyst used in simulation contained 14,5% nickel, supported on calcium aluminate with BET surface area of 57 m^2, nickel surface area of 12,0 m^2/g_{cat} and with the void fraction of 0,51963. The mentioned catalyst characteristics are in good alignment with the work of Xu and Froment [58, 59]. Therefore, literature kinetics data can apply to the model, although different catalyst support was used in the model.

The average conversion rate of hydrogen from hydrocarbons and water in standard SMR reformers within ammonia production is in the range from 60 to 70%, so the methane slip of the reformer is between 10 and 14 mol.% per dry basis [1, 60, 62]. Term methane slip is commonly used in industrial practice to describe methane molar concentration per dry basis at the outlet of reformer tubes.

Important considerations during operation of SMR are: the type of furnace used to transfer heat to the reactants, the catalyst properties such as activity, lifetime, size, and strength, operating conditions such as feedstock composition, pressure, temperature, and desired product composition [62, 63].

From the mentioned it can be concluded that the hydrogen production depends on the reforming tube outer wall temperature and steam–to–carbon molar ratio. A higher outer reforming tube wall temperature and higher steam–to–carbon molar ratio will cause higher hydrogen conversion and lower methane slip. To satisfy benefits and constraints during operation, all process parameters which influence reformer behavior must be appropriately controlled to minimize the operator's interference [64-68].

The schematic diagram of the top–fired SMR based on M. W. Kellogg Inc. design in Petrokemija Plc., Kutina, used in the model is given in Figure 3. Characteristic process data of the top–fired SMR for data reconciliation are given in Table 3.

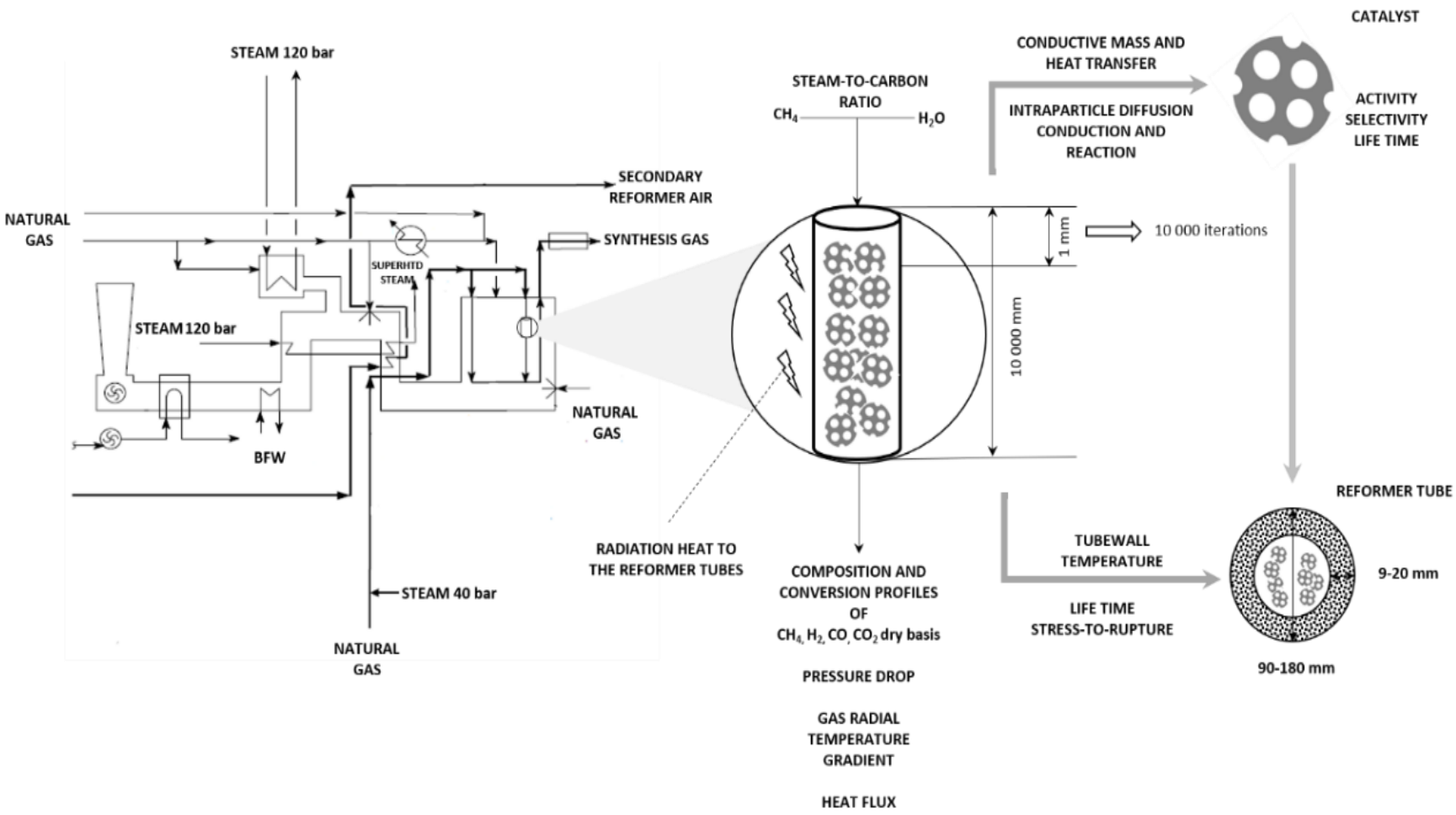

Figure 3. The schematic diagram of the top–fired SMR based on M. W. Kellogg Inc. design.

The radiant section of the reformer is composed of 198 arch burners distributed across 11 rows of 18 burners, and 520 reformer tubes (MANAURITE XM and 900 alloy) distributed across 10 rows of 52 tubes. Waste gas tunnels with related 11 tunnel burners are located at the bottom of the furnace to evacuate the waste gas generated by the combustion reactions inside the furnace chamber. The reforming tubes are packed with commercially available nickel oxide over alpha alumina (*i.e.* $Ni/\alpha{-}Al_2O_3$) support in the shape of rings with 12 evenly distributed holes, which facilitate the reactions within the reformer and heat transfer from the reforming tube walls to the inside of the tube. The external diameter, internal diameter, and exposed length of the reforming tube are 8,5 cm, 11,3 cm, and 12,5 m, respectively. The catalyst length of each reformer tube is adjusted to be 10000 mm. The reforming tubes are heated mainly by radiation inside the high–temperature furnace chamber to drive the net endothermic reactions given in Table 2.

For a set of operating conditions – fuel flow rate, temperature and molar composition of the process gas at the reformer tube inlet, the model predicts the heat duty of the reformer, temperature and pressure profiles of the reformed gas, concentration profiles of the process gas stream constituents, and waste gas temperature profiles.

The reformer furnace model calculates adiabatic and real flame temperatures and determines waste gas quality and quantity composition according to the known composition of the fuel gas, inlet temperatures of fuel and combustion air, with possibility to adjust automatically air–to–fuel ratio regarding to required oxygen content in the waste gas.

The following equations are used for determination of the adiabatic and real gas flame temperatures. Adiabatic flame temperature (*TAD*) in K is determined by:

$$TAD = \frac{Q_{\mathrm{wg}}}{V_{\mathrm{wg}} \cdot c_{\mathrm{pwg}}} \tag{3}$$

where Q_{wg} represents heat absorbed due to combustion of fuel in J, V_{wg} stands for waste gas volume from 1 m^3 of fuel in m^3, and c_{pwg} denotes waste gas specific heat at constant pressure in kJ/m^3K.

Heat absorbed due to dissociation of combustion products is determined from the heat balance:

$$Q_{\mathrm{WG}} = Q_{\mathrm{FUEL}} + Q_{\mathrm{AIR}} + Q_{\mathrm{CHEM}} \tag{4}$$

where Q_{FUEL} represents heat in the fuel in J, Q_{AIR} stands for the heat in the combustion air in J, and Q_{CHEM} denotes heat of combustion in J.

Heat in the fuel is determined from:

$$Q_{\mathrm{FUEL}} = c_{\mathrm{pFUEL}} \cdot \Delta T_{\mathrm{FUEL}} \tag{5}$$

where c_{pFUEL} represents fuel gas specific heat at constant pressure in kJ/m^{3}K, while ΔT_{FUEL} stands for fuel temperature in K.

Heat in the combustion air is determined by:

$$Q_{\mathrm{AIR}} = \frac{V_{\mathrm{AIR}} \cdot c_{\mathrm{pAIR}} \cdot \Delta T_{\mathrm{AIR}}}{V_{\mathrm{FUEL}}} \tag{6}$$

where V_{AIR} represents volume flow of combustion air in m^3/h, c_{pAIR} stands for combustion air specific heat at constant pressure in kJ/m^{3}K, ΔT_{AIR} is combustion air temperature in K and V_{FUEL} denotes volume flow of fuel gas in m^3/h.

Heat of combustion is determined from:

$$Q_{\mathrm{CHEM}} = FCV \tag{7}$$

where *FCV* represents fuel calorific value in kJ/m^3.

Real gas temperature (*TRE*) is determined from:

$$TRE = TAD \cdot \frac{\eta}{100} \tag{8}$$

where η represents efficiency of combustion in %.

Specific heat of different gases (fuel, combustion air, waste gas) vary with temperature, and analytical expressions for their determination are given in the literature [69].

Table 3. Summary of process data of the top-fired SMR.

Reformer Tubes	**Value/Unit**	**Catalyst Pellets**	**Value/Unit**
Heated length of reformer tubes	10,00 m	Shape	Raschig rings with 12 holes
Inside diameter of reformer tubes	0,085 m	Dimensions	19×12 mm/30%; 19×16 mm/70%;
Outside diameter of reformer tubes	0,110 m	Bulk density	800 kg/m^3
Number of reformer tubes	520	Porosity	0,51963
Construction material of reformer tubes	MANAURITE XM and 900	Tortuosity	2,74
Number of rows	10	Mean pore radius	80 Å
Number of arch burners	198	Catalyst characteristic length	0,001948 cm
Heat duty of reformer	204,80 MWh	Catalyst material	$NiO+CaAl_{12}O_{19}$
Skin temperature	840ºC	Catalyst quantity	32,0 tons
Process gas flow rate and composition	**Value/Unit**	**Fuel characteristics**	**Value/Unit**
Molar flow rate	1530 kmol/h	Molar flow rate	792 kmol/h; 3% of O_2 excess air at 503 K
Composition	mol.%, dry basis	Composition	mol.%, dry basis
CH_4	96,6591	CH_4	96,6591
C_2H_6	0,00	C_2H_6	0,00
C_3H_8	0,00	C_3H_8	0,00
i-C_4H_{10}	0,00	i-C_4H_{10}	0,00
C_2H_5SH	0,0009	C_2H_5SH	0,0009
H_2	1,43	H_2	1,43
CO_2	0,95	CO_2	0,95
N_2	0,95	N_2	0,95
Ar+He	0,01	Ar+He	0,01
Inlet conditions	**Value/Unit**	**Outlet conditions**	**Value/Unit**
Temperature	773 K	Temperature	800ºC
Pressure	30,5 bar	Pressure	30,0 bar
S/C ratio	3,60	S/C ratio	3,60
Maximum allowable temperature			900ºC
Ammonia production capacity			1.360 t/day

Dynamic energy balance on the reformer tubes by radiation and convection transfer of the heat is following:

$$V_{\mathrm{m}}\rho_{\mathrm{m}}C_{\mathrm{m}}\frac{dT_{\mathrm{p}}(t)}{dt} = h_{\mathrm{e}}A_{\mathrm{e}}\left[T_{\mathrm{wg}}(t) - T_{\mathrm{wtt}}(t)\right] - h_{\mathrm{i}}A_{\mathrm{j}}\left[T_{\mathrm{wtt}}(t) - T_{\mathrm{rgo}}(t)\right] \quad (9)$$

where V_{m} is the volume of reformer tube in m^3, ρ_{m} is the density of the reformer tube material in kg/m^3, C_{m} denotes heat capacity of the reformer tube material in kJ/kgK, T_{wg} is the temperature of the waste gas in K, T_{wtt} stands for reformer tube wall temperature, T_{rgo} is the outlet temperature of the reformed syngas in K, h_{i} is the heat transfer coefficient of the catalyst in kJ/kg, while A_{j} is the internal heat transfer area in m^2.

Dynamic energy balance of the combustion gas is determined by:

$$M_{\mathrm{B}} C_{\mathrm{B}} \frac{dT_{\mathrm{s}}(t)}{dt} = F_{\mathrm{f}}(t) H_{\mathrm{f}} \eta_{\mathrm{RF}} - h_{\mathrm{e}} A_{\mathrm{e}} [T_{\mathrm{rf}}(t) - T_{\mathrm{wtt}}(t)] \quad (10)$$

where M_{B} stands for effective mass flow of the waste gas in kg/h, C_{B} is the specific heat of the waste gas in kJ/kgK, F_{f} is the mass flow rate of the fuel in kg/h, H_{f} denotes calorific value of the fuel in kJ/kg, η_{RF} is the reformer furnace efficiency in %, h_{e} is the heat transfer coefficient of the reformer tube material in kJ/kg, while A_{e} is the external heat transfer area of the reformer tubes in m^2.

The reformer tube side model uses a combination of steam–methane reforming reactions 1 and 2 (SR1 and SR2) and water gas shift reaction (WGS) to calculate the product compositions. The carbon dioxide–methane reforming reaction is not considered in the model because natural gas as the main feedstock contains negligible concentrations of carbon dioxide. For establishing chemical equilibrium at a particular temperature, the equilibrium constants for the SR1, WGS and SR2 reactions are as follows [57-60, 62-63]:

$$K_{\mathrm{SR1}} = \frac{p_{\mathrm{CO}} \cdot p_{\mathrm{H_2}}^3}{p_{\mathrm{CH_4}} \cdot p_{\mathrm{H_2O}}} = 1{,}198 \cdot 10^{17} exp\left(\frac{-26830}{T}\right) \quad (11)$$

$$K_{\mathrm{WGS}} = \frac{p_{\mathrm{CO_2}} \cdot p_{\mathrm{H_2}}}{p_{\mathrm{CO}} \cdot p_{\mathrm{H_2O}}} = 1{,}767 \cdot 10^{-2} \exp\left(\frac{4400}{T}\right) \quad (12)$$

$$K_{SR2} = \frac{p_{\mathrm{CO_2}} \cdot p_{\mathrm{H_2}}^4}{p_{\mathrm{CH_4}} \cdot p_{\mathrm{H_2O}}^2} = K_{\mathrm{SR1}} \cdot K_{\mathrm{WGS}} = 2{,}117 \cdot 10^{15} exp\left(\frac{-22430}{T}\right) \quad (13)$$

where K represents apparent chemical equilibrium constant (the true one would require activities instead of equilibrium pressures), p stands for the partial pressure of corresponding component (in bar) and T denotes gas temperature inside of reformer tubes (in K).

The corresponding rate equations according to Xu and Froment are [58-59]:

$$r_{\mathrm{SR1}} = \frac{k_{\mathrm{SR1}}}{p_{\mathrm{H_2}}^{2.5}} \left(p_{\mathrm{CH_4}} \cdot p_{\mathrm{H_2O}} - \frac{p_{\mathrm{H_2}}^3 \cdot p_{\mathrm{CO}}}{K_{\mathrm{SR1}}}\right) / D^2 \quad (14)$$

$$r_{\mathrm{WGS}} = \frac{k_{\mathrm{WGS}}}{p_{\mathrm{H_2}}}\left(p_{\mathrm{CO}} \cdot p_{\mathrm{H_2O}} - \frac{p_{\mathrm{H_2}} \cdot p_{\mathrm{CO_2}}}{K_{\mathrm{WGS}}}\right)/D^2 \quad (15)$$

$$r_{\mathrm{SR2}} = \frac{k_{\mathrm{SR2}}}{p_{\mathrm{H_2}}^{3.5}}\left(p_{\mathrm{CH_4}} \cdot p_{\mathrm{H_2O}}^{2} - \frac{p_{\mathrm{H_2}}^{4} \cdot p_{\mathrm{CO_2}}}{K_{\mathrm{SR1}} \cdot K_{\mathrm{WGS}}}\right)/D^2 \quad (16)$$

$$D = 1 + K_{\mathrm{CO}} \cdot p_{\mathrm{CO}} + K_{\mathrm{H_2}} \cdot p_{\mathrm{H_2}} + K_{\mathrm{CH_4}} \cdot p_{\mathrm{CH_4}} + K_{\mathrm{H_2O}} \frac{p_{\mathrm{H_2O}}}{p_{\mathrm{H_2}}} \quad (17)$$

where r stands for the rate of reaction in kmol/(kg_{cat}hr) and k denotes the rate coefficient. The units of k_{SR1} and k_{SR2} are kmol·$bar^{0.5}$/(kg_{cat}hr) and unit of k_{WGS} is kmol/(kg_{cat}hrbar). K_{CH4}, K_{CO} and K_{H2} are the apparent adsorption constants for CH_4, CO and H_2 in bar^{-1}, and K_{H2O} is the apparent dissociative adsorption constant of H_2O (dimensionless). As before, p is the partial pressure of component in bar, and D, defined in Equation (13), stands for the denominator of Equations (14-16). Since the three reactions are assumed to take place on the same active sites of the primary reformer catalyst, the above mentioned three rate equations have the same denominator [70].

Reaction rates for the formation of CO and CO_2 and for the disappearance of methane and water in steam reforming reactions (1) and (2) are getting from [58-59, 70]:

$$r_{\mathrm{CO}} = r_{\mathrm{SR1}} - r_{\mathrm{WGS}} \quad (18)$$

$$r_{\mathrm{CO_2}} = r_{\mathrm{WGS}} + r_{\mathrm{SR2}} \quad (19)$$

$$r_{\mathrm{CH_4}} = r_{\mathrm{SR1}} + r_{\mathrm{SR2}} \quad (20)$$

$$r_{\mathrm{H_2O}} = r_{\mathrm{SR1}} + r_{\mathrm{WGS}} + r_{\mathrm{SR2}} \quad (21)$$

Reaction rates for CO_2 disappearance and for CO and CH_4 formation in the reverse of the water–gas shift reaction and methanation (CO_2 and H_2 as feed) are obtained from [58-59, 70]:

$$r'_{\mathrm{CO}} = -(r_{\mathrm{SR1}} - r_{\mathrm{WGS}}) \quad (22)$$

$$r'_{\mathrm{CO_2}} = -(r_{\mathrm{WGS}} + r_{\mathrm{SR2}}) \quad (23)$$

$$r'_{\mathrm{CH_4}} = -(r_{\mathrm{SR1}} + r_{\mathrm{SR2}}) \tag{24}$$

$$r'_{\mathrm{H_2O}} = -(r_{\mathrm{SR1}} + r_{\mathrm{WGS}} + r_{\mathrm{SR2}}) \tag{25}$$

The WGS reaction is assumed to reach equilibrium in steam reformer catalyst filled tubes, but SR1 and SR2 reactions do not. However, an allowance can be made for the deviation from equilibrium by a „temperature approach to equilibrium (ATE)“, and thus at given outlet temperature both K_{SR1} and K_{WGS} are known. The temperature approach to equilibrium at the exit of a catalyst bed is the difference between the gas temperature at the exit of the catalyst bed and the equilibrium temperature that corresponds to the exit gas composition, specifically to the methane slip [60]. This value can be used as a good measure of the performance of the catalyst bed when the reactor operating temperature is held constant and when the reaction is equilibrium–limited, such as with primary and secondary reformers. The above rate equations cannot be used when the concentration of hydrogen is zero because the calculated reaction rates become infinite in that case. Hence, the presence of hydrogen is necessary for these equations be applicable. From the technical point of view, the feedstock material must not be hydrogen–free; hydrogen will reduce nickel oxide within the packed catalyst to metallic nickel, which is necessary to maintain the appropriate level of catalyst activity within the primary reformer. Therefore, the appearance of the partial pressure of hydrogen, p_{H2}, in the denominator of Equation (17) would not cause any practical modelling problems.

For the catalyst tubes of a fixed–bed catalytic reactor under consideration, an extensive amount of physical–chemical data is needed for precise modelling and simulation. The heart of this data is related to the catalyst pellets, namely the intrinsic kinetics and diffusional resistances. However, other data are also needed, including physical properties of the gas mixture and the heat–transfer coefficients. The fact that the composition and temperature of the mixture changes with the progress of the reaction is important for modelling. Therefore, the physical data should be updated along the reformer catalyst tubes in order to achieve an accurate simulation of the reactor. The relevant temperature range is from 600 K to 1310 K for a nickel catalyst applied either to $MgAl_2O_4$ or $CaAl_{12}O_{19}$ support [58-59, 70-75]. Therefore, the calculations inside of the model were limited to that range only to make the model control performance convergence faster. A kinetic rate coefficient is given by Arrhenius–type equation:

$$k_{\mathrm{i}} = A_{\mathrm{i}} \exp\left[-\frac{E_{\mathrm{i}}}{RT}\right] \tag{26}$$

where A_i is the pre–exponential factor, E_i is the activation energy in kJ/mol, R is gas constant in kJ/kmolK, and T is the temperature in K.

Apparent adsorption equilibrium constants are given by:

$$K_j = B_j \exp\left[-\frac{\Delta H_j}{RT}\right] \tag{27}$$

where B_j is the pre-exponential factor and ΔH_j is enthalpy change of adsorption.

For a nickel catalyst on either $MgAl_2O_4$ or $CaAl_{12}O_{19}$ support, the activation energies E_i, are shown in Table 4, pre-exponential factors A_i, are shown in Table 5, absorption enthalpy changes ΔH_j are shown in Table 6 and pre–exponential factors B_j are shown in Table 7 [58-59, 70-75].

Mass balances equations for the reformer catalyst tubes within primary reformer furnace are [73-75]:

$$\frac{dX_{CH_4}}{dl} = A\rho_B\eta_{CH_4}\frac{r_{CH_4}}{F_{CH_4}} \tag{28}$$

$$\frac{dX_{H_2O}}{dl} = A\rho_B\eta_{H_2O}\frac{r_{H_2O}}{F_{H_2O}} \tag{29}$$

where X_{CH4} and X_{H2O} are conversions of CH_4 and H_2O, respectively, given by

$$X_{CH_4} = \frac{F_{CH_4 in} - F_{CH_4 out}}{F_{CH_4 in}} \tag{30}$$

$$X_{H_2O} = \frac{F_{H_2O in} - F_{H_2O out}}{F_{H_2O in}} \tag{31}$$

η_{CH4} and η_{H2O} are effectiveness factors [58-59, 72-75], while F_{CH4in}, $F_{CH4iout}$, F_{H2Oin} and F_{H2Oout} are the molar flow rate of the CH_4 and H_2O at the inlet and outlet of the primary reformer tubes, respectively, in kmol/h [74-75]. l is the distance along the reactor tube in m, A is the reformer tube cross sectional area in m^2, ρ_B is the catalyst bed density in kg/m^3.

Table 4. Parameters for the activation energies E_i used in the model [58-59, 70-75].

Reaction	E_i [kJ/mol]
SR1	240,10
SR2	67,13
WGS	243,90

Table 5. Parameters for the pre-exponential factors A_i used in the model [58-59, 70-75].

Pre-exponential factor	Reactions		
	SR1	SR2	WGS
A_i [kmol·bar$^{0.5}$/(kg$_{cat}$hr)]	$4{,}225\times10^{15}$	-	-
A_i [kmol·bar$^{0.5}$/(kg$_{cat}$hr)]	-	$1{,}020\times10^{15}$	-
A_i [kmol/(bar·kg$_{cat}$hr]	-	-	$1{,}955\times10^{6}$

Table 6. Parameters for the absorption enthalpy changes ΔH_j used in the model [58-59, 70-75].

Species	H_2O	CH_4	CO	H_2
ΔH_i [kJ/mol]	88,68	-38,28	-70,61	-82,90

Table 7. Parameters for the pre–exponential factors B_j used in the model [58-59, 70-75].

Species	H_2O	CH_4	CO	H_2
B_i [-]	$1{,}77\times10^{5}$	-	-	-
B_i [bar-1]	-	$6{,}65\times10^{-4}$	$8{,}23\times10^{-5}$	$6{,}12\text{x}10^{-9}$

In the heterogeneous reaction (as in SR1, SR2 and WGS are given in Table 2), the actual reaction rate is affected by the molecular diffusion into the micropore inside the catalyst. Therefore, the effectiveness factor should be considered in order to apply the kinetic equations to the industrial reactor design. The effectiveness factor can be estimated using the following equation as proposed by Xu and Froment [58-59]:

$$\eta_k = \left(\frac{1}{\phi_k}\right)\left(\left(\frac{1}{\tanh\,(3\phi_k)}\right) - \left(\frac{1}{3\phi_k}\right)\right) \tag{32}$$

where η_k is the reaction effectiveness factor for reaction k (dimensionless unit) and the ϕ is the Thiele modules (dimensionless unit).

If the catalyst pellet is a spherical, the Thiele modulus can be defined by the following equation with a characteristic length, $D_s/6$, as noted by previous researchers including Rostrup-Nielsen [57] and Xu and Froment [58-59]:

$$\phi_k = \frac{D_s}{6}\sqrt{\frac{k_{vk}\cdot\rho_b(1+K_{e,k})}{K_{e,k}\cdot D_{e,k}}} \tag{33}$$

where D_s is the equivalent pellet diameter in m, k_{vk} is the volumetric kinetic constant for reaction k (to convert the unit of constant of reaction rate) given in $m^3/kg_{cat}h$, ρ_B is the bulk density in kg/m^3, $K_{e,k}$ is the apparent adsorption equilibrium constant, and D_{KA} is the Knudsen diffusivity, in m^2/s.

The equivalent pellet diameter is defined as the diameter of a sphere with the same external surface area per unit volume of the catalyst pellet, given by:

$$D_s = 6\cdot\frac{(1-\epsilon_B)}{S_B} \tag{34}$$

where S_B is the specific surface area of the catalyst bed in m^3/m^2, while ϵ_B is the porosity of packed catalyst bed in m^3_{void}/m^3_{cat}.

Effective diffusivity is adjusted to account for the nature of the primary reformer catalyst pores using the catalyst pellet porosity and pore tortuosity [77]. Diffusion coefficients are dependent on both molecular and Knudsen diffusivity. The Knudsen diffusivity, D_{KA}, in m^2/s is given by [77]:

$$D_{KA} = \frac{d_{pore}}{3}\cdot\sqrt{\frac{8RT}{\pi M}} \tag{35}$$

where d_{pore} is the average pore radius of the primary reformer catalyst in m, M is the molar mass of the process gas in kg/kmol.

The molecular diffusivity for process gas is given by [78]:

$$D_{\mathrm{i,j}} = \frac{Z \cdot T^{1.5} \sqrt{1/M_{\mathrm{i}} + 1/M_{\mathrm{j}}}}{p \sigma_{\mathrm{ij}}^2 \Omega} \tag{36}$$

where D_{ij} is in m^2/h, Z is an empirical coefficient equal to $1{,}859 \times 10^{-3}$ in $atm \cdot Å^2 \cdot cm^2(kg/kmol)^{1/2}/(K^{3/2}s)$, M_{i} and M_{j} denote the molecular weight of component *i* and *j*, respectively, in kg/kmol, p is the total pressure in atm, Ω is a dimensionless temperature dependent collision integral equal to 1 in the presented model and $\sigma_{\mathrm{i,j}}$ is the average collision diameter in Å, given by [78]:

$$\sigma_{\mathrm{i,j}} = \frac{\sigma_{\mathrm{i}} + \sigma_{\mathrm{j}}}{2} \tag{37}$$

A simple, non-isothermal model that takes into consideration the temperature variation along of the reformer tube is used for the description of energy balance of the reformer tube element, assuming a constant tube wall temperature of the reformer tubes [75]:

$$\frac{dT}{dl} = \frac{A \rho_{\mathrm{B}} \left[\sum_{i=1}^{3} \eta_i r_{\mathrm{i}} (-\Delta H_{\mathrm{i}})\right] + U \pi d_{\mathrm{e}} \cdot (T_{\mathrm{wtt}} - T)}{\sum_{i=1}^{5} F_{\mathrm{i}} C_{\mathrm{p,i}}} \tag{38}$$

where U is the heat transfer coefficient in $kJ/(m^2hK)$, d_{e} is the external reformer tube diameter in m, T_{wtt} is the reformer tube wall temperature in K and $C_{\mathrm{p,i}}$ is the specific heat of components *i* = CH_4, H_2O, H_2, CO and CO_2 at operating temperature range expressed in kJ/(kmolK).

Heat transfer coefficient U between the catalyst reformer tubes and their surroundings is given by the equation [74-75]:

$$\frac{1}{U} = \frac{d_{\mathrm{i}}}{2\lambda_{\mathrm{st}}} \ln\left(\frac{d_{\mathrm{e}}}{d_{\mathrm{i}}}\right) + \frac{1}{\alpha} \tag{39}$$

where d_{i} and d_{e} are the internal and external reformer tube diameter, respectively, in m, λ_{st} is the thermal conductivity of the reformer tube metal in $kJ/(m^2hK)$, and α is the convective heat transfer coefficient in the packed bed in $kJ/(m^2hK)$. Convective heat transfer coefficient α in the packed bed is obtained from the correlation of Leva *et al.* by the following equation [76]:

$$\alpha = \frac{\lambda_g \cdot 0{,}813\left(\frac{d_p \cdot G}{\mu}\right)^{0.9} \exp\left(-\frac{6 d_p}{d_i}\right)}{d_i} \quad (40)$$

where λ_g is the process gas thermal conductivity in kJ/(m^{2}hK), d_p is the (equivalent spherical) catalyst particle diameter in m, G is the mass velocity of the process gas at the inlet of the reformer tubes in kg/(m^{2}h), μ is the viscosity of the process gas in Pas.

The differential equation for the pressure drop across the differential element is modelled by the Ergun equation [77-78]:

$$\frac{dp}{dl} = \frac{\rho v^2}{d_p} \cdot \frac{1-\epsilon}{\epsilon} \cdot \left[\frac{150 \cdot (1-\epsilon)}{\mathrm{Re}} + 1{,}75\right] \quad (41)$$

where p is the pressure in bar, ρ is the density of the fluid in kg/m^3, v is the velocity of the fluid in m/s, d_p is the (equivalent spherical) catalyst particle diameter in m, ϵ is the void fraction of the primary reformer catalyst, and Re is the particle Reynolds number.

In the model, the state variables are the molar flow rates of each species i ($\dot{n}_i$) in kmol/h and temperature T in K. Process gas, the mass balance equation for species i is:

$$\frac{d}{dt}(C_i) = -\frac{1}{A}\frac{d}{dl}(\dot{n}_i) + \sum_{rxnsj} \nu_{i,j} r_j \qquad i = \{CH_4, H_2O, H_2, CO, CO_2\} \quad (42)$$

and the energy balance is:

$$\frac{d}{dt}(C_v T \sum_i C_i) == -\frac{1}{A}\frac{d}{dl}(C_p T \sum_i \dot{n}_ı) + \frac{(2h_c)}{d_i}(T_{wtt} - T_{wg}) \sum_{rxnsj} r_j \Delta H_j \quad (43)$$

where C_i is the molar concentration of species i in kmol/L, A is the cross–sectional area of a process tube in m^2, $\nu_{i,j}$ is the stoichiometric coefficient of species i in reaction j, C_v is the molar heat capacity at constant volume in kJ/kgK, C_p is the molar heat capacity at constant pressure in kJ/kgK, h_c is the heat-transfer coefficient in kJ/kg, d_i is the inner tube radius in m, r_j is reaction j, T_{wtt} is the tube wall temperature, T_{wg} is the temperature of the waste gas in K, l is reformer tube heated length in m and ΔH_j is the enthalpy of reaction j in kJ/kmol.

The heat capacities are functions of C_i, which are functions of T and $\dot{n}_i$:

$$C_{\mathrm{i}} = f_1\left(\dot{n}_{\mathrm{CH_4}}, \dots, \dot{n}_{\mathrm{CO_2}}, T\right) \qquad i = \{CH_4, H_2O, H_2, CO, CO_2\} \tag{44}$$

$$C_{\mathrm{v}} = f_2\left(\dot{n}_{\mathrm{CH_4}}, \dots, \dot{n}_{\mathrm{CO_2}}, T\right) \tag{45}$$

$$C_{\mathrm{p}} = f_2\left(\dot{n}_{\mathrm{CH_4}}, \dots, \dot{n}_{\mathrm{CO_2}}, T\right) \tag{46}$$

These functions are used in Equations (42) and (43).

From the mentioned it can be concluded that the behavior of the steam methane reformer is dominated by convective and radiative transfer generated through combustion in reformer furnace box, reaction kinetics and the bulk motion of the reformed gas. Key variables are the methane slip and the outlet temperature of the reformed gas as the most reliable process indicators. The unique manipulated variable is the fuel flow rate for appropriate control of the waste gas temperature. The input process variables – the natural gas volume flow, steam mass flow and the temperature of their mixed flow are measurable variables, but normally are not manipulated. The control strategy of air–to–fuel ratio was used for keeping the combustion temperature and oxygen concentration in the waste gas of the reformer furnace at a constant value.

In practical operation reformer tubes wall temperature is not set directly because of difficulties with reliable and accurate measurement. Thus, it is proposed that the optimal reformer tube wall temperature can be achieved by adjusting the combustion conditions through air–to–fuel ratio control. As an assumption in the model, reformer tubes wall temperature can be controlled by keeping appropriate air–to–-fuel ratio additionally trimmed by the oxygen concentration in the waste gas measured at different locations inside of the reformer box.

4.1.1.3.Secondary reforming unit

In the secondary reforming unit the effluent from the primary reformer tubes is combined with the preheated mixture (490^{o}C) of air and MP steam, before entering the secondary reformer burner which is located over nickel catalyst to ensure a 3:1 molar mixture of H_2 and N_2. The

secondary reformer unit comprises two zones, namely combustion and catalyst zone. The schematic diagram of the secondary reformer is given in Figure 4.

The following homogeneous (non–catalytic), exothermic, irreversible reaction takes place in the combustion zone which is modelled as conversion reactor:

$$CH_4 + 2O_2 \rightarrow CO_2 + 2H_2O \tag{47}$$

The above reaction follows reaction rate given by Wolf *et al*. [79]:

$$-r_{CH_4} = \frac{k_3 \exp\left(\frac{-E_3}{RT}\right) \cdot p_{CH_4} p_{O_2}}{\left(1 + K_{CH_4} p_{CH_4} + K_{O_2} p_{O_2} + K_{CO_2} p_{CO_2} + K_{H_2O} p_{H_2O}\right)^2} \tag{48}$$

The reaction rate r is in kmol/m^{3}s, p stands for the partial pressures (in kPa) and T is the temperature (in K), R is the universal gas constant (in kJ/kmolK), with E_3 = 32000 kJ/kmol and k_3 = 1000 kJ/kmol, respectively.

According to Wolf *et al*. [79] kinetic parameters are defined as:

$$K_{CH_4} = 1{,}1 \text{x} 10^{-6} \left(\frac{-E_{CH_4}}{RT}\right) \tag{49}$$

$$K_{O_2} = 1{,}1 \text{x} 10^{-2} \left(\frac{-E_{O_2}}{RT}\right) \tag{50}$$

$$K_{CO_2} = 1{,}5 \text{x} 10^{-4} \left(\frac{-E_{CO_2}}{RT}\right) \tag{51}$$

$$K_{H_2O} = 5{,}3 \left(\frac{-E_{H_2O}}{RT}\right) \tag{52}$$

Activation energies are as follows: E_{CH_4}=32200 kJ/kmol, E_{O_2}=28400 kJ/kmol, E_{CO_2}=32900 kJ/kmol, E_{O_2}=27300 kJ/kmol.

An input–output model of the combustion zone based on mass and energy balance was used, based on an assumption that the primary reformer effluent feedstock and air/steam feed to the burner are completely mixed along the flame. Besides that, in conversion reactor complete

oxygen consumption is considered, with the assumption that the conditions inside and outside of the combustion zone are equal.

For the combustion zone, the molar balance according to Figure 4 can be derived as follows [80]:

for argon:

$$F_{\mathrm{IN},1} + F_{\mathrm{IN},2} = F_{\mathrm{OUT}} \tag{53}$$

for nitrogen:

$$F_{\mathrm{IN},1}x2 + F_{\mathrm{IN},2}x2 = F_{\mathrm{OUT}}x2 \tag{54}$$

for carbon:

$$F_{\mathrm{IN}(CH_4),1} + F_{\mathrm{IN}(CO),1} + F_{\mathrm{IN}(CO_2),1} + F_{\mathrm{IN}(CO_2),2} = F_{\mathrm{OUT}(CH_4)} + F_{\mathrm{OUT}(CO)} + F_{\mathrm{OUT}(CO_2)} \tag{55}$$

for hydrogen:

$$F_{\mathrm{IN}(CH_4),1}x4 + F_{\mathrm{IN}(H_2O),1}x2 + F_{\mathrm{IN}(H_2),1}x2 + F_{\mathrm{IN}(H_2O),2}x2 = F_{\mathrm{OUT}(CH_4)}x4 + F_{\mathrm{OUT}(H_2O)}x2 + F_{\mathrm{OUT}(H_2)}x2 \tag{56}$$

for oxygen:

$$F_{\mathrm{IN}(H_2O),1} + F_{\mathrm{IN}(CO),1} + F_{\mathrm{IN}(CO_2),1}x2 + F_{\mathrm{IN}(O_2),2}x2 + F_{\mathrm{IN}(H_2O),2} + F_{\mathrm{IN}(CO_2),2}x2 = F_{\mathrm{OUT}(H_2O)} + F_{\mathrm{OUT}(CO)} + F_{\mathrm{OUT}(CO_2)}x2 \tag{57}$$

and

overall molar balance:

$$F_{\text{tot}} = F_{\text{OUT}(\text{CH}_4)} + F_{\text{OUT}(\text{H}_2\text{O})} + F_{\text{OUT}(\text{H}_2)} + F_{\text{OUT}(\text{CO})} + F_{\text{OUT}(\text{CO}_2)} + F_{\text{OUT}(\text{N}_2)} + F_{\text{OUT}(\text{Ar})} \quad (58)$$

where $F_{\text{IN},1}$ is the molar flow rate of inlet process gases in the stream number 1 in kmol/h, $F_{\text{IN},2}$ is the molar flow rate of inlet air/steam in the stream number 2 in kmol/h, F_{OUT} is the molar flow rate of each gas from the combustion zone in kmol/h, F_{tot} is the total molar flow rate of outlet gases from the combustion zone in kmol/h.

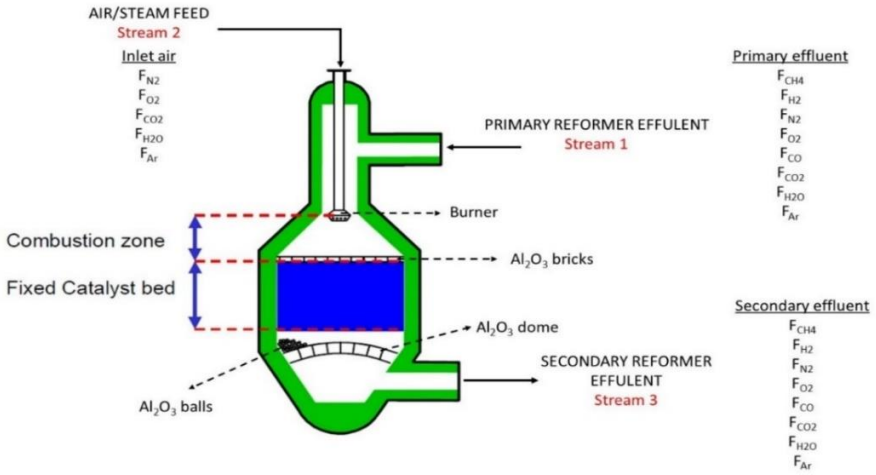

Figure 4. Schematic diagram of the secondary reformer.

The secondary reformer combustion zone is operated close to adiabatic conditions, and hence, the temperature is given by the adiabatic heat balance. Adiabatic flame temperature can be described by the following equation:

$$\Delta H = \sum_{\text{OUT}} F_{\text{i}} \cdot H_{\text{i}} - \sum_{\text{IN}} F_{\text{i}} \cdot H_{\text{i}} = 0 \quad (59)$$

where, ΔH is the enthalpy change in kJ/kmol, F_{i} is the molar flow rate of the *i*-component in kmol/h, and H_{i} is the specific enthalpy of the *i*-component in kJ/kmol.

The product gas of the combustion zone is directed to the catalytic zone of the secondary reformer unit. The catalytic zone is modelled as adiabatic PFR, followed by heterogeneous endothermic reversible reactions (SR1, SR2 and WGS) given in Table 2. Everything stated for the primary reformer tubes and related catalyst was applied during the modelling procedure of the secondary reformer unit catalytic zone.

The secondary reformer unit is a refractory lined water jacketed vessel containing 38,5 m^3 of catalyst. The top 6,7 m^3 of catalyst is a nickel catalyst resistant to withstand the high

temperature in this part of the reactor. The chemical content of the nickel is 9,0% and the balance is $CaAl_{12}O_{19}$ support resistant to temperature over 1600°C. The remaining 31,8 m^3 of catalyst is a high activity nickel reforming catalyst with the nickel content is also 9,0%, and the balance is Al_2O_3. The shape of the catalysts is the Rashig ring with 8 holes. Both catalysts have an approximate charged bulk density of 1,0 kg/L. All other data necessary for the modelling are the same as was with the primary reforming catalyst. The top bed of catalyst is protected against direct flame impingement from the air burner by a 75 mm layer high alumina spheres with 25 mm in diameter.

Downstream of the secondary reformer is located three heat exchangers which reduces the effluent temperature of approx. 980°C to 352°C before the next process step. This three heat exchangers generate high pressure steam (125 bar and 358°C), providing a revenue source in the amount of 76,4 MW.

4.1.2. Synthesis gas purification model

The major drawback of the synthesis gas generation unit (purification and SMR units) is generation of significant amounts of CO (approx. 935 kmol/h or approx. 12,34 mol.% and per dry basis) and CO_2 (approx. 608 kmol/h or approx. 8,00 mol.% and per dry basis), which poisons the ammonia synthesis catalyst. To resolve this issue synthesis gas purification model was set up. This part of the model consists of four process steps, namely high and low temperature water gas shift units, CO_2 washing unit (in the reference ammonia plant this is Benfield unit) and methanation unit. The steady–state flowsheet of the synthesis gas purification model build in UniSim Design R470 is shown in Figure 5.

From the secondary waste heat boiler 102–C, the synthesis gas passes to the WGS conversion units going first to the high temperature (HT) WGS converter 104–D1. The inlet temperature of the synthesis gas to 104–D1 are controlled by the control valve TV–124 and design inlet temperature being 371°C. The synthesis gas passes down through a bed of promoted iron catalyst in which the bulk of the CO in the synthesis gas is converted to CO_2 and H_2 in the presence of steam. The effluent gas from 104–D1 containing about 3,18 mol.% of CO per dry basis (inlet value is about 13 mol.% per dry basis) goes to the shift effluent waste heat boiler 103–C. The process gas enters the tube side of this exchanger at a temperature of about 432°C and in generating steam at 125 bars is cooled to about 340°C. From 103–C the process gas is cooled to about 235°C by exchanging with methanator feed in the methanator feed heater 104–C. The synthesis gas is next cooled against water in the low temperature (LT) converter inlet

trim cooler 112–C. This cooler is provided to give fine control over the inlet temperature to the LT WGS converter. The process gas outlet temperature from 112–C is controlled by control valve TV–149 which throttles the boiler feed water flow to 112–C.

The effluent gas from 112–C goes to the last stage of shift conversion in the LT WGS converter 104–D2. The catalyst in this vessel is a complex of copper oxide, zinc oxide and alumina, and the CO content of the synthesis gas is reduced to 0,2 mol.% on a dry gas basis. The outlet temperature of this reactor is about 221^{o}C.

The effluent line from 104–D2 goes to two CO_2 reboiler shift effluent coolers 105–CA and CB. These two exchangers are in parallel and cool the LT WGS effluent gas, by providing heat for the CO_2 washing unit. Upstream of the 105–C's, the shift effluent gas is quenched to its dew point, which is about 177^{o}C during normal operation. From the 105–C's the shift effluent gas with condensed steam goes to the raw gas separator 102–F, where disengagement of the gas and condensate takes place. Disengaged synthesis gas passes from the top of 102–F to the next processing stage, which is CO_2 washing unit.

Removal of CO_2 from the raw synthesis gas is accomplished by absorption using an activated solution of K_2CO_3 (Benfield solution). The activator is diethanolamine (DEA) and solution also contains V_2O_5 as a corrosion inhibitor. The raw synthesis gas from 102–F flows in the bottom of the CO_2 absorber 101–E and flows upwards through six trays filled with rings. As the gas flows up the absorber, it continuously contacts Benfield solution which progressively absorbs the CO_2. The process gas leaves the CO_2 absorber and contain up to 0,05 mol.% of CO_2 per dry basis. The inlet gas contains about 18,40 mol.% per dry basis of CO_2. Benfield solution enters 101–E at two levels as partially regenerated or semi–lean solution and as completely regenerated or lean solution. The semi–lean solution enters the middle of absorber with temperature of 115^{o}C and removes the bulk of the CO_2. The lean solution enters at the top of the absorber with the temperature of 70^{o}C and removes the remaining CO_2 from the process gas. After absorption stage "rich" Benfield solution from the bottom of the absorber passes through a hydraulic turbine and enters the top of the CO_2 stripper. The CO_2 from the "rich" solution is stripped or flashed and with temperature at 96^{o}C leaves the top of the CO_2 stripper and goes to the CO_2 stripper condenser 110–C. The cooled CO_2 at 40^{o}C, together with condensed water flows to the CO_2 knock-out drum 113–F where the water disengages, while CO_2 is vented or consuming from the *e.g.* urea plant. Process gas from the top of the CO_2 absorber 101–E passes to the CO_2 absorber knock-out drum 103–F where any entrained Benfield solution is disengaged. From the 103–F the process gas flows to the synthesis gas compressor inter-stage methanator feed exchanger 136–C. Leaving the 136–C, the process gas

is further heated in the methanator feed heater 104–C, by shift effluent. From 104–C the process gas passes to the methanator 106–D to be finally purified from CO and CO_2. The preheated synthesis gas enters the top inlet of the methanator 106–D. It passes down through a bed of high nickel catalyst where remaining carbon oxides react with H_2 to form CH_4 and H_2O. The inlet CO concentration is about 0,24 mol.% and the CO_2 is 0,05 mol.% on a dry basis. At the exit of the methanator the combined concentration of oxides of carbon is almost zero. Purified synthesis gas flows from the methanator through heat exchangers 114–C (boiler feed water heater), 168–C (boiler feed water heater) and 115–C (cooling water) and cools down to 33^{o}C before entering the synthesis gas compressor suction drum 104–F. In this vessel, water formed in methanation reaction is disengaged and pressured to the condensate stripper.

4.1.2.1.Water–gas shift (WGS) conversion unit

The principal task of the WGS conversion reactors is to carry out the WGS reaction from Table 2, reducing the CO fraction from the secondary reformer effluent and increasing the H_2 yield. The WGS reaction is heterogenous, exothermic and reversible one. According to this ,the WGS conversion unit was modelled as an adiabatic equilibrium reactor. As it was mentioned the WGS reaction is performed in a series of HT WGS followed by LT WGS based reactors with intercooling stage to increase the overall conversion and to achieve high purity hydrogen. The HT WGS reactor uses an iron oxide–chromium oxide based catalyst (88% Fe_2O_3, 9% Cr_2O_3, 3% CuO) with the inlet temperature of 371^{o}C, while the LT WGS reactor uses a copper-zinc based catalyst (59% CuO, 31% ZnO, 9% Al_2O_3 and 1% Cs) with the inlet temperature of 221^{o}C. Both WGS catalysts have a pellet form with the following dimensions: HT pellet has a diameter of 5,4 mm and a length of 3,6 mm, while LT pellet has a diameter of 5,0 mm and a length of 3,0 mm. The bulk density for HT catalyst is 1220 kg/m^3, and the same for the LT catalyst is 1140 kg/m^3. The overall volume of the catalysts is 80,6 m^3 for the HT WGS and 108,8 m^3 for the LT WGS.

According to the Arrhenius law of kinetics, increasing the temperature increases the reaction rate. On the other side, the Le Châtelier principle states that increasing the temperature of an exothermic reaction shifts the reaction to reactants side, decreasing its equilibrium conversion. Therefore, the WGS reaction is a balance between these two effects and the reactor optimal operational point considers the trade-off between kinetics and equilibrium driving forces. Chen *et al*. [81] demonstrated by experimental data that increasing temperature in HT WGS reactor will promote the performance of WGS reaction.

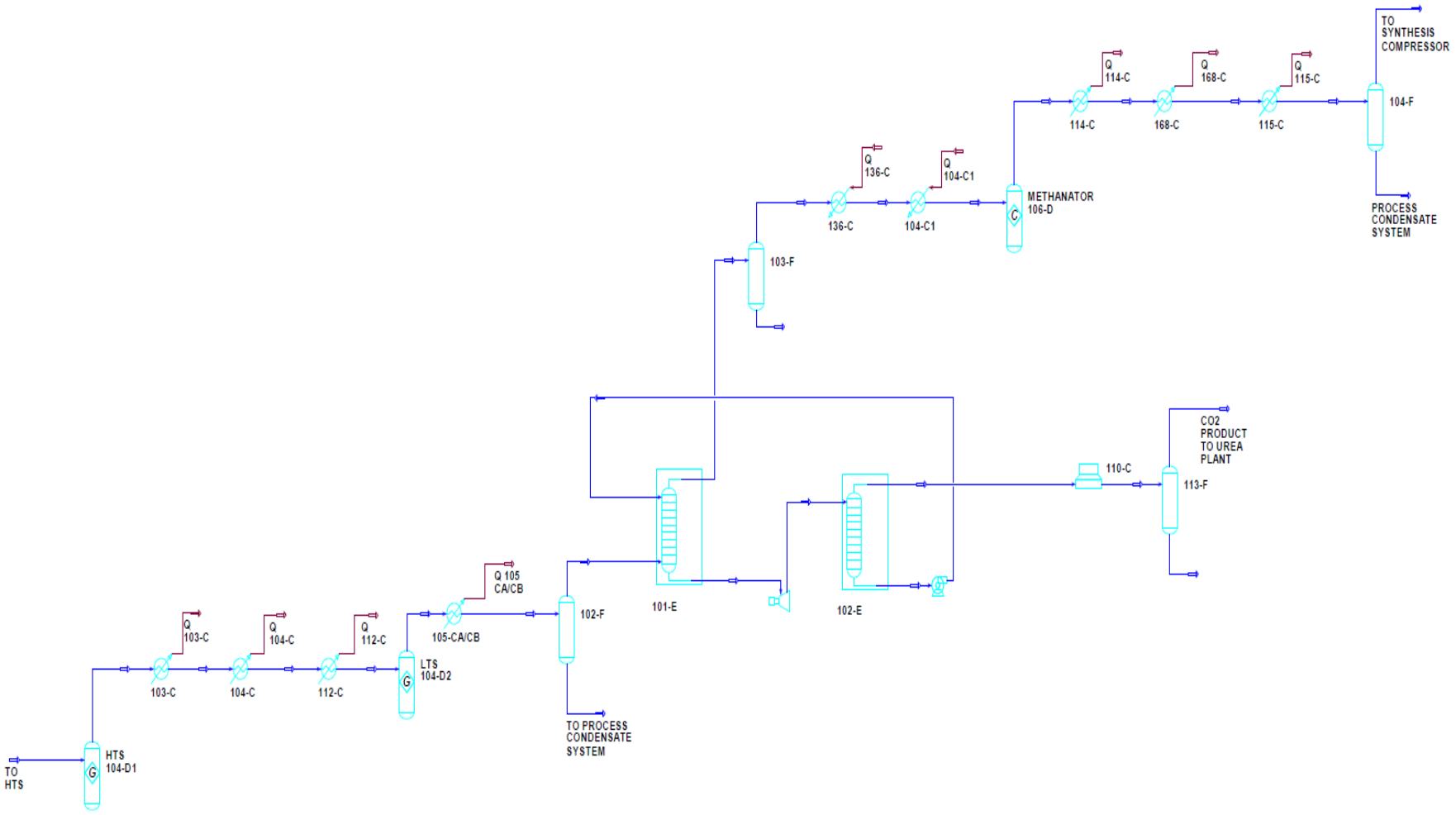

Figure 5. Synthesis gas purification steady–state flowsheet.

For the LT WGS reactor, the reaction is not excited if the reaction is below 200ºC. Once the temperature reaches 200ºC the reaction occurs, but the CO conversion decreases with increasing temperature. This reveals that the WGS reactions with the HT WGS and the LT WGS reactors are governed by chemical kinetics and thermodynamic equilibrium, respectively in industrial conditions.

Smith *et al*. [82] classifies the reaction kinetic models in microkinetic approach and the empirical method. Basically, the micro kinetic approach explores the detailed chemistry of the reaction. The empirical models are based on the experimental results and are typically expressed in the Arrhenius model and provide an easy and computationally lighter way to predict the rate of reaction. The major disadvantage is the fact that the adjusted model cannot be extrapolated to different composition and types of catalysts. Many empirical expressions have been reported in literature for HT WGS and LT WGS according to Newsome [83] and Smith *et al*. [82]. An empirical rate expression successfully used to describe the WGS reaction in HT and LT WGS catalysts is a power law type [83]:

$$r = k_0 exp\left(-\frac{E_a}{RT}\right) p_{CO}^{l} p_{H_2O}^{m} p_{CO_2}^{n} p_{H_2}^{q} \left(1 - \frac{p_{co_2} p_{H_2}}{K_{eq} p_{CO} p_{H_2O}}\right) \quad (60)$$

where r is the reaction rate in kmol/(kg_{cat}hr), k_0 is the pre-exponential factor, E_a is the activation energy in kJ/mol, p denotes partial pressure of each species in reaction mixture in atm, R is the universal gas constant in kJ/kmolK, T is the thermodynamic temperature in K, l, m, n, and q are estimated parameters by experimental data and K_{eq} is the reaction equilibrium constant.

The reaction equilibrium constant K_{eq} is derived from thermodynamics as a function of temperature and the same is given by Smith *et al*. [82]:

$$\ln\left(K_{eq}\right) = \frac{5693,5}{T} + 1,077\ln(T) + 5,44x10^{-4}T - 1,125x10^{-7}T^2 - \frac{49170}{T^2} - 13,148 \quad (61)$$

Values for k_0, E_a, l, m, n, and q are given in Table 8 and the same are characteristic experimental parameters for the HT and LT WGS catalysts used in the model:

Table 8. Characteristic experimental parameters for HT and LT WGS catalysts used in the model.

WGS catalyst	Arrhenius parameters		Order of reaction				Reference
	k_0	E_a (kJ/mol)	l	m	n	q	
HT	2,693	79797.77	0,74	0,47	-0,18	0.0	[84]
LT	2,533	47,40	1	1	-	-	[85]

The differential molar balance simplified to a fixed bed reactor can be expressed with the following equation given by Froment *et al*. [86]:

$$\frac{dX_a}{dW} = \frac{r_a}{F_{a0}} \tag{62}$$

where X_a is the component conversion in mol. %, W is the catalyst weight in kg, r_a is the rate of reaction of component a, F_{a0} is the molar feed rate of the component a in kmol/h, and F_a is the molar flow of component a leaving the reactor in kmol/h.

The ideal model assumes that concentration and temperature gradients only occur in the axial direction. The only transport mechanism operating in this direction is the overall flow itself, and is considered being of the plug flow type. In case of a reactor bed with a fixed cross-sectional area (S), the differential molar balance can be rewritten as a function of the reactor differential length as can be seen in the following equation:

$$\frac{dX_a}{dz} = \frac{r_a \cdot \rho_B \cdot S}{F_{a0}} \tag{63}$$

where ρ_B is the catalyst bulk density in kg/m^3, S is the reactor bed constant section area in m^2 and z is the length of reactor (z axis – axial direaction).

The differential equation of energy conservation may be written as the following equation:

$$\sum F_i \cdot c_{pi} \cdot \frac{dT}{dz} = (-\Delta H_r) \cdot r_a \cdot \rho_B \cdot S - 4\frac{U}{d_t} \cdot (T - T_R) \tag{64}$$

where ΔH_r is the enthalpy of reaction in kJ/mol, c_{pi} is the specific heat of component *i* in kJ/molK, F_i is the component i molar flow in kmol/h, *T* and T_R are the reactor temperature and temperature at radius in K, *R* of internal tube, d_t is the internal tube diameter in m, and *U* is the overall heat transfer coefficient in kJ/kg.

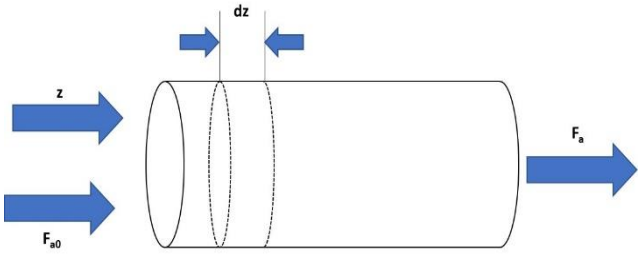

Figure 6. WGS reactor differential volume representation.

For an adiabatic reactor, *U* equals zero and equation (64) can be simplified to:

$$\sum F_i \cdot c_{pi} \cdot \frac{dT}{dz} = (-\Delta H_r) \cdot r_a \cdot \rho_B \cdot S \tag{65}$$

The differential pressure equation is defined according to the Ergun type equation:

$$-\frac{dp}{dz} = -f \cdot \frac{\rho_g \cdot u_s^2}{d_p} \tag{66}$$

where *p* is the reactor pressure in position *z* in atm, *f* is the friction factor, ρ_g is the gas density in kg/m^3, u_s is the superficial velocity in m/s and d_p is the particle diameter in mm.

Bed dimensions in the case of HT WGS catalyst are 5024 mm in diameter and 4070 mm in depth, while in the case of the LT WGS reactor the same dimensions are 5052 mm and 5430 mm, respectively.

4.1.2.2.CO_2 washing unit

The CO_2 washing unit (the Benfield CO_2 removal system) is a proprietary commercial process for CO_2 removal from gas streams of high CO_2 concentrations. The CO_2 in the raw synthesis gas is a poison to the ammonia synthesis catalyst and therefore must be removed from

the syngas stream before delivery to ammonia synthesis. Removal of the bulk of the CO_2 from the process gas is accomplished by absorption in counter–current flow of catalysed potassium carbonate (K_2CO_3) solution in the CO_2 absorber.

The following elementary reactions take place when CO_2 is absorbed in potassium carbonate and bicarbonate solution:

$$CO_2 + OH^- \rightarrow HCO_3^- \tag{67}$$

$$CO_2 + H_2O \rightarrow HCO_3^- + H^+ \tag{68}$$

$$HCO_3^- \rightarrow CO_3^{2-} + H^+ \tag{69}$$

$$H_2O \rightarrow OH^+ + H^+ \tag{70}$$

The overall stoichiometric reaction can be represented in the following reaction:

$$CO_2 + CO_3^{2-} + H_2O \rightarrow 2HCO_3^- \tag{71}$$

Reactions (68) and (70) are assumed to be always in equilibrium condition. The equilibrium constant of these reactions is available in the literature [87] and the same is expressed in a general form:

$$K_{\mathrm{i}} = exp\left(\frac{a_{\mathrm{i}}}{T} + b_{\mathrm{i}} lnT + c_{\mathrm{i}} T + d_{\mathrm{i}}\right) \tag{72}$$

According to this general form, the specific equilibrium constants for the equation (68) to (70) are:

$$K_{68} = \frac{C_{\mathrm{HCO_3^-}} \cdot C_{\mathrm{H^+}}}{C_{\mathrm{CO_{2,g}}}} = exp\left(-\frac{12{,}092.1}{T} - 36{,}7816 lnT + 231{,}4\right) \tag{73}$$

$$K_{69} = \frac{C_{\mathrm{CO_3^{2-}}} \cdot C_{\mathrm{H^+}}}{C_{\mathrm{HCO_3^-}}} = exp\left(-\frac{12431{,}7}{T} - 35{,}4819 lnT + 216{,}067\right) \tag{74}$$

$$K_{70} = K_{\mathrm{w}} = C_{\mathrm{H^+}} \cdot C_{\mathrm{OH^-}} = exp\left(-\frac{13445{,}9}{T} - 22{,}4773lnT + 132{,}932\right) \quad (75)$$

where C_i denotes molar concentration of component i in kmol/m^3 and T is the temperature in K. Subscripts 68 to 70 are referred to the Equations (67) to (70).

From equations (73) to (75), the concentration of OH^- ion and equilibrium concentration of CO_2 in liquid phase can be obtained as follows:

$$C_{\mathrm{CO_{2,e}}} = \frac{K_{69} \cdot C_{\mathrm{HCO_3^-}}^2}{K_{68} \cdot C_{\mathrm{CO_3^{2-}}}} \quad (76)$$

$$C_{\mathrm{OH^-}} = \frac{K_{\mathrm{w}} \cdot C_{\mathrm{CO_3^{2-}}}}{K_{69} \cdot C_{\mathrm{HCO_3^-}}} \quad (77)$$

where $C_{CO2,e}$ denotes equilibrium concentration in kmol/m^3.

Reaction (67) is the rate-controlling step for CO_2 absorption in hot K_2CO_3 solution. When the forward reaction is pseudo-first order and reverse reaction rate is constant, then the reaction rate can be expressed as follows [88-90]:

$$r_{\mathrm{OH}} = k_{1,\mathrm{OH}}\left(C_{\mathrm{CO_2}} - C_{\mathrm{CO_{2,e}}}\right) \quad (78)$$

$$k_{1,\mathrm{OH}} = k_{\mathrm{OH}} \cdot C_{\mathrm{OH^-}} \quad (79)$$

where r_{OH} denotes reaction rate of CO_2 with OH^- in kmol/m^{3}s, $k_{1,\,OH}$ is the overall pseudo–first order reaction rate constant in s^{-1}, and k_{OH} is second order reaction rate constant of the forward reaction with OH^- in m^3/kmols.

In Equation (79), k_{OH} is a second order reaction rate constant of the forward reaction and is obtained from the following correlation [91]:

$$k_{\mathrm{OH}} = 2{,}53x10^{11}e^{-4{,}311/T} \quad (80)$$

It is industry practice to add promoter to the carbonate-bicarbonate solution to increase the reaction rate. In the reference ammonia plant, diethanolamine (DEA) is used as a promotor. Reaction of CO_2 with DEA and their rate constants can be described with the following expressions [92-94]:

$$CO_2 + R_2NH \rightarrow R_2N^+HCOO^- \tag{81}$$

$$R_2NH_2^+ \rightarrow R_2NH + H^+ \tag{82}$$

$$K = \frac{C_{R_2NH} \cdot C_{H^+}}{C_{R_2NH_2^+}} = exp\left(-\frac{3071,15}{T} + 6,776904lnT - 48,7594\right) \tag{83}$$

$$R_2N^+HCOO^- + OH^- \rightarrow R_2NH + HCO_3^- \tag{84}$$

$$K = \frac{C_{R_2NH} \cdot C_{HCO_3^-}}{C_{R_2NHCOO^-} \cdot C_{OH^-}} = exp\left(-\frac{17067,2}{T} + 66,8007lnT - 439,709\right) \tag{85}$$

Reactions (81) and (82) are the controlling step for the reaction between CO_2 with promoter DEA. When the forward reaction is pseudo–first order and reverse reaction rate is constant, then the reaction rate can be expressed as follows:

$$r_{cat} = k_{1,cat}\left(C_{CO_2} - C_{CO_{2,e}}\right) \tag{86}$$

$$k_{1,cat} = k_{cat} \cdot C_{cat} \tag{87}$$

where r_{cat} is the reaction rate of CO_2 with catalyst in kmol/m^{3}s, $k_{1,\,cat}$ is the overall pseudo–first order reaction rate constant in s^{-1}, k_{cat} is the second order reaction rate constant of the forward reaction with the catalyst in m^3/kmols, and the value for the same in case of DEA catalyst is $5,65x10^{11}e^{-5284,4/T}$ [95].

If the operating condition of absorption process is in a fast reaction regime, then the absorption rate can be got from the following equation:

$$N_{CO_2}a = Ek_{L,CO_2}a(C^*_{CO_2} - C_{CO_{2,e}}) \tag{88}$$

where N_{CO2} is the molar flux (absorption flux) of CO_2 in kmol/m^{2}s, a is the gas-liquid interfacial area per unit volume of packed column in m^2/m^3, E is the enhancement factor, $k_{L,CO2}$ is the mass transfer coefficient of liquid side in kmol/m^{2}s, C^*_{CO2} is the CO_2 concentration at interface in kmol/m^3 and $C_{CO2,e}$ is the equilibrium concentration of CO_2 in the liquid phase in kmol/m^3.

$$E = H_a \tag{89}$$

H_a is the Hatta number which can be obtained from the following equation:

$$H_a^2 = \frac{D_a \cdot k_1}{k_{L,CO_2}^2} \tag{90}$$

where D_a is the diffusivity in m^2/s, k_1 is the overall pseudo–first order reaction rate constant in s^{-1}, and $k_{L,\,CO2}$ is the mass transsfer coefficient of liquid side in kmol/m^{2}s.

The overall pseudo-first order reaction rate constant k_1 is defined as:

$$k_1 = k_{OH} \cdot C_{OH} + k_{cat} \cdot C_{cat} \tag{91}$$

where k_{OH} is the second order reaction rate constant of the forward reaction with OH^- in m^3/kmols, and k_{cat} is the second order reaction rate constant of the forward reaction with catalyst in m^3/kmols.

Fast pseudo first order reaction assumption is valid under the following condition:

$$3 < H_a < 0{,}5E_\infty \tag{92}$$

where E_∞ is enhancement factor for instantaneous reaction which can be obtained using film theory described with following equation:

$$E_\infty = 1 + \frac{D_{CO_3^{2-}} \cdot C_{CO_3^{2-}}}{D_{CO_2} \cdot C^*_{CO_2}} \tag{93}$$

where D is the diffusivity in m^2/s, and C^*_{CO2} is the CO_2 concentration at interface in kmol/m^3.

The solubility of gases in promoted carbonate solutions was estimated using modified Henry law with an empirical model of Schumpe [96] which describes the solubility of gases in mixed electrolyte solutions considering salting out effects:

$$log\left(\frac{H_{\mathrm{e,jw}}}{H_{\mathrm{e,j}}}\right) = \sum\left(h_{\mathrm{i}} + h_{\mathrm{g}}\right) \cdot c_{\mathrm{i,L}} \tag{94}$$

where $H_{\mathrm{e,jw}}$ is the Henry constant of gas-water system in Pam^3/kmol, $H_{\mathrm{e,j}}$ is the Henry constant of gas-aqueous electrolyte solution system in Pam^3/kmol, h_{i} is the ion-specific parameter in m^3/kmole, h_{G} is the gas-specific parameter in m^3/kmole and $c_{\mathrm{i,L}}$ is the molar concentration of ion *i* in kmole/m^3.

The Henry constant of gas–water system can be obtained from the following equation:

$$H_{\mathrm{e,jw}}(T) = H_{\mathrm{e,jw}}(298K)exp\left(\frac{-dlnk_{\mathrm{H}}}{d\left(\frac{1}{T}\right)} \cdot \left(\frac{1}{T} - \frac{1}{298}\right)\right) \tag{95}$$

where k_{H} is the reverse of Henry constant in kmol/m^{3}Pa.

The value of $H_{\mathrm{e,jw}}$ (298 K) and $-d$ ln kH /d(1/T) are shown in Table 9 [96]. Gas–specific parameter was extended from Equation (94) to wider temperature range using Weissenberger and Schumpe method [96] and expressed in the following equation:

$$h_{\mathrm{G}} = h_{\mathrm{G,0}} + h_{\mathrm{T}}(T - 298{,}15) \tag{96}$$

Table 9. The values of $H_{\mathrm{e,jw}}$ (298 K) and $-d$ ln kH / d(1/T) for various gases [96].

Component	$1/He^{o}_{298K}$ (kmol/m^{3}Pa)	-dlnk_h/d(1/T) (K)
CO_2	3600	2200
CO	99	1300
H_2	78	500
N_2	61	1300
CH_4	140	1600
Ar	140	1500

Table 10. The value of gas parameters [96].

Component	$h_{G,0}$ (m^3/kmol)	h_T (m^3/kmolK)
CO_2	-1,72x10^{-5}	-3,38x10^{-7}
CO	-	-
H_2	-2,18x10^{-5}	-2,99x10^{-7}
N_2	-1,0x10^{-6}	-6,05x10^{-7}
CH_4	2,2x10^{-6}	-5,24x10^{-7}
Ar	5,7x10^{-6}	-4,85x10^{-7}

In equation (96), h_T is the temperature correction in m^3/kmolK. The values of h_{i+}, h_{i-}, $h_{G,0}$, and h_T can be seen in Table 10 [96] and Table 11 [96]. Equations (95) and (96) are substituted into Equation (94) to obtain the value of $H_{e,j}$.

Table 11. The value of ion specific parameters [96].

Cation	h_i^+ (m^3/kmol)	Anion	h_i^- (m^3/kmol)
K^+	0,0922	HCO_3^-	0,0967
$DEAH^+$	0,0470	CO_3^{2-}	0,1423
		OH^-	0,0610
		$DEACOO^-$	0,0430

Gas side mass transfer coefficient in kmol/m^2s is obtained from the empirical correlation by Onda *et al.* [97] shown in Equation (97) where constant *A* equal to 2 for packing diameter less than 0,012 m and equal to 5,23 for packing diameter greater than 0,012 m (in this work it is used 5.23).

$$k_G = \frac{A}{RT}(Re)^{0,7}(S_{cG})^{1/3}\left(a \cdot d_p\right)^{-2,0}(a \cdot D_{kG}) \quad (97)$$

where *R* is the universal gas constant in kJ/kmolK, *T* is the thermodynamic temperature in K, *Re* is the Reynold number of gas, S_{cG} is the Schmidt number of gas, *a* is the gas–liquid interfacial area per unit volume of packed column in m^2/m^3, d_p is the packing diameter in m, *D* is the diffusivity in m^2/s.

Reynold and Schmidt number of liquid are defined as:

$$R_{\mathrm{eL}} = \frac{L}{a \cdot \mu_{\mathrm{L}}} \tag{98}$$

$$S_{\mathrm{cL}} = \frac{\mu_{\mathrm{L}}}{\rho_{\mathrm{L}} \cdot D_{\mathrm{kL}}} \tag{99}$$

where L is the mass velocity of liquid in kg/m^{2}s, a is the gas-liquid interfacial area per unit volume of packed column in m^2/m^3, μ is the viscosity in Pas, ρ is the density in kg/m^3 and D is the diffusivity in m^2/s.

Liquid side mass transfer coefficient $k_{\mathrm{L,k}}$ in kmol/m^{2}s is obtained from the empirical correlation by Taylor and Krishna [98] shown in the following equation:

$$k_{\mathrm{L,k}} = 0{,}0051 (R_{\mathrm{eL}})^{2/3} (S_{\mathrm{cL}})^{-0{,}5} \left(a_{\mathrm{p}} \cdot d_{\mathrm{p}}\right)^{0.4} \left(\frac{\mu_{\mathrm{L}} \cdot g}{\rho_{\mathrm{L}}}\right)^{1/3} \tag{100}$$

where a_{p} is the specific area of packing in m^2/m^3, d_{p} is the packing diameter in m and g is gravity acceleration in m/s^2.

The liquid Reynold and Schmidt number are defined as, respectively:

$$R_{\mathrm{eL}} = \frac{L}{a \cdot \mu_{\mathrm{L}}} \tag{101}$$

$$S_{\mathrm{cL}} = \frac{\mu_{\mathrm{L}}}{\rho_{\mathrm{L}} \cdot D_{\mathrm{kL}}} \tag{102}$$

where L is the mass velocity of liquid in kg/m^{2}s.

Gas–liquid interfacial area per unit volume of packed column, a in m^2/m^3 is obtained from packing specific area from the correlation provided by Onda *et al.* [97].

$$\frac{a}{a_{\mathrm{p}}} = 1 - exp\left[-1{,}45 \left(\frac{\sigma_{\mathrm{c}}}{\sigma_{\mathrm{L}}}\right)^{0{,}75} (R_{\mathrm{eL}})^{0{,}1} (F_{\mathrm{rL}})^{-0{,}05} (W_{\mathrm{eL}})^{0{,}2}\right] \tag{103}$$

where σ_C is the critical surface tension of liquid in N/m, σ_L is the surface tension of liquid in N/m, F_{rL} is the Froude number and W_{eL} is the Weber number.

Froude and Weber number are defined as:

$$F_{\mathrm{rL}} = \frac{a_{\mathrm{p}} \cdot L^2}{\rho_{\mathrm{L}}^2 \cdot g} \tag{104}$$

$$W_{\mathrm{eL}} = \frac{L^2}{\rho_{\mathrm{L}} . a_{\mathrm{p}} \cdot \sigma} \tag{105}$$

where a_p is the specific area of packing in m^2/m^3, L is the mass velocity of liquid in kg/m^2s, ρ is the density in kg/m^3, g is the gravity acceleration in m/s^2, and σ is the surface tension in N/m.

The diffusion coefficient of a species in gas phases was determined from binary diffusion coefficient using Maxwell–Stefan equation as follows:

$$\frac{1}{D_{\mathrm{im}}} = \frac{\sum\left(\frac{1}{D_{\mathrm{i,j}}}\right) \cdot \left(x_{\mathrm{j}} N_{\mathrm{i}} - x_{\mathrm{i}} N_{\mathrm{j}}\right)}{N_{\mathrm{i}} - x_{\mathrm{i}} \sum N_{\mathrm{j}}} \tag{106}$$

where D is the diffusivity in m^2/s, N_i is the molar flux of component i in $kmol/m^2s$ and x_i is the mole fraction of component i in liquid phase.

The binary diffusion coefficient was obtained from correlation by Fuller *et al.* [99] recommended by Taylor and Krishna [98] as follows:

$$D_{\mathrm{i,j,G}} = \frac{1x10^{-7} T^{1,75} \left(\frac{1}{M_{\mathrm{i}}} - \frac{1}{M_{\mathrm{j}}}\right)}{p\left(v_{\mathrm{i}}^{1/3} + v_{\mathrm{j}}^{1/3}\right)^2} \tag{107}$$

where M is the molecular weight of component i in kg/kmol, p is the prressure in Pa, and v is the molar volume of component in $m^3/kmol$.

Because of the dilute solution condition, the diffusion coefficient of a species in liquid phase was assumed binary regarding water and determined using Wilke and Chang Equation [90]:

$$D_{\mathrm{iw,L}} = \frac{7{,}4x10^{-8}T(\phi \cdot M_{\mathrm{w}})^{0,5}}{\mu_{\mathrm{L}} \cdot v_{\mathrm{i}}^{0,6}} \qquad (108)$$

where ϕ is the association factor for solvent (ϕ=2,6 for water), M_{w} is the molecular weight in kg/kmol, μ is the viscosity in Pas, v_{i} is the molar volume of component *i* in m^3/kmol.

Heat transfer coefficient in the gas phase was determined from mass transfer coefficient in the gas phase using Chilton–Colburn analogy, while the heat transfer resistance in liquid phase was neglected.

The model was constructed by differential mass balances in the packed column. Figure 7 shows a schematic diagram of the packed bed absorption column showing an infinitesimal element of mass and energy balances. Microscopic or differential mass and energy balance was constructed based on System 1, while macroscopic balance to correlate several process variables in the packed column was constructed through System 2.

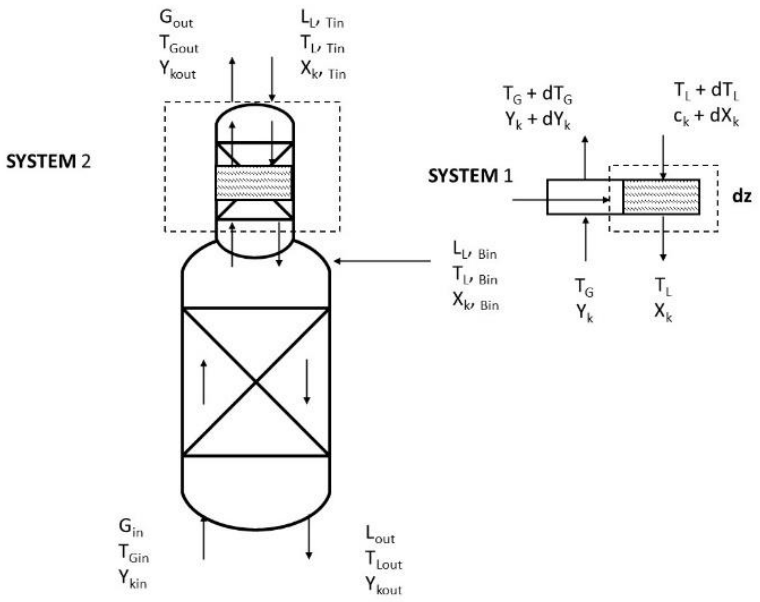

Figure 7. Schematic diagram of packed bed absorption column showing an infinitesimal element of mass and energy balances.

Microscopic or differential mass and energy balance was constructed based on System 1, while macroscopic balance to correlate several process variables in the packed column was constructed through System 2.

Differential mass balances for System 1 is:

CO_2 $$N_{CO_2} \cdot a \cdot A \cdot dz = r_{CO_2} \cdot \phi_L \cdot A \cdot dz \quad (109)$$

K_2CO_3 $$-L_{in} \cdot dX_{CO_3^{2-}} - v \cdot r_{CO_2} \cdot \phi_L \cdot A \cdot dz = 0 \quad (110)$$

where N_{CO2} is the molar flux (absorption flux) of CO_2 in kmol/m^{2}s, a is the gas liquid interfacial area per unit volume of packed column in m^2/m^3, A is the sectional area of the column in m^2, z is the axial position in packed column in m, L_{in} is the inlet molar flow rate of liquid in kmol/s, X is the molar ratio of component, v is the stoichiometric coefficient, r_{CO2} is the reaction rate of CO_2 in kmol/m^{3}s, and ϕ_L is the liquid hold up in packed column.

By rearrangement of the Equations (109) and (110) the following expressions can be obtained:

$$-L_{in} \cdot dX_{CO_3^{2-}} - v \cdot N_{CO_2} a \cdot A \cdot dz = 0 \quad (111)$$

$$\frac{dX_{CO_3^{2-}}}{dz} = -\frac{v \cdot N_{CO_2} \cdot a \cdot A}{L_{in}} \quad (112)$$

When $N_{CO2}a$ was substituted from Equation (88), then the following equation was obtained after some rearrangements:

$$\frac{dX_{CO_3^{2-}}}{d\zeta} = -\frac{v \cdot E \cdot k_{L,CO_2} \cdot a \cdot C \cdot \left(x^*_{CO_3^{2-}} - x^e_{CO_3^{2-}}\right) \cdot Z_T \cdot A}{L_{in}} \quad (113)$$

where $\zeta = Z/Z_T$ and $x_{CO_3^{2-}} = C_{CO_3^{2-}}/C$.

ζ denotes dimensionless axial position in packed column, $x^*_{CO_3^{2-}}$ is the mole fraction of CO_3^{2-} at interface, $x^e_{CO_3^{2-}}$ is the equilibrium mole fraction of CO_3^{2-} in liquid phase, and Z_T is the height of packing in m.

$$k(dissolved\ gas): L_{in} \cdot dX_k = N_k \cdot a \cdot A \cdot dz \quad (114)$$

$$\frac{dX_k}{dz} = \frac{N_k \cdot a \cdot A}{L_{in}} \quad (115)$$

where $N_k a$ was obtained from $N_k \cdot a = k_{L,K} \cdot a \cdot (C_k^* - C_{k^0})$, after which the Equation (115) can be rearranged as follows:

$$\frac{dX_k}{d\zeta} = \frac{k_{L,k} \cdot a \cdot C \cdot (x_k^* - x_k^0) \cdot Z_T \cdot A}{L_{in}} \quad (116)$$

where x_k^* is the mole fraction of component k at interface, x_k^0 is the mole fraction of component k in the bulk liquid phase, C_k^* is the molar concentration of component k at interface in kmol/m^3, and C_{k^0} is the molar concentration of component k in the bulk liquid phase in kmol/m^3.

The concentration of bicarbonate ion was determined using stoichiometry as follows:

$$X_{HCO_3^-} - X_{HCO_3^-,in} = 2 \cdot \left[X_{CO_3^{2-},in} - X_{CO_3^{2-}}\right] \quad (117)$$

The concentration of other species (expressed as mole ratio) in liquid phase was determined using equilibrium and electro neutrality constraint. The molar concentration of various species in liquid phase was determined from $c_i = x_i\, c$, where mole-fraction, x_i, was determined from the mole ratio as follows:

$$x_i = \frac{X_i}{\sum X_k} \cdot y_i = \frac{Y_i}{\sum Y_k} \quad (118)$$

and molar density, c, was calculated from liquid mass density as $c = \rho_L/M$, where M is molecular weight of liquid mixture, $M = \Sigma M_i\, x_i$, and ρ is its density which was obtained by regression fitting of data from literature [100] as follows:

$$\rho_L = \rho_{L,293} + 17816{,}45\left(\frac{1}{T} - \frac{1}{293}\right) \quad (119)$$

$$\rho_{L,293} = \frac{49196{,}07}{49{,}693 - 39{,}1902 \cdot w_{K_2CO_3} - 29{,}4723 w_{KHCO_3}} \quad (120)$$

where w is the mass fraction.

The presence of a catalyst in the liquid phase does not affect significantly liquid density. The concentration of CO_2 and carrying gases in the gas phase can be obtained by performing a mass balance over System 2:

CO_2 $$G_{\mathrm{m,in}} \cdot \left[Y_{\mathrm{CO_2}} - Y_{\mathrm{CO_{2,out}}}\right] = \frac{L_{\mathrm{m,in}}}{v} \cdot \left[X_{\mathrm{CO_3^{2-},in}} - X_{\mathrm{CO_3^{2-}}}\right] \quad (121)$$

k(carrying gases): $$G_{\mathrm{m,in}} \cdot \left[Y_{\mathrm{k}} - Y_{\mathrm{k,out}}\right] = L_{\mathrm{m,in}} \cdot \left[X_{\mathrm{k,in}} - X_{\mathrm{k}}\right] \quad (122)$$

where G is the mass velocity of gas in kg/m^{2}s, Y is the molar ratio of component i (mole component i per mole of inlet gas), L is the mass velocity of fluid in kg/m^{2}s, v is stoichiometric coefficient of K_2CO_3 and X is the molar ratio of component i (mole component i per mole of inlet liquid).

The CO_2 concentration on the interface (C^*_{CO2}) in kmol/m^3:

$$C^*_{\mathrm{CO_2}} = \frac{k_{\mathrm{G,CO_2}} \cdot y_{\mathrm{CO_2}} \cdot p + E \cdot k_{\mathrm{L,CO_2}} \cdot C_{\mathrm{CO_2,e}}}{E \cdot k_{\mathrm{L,CO_2}} + k_{\mathrm{G,CO_2}} \cdot H_{\mathrm{CO_2}}} \quad (123)$$

where k_G is the mass transfer coefficient of gas side in kmol/m^{2}s, y_i is the mol fraction of component i (mole component i per mole of inlet gas), p is the pressure in Pa, E is the enhancement factor, k_L is the mass transfer coefficient of liquid side in kmol/m^{2}s, $C_{CO2,e}$ is the equilibrium concentration of CO_2 in liquid phase in kmol/m^3 and H_{CO2} is the Henry constant of CO_2 in aqueous electrolyte solution system in Pam^3/kmol.

Concentration of other gases on the interface (C^*_k) in kmol/m^3:

$$C^*_{\mathrm{k}} = \frac{k_{\mathrm{G,k}} \cdot y_{\mathrm{CO_2}} \cdot p + k_{\mathrm{L,k}} \cdot C_{\mathrm{k}}}{k_{\mathrm{L,k}} + k_{\mathrm{G,k}} \cdot H_{\mathrm{k}}} \quad (124)$$

where k_G is the mass transfer coefficient of gas side in kmol/m^{2}s, y_i is the mole fraction of component i in gas phase, p is the pressure in Pa, k_L is the mass transfer coefficient of liquid side in kmol/m^{2}s, C_k is the molar concentration of component k in kmol/m^3 and H_k is the Henry constant of the component k.

The differential heat balance on the gas side is given by following equation:

$$\frac{dT_{\mathrm{G}}}{dz} = -\frac{h_{\mathrm{G}} \cdot a}{C_{\mathrm{pG}} \cdot G}\left(T_{\mathrm{G}} - T_{\mathrm{L}}\right) \quad (125)$$

where T_G od the temperature of gas stream in K, z is the axial position in packed column in m, h_G is the gas specific parameter in m^3/kmol, a is the gas-liquid interfacial area per unit volume of packed column in m^2/m^3, C_{pG} is the heat capacity of gas in J/kgK, G is the mass velocity of gas in kg/m^2s, and T_L is the temperature of the liquid stream in K.

The liquid temperature was calculated from energy balance for System 2:

$$T_L = T_{L,in} + \frac{G \cdot C_{pG}}{C_{pL}}\left[c_{pG}\left(T_G - T_{G,in}\right)\right] - \left(-\Delta H_{rx}\right)\frac{G_{in}}{L \cdot C_{pL}}\left[Y_{CO_{2,in}} - Y_{CO_2}\right] \quad (126)$$

where $T_{L,in}$ is the temperature of the inlet liquid in K, G is the mass velocity of gas in kg/m^2s, C_{pG} is the heat capacity of gas in J/kgK, C_{pL} is the heat capacity of liquid in J/kgK, T_G od the temperature of gas stream in K, $T_{G,in}$ is the temperature of the inlet gas in K, ΔH_{rx} is the heat of reaction in J/kmol, G_{in} is the inlet mass velocity of gas in kg/m^2s, L is the mass velocity of liquid in kg/m^2s, and Y is the molar ratio of component i (mole component i per mole of inlet gas).

Equations (113) and (115) were solved numerically using the orthogonal collocation method with 6 internal collocation points, thus:

$$X_{CO_3^{2-},j} = X_{CO_3^{2-},in} - \frac{v \cdot Z_T}{H_{T,CO_3^{2-}}} \sum_{m=1}^{NC+2} H_{jm} \cdot E_m \left(x^*_{CO_3^{2-},m} - x^e_{CO_3^{2-},m}\right) \quad (127)$$

$$X_{k,j} = X_{k,in} + \frac{Z_T}{H_{T,k}} \sum_{m=1}^{NC+2} H_{jm} \left(x^*_{k,m} - x^0_{k,m}\right) \quad (128)$$

where X is the molar ratio of component i (mole component i per mole of inlet liquid), v is the stoichiometric coefficient of K_2CO_3, Z_T is the height of packing in m, $H_{T,k}$ is the height of transfer unit for component k, H_{jm} is the quadrature weight, E_m is the enhancement factor, $x^*_{CO_3^{2-},m}$ is the mole fraction of CO_3^{2-} at interface, $x^e_{CO_3^{2-},m}$ is the equilibrium mole fraction of CO_3^{2-} in liquid phase, $x^*_{k,m}$ is the mole fraction of component k at interface in collocation points m in packed column and $x^0_{k,m}$ is the mole fraction of component k in the bulk liquid phase in collocation points m in packed column.

$$H_{T,CO_3^{2-}} = \frac{L_{in}}{A \cdot k_{L,CO_3^{2-}} \cdot a \cdot C} \quad (129)$$

$$H_{\mathrm{T,k}} = \frac{L_{\mathrm{in}}}{A \cdot k_{\mathrm{L,k}} \cdot a \cdot C} \tag{130}$$

where L_{in} is the inlet molar flow rate of liquid in kmol/s, A is the sectional area of the column in m^2, k_L is the mass transfer coefficient of liquid side in kmol/m^2s, a is the gas-liquid interfacial area per unit volume of packed column in m^2/m^3 and C is the molar density in kmol/m^3.

With collocation orthogonal method on Equation (125), the result of gas temperature distribution in the column was shown by following expression:

$$T_{\mathrm{G,j}} = T_{\mathrm{G,out}} - N_{\mathrm{G}} \sum_{\mathrm{m=1}}^{\mathrm{NC+2}} H_{\mathrm{jm}} \left(T_{\mathrm{G,m}} - T_{\mathrm{L,m}} \right) \tag{131}$$

where N_G is the dimensionless quantity, H_{jm} is the quadrature weight, $T_{G,m}$ is the temperature of the gas in collocation points in packed column in K, and $T_{L,m}$ is the temperature of the liquid in collocation points m in packed column in K.

The dimensionless quantity N_G is defined as:

$$N_{\mathrm{G}} = \frac{h_{\mathrm{G}} \cdot a \cdot Z_{\mathrm{T}}}{C_{\mathrm{pG}} \cdot G} \tag{132}$$

where h_G is the gas specific parameter in m^3/kmol, a is the gas-liquid interfacial area per unit volume of packed column in m^2/m^3, Z_T is the height of packing in m, C_{pG} is the heat capacity of the gas in J/kgK and G is the mass velocity of gas in kg/m^2s.

The solution of nonlinear algebraic equation obtained from orthogonal collocation method was conducted by successive approximation method. Thus, %CO_2 removal can be calculated by following equation:

$$\%Removal = 1 - \frac{Y_{\mathrm{A,out}}}{Y_{\mathrm{A,in}}} \tag{133}$$

where Y is the molar ratio of component i (mole component i per mole of inlet gas).

The CO_2 washing system is in charge to remove CO_2 from the raw synthesis gas stream containing 18,00 mol.% of CO_2, 60,83 mol.% of H_2, 20,49 mol.% of N_2, 0,27 mol.% of CH_4, 0,16 mol.% of CO and 0,25 mol.% of Ar per dry basis with the mass flow rate of 130227 kg/h. The CO_2 is removed from the gas stream by counter–current absorption in two stages column, lower part with a diameter of 4,30 m and upper part with a diameter of 2,69 m. The lower part column is filled with 5 cm ring packing distributed in three beds with the height of 6,6 m, while the upper part is filled also with 5 cm ring packing distributed in three beds with the height of 4,85 m. Lean solution, containing 21,22 mas.% of K_2CO_3 and 5,60 mas.% of $KHCO_3$, was fed into the top of the upper part column while semi–lean solution containing 18,12 mas.% of K_2CO_3 and 9,76 mas.% of $KHCO_3$ were fed into the top of the lower part column. To enhance the absorption rate, an amine promoter, DEA, was added into the carbonate–bicarbonate solution. The volume flow of lean and semi-lean solution was controlled to achieve the outlet CO_2 in the absorber overhead stream at the level of 0,04 mol.% per dry basis.

4.1.2.3.Methanation unit

The objective of the methanation reaction is to complete the removal of the carbon oxides (CO and CO_2) from the raw synthesis gas, since the carbon oxides are harmful to the ammonia synthesis catalyst. Removal of the carbon oxides is accomplished by their conversion to CH_4, which acts as an inert gas in the ammonia converter. The methanation reactions are:

$$CO + 3H_2 \rightarrow CH_4 + H_2O \quad \Delta H_{298} = -206{,}2\ kJ/mol \tag{134}$$

$$CO_2 + 4H_2 \rightarrow CH_4 + 2H_2O \quad \Delta H_{298} = -165{,}0\ kJ/mol \tag{135}$$

Both reactions are strongly exothermic, causing a theoretical temperature rise of about 72°C for each mol percent of carbon oxide in the inlet gas. Under normal operating conditions, with a CO content of 0,24 mol.% in the inlet gas per dry basis, the expected temperature rise in the methanator will be about 19°C resulting in an outlet temperature of about 335°C. However, during methanation step in the presence of a nickel catalyst the WGS reaction (Table 2) simultaneously occurs.

The methanation reactor is modelled as an adiabatic equilibrium reactor. Kinetics are based on the work developed by Kopyscinski [101]. The reaction uses a commercial catalyst Ni/Al_2O_3

(20% of Ni and the balance is Al_2O_3) with the BET surface area of 183 m^2/g in the shape of pellets with a diameter of 3 mm and a length of 5 mm, porosity of 0,625, tortuosity factor of 2,74 and bulk density of 1014 kg/m^3.

The corresponding rate equations (14) to (16) and reaction rate equations (22) to (25) defined in the steam–natural gas reformer unit was used for determination of methanation kinetics. Kinetic rate coefficients and apparent adsorption equilibrium constants are defined according to Equations (26) and (27) with the corresponding parameters for the pre–exponential factors A_i and B_j, and activation energies E_i, given in Table 4, Table 5 and Table 7.

Considering that two of the three major reactions are independent from each other, and by definition of two corresponding variables, by the conversion rate, it is possible to determine all the concentration variables from the following expressions:

$$X_{\mathrm{CH_4}} = \frac{F_{\mathrm{CH_{4,0}}} - F_{\mathrm{CH_4}}}{F_{\mathrm{CH_{4,0}}}} \tag{136}$$

$$X_{\mathrm{H_2}} = \frac{F_{\mathrm{H_2}} - F_{\mathrm{H_{2,0}}}}{F_{\mathrm{CH_{4,0}}}} \tag{137}$$

$$X_{\mathrm{CO_2}} = \frac{F_{\mathrm{CO_2}} - F_{\mathrm{CO_{2,0}}}}{F_{\mathrm{CH_{4,0}}}} \tag{138}$$

$$X_{\mathrm{CO}} = \frac{F_{\mathrm{CO}} - F_{\mathrm{CO,0}}}{F_{\mathrm{CH_{4,0}}}} \tag{139}$$

where X denotes the conversion rate in %, while F is the molar flow rate in kmol/h.

With the above definitions, it was possible to drive all the model's flow rates in terms of X_{CO2}, X_{CO}, X_{H2} and X_{CH4}. For example, the molar flow rate of methane F_{CH4} is:

$$F_{\mathrm{CH_4}} = F_{\mathrm{CH_{4,0}}}\left(1 - X_{\mathrm{CH_4}}\right) \tag{140}$$

The partial pressures are defined based on the components molar flow rates:

$$p_{\mathrm{H_2O}} = p_{\mathrm{total}}\left[\frac{F_{\mathrm{H_2O,0}} - F_{\mathrm{CH_{4,0}}}\left(X_{\mathrm{CH_4}} + X_{\mathrm{CO_2}}\right)}{F_{\mathrm{total,0}} + 2F_{\mathrm{CH_{4,0}}}X_{\mathrm{CH_4}}}\right] \tag{141}$$

$$p_{\mathrm{CH_4}} = p_{\mathrm{total}} \left[\frac{F_{\mathrm{CH_{4,0}}}(1 - X_{\mathrm{CH_4}})}{F_{\mathrm{total,0}} + 2F_{\mathrm{CH_{4,0}}} X_{\mathrm{CH_4}}} \right] \tag{142}$$

$$p_{\mathrm{H_2}} = p_{\mathrm{total}} \left[\frac{F_{\mathrm{H_{2,0}}} - F_{\mathrm{CH_{4,0}}}(3X_{\mathrm{CH_4}} + X_{\mathrm{CO_2}})}{F_{\mathrm{total,0}} + 2F_{\mathrm{CH_{4,0}}} X_{\mathrm{CH_4}}} \right] \tag{143}$$

$$p_{\mathrm{CO}} = p_{\mathrm{total}} \left[\frac{F_{\mathrm{CH_{4,0}}}(3X_{\mathrm{CH_4}} + X_{\mathrm{CO_2}})}{F_{\mathrm{total,0}} + 2F_{\mathrm{CH_{4,0}}} X_{\mathrm{CH_4}}} \right] \tag{144}$$

where p is the partial pressure in Pa.

Substituting the above partial pressure equations of feedstock and product in reaction rate equations will cause the rate equations to be in terms of conversion rate variables. Now it is possible to derive the balance equations. Mass balance equations for CH_4, CO_2, CO, and H_2O are:

$$\frac{dF_{\mathrm{CH_4}}}{dz} = -\pi \cdot \rho_{\mathrm{B}} \cdot (\eta_1 \cdot r_1 + \eta_3 \cdot r_3) \tag{145}$$

$$\frac{dF_{\mathrm{CO_2}}}{dz} = -\pi \cdot \rho_{\mathrm{B}} \cdot (\eta_2 \cdot r_2 + \eta_3 \cdot r_3) \tag{146}$$

$$\frac{dF_{\mathrm{CO}}}{dz} = -\pi \cdot \rho_{\mathrm{B}} \cdot (\eta_2 \cdot r_2 - \eta_1 \cdot r_1) \tag{147}$$

$$\frac{dF_{\mathrm{H_2O}}}{dz} = -\pi \cdot \rho_{\mathrm{B}} \cdot (\eta_1 \cdot r_1 + \eta_2 \cdot r_2 + \eta_3 \cdot r_3) \tag{148}$$

where z is the length of the reactor in m, π is the cross section of the reactor in m^2, ρ_B is the catalyst mass density in kg/m^3 and η_1, η_2, and η_3 are the effectivness factors of the reaction, while r_1, r_2, and r_3 are rection rates in $kgmol/kg_{cat}h$.

The catalyst effectiveness factors were calculated according to the Equations (32) to (37) defined in the steam–natural gas reformer unit.
Substitution of molar flow with conversion variables yields:

$$\frac{dX_{\mathrm{CH_4}}}{dz} = \frac{-\pi \cdot \rho_{\mathrm{B}} \cdot (\eta_1 \cdot r_1 + \eta_3 \cdot r_3)}{F_{\mathrm{CH_{4,0}}}} \tag{149}$$

$$\frac{dX_{\mathrm{CO_2}}}{dz} = \frac{-\pi \cdot \rho_{\mathrm{B}} \cdot (\eta_2 \cdot r_2 + \eta_3 \cdot r_3)}{F_{CH_{4,0}}} \tag{150}$$

$$\frac{dX_{\mathrm{CO}}}{dz} = \frac{-\pi \cdot \rho_{\mathrm{B}} \cdot (\eta_2 \cdot r_2 - \eta_1 \cdot r_1)}{F_{\mathrm{CH_{4,0}}}} \tag{151}$$

$$\frac{dX_{\mathrm{H_2O}}}{dz} = \frac{-\pi \cdot \rho_{\mathrm{B}} \cdot (\eta_1 \cdot r_1 + \eta_2 \cdot r_2 + \eta_3 \cdot r_3)}{F_{\mathrm{CH_{4,0}}}} \tag{152}$$

Energy balance equation, with considering that the reactor is adiabatic is following:

$$\frac{dT}{dz} = \frac{1}{\rho_{\mathrm{g}} \cdot C_{\mathrm{pg}} \cdot u_{\mathrm{s}}} \left[\rho_{\mathrm{B}} \left((-\Delta H_1) \cdot \eta_1 \cdot r_1 \right) + (-\Delta H_2) \cdot \eta_2 \cdot r_2 + (-\Delta H_3) \cdot \eta_3 \cdot r_3 \right] \tag{153}$$

where ρ_{g} is the density of gas mixture in kg/m^3, C_{pg} is the heat capacity in kJ/kmolK, u_{s} is the gas mixture speed in the reactor in m/s, and ΔH is the reaction enthalpy change in kJ/kmol.

The Ergun momentum balance equation is used for determination of the pressure drop along the reactor:

$$\frac{dP}{dz} = 150 \cdot \frac{(1-\epsilon)^2 \cdot \eta \cdot u_{\mathrm{g}}}{\epsilon^3 \cdot d_{\mathrm{p}}^3} + 1{,}75 \cdot \frac{(1-\epsilon) \cdot u_{\mathrm{g}} \cdot \rho}{\epsilon^3 \cdot d_{\mathrm{p}}} \tag{154}$$

where ϵ is the void fraction of the catalytic bed, η is the effectivness factor used for the intra particle transport limitation, u_{g} is the linear velocity of fluid phase in m/s, d_{p} is the particle diameter in m, and ρ is the density of catalyst bed in kg/m^3.

Bed dimension of the methanation catalyst is 3684 mm in diameter and 3165 mm in depth.

4.1.3. Ammonia synthesis loop model

The last part of the model is an ammonia synthesis loop which comprises synthesis gas compression unit, conversion of synthesis gas to ammonia and liquefaction of gas ammonia to

liquid ammonia with subsequent separation from the recycle gas. The steady–state flowsheet of the ammonia synthesis loop is shown in Figure 8.

Pure synthesis gas leaves 104–F and enters the first case of the synthesis gas compressor 103–J at a pressure of 25 bar and is compressed to about 52 bars. The compressor 103–J is the centrifugal compressor with four casings driven by a steam turbine. This stream is cooled in two heat exchangers: 136–C and 170–C. Cooled gas at about 33^{o}C goes to separator 142–F where entrained water is removed. Liquid collecting in this drum is drained to the condensate stripper system. During normal operation, the pressure in 104–F is controlled by pressure control valve PV–176 and accordingly the compressor speed.

Synthesis gas leaves 142–F and goes to the second case of the compressor where it is compressed to about 95 bars. The gas is then cooled in two heat exchangers: 116–C and 129–C. The cooled synthesis gas goes to the separator 105–F where any further liquid condensed is separated and the liquid flow goes into the condensate stripper system. From the 105–F the synthesis gas goes to the third and fourth case of 103–J where it is compressed in two steps to about 170 bars. The first step is compressed to about 156 bar at a temperature of about 121^{o}C. The synthesis gas at this level leaves the compressor and is cooled by the 156–C and 140–C. The synthesis gas stream is then joined by the effluent stream from the synthesis converter which contains approximately 13% of ammonia. The combined stream is then cooled by chiller 118–C to a temperature of approximately -5.6^{o}C. Further cooling by 158–C and 119–C takes place after which the gas enters the ammonia separator 106–F at about -23^{o}C.

The chilled gas enters the ammonia separator 106–F where the condensed ammonia is disengaged from the feedstock and recycle gas stream. The gas leaves the drum, now containing about 2% ammonia, passes through 158–C and then the 120–C and returns to the fourth recycle case of 103–J.

The recycle section of 103–J increases the synthesis gas pressure by about 14 bar to 170 bar. The synthesis gas leaves the compressor at a temperature of about 28^{o}C, through exchanger 121–C after which the synthesis gas is heated to about 140^{o}C.

After pre-heating in 121–C, the high-pressure synthesis gas flows to the synthesis gas convertor 105–D, which is an axial-radial design. The mainstream of the synthesis gas enters near the bottom of the vessel and flows upwards through an annular space which is between the outer shell of the vessel and the wall of the catalyst section. The synthesis gas flows through the shell side of the interchanger 122–C where it is further heated by effluent gas flowing through the tubes.

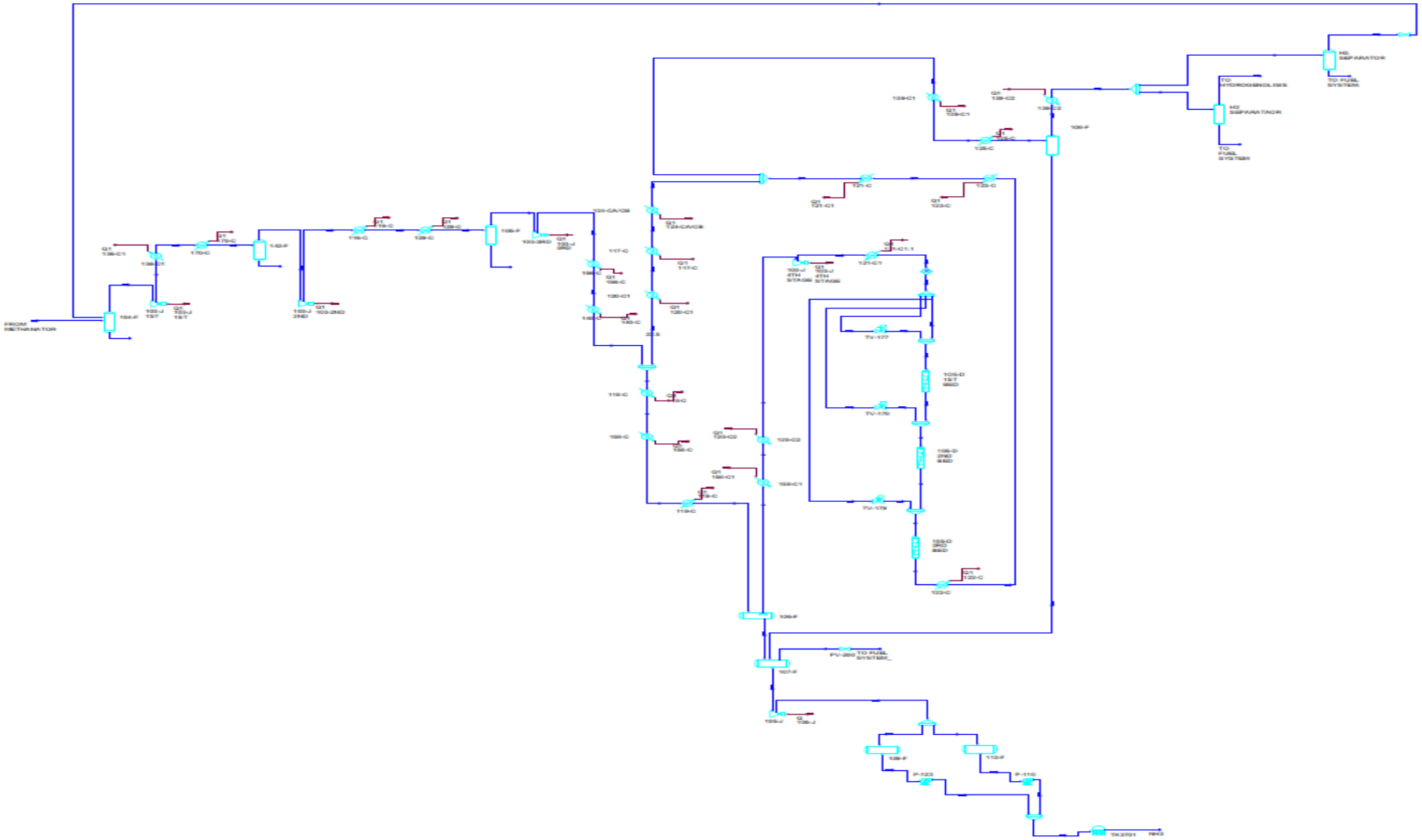

Figure 8. Ammonia synthesis loop flowsheet.

Leaving the interchanger, the synthesis gas passes down through the three beds of increasing depth of promoted iron ammonia synthesis catalyst in the catalyst basket. Between each catalyst bed, there is space. Quench gas for temperature control is introduced as required above each bed of catalyst. Synthesis gas bypassing the interchanger is used as a quench with each quench stream being controlled by control valves TV–177, TV–178, and TV–179.

Effluent gas leaves 105–D via the tube side of the boiler feed water exchanger 123–C. In heating boiler feed water to about 278^{o}C, the converter effluent is cooled to about 156^{o}C and then preheats feed gas in 121–C. Leaving the 121–C at about 43^{o}C, the cooled converter effluent joins the make-up gas discharge from the third case of the 103–J after cooling in exchangers 124–C, 117–C, and 120–C.

The synthesis loop purge gas is also taken off the 121–C. The purge gas stream is first cooled to about 23^{o}C in the 139–C before being chilled to -23^{o}C in 125–C. The chilled purge gas enters the separator 108–F where the ammonia condenses out. The purge gas leaves the separator and flows to the hydrogen membrane unit where the hydrogen is separated. One part of hydrogen is used in the process of hydrogenolysis for sulphur removal, while another part is used as make-up hydrogen at the suction of 103–J. The rest of the purge gas flows to the fuel system via control valve FV–166, while the liquid ammonia from the 108–F is pressured to the refrigeration system in vessel 107–F. Liquid ammonia from 106–F and from 108–F is pressured in the ammonia letdown drum 107–F. A control valve LV–161 and LV–187 are used to control the levels in the 106–F and 108–F.

The pressure in 107–F is held at about 17,6 bars, by venting gas to the separation unit to recover of ammonia and the rest of the gas flows to the fuel system. The liquid ammonia collecting in 107–F flows to the refrigeration compressor 105–J. After the process of refrigeration, the liquid ammonia flows in two separator drums 109–F and 112–F. From separator 109–F the warm liquid ammonia with the temperature of about 26^{o}C flows to the pump 123–J and from that location to the ammonia storage tank, while from the separator 112–F the liquid ammonia flows to the pump 110–J with the temperature of about -33^{o}C and from that location again in the ammonia storage tank. These two streams comprises the total flow of produced ammonia, which in the reference case is at the level of 56,666 t/h.

4.1.3.1.Ammonia synthesis unit

The ammonia synthesis converter is modelled as 3 catalyst beds with three quench between the first, the second and the third bed and one interchanger between the second and the third

bed. Axial–radial gas distribution concept uses the full catalyst efficiency and to ensure lower pressure drop thanks to the shorter gas path through the catalytic beds. The axial–radial distribution concept according to the Casale design is shown in Figure 9.

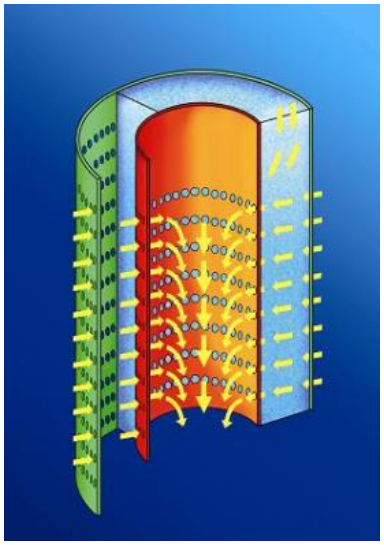

Figure 9. The axial–radial distribution concept according to the Casale design [102].

Regarding process description the pressurised nitrogen and hydrogen mixture in the molar ratio of 1 to 3 flow in the ammonia synthesis converter where only a fraction of the synthesis mixture is converted to ammonia in a single pass through the converter because of thermodynamic equilibrium of the ammonia synthesis reaction as shown:

$$N_2 + 3H_2 \rightarrow 2NH_3 \quad \Delta H = -46{,}22\ kJ/mol \tag{155}$$

Different kinetic models for ammonia synthesis have been proposed over the past couple of decades. However, the rate expression of Temkin–Pyzhez [103] is widely accepted to represent accurately the ammonia synthesis reaction over wide and varying process conditions. The changed form of the Temkin–Pyzhez equation expressed in activities as developed by Dyson and Simon [104] is used for modelling the ammonia synthesis converter. The reaction rate expression is given by:

$$r_{\mathrm{NH_3}} = 2k\left(K_{\mathrm{a}}^2 a_{\mathrm{N_2}}\left[\frac{a_{\mathrm{H_2}}^3}{a_{\mathrm{NH_3}}^2}\right]^{\alpha} - \left[\frac{a_{\mathrm{NH_3}}^2}{a_{\mathrm{H_2}}^3}\right]^{1-\alpha}\right) \tag{156}$$

where k is the rate constant for the reverse reaction, K_a is the equilibrium constant, a_i is the activity of component i and α is a constant which takes a value from 0,5 to 0,75 according to Dashti *et. al.* [105].

The equilibrium constant was obtained using the expression of Gunorubon and Raphael [106] as follows:

$$logK_a = \left(-2{,}6911logT - 5{,}51925x10^{-5}T + 1{,}848863x10^{-7}T^2 + \frac{2001{,}6}{T} + 2{,}689\right) \quad (157)$$

The rate constant values were obtained using the Arrhenius relation with values for synthesis relation obtained from Gunorubon and Raphael [106]:

$$k = k_0 exp\left(\frac{-E_a}{RT}\right) \quad (158)$$

where k_0 is the Arrhenius coefficient ($8{,}849x10^{14}$), E_a is the activation energy in kJ/mol, R is the universal gas constant in J/Kmol, while T is the thermodynamic temperature in K.

The component activities in the reaction rate equation were expressed in terms fugacity as:

$$a_i = \frac{f_i}{f_i^o} \quad (159)$$

where f_i^o is the reference fugacity at 1 atm.

The fugacity of component i can be determined from the expression of the dimensionless fugacity coefficient:

$$\phi_i = \frac{f_i}{p_i} \quad (160)$$

where p_i is the component partial pressure in atm.

The component partial pressures were converted to molar concentrations using the expression:

$$p_{\mathrm{i}} = y_{\mathrm{i}} \cdot p_{\mathrm{total}} = \left(\frac{N_{\mathrm{i}}}{\sum N_{\mathrm{i}}}\right) p_{\mathrm{total}} \tag{161}$$

where y_{i} is the mole fraction of component *i*, p_{total} is the total pressure in atm, and N_{i} is the mole of component *i* in kmol.

By rearrangement of the Equations (159) to (161), the component activities can be expressed as:

$$a_{\mathrm{i}} = \phi_{\mathrm{i}} \cdot y_{\mathrm{i}} \cdot p_{\mathrm{total}} \tag{162}$$

The fugacity coefficients for all the components were determined using the expressions given by Ukpaka *et al.* [107]:

$$\phi_{\mathrm{H_2}} = \left(exp\left(exp(-3{,}802T^{0{,}125} + 0{,}541)p - exp(-0{,}1263T^{0{,}5} - 15{,}98)p^2 + \left(300\left(exp(-0{,}011901T - 5{,}941)\left(exp\frac{p}{300}\right)\right)\right)\right)\right) \tag{163}$$

$$\phi_{\mathrm{N_2}} = 0{,}93431737 + 0{,}2028538x10^{-3}T + 0{,}295896x10^{-3}p - 0{,}270727x10^{-6}T^2 + 0{,}4775207x10^{-6}p^2 \tag{164}$$

$$\phi_{\mathrm{NH_3}} = (0{,}1438996 + 0{,}2028538x10^{-3}T + 0{,}4487672x10^{-3}p - 0{,}1142945x10^{-5}T^2 + 0{,}276121x10^{-6}p^2) \tag{165}$$

The reaction rate equations for the reactants were determined using the stoichiometry of the reaction (155) to relate the individual rates of reactions as follows:

$$-r_{\mathrm{N_2}} = -\frac{1}{3}r_{\mathrm{H_2}} = \frac{1}{2}r_{\mathrm{NH_3}} \tag{166}$$

The molar concentrations of each component (Y_{i}) were expressed in terms of fractional conversion of the limiting reactant nitrogen (*X*) using the expressions given in Table 12. In

Table 12, expressions are developed by performing a mole balance on the ammonia synthesis converter. With this relation, it is possible to express the component activities in terms of fraction conversion of the limiting reactant nitrogen.

Table 12. Model stoichiometric relationships.

Component	Initial molar concentration [kmol/h]	Amount of reactant used/product produced	Exit molar concentration [kmol/h]	Mole fraction [y_i]
N_2	$FY_{N_2,0}$	$-FXY_{N_2,0}$	$F(Y_{N_2,0} - XY_{N_2,0})$	$\frac{Y_{N_2,0}(1-X)}{1-2XY_{N_2,0}}$
H_2	$FY_{H_2,0}$	$-3FXY_{N_2,0}$	$F(Y_{N_2,0} - 3XY_{N_2,0})$	$\frac{Y_{H_2,0} - 3XY_{N_2,0}}{1-2Y_{N_2,0}}$
CH_4	$FY_{CH_4,0}$	0	$FY_{CH_4,0}$	$\frac{Y_{CH_4,0}}{1-2XY_{N_2,0}}$
Ar	$FY_{Ar,0}$	0	$FY_{Ar,0}$	$\frac{Y_{Ar,0}}{1-2XY_{N_2,0}}$
NH_3	$FY_{NH_3,0}$	$2FXY_{N_2,0}$	$F(Y_{NH_3,0} + 2XY_{N_2,0})$	$\frac{Y_{NH_3,0} + 2YX_{N_2,0}}{1-2XY_{N_2,0}}$
Total		$\left(\sum_{i=1}^{5} Y_i\right) = F(1-2XY_{N_2,0})$		

The respective component activities were substituted into the rate expression Equation (156) to yield the reaction rate expression in terms of fractional conversion of the limiting reagent (nitrogen).

$$r_{NH_3} = 2k\left(K_a^2\phi_{N_2}\frac{Y_{N_2,0}(1-X)}{1-2XY_{N_2,0}}p\left[\frac{p\left(\phi_{H_2}\left(Y_{H_2,0}-3XY_{N_2,0}\right)\right)^3}{\left(1-2XY_{N_2,0}\right)\left(\phi_{NH_3}\left(Y_{NH_3,0}+2XY_{N_2,0}\right)\right)^2}\right]^{\alpha} - \left[\frac{\left(1-2XY_{N_2,0}\right)\left(\phi_{NH_3}\left(Y_{NH_3,0}+2XY_{N_2,0}\right)\right)^2}{p\left(\phi_{H_2}\left(Y_{H_2,0}-3XY_{N_2,0}\right)\right)^3}\right]^{1-\alpha}\right) \quad (167)$$

Substituting the reaction rate expression Equation (167) into the model Equations (171) and (172) gives the model equations in terms of fractional conversion of the limiting reactant nitrogen.

The reactor is modelled as PFR based on a pseudo-heterogeneous one-dimensional model for the reacting species by applying the principle of mass and energy on an elemental section (differential section) of the converter as shown in Figure 10.

The overall mass balance can be written in the following general form:

$$u\frac{dC_{N_i}}{dL} = \eta r_{N_i} \tag{168}$$

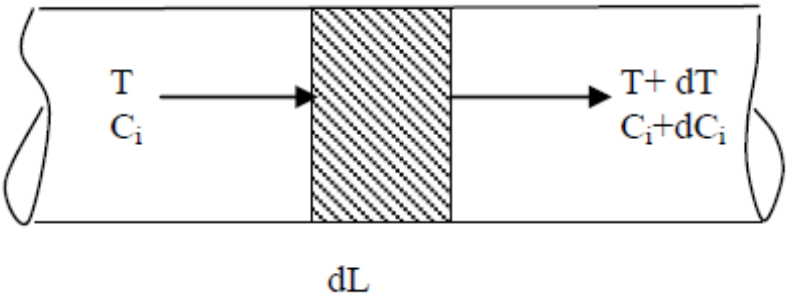

Figure 10. Elemental portion of the packed bed reactor.

The Equation (168) can be written for the limiting reactant (nitrogen) as:

$$u\frac{dC_{N_2}}{dL} = \eta r_{N_2} \tag{169}$$

where u is the velocity of gas in m/s, C_i is the molar concentration in the kmol/m^3, L is the length of the catalyst bed in m, r is the reaction rate, and η is the effectiveness factor.

The Equation (159) can be expressed in terms of nitrogen conversion X and initial flow rate $F_{N2,0}$ as follows:

$$\frac{dX}{dL} = -\eta\frac{r_{N_2}A}{F_{N_2,0}} \tag{170}$$

where X is the rate of the nitrogen conversion in %, $F_{N2,0}$ is the initial flow rate of nitrogen in kmol/h, and A is the cross-sectional area of the catalyst bed in m^2.

Equation (160) can be expressed in terms of ammonia production rate using the relationship given in Equation (157) by following expression:

$$\frac{dX}{dL} = \eta\frac{r_{NH_3}A}{2F_{N_2,0}} \tag{171}$$

The change in temperature of synthesis gas over a catalyst bed divided into infinitesimal length is defined as follows:

$$\frac{dT}{dL} = \eta \frac{(-\Delta H_r) r_{NH_3} A}{m C_{pmix}} \quad (172)$$

where m is the total mass flow rate in kg/h, (- ΔH_r) is the heat of reaction in kJ/kmol, T is the temperature in the ammonia synthesis converter in K, and C_{pmix} is the specific heat capacity of the gas mixture in kJ/kmol.

The specific heat capacity of the reactant gas mixture was obtained using the equation:

$$C_{pmix} = \sum_{i=1}^{n} y_i \cdot C_{pi} \quad (173)$$

where y_i is the mole fraction of component i, and C_{pi} is the specific heat capacity of component i in kJ/kmol.

The specific heat capacities of the components of the reactant gases were obtained according to the expression given by Gunorubon and Raphael [106]:

$$C_{pi} = 4{,}1884(a_i + b_i T + c_i T^2 + d_i T^3) \quad (174)$$

where a_i, b_i, c_i, and d_i are constants with values given in the Table 13.

Table 13. Coefficient for specific heat capacity of gas mixture [107].

Constants	Component			
	H_2	N_2	CH_4	Ar
a	6,952	6,903	4,750	4,9675
b x 10^2	-0,04567	-0,03753	1,2	-
c x 10^5	0,095663	0,193	0,303	-
d x 10^5	-0,2079	-0,6861	-2,63	-

The heat capacity of the ammonia (product) was obtained by the expression given by Elverse *et al.* [108]:

$$C_{pNH_3} = (6{,}5846 - 0{,}61251x10^{-2}T + 0{,}23663x10^{-5}T^{-2} - 1{,}5981x10^{-9}T^3 + 96{,}1678 - 0{,}067571p + (0{,}2225 + 1{,}6847x10^{-4}p)T + (1{,}289x10^{-4} - 1{,}0095x10^{-7}p)T^2) \quad (175)$$

The equation developed by Mahfouz *et al*. [109] was used to calculate the exothermic heat of reaction and the same is following:

$$\Delta H_r = \left(-\left(0{,}54426 + \frac{846{,}609}{T} + \frac{459{,}734x10^6}{T^3}\right)p - 5{,}34685T - 0{,}2525x10^{-3}T^2 + 1069197x10^{-6}T^3 - 9157{,}09\right) \quad (176)$$

Effectiveness factor which defines the effects of temperature and density of the catalyst interior and the difference between these parameters with those of the catalyst surface is given by the following general form:

$$\eta = b_0 + b_1T + b_2X + b_3T^2 + b_4X^2 + b_5T^3 + b_6X^3 \quad (177)$$

The values of effectiveness factor coefficients at different pressures are defined in Table 14.

Table 14. Coefficients of effectiveness factor at different pressures.

p [bar]	b_0	b_1	b_2	b_3	b_4	b_5	b_6
150	-17,539096	0,07697849	6,900548	-1,08279x10^{-4}	-26,42469	4,927648x10^{-8}	38,937
225	-8,2125534	0,03774149	6,190112	-5,354571x10^{-5}	-20,86963	2,379142x10^{-8}	27,88
300	-4,6757259	0,02354872	4,687353	-3,463308x10^{-5}	-11,28031	1,540881x10^{-8}	10,46

To calculate the pressure drop inside catalytic beds, Ergun relationship, according to Equation (41) has been applied.

The ammonia synthesis converter (105-D) contains about 70,65 m^3 of magnetite catalyst activated with K_2O, CaO, Al_2O_3, and MgO in the irregular shape with particle size 1,5 to 3,0 mm. The equivalent particle size is 1,38 mm, void fraction is 0,36 and the bulk density of the catalyst is 2300 kg/m^3. The first bed is the smallest and the same holds 13,75 m^3 with each succeeding bed containing a greater volume of the catalyst, namely the second bed holds 21,25 m^3, while the third bed holds 35,65 m^3. All three beds possess the same diameter of 2946 mm. The more detailed schematic drawing of the ammonia synthesis converter used in the model and in the ammonia reference plant is shown in Figure 11.

The main process parameters which influence the conversion efficiency are temperature, pressure, space velocity, H_2–to–N_2 molar ratio, the molar content of inert gases (Ar + CH_4), and synthesis gas rate. The most important controlling variables which can be changed to alter the

synthesis loop operation are synthesis feed gas rate, synthesis gas circulation rate, inert purge gas rate, converter bed temperature, converter feed gas temperature, H_2–to–N_2 molar ratio, and purity of feed gas.

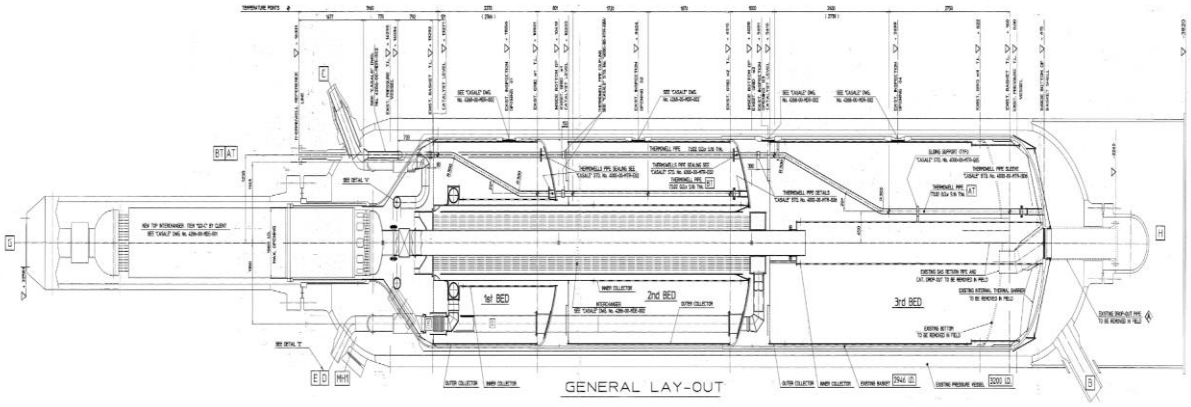

Figure 11. The detail schematic drawing of the ammonia synthesis converter (axial–radial design).

The refrigeration part of the ammonia synthesis unit with all system components was modelled based on the mass and energy conversation principles, according to the work of Mogaji [110].

Regarding all given steady–state flowsheets described in the previous sections, each part of the model with related process equipment was solved to get a satisfactory agreement with the real process data. The steady–state solution procedure uses modular operations, which are combined with a non–sequential algorithm. It means that the information is processed as soon as it is supplied. The results of any calculation are automatically propagated throughout the flowsheet, both forwards and backward. Material, energy, and composition balances are considered simultaneously. Pressure, flow, temperature, and composition specifications are considered equally. For example, a column overhead flow rate specification is replaced by a composition specification in the condenser. The column can solve with either specification.

Using all analyzed reaction rates, equilibrium equations, thermodynamic relationship, pressure drop relations, and assuming that the reactors can be modelled as a PFR and/or equilibrium reactor, a set of ODE's can be written to solve for the flux profile of each species occurring in the reaction scheme.

$$\frac{dF_{\mathrm{i}}}{dl} = r_{\mathrm{i}} \tag{178}$$

where F_{i} is the molar flux of species *i*, r_{i} is the rate of formation or disappearance of species *i* and *l* is the distance along the reactor.

The reaction rate equations are used with mass and heat balance to determine the temperature and the composition profile for each component as a function of reactor length in the catalyst zone. In addition, ODEs for pressure drop and energy balance are included to calculate the pressure and temperature profile along the reactor. Newton–Raphson and/or Euler technique of solving ODEs was used to getting a rapid convergence in order to determine the composition at the outlet of each of the mentioned reactors/converters. The technique uses previous values of the component outlet molar concentration ($d_{\mathrm{n\text{-}2}}$ and $d_{\mathrm{n\text{-}1}}$) to predict the value of the next calculation according to the following relationship:

$$d_{\mathrm{n-1}} = d_{\mathrm{n}} - \frac{(p_{\mathrm{n}} - p)}{(p_{\mathrm{n}} - p_{\mathrm{n-1}})}(d_{\mathrm{n}} - d_{\mathrm{n-1}}) \tag{179}$$

where *p* denotes the pressure of the components in the reacting mixture.

The iteration is repeated until the molar fraction calculation and reaction temperature will agree with the reference case values. Otherwise, a new assumption for the total molar flow rates of outlet gases is generated. The solution time in the model is directly connected with the number of iterations and solution method (*e.g.* ode23). Typically, it is expected that the solution time will increase with the higher number of iterations, which needs more computational time. The best fit between the model and process data for all relevant process parameters was achieved with the 10000 iterations. This number of iterations are proportional to the length of the catalyst in the reformer tube; therefore, the model parameters are calculated at each millimeter per catalyst bed length. The solution time for 10000 iterations is 30 seconds, which is again in excellent alignment with the industrial process data. This time was also used in all other reactors/converters and during the design phase of an advanced control structure in a closed–loop system.

All other parts of the process equipment (process streams, piping equipment, rotating equipment, separation operations, column) were adjusted according to recommendations from the UniSim Design R470 Operations Guide [111].

4.2.Calculation basis

In this part, the fundamental assumptions and limitations of the steady–state model have been considered. Besides that, a method of dynamic modelling has been given. In the end, details related to the control strategy design together with advanced ratio–cascade controller design have been explained.

4.3.Assumptions and limitations of steady-state model

Assumptions and limitations of the steady–state model are the following:

Assumptions

1. The basis for the fluid modelling is the Peng–Robinson equation of state (EOS);
2. All SMR tubes within the furnace are assumed to behave in the same way; the behavior of a set of tubes can be obtained by multiplying the behavior of one tube by the number of tubes in the set;
3. The system operates both in a steady–state and dynamic mode of operation;
4. A one–dimensional model for mass, heat, and momentum transfer has been used. This means that the composition, heat, and pressure are uniform at any cross section of the reactors/converters;
5. All hydrocarbons in the natural gas feed higher than methane are assumed to be instantly cracked into CH_4, CO_2, H_2, and CO. The reaction system inside a reformer tube is described by the kinetic expressions for SR1, SR2, and WGS reactions only;
6. The axial diffusion of mass and heat is negligible;
7. The system in all catalytic steps is heterogeneous, external mass and heat transfer resistance between the pellet and the bulk gas is negligible but the intraparticle diffusion resistance is considerable and cannot be neglected;
8. Outlet concentrations of the reaction mixture with related temperatures and pressures are available at all sampling instances;
9. The combustion gas is well mixed inside the reformer furnace, and its temperature is uniform;
10. The radiation heat transfer between reformer tubes is neglected;

11. The radial temperature profiles of reactors/converters are neglected, but the axial temperature changes are considered;
12. The initial conditions along each tube are the same as the boundary conditions on tube entrances;
13. Tube wall temperature data are measured by optic pyrometry and it was assumed that they are accurate between ±5^{o}C;
14. CH_4 reforming reaction with CO_2 (dry reforming) is neglected, because of very low intrinsic activity, unfavourable thermodynamics, small amounts of "pure" CO_2, and avoidance of carbon deposition which is in the model prevented with higher S/N.G. molar ratios;
15. Axial dispersion is neglected because the flow rate is sufficiently high to create a turbulent flow (Re>40);
16. Radial dispersion is neglected, because the reformer tubes/reactors/converters diameter are narrow, the reactor is adiabatic and the WGS and ammonia synthesis reaction are a moderately exothermic. Under these conditions, radial gradients of concentrations and temperatures are not important;
17. The heat and mass transfer and the diffusion in the catalyst were lumped in the rate constant;
18. Penetration of mass and heat is ignored, as the fluid velocity is very high in industrial scale;
19. Concentration and temperature on catalyst surface and bulk of gas are equal;
20. The effects of penetration resistance in catalyst, temperature gradient and catalyst inside concentration have been incorporated in the equations by an effectiveness coefficient for each of the catalyst.

Limitations

1. Impossibility to evaluate carbon forming potential with higher hydrocarbon feed streams, because of reasons that model converts these compounds to equivalent methane before any tube integrations take place. However, it is believed that from about 30% tube level down all higher hydrocarbons have been broken down. Carbon forming predictions from this point in the tube to the bottom are accurate;
2. The model does not provide any information about tube hot band problems. The model with the heat flux profile shows the region of the highest heat transfer, but nothing more as to the hot band formation;

3. All the SMR tubes within the furnace are assumed to behave in the same way. Of course, this is not true in actual conditions since the tubes close to the refractory brick wall are under different heat fluxes in comparison with the tubes in the middle part of the furnace. In order to compensate this non–uniformity set of simulations were performed and results are adjusted against real process data;
4. The model cannot predict tube wall temperatures and the same must be assumed or measured in the plant;
5. The model cannot provide any information about the hot spot and/or hot band problems regarding the reformer tube performance.

4.4.Dynamic modelling

The UniSim Design R470 steady–state model is embedded into a "lumped" dynamic model for all unit operations in an ammonia plant. If the x, y, and z gradients are ignored, the system is "lumped", and all physical properties are considered being equal in the segment. Only the time gradients are considered in such an analysis. This consideration allows that the process model can be described using ODEs. The lumped method gives a solution that is a reasonable approximation of the distributed model. With respect, that the "lumped" method gives enough reliability for describing the ammonia plant, the same was used in a model which served for designing the advanced control structure.

The approximation of the mass, component, and energy balances were taken into consideration to maintain the flowsheet requirements of the ammonia plant. The conservation of mass is defined by the following general relationship:

$$rate\ of\ accumuation\ of\ mass = mass\ flow\ into\ system - mass\ flow\ out\ of\ system$$

Component balances are calculated as follows:

$$rate\ of\ accumulation\ of\ component\ j = flow\ of\ component\ j\ into\ system\ -\ flow\ of\ component\ j\ out\ of\ system + (rate\ of\ formation\ of\ component\ j\ by\ reaction$$

The energy balance is determined as follows:

rate of accumulation of energy = flow of energy into system - flow of energy out of system + heat added to system across its boundary + heat generated by reaction - work done by system on surroundings

Based on all mentioned general balances for the main process streams, the ODE's are solved using the implicit Newton–Raphson and/or Euler method with maximum speed performance. Dynamic calculations are performed at three different frequencies: volume (pressure–flow), energy and composition. These relations are not solved simultaneously at every time step. The balances are solved at different time step frequencies. Pressure flow equations are solved at every time step while composition balances are solved at every 10^{th} time step. Since the composition changes much more gradually than the pressure, flow, or energy in a system, the equations associated with composition can be solved less frequently. An approximate flash is used for each pressure-flow integration time step. A rigorous flash is performed at every composition integration time step.

Holdup values of all process units (vessel volumes, pump heads, valves, heat exchangers, compressors, reactors, *etc*.) have been specified according to the detailed engineering design documentation of the reference ammonia plant and reconciled against actual process conditions to reflect the proper behaviour of the process. A holdup model is necessary because changes in the composition, temperature, pressure, or flow in an inlet process stream to a vessel with volume (holdup) are not immediately seen in the exit stream. The model predicts how the holdup and exit process streams of particular unit equipment respond to input changes to the holdup over time. Calculations included in the holdup model are material and energy accumulation, thermodynamic equilibrium, heat transfer, and chemical reactions. Process flows exiting from holdup are calculated from a resistance equation. In order to solve a resistance equation that realistically describes the ammonia production process, the characteristic parameters of unit equipment are defined according to the detailed engineering design documentation.

The assumptions of the holdup model are:

1. each phase is assumed to be well mixed;
2. mass and heat transfer occur between feed to the holdup and material in the holdup;
3. mass and heat transfer occur between phases in the holdup.

One recycles operator (logic operator) was added to the ammonia synthesis loop to predict how the holdup conditions change over time and to satisfy the primary requirement of the ammonia synthesis loop. The general relationship which describes the material accumulation is following:

$$material\ accumulation_{new} = material\ flow\ into\ system + material\ accumulation_{old}(recycle\ stream) - material\ flow\ out\ of\ system$$

The pressure and flow profiles of a dynamic flowsheet are calculated through the network of pressure nodes, which are conceived across the entire simulation case and the same are solved by a pressure–flow solver. A pressure–flow matrix is set up to solve required process variables. The pressure-flow matrix comprises volume balance equations, resistance equations, and pressure-flow specifications from the detailed engineering design documentation of the reference ammonia plant. In dynamic mode calculation, it is supposed that there is no accumulation of the mass in the process equipment:

$$V = Constant = f(w, h, p, T) \tag{180}$$

$$\frac{dV}{dt} = 0 \tag{181}$$

where V is the volume of the equipment in m^3, t is the time in hours, w is the mass flow rate in the kg/h, h is the holdup, p is the pressure in bar and T is the thermodynamic temperature in K.

The volume balance equation allows observation of the pressure effects in the vapour holdup because of disturbances in the feed which is used during the testing procedure of the control structure.

The resistance equations calculate flow rates from the pressure difference of the surrounding nodes based on the assumption of turbulent flow with the following form:

$$w = k\sqrt{\Delta p} \tag{182}$$

where *w* is the mass flow rate in kg/h, *k* is the conductance, which is a constant representing the reciprocal of resistance to flow, and Δp is the frictional pressure loss, which is the pressure drop across the unit operation without static head contributions.

Valves, pumps, compressors, columns, and heat exchangers have a resistance equation associated with them, and the same is specified in their specification tabs inside the dynamic flow sheet.

The number of pressure–flow specifications that need to be provided is defined by the degrees–of–freedom analysis. The modelled dynamic flow sheet in total comprises 1245 equations. The total number of material streams is 134, the number of energy streams is 44, and the number of unit operations is 134. According to this, the total number of pressures–flow variables is 490 as follows:

134 material streams x 2 + 44 energy streams x 2 + 134 unit operations x 1 = 490 pressure – flow variables

With 490 variables to solve for in the network and 1245 available equations, the degrees of freedom of this network are 755. Therefore, 755 variables need to be specified to define this system. This is the same number of flowsheet boundary streams. These 755 variables were taken from the detailed engineering design documentation and the actual process parameters of the reference ammonia plant.

Control valves and actuators are modelled in instantaneous mode. The assumption is that the actuator moves instantaneously to the desired position defined by the controller output. The equation defining this relationship is:

$$Act\% = Act_{Desired}\% \tag{183}$$

Rating information for the valve operation includes the valve type, *C*v value, and the pressure drop over the valve.

Heat exchanger dynamics are specified by pressure drop and temperature difference.

The separators are specified by the volume of the vessel, boot capacity, nozzle location, and inlet pressure and flow.

The condensers are specified by vessel volume, boot capacity, nozzle location, inlet flow stream, overhead vapour stream, outlet liquid stream, and with inlet pressure and flow.

The absorber and stripper columns are defined by tray diameter, weir length, weir height, and tray spacing. Pressure and temperature specifications are defined for the liquid product stream leaving the bottom of the column and for the vapour product of the columns. Flow specifications for the feed stream are also defined. Compressors are defined by the pressure rise based on the inlet pressure value and by the inlet flow value. Mixers and tees are defined by pressures and resistance through the flow sheet according to which the flow to and from these operations are calculated. The reformer tubes/reactors/converters are defined by the characteristics of each catalyst, type of the reactions, and inlet specifications for the flow composition, temperature, and pressure.

4.5.Control strategy design

From the previous discussion, it can be concluded that the ammonia plant is a complex system that comprises different unit operations mutually interlinked and with a strong interdependency. Regarding this complexity, it is necessary to have the control possibility to attain maximum production efficiency for the minimum feedstock and energy input and to minimize operator interventions. One approach to guarantee the entire plant is continually working within the best process conditions is to execute a continuous optimization that can control main process parameters. The final result is an improvement of the plant's key performance and economic indicators.

Regarding the literature review, so far, all the practical and already proven control solutions are primarily concentrated on single control schemes in isolated parts of the ammonia production process with a special emphasis on the SMR process unit [5, 11-12]. As per the literature findings, the best accomplishment until now is the arrangement in the shape of an integrated module for the management of interactions and constraints control between different independent modules to control the front–end of the ammonia plant [11]. A couple of control schemes were proposed as APC control techniques by the implementation of PI and PID controllers [5, 13-14]. Implementation of the APC control strategy with subsequent MPC techniques specifically related to different SMR units has been also proposed in the literature [64-67]. All of them have been shown different benefits and control mechanisms against the dynamic relationship between the temperature of the reformed gas or the reforming tube wall temperatures (process outputs) and manipulated variables and disturbances (process inputs). The main constraints of proposed control strategies are difficulties in reliable and accurate measurement of the reforming tube wall temperatures, which is the key variable of the complete

system. Recently, Wu *et al.* [64] demonstrated the development of a computationally efficient closed–loop system with the MPC where a computational fluid dynamics (CFD) process model is used to represent the process behaviour. The CFD model is based on the single reformer tube to control the hydrogen production and to obtain a desired dynamic response. One of the fundamental assumptions of the above–mentioned work is that the outer reforming tube wall temperature can be directly controlled. Besides that, Tran *et al.* [68] introduced a new furnace–balancing scheme which is based on an optimizer, that is formulated as an optimization problem within which the valve position distribution is the decision variable. By minimization of the weighted squared sum deviations of the outer reforming tube wall temperatures from a set point for all reforming tubes, they proposed a penalty term on the deviation of the valve positions from their fully open positions as the objective function. Considering multiple reformer tubes (in average between 300 and 500) and the high possibility to have different temperature profiles inside of radiation section of the top–fired steam reformer (different temperatures between the sidewalls and the central part) it can be concluded that the main challenge is application of appropriate and reliable measurement device (extremely harsh temperature conditions) for temperature readings of the main controlled variable.

Another part that covers only the ammonia synthesis loop and has the most influence on the further development of the APC structures are works by Araújo and Skogestad [16] and Luyben [15]. These works are based on the PWC theory and heuristic approach.

However, the use of PID to control such complex systems has not yet been fully explored [5, 13-14], especially the control structures that exhibit higher levels of performance like a combination of feedforward, feedback, ratio, and cascade controllers.

To overcome this limitation and to achieve better control of the whole ammonia plant a novel approach based on the first–principal plant model with the background of actual process industrial data was proposed. It describes a dynamic relationship between the two parts of the ammonia plant front–end (synthesis gas preparation and purification) and ammonia synthesis loop. On the front–end of the ammonia plant, the APC control structure is based on control of SMR by methane slip which is one of the key process outputs and it can be reliably and accurately measured by the standard industrial gas chromatograph. The proposed approach is based on an optimization strategy for manipulating heat release on the burners at different locations in the reformer box to provide smooth heat flux profiles that can prolong reformer tube lifetime and uniform value of methane slip. The major goals are to achieve maximum selectivity and activity of the installed catalyst and to keep the optimal temperature profile of

the reformer tubes with higher hydrogen conversion. To achieve maximum production efficiency the present work demonstrates, for the first time, the assembly of a discrete computationally efficient closed–loop system with the additional feature of the gain–scheduled structure. The design of the gain–scheduled structure was derived according to the high–fidelity data–driven discrete–time linear model based on dynamic closed–loop simulation results. The linear model computes optimal temperature trajectory for a waste gas in the reformer furnace and accounts for the temperature limitations of the reforming tube to achieve fast control of methane slip regarding higher hydrogen production efficiency. Three typical process conditions of S/N.G. molar ratios (3,0; 3,3, and 3,6) are characterized by gain–scheduling to assure that the methane slip values approach their set point faster than under the standard control. The production process can satisfy higher conversion of hydrogen and closely keep safety concerns related to the lifetime of the reformer tubes. The additional benefit can be achieved for older installations with higher S/N.G. molar ratios to safely elevate energy efficiency.

Further improvement of the ammonia plant control was achieved by the implementation of feedforward, ratio, and cascade techniques, with possibility for disturbance rejection. Another important process variable during ammonia production is the air volume flow rate into the secondary reformer unit. By control of the airflow, the H_2–to–N_2 molar ratio is determined. This molar flow is one of the most influencing process variables in the ammonia synthesis loop unit. To control H_2–to–N_2 molar ratio, another controller was designed according to the molar ratio between the natural gas feedstock and the air for the secondary reformer. The third controller controls the molar ratio between the ammonia production rate and natural gas feedstock. Combination of all benefits given by feedforward, feedback, ratio, and cascade control techniques in relation with three controllers enables optimization and maximum throughput of the ammonia plant. Master controller manipulates the ammonia production rate by a ratio controller in charge of keeping the molar ratio between the ammonia production rate and natural gas flow rate. Finally, advanced strategy delivers the maximum ability to reject process disturbances.

4.5.1. Advanced ratio–cascade controller design

Based on dynamic simulation and analysis, which takes into account process data from the reference ammonia plant, the list of manipulated and controlled variables (MVs/CVs) was identified and shown in Table 15.

According to MVs/CVs list, the control matrix for the ammonia plant is determined and mutual relationships are shown in Table 16. The boxes marked "+" (green colour) indicates that the increase of MVs will increase the value of CVs (direct acting), a "- "sign (red colour) indicates that the increase of MVs will decrease the value of CVs (reverse acting), and "x" sign (yellow colour) indicates no relationship is used.

The relationship between various MVs and CVs was determined based on industrial practice and observation during the normal operation of the ammonia plant (reference case).

Table 15. List of manipulated and controlled variables (MVs/CVs) used in the model.

Name	Manipulated variables	Unit	Name	Controlled Variables	Unit
MV1	Natural gas flow to primary reformer	m^3/h	CV1	Steam – to – natural gas molar ratio	-
MV2	Steam flow to primary reformer	t/hr	CV2	Primary reformer outlet temperature	^oC
MV3	Fuel flow to primary reformer	m^3/h	CV3	CH_4 slip after primary reformer	mol. %
MV4	Air flow to secondary reformer	m^3/h	CV4	H_2/N_2 ratio after secondary reformer	-
MV5	Temperature in HT WGS reactor	^oC	CV5	CO slip after HT WGS reactor	mol. %
MV6	Temperature in LT WGS reactor	^oC	CV6	CO slip after LT WGS reactor	mol. %
MV7	Volume flow of Benfield solution	m^3/h	CV7	CO_2 slip after absorber overhead	mol. %
MV8	Synthesis gas flow in 1st bed of ammonia convertor	m^3/h	CV8	Temperature in 1st bed of ammonia convertor	^oC
MV9	Synthesis gas flow in 2nd bed of ammonia convertor	m^3/h	CV9	Temperature in 2nd bed of ammonia convertor	^oC
MV10	Synthesis gas flow in 3rd bed of ammonia convertor	m^3/h	CV10	Temperature in 3rd bed of ammonia convertor	^oC
MV11	Purge flow gas	m^3/h	CV11	Inert (CH_4 + Ar) molar concentration	^oC
			CV12	Ammonia product rate	metric tons/h

Table 16. Ammonia plant control matrix with mutual relationships between MVs and CVs.

MV/CV	MV1	MV2	MV3	MV4	MV5	MV6	MV7	MV8	MV9	MV10	MV11
CV1	-	+	x	x	x	x	x	x	x	x	x
CV2	-	-	+	x	x	x	x	x	x	x	x
CV3	+	-	-	x	x	x	x	x	x	x	x
CV4	-	-	x	-	x	x	x	x	x	x	x
CV5	+	-	-	-	-	x	x	x	x	x	x
CV6	+	-	-	-	-	-	x	x	x	x	x
CV7	+	-	x	x	+	+	-	x	x	x	x
CV8	x	x	x	x	x	x	x	-	x	x	+
CV9	x	x	x	x	x	x	x	-	-	x	+
CV10	x	x	x	x	x	x	x	-	-	-	+
CV11	+	-	-	+	x	x	x	x	x	x	-
CV12	+	+	x	+	+	+	x	+	+	+	-

According to the list of MVs/CVs and related control matrix a control structure is identified which uses feedforward, feedback, ratio and cascade control schemes for disturbance rejection. The proposed control structure is shown in Figure 12.

As it can be seen from Figure 12 the control structure comprises the three molar ratio controllers, S/N.G. molar ratio, H_2–to–N_2 molar ratio, and NH_3–to–natural gas molar ratio. In all three controllers, it can be recognized two streams where one stream is a "wild" stream (disturbance) and it is desirable to maintain the flow rate of another stream at a constant ratio to the "wild" stream. In S/N.G. molar ratio controller the "wild" stream is the natural gas volume flow, in the H_2–to–N_2 molar ratio controller the "wild" stream is the air volume flow rate, while in the NH_3–to–natural gas molar ratio the "wild" stream is the natural gas volume flow rate .

The main raw materials for ammonia production are natural gas (the source of H_2) and air (the source of N_2) and these two present the process parameters which must be appropriately controlled to achieve as much as possible stable throughput of production capacity. At the same time, natural gas is under the influence of quality composition and also under the influence of pressure changes because of fluctuations in the outside natural gas grid which must be rejected. The air volume flow is under the influence of atmospheric temperature fluctuations (day/night and seasons) which significantly influence the air density fluctuations and subsequently to the amount of N_2 needed for ammonia synthesis. Consequently, these changes must be appropriately rejected with the help of an adequate controller.

According to consecutive chemical reactions in an ammonia plant, the overall reaction of syngas and ammonia production based on the reforming of methane is given by the following expression:

$$CH_4 + 0{,}358O_2 + 1{,}333N_2 + 1{,}395H_2O \rightarrow 1{,}055CO_2 + 1{,}333N_2 + 4H_2 \rightarrow 1{,}055CO_2 + 2{,}667NH_3$$

This general stoichiometry for ammonia production brings the following ideal molar ratios between NH_3 –to–CH_4 = 2/0,75 = 2,667 and AIR–to–CH_4 = 0,641/0,375 = 1,709, respectively, shown in Figure 13.

To achieve full nameplate capacity at the level of 56666 kg/h of liquid ammonia in actual conditions, it is needed 34440 Nm^3/h of natural gas (mainly CH_4), 99 t/h of 40 bar steam (S/N.G. molar ratio = 3,6), and 49430 Nm^3/h of air. Regarding these values the following molar ratios are achieved: NH_3–to–natural gas = 3326,48/1530,03 = 2,174 and AIR–to–natural gas = 2205,32/1530,03 = 1,441, respectively. The purge gas rate was at the level of 8000 Nm^3/h which insures the inert gas (CH_4 + Ar) molar concentration in the synthesis loop at the level of 13,50

mol.% per dry basis. The S/N.G. molar ratio of 3,6 insured the methane slip molar concentration of 10,25 mol.% per dry basis at the outlet of the reformer tubes with hydrogen conversion of 65,54%. At the same time, the methane slip molar concentration at the outlet of the secondary reformer is 0,256 mol.% per dry basis. The temperature of the reformer tube skin is 983^{o}C which keeps the reformer tube material in the safe temperature range preventing any damages regarding the effect of creep damage and stress–to–rupture.

These molar ratios were used as molar ratios for ammonia–to–natural gas and air–to–natural gas in the proposed advanced ratio and cascade control system as the main control variables. The main manipulated variables were natural gas volume flow rate and steam mass rate to the steam reforming and air volume flow rate to the secondary reformer.

The objective of the molar ratio control is to maintain the molar ratio of two process variables as a specified value. There are two alternatives to control the molar ratio shown in Figure 14 and the same are:

1. the flow rate between two streams is calculated and sent to ratio controller;
2. the flow rate of the "wild" stream is measured and multiplied by the desired ratio to determine the set point for the other process stream flow rate.

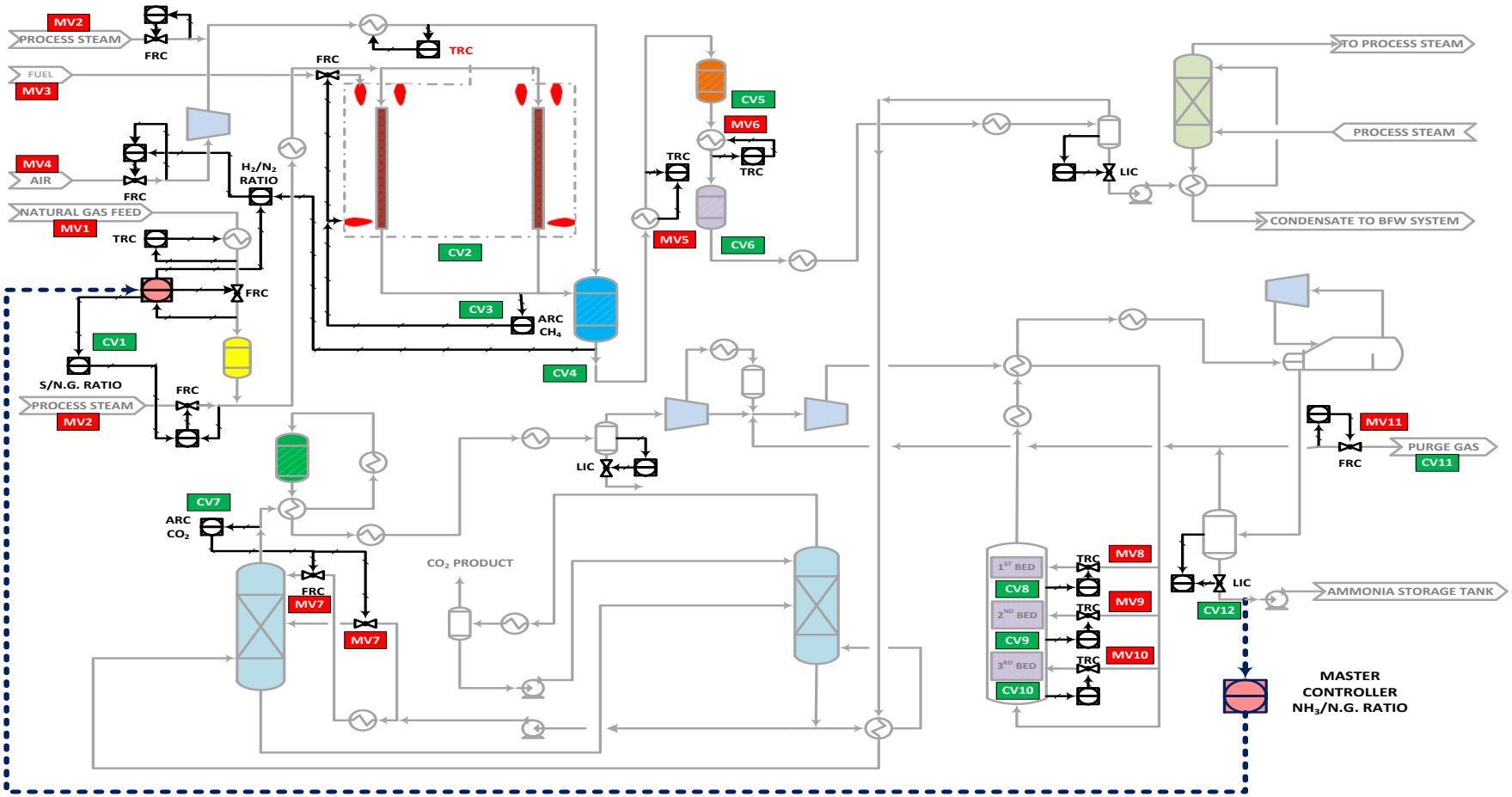

Figure 12. Ammonia plant flowsheet with control structure and list of MVs and CVs.

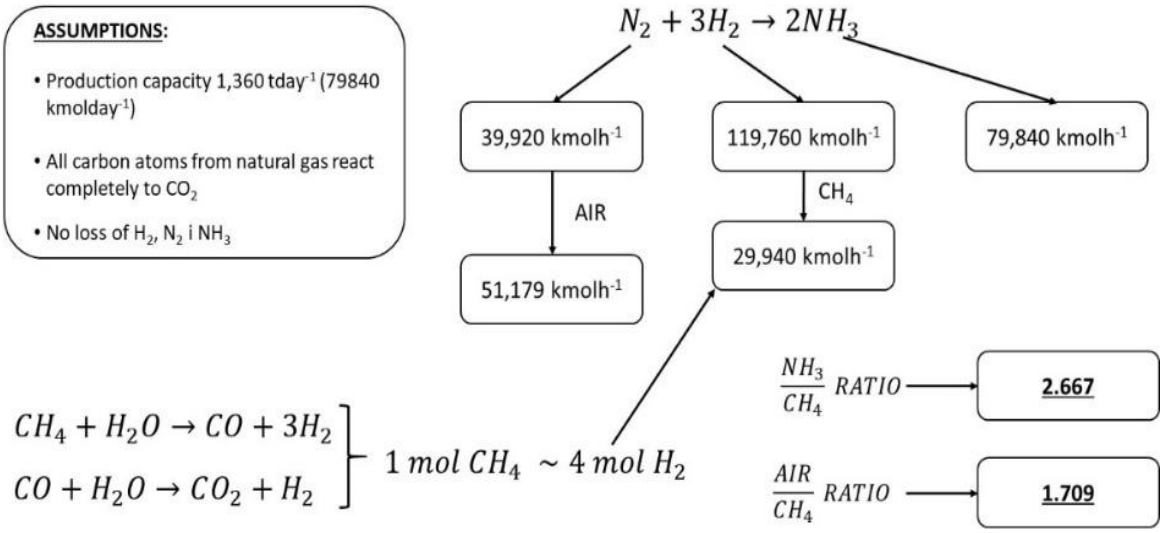

Figure 13. Ideal stoichiometry ratios between ammonia–to–methane and air–to–methane during ammonia production.

In direct control, the two process variables (usually flow rates), a manipulated variable *u*, and disturbance variable *d* are in the following relationship and according to this, the ratio is controlled rather than the individual variables:

$$Ratio = \frac{u}{d} \tag{184}$$

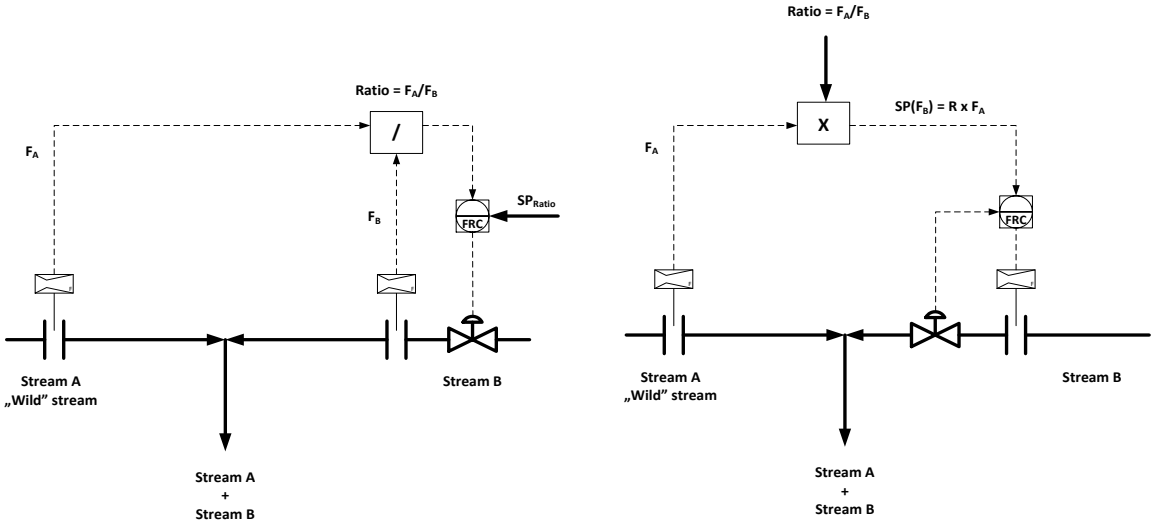

Figure 14. Direct and indirect ratio control.

A key disadvantage of direct control is that a divider element must be included in the control loops, and this element makes the process gain vary in a nonlinear fashion. From Equation (184), the process gain in direct control is following:

$$K_{\mathrm{p}} = \left(\frac{\partial Ratio}{\partial u}\right)_d = \frac{1}{d} \tag{185}$$

where d is the disturbance flow rate [112, 119].

Indirect ratio control is favoured over direct control since it results in a linear input–output relationship. The relationship between the manipulated input (valve position, related to F_{B}) and the measured output (F_{B}) for the flow controller in indirect control is following:

$$y = F_{\mathrm{B}} = u \tag{186}$$

so, the gain is:

$$K_{\mathrm{p}} = \frac{\partial y}{\partial u} = 1 \tag{187}$$

which is constant.

Stream A represents the natural gas flow or the ammonia production rate, while stream B is either steam flow or air flow in the S/N.G. controller and air–to–natural gas controller (H_2–to–N_2 molar ratio) or natural gas flow in the master controller which is in charge of the ammonia–to–natural gas molar ratio. The mixed stream could also have a composition or product property measurement and control; the output of this controller would be cascaded to the ammonia production rate in the proposed advanced control structure.

Feedforward control uses the measurement of an input disturbance to the plant as additional information for enhancing single–loop PID control performance. This measurement provides an "early warning" that the controlled variable will be upset sometime in the future. With this warning, the feedforward controller adjusts the manipulated variable before the controlled variable deviates from its set point. This feature of the feedforward technique is used for control of the main streams in the controller for controlling the “wild” streams of the volume flow of natural gas in the S/N.G. molar ratio controller, air volume flow rate in the air–to–natural gas stream and ammonia production rate in the ammonia–to–natural gas controller.

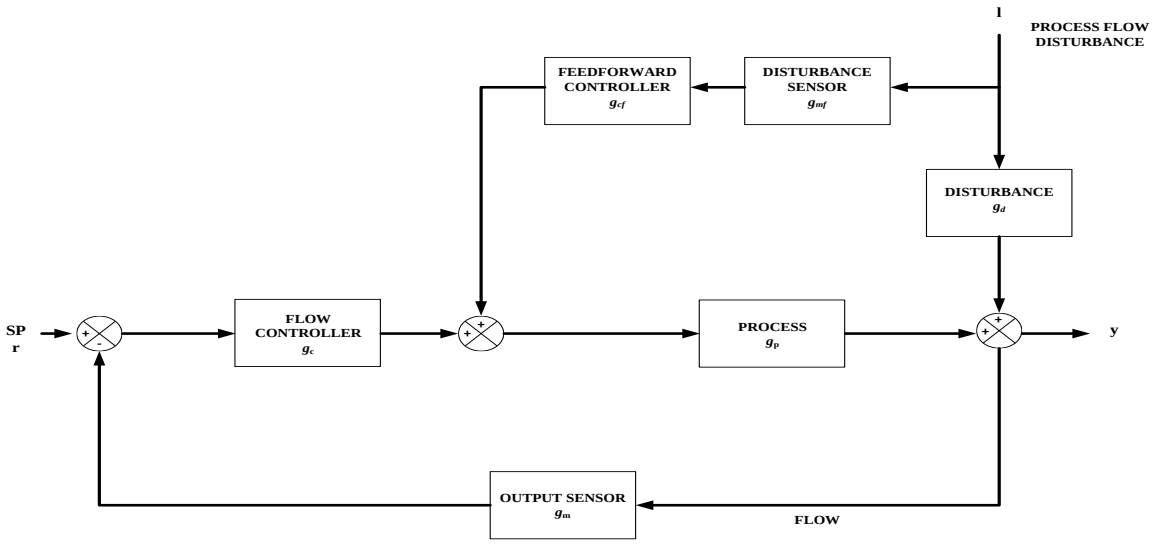

Figure 15. Feedforward block diagram.

Considering the feedforward block diagram shown in Figure 15, the closed–loop transfer function was developed by using the following steps:

$$y(s) = g_{\mathrm{d}}(s)l(s) + g_{\mathrm{p}}(s)u(s) = g_{\mathrm{d}}(s)l(s) + g_{\mathrm{p}}(s)[u_{\mathrm{f}}(s) + u_{\mathrm{c}}(s)] \quad (188)$$

$$y(s) = g_{\mathrm{d}}(s)l(s) + g_{\mathrm{p}}(s)[g_{\mathrm{cf}}(s)g_{\mathrm{mf}}(s)l(s) + g_{\mathrm{c}}(s)(r(s) - g_{\mathrm{m}}(s)y(s))] \quad (189)$$

$$y(s) = \left[g_{\mathrm{d}}(s) + g_{\mathrm{p}}(s)g_{\mathrm{cf}}(s)g_{\mathrm{mf}}(s)\right]l(s) + g_{\mathrm{p}}(s)g_{\mathrm{c}}(s)r(s) - g_{\mathrm{p}}(s)g_{\mathrm{c}}(s)g_{\mathrm{m}}(s)y(s) \quad (190)$$

Rearranging, to solve for *y(s)* it can be find:

$$\left(1 + g_{\mathrm{p}}(s)g_{\mathrm{c}}(s)g_{\mathrm{m}}(s)\right)y(s) = \left[g_{\mathrm{d}}(s) + g_{\mathrm{p}}(s)g_{\mathrm{cf}}(s)g_{\mathrm{mf}}(s)\right]l(s) + g_{\mathrm{p}}(s)g_{\mathrm{c}}(s)r(s) \quad (191)$$

or

$$y(s) = \frac{g_{\mathrm{d}}(s)+g_{\mathrm{p}}(s)g_{\mathrm{cf}}(s)g_{\mathrm{mf}}(s)}{1+g_{\mathrm{p}}(s)g_{\mathrm{c}}(s)g_{\mathrm{m}}(s)}l(s) + \frac{g_{\mathrm{p}}(s)g_{\mathrm{c}}(s)}{1+g_{\mathrm{p}}(s)g_{\mathrm{c}}(s)g_{\mathrm{m}}(s)}r(s) \quad (192)$$

Equation (192) is the closed–loop relationship for feedforward/feedback control. The stable feedforward controller does not affect the closed–loop stability, since the feedforward

controller transfer function does not appear in the closed–loop characteristic equation (denominator polynomial).

In case that there is no setpoint change (*r(s)* = 0), the output variable will no change, so the *y(s)* = 0. This condition in Equation (192) can be obtained only if the following relationship is achieved:

$$g_{\mathrm{d}}(s) + g_{\mathrm{p}}(s)g_{\mathrm{cf}}(s)g_{\mathrm{mf}}(s) = 0 \tag{193}$$

In this expression, all the transfer functions are determined for a particular system, except for the feedforward controller, $g_{\mathrm{cf}}(s)$. Solving Equation (193) for $g_{\mathrm{cf}}(s)$, the following expression is valid:

$$g_{\mathrm{cf}}(s) = -\frac{g_{\mathrm{d}}(s)}{g_{\mathrm{p}}(s)g_{\mathrm{mf}}(s)} \tag{194}$$

In case of simplification that the disturbance measurement has no dynamics, then Equation (194) becomes:

$$g_{\mathrm{cf}}(s) = -\frac{g_{\mathrm{d}}(s)}{g_{\mathrm{p}}(s)} \tag{195}$$

Equation (195) requires the inverse of the process model, so there will be problems if the process model has right half plane (RHP) zeros, or if the process overall lag is greater than the disturbance time delay.

The first-order process and disturbance transfer functions can be defined as:

$$g_{\mathrm{p}}(s) = \frac{K_{\mathrm{p}}}{\tau_{\mathrm{p}}s+1} \tag{196}$$

$$g_{\mathrm{d}}(s) = \frac{K_{\mathrm{d}}}{\tau_{\mathrm{d}}s+1} \tag{197}$$

According to the Equations (196) and (197) and Equation (195) the feedforward controller is defined as:

$$g_{\mathrm{cf}}(s) = -\frac{\frac{K_{\mathrm{d}}}{\tau_{\mathrm{d}}s+1}}{\frac{K_{\mathrm{p}}}{\tau_{\mathrm{p}}s+1}} = -\left(\frac{K_{\mathrm{d}}}{K_{\mathrm{p}}}\right)\frac{\tau_{\mathrm{p}}s+1}{\tau_{\mathrm{d}}s+1} \tag{198}$$

Following the proposed structure given in Figure 12 and considering the benefits of the ratio and feedforward control structures given in Figures 14 and 15, a detailed control structure represented by transfer functions was developed as shown in Figure 16. This advanced control structure adds the benefits of the cascade control technique. In the proposed solution, the primary control variable is the ammonia production rate, which is cascaded from the outer control loop to the inner control loops. The outer loop controls ammonia production rate by NH_3–to–natural gas molar ratio controller (gc1 – controller transfer function), while two inner loops control by S/N.G. molar ratio controller (gc2 – controller transfer function) and by air–to–natural gas molar ratio controller (gc3 – controller transfer function).

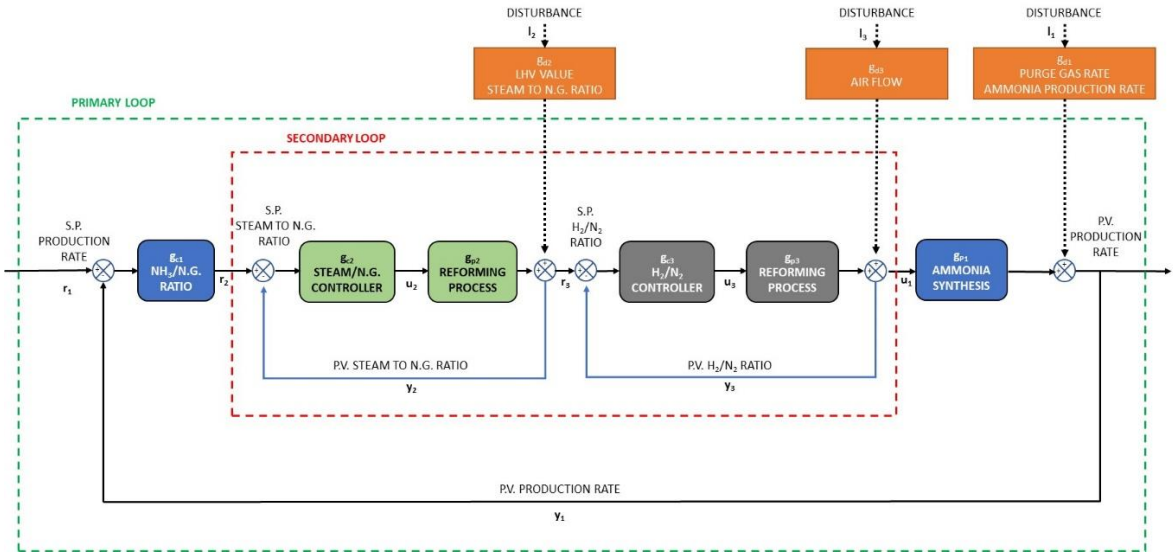

Figure 16. Advanced ratio–cascade control structure in ammonia production.

g_{p1}, g_{p2} and g_{p3} represent the process transfer functions, g_{d1}, g_{d2} and g_{d3} denotes disturbance transfer functions, *r* is the respective setpoint (reference signal), *u* is the manipulated input (also known as the controller output), *l* is the load (disturbance) input, while *y* is the process output (also known as the controlled variable or process variable).

The secondary outputs (y_2 and y_3) of the two inner-loops for control of S/N.G. molar ratio (Equation 199) and air–to–natural gas ratio (Equation. 200) can be defined as:

$$y_2(s) = \frac{g_{c2}(s)g_{p2}(s)}{1+g_{c2}(s)g_{p2}(s)} r_2(s) + \frac{g_{d2}(s)}{1+g_{c2}(s)g_{p2}(s)} l_2(s) \quad (199)$$

$$y_3(s) = \frac{g_{c3}(s)g_{p3}(s)}{1+g_{c3}(s)g_{p3}(s)} r_3(s) + \frac{g_{d3}(s)}{1+g_{c3}(s)g_{p3}(s)} l_3(s) \quad (200)$$

The secondary closed–loop transfer functions of the two inner–loops for control of S/N.G. molar ratio (Equation 201) and air–to–natural gas molar ratio (Equation 202) with feedforward characteristics can be defined as:

$$g_{c2cl}(s) = \frac{g_{c2}(s)g_{p2}(s)}{1+g_{c2}(s)g_{p2}(s)} \quad (201)$$

$$g_{c3cl}(s) = \frac{g_{c3}(s)g_{p3}(s)}{1+g_{c3}(s)g_{p3}(s)} \quad (202)$$

The primary output (y_1) of the outer loop for control of ammonia production capacity (t/h) by ammonia–to–natural gas molar ratio controller is:

$$y_1(s) = y_2(s)g_{p1}(s) + y_3(s)g_{p1}(s) + g_{d1}(s)l_1(s) \quad (203)$$

The following transfer function is used for the design of the outer controller in charge of ammonia production by ammonia–to–natural gas molar ratio:

$$g_{p1,eff}(s) = g_{c2cl}(s)g_{p1}(s) + g_{c3cl}(s)g_{p1}(s) \quad (204)$$

The closed–loop relationship for a primary set point change is given by following equation:

$$y_1(s) = \frac{g_{c1}(s)g_{p1,eff}(s)}{1+g_{c1}(s)g_{p1,eff}(s)} r_1(s) = \frac{g_{c1}(s)g_{c2cl}(s)g_{p1}(s)+g_{c1}(s)g_{c3cl}(s)g_{p1}(s)}{1+g_{c1}(s)g_{c2cl}(s)g_{p1}(s)+g_{c1}(s)g_{c3cl}(s)g_{p1}(s)} r_1(s) \quad (205)$$

From Equation (205) it is clear that two secondary closed–loop transfer functions affect the primary control loop. The secondary control loops are much faster than the primary loop, so that g_{c2CL} = 1 and g_{c3CL} = 1 (on a relative time scale to the primary control loop), then the closed–loop transfer function for the primary loop is:

$$y_1(s) \approx \frac{2g_{c1}(s)g_{p1}(s)}{1+2g_{c1}(s)g_{p1}(s)} r_1(s) \quad (206)$$

For controllers arranged in series the controller transfer function is defined as:

$$g_c(s) = K_c \left(\frac{\tau_I s+1}{\tau_I s}\right)\left(\frac{\tau_D s+1}{\tau_F s+1}\right) \quad (207)$$

where K_c denotes proportional gain, τ_I is the integral time constant, τ_D is the derivative time constant and τ_F is the filter time constant.

The manipulated input was defined as:

$$u(s) = K_c \left(\frac{\tau_I \tau_D s^2+\tau_I s+1}{\tau_I s}\right) e(s) \quad (208)$$

where *e* represents the error (setpoint–measured process output) defined with following expression:

$$e(t) = \bar{x}_{S.P.} - \bar{x}_{P.V.}(t) \quad (209)$$

where *t* denotes current time in s, while *e(t)* is the error between a measured/controlled process variable (P.V.) and its set point value (S.P.).

In order to design advanced ratio and cascade control structure, data–driven modelling was used to derive a linear model from UniSim Design R470 flow sheet simulation results. The preliminary design of the controllers was determined according to general guidelines given in UniSim Design R470. Different control loops were selected from the dynamic model behavior and analyses were performed.

Parameters of the controllers were estimated by built-in Auto Tuning Variation (ATV) technique [111] with the following auto tuner parameters:

- α (ratio T_i/T_d) = 4,50;
- β (gain ratio) = 0,25;
- φ (phase angle) = 60,0;

- h (relay hysteresis) = 0,1%
- a (relay amplitude) = 5,00%.

In the present version of the UniSim Design software, the above–mentioned auto tuner parameters are default values specified for the PID tuning. These tuning parameters have been optimized for a quarter decay ratio error criterion. However, there is no single correct way to define the same, and the same has been chosen as the starting values and should not be treated as a catholicon [111]. Based on these approximate parameters, the further adjustment of controllers has been conducted in MATLAB by System Identification Tool and Control System Designer.

The tuning parameters were calculated according to equations given in Table 17, while their relationship is shown in Figure 17.

Table 17. ATV stability limit parameters.

Tuning parameter	Equation
Ultimate gain	$K_u = \frac{4h}{\pi a}$
Ultimate period	P_u = period taken from limit cycle
Controller gain	$K_\mathrm{c} = \frac{K_\mathrm{u}}{3,2}$
Controller integral time	$T_\mathrm{i} = 2,2P_\mathrm{u}$

A tightly tuned or aggressive controller gives an excellent performance but is not robust to process changes. It could become unstable if working conditions change. A sluggishly tuned controller delivers poor performance, but is very robust. It is less likely to become unstable [111, 119].

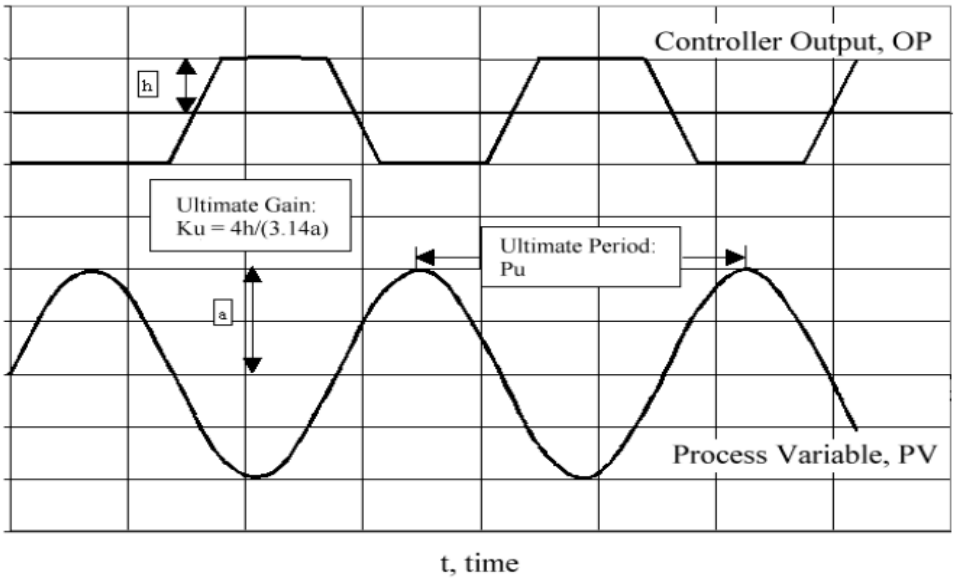

Figure 17. ATV stability limit parameters.

Finally, the controller parameters were fine–tuned until the process response of the closed–loop system appears to be critically damped. The fine–tuning was performed in MATLAB by System Identification Tool and Control System Designer. System Identification Tool was used for the determination of the transfer functions based on step response tests and linear dynamic model (performed in dynamic UniSim Design R470 flowsheet). Following process streams were tested: natural gas flow rate and steam mass flow rate (primary SMR unit), airflow rate (secondary SMR unit), and ammonia production rate. According to the linear dynamic model and step response test results, the discrete transfer functions with the input/output response were determined for the secondary/slave and primary/master controllers.

Based on the dynamic plant model and calculated transfer functions for each PID controller the Control System Designer in MATLAB was used for the final tuning of the stability parameters. Performance requirements were analyzed in terms of step response and root locus editors to satisfy the maximum allowed overshoot percentage, rise and settling time, and an oscillation frequency to be able to optimally control the ammonia plant process in actual conditions. The overshoot percentage, rise and settling time, and oscillation frequency are adjusted by changing the pole and zero locations in the root locus editor which finally drives to adequate PID controller design. The objective of controller design is to provide a reasonable compromise between performance and robustness in the closed–loop response. According to design performance requirements, the final control structure was tested and validated in SIMULINK. The overall designing approach is shown in Figure 18.

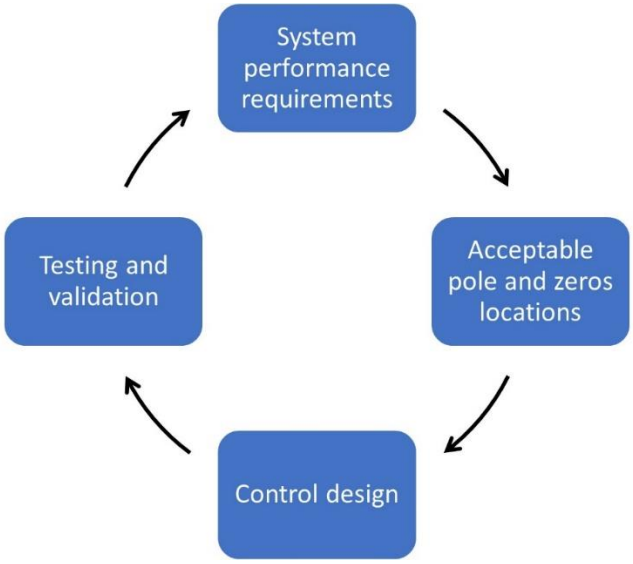

Figure 18. The overall designing approach.

5. RESULTS AND DISCUSSION

5.1. Stability tuning parameters determination and tuning of the advanced ratio–cascade control system

As was mentioned in the introduction, the focus of this thesis was how to compensate for measuring disturbances that affect the ammonia production rate to achieve production with minimum raw material and energy consumption. Based on reliable steady–state and dynamic models, an adequate control strategy could be designed.

Regarding practical solutions for the control structure, the first objective was the development of steady–state and dynamic reliable models, that can identify process variables having the greatest effect on the stability, quality, and profitability of the ammonia plant based on operational experience. The design of the control structure is based on data–driven modelling and determination of the related transfer functions. In order to determine the plant model transfer functions from the developed steady–state and dynamic models, the general representation of the APC control system is given in Figure 19.

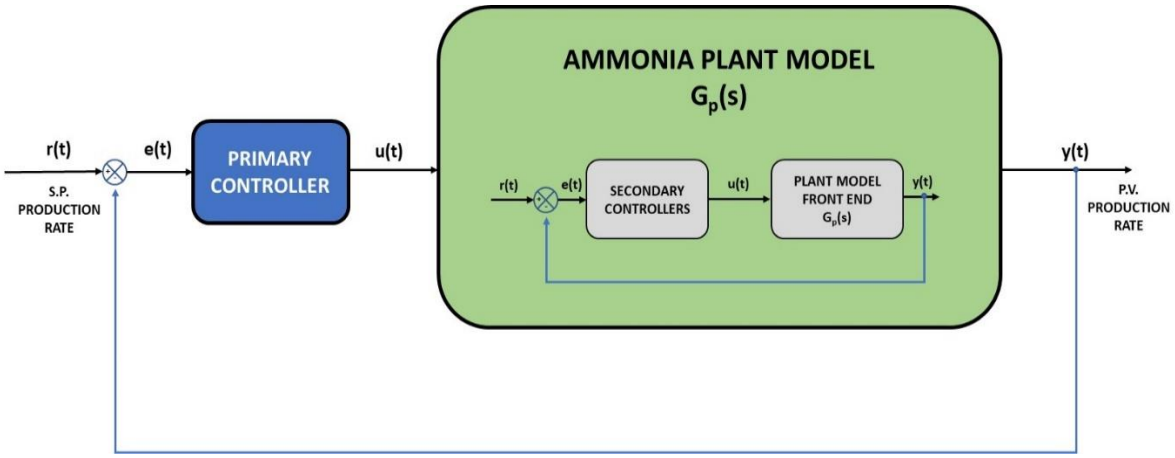

Figure 19. General representation of the APC control system by transfer functions.

Two principal parts must be defined, the plant model for each part of the APC control structure and stability tuning parameters of the outer and inner control loops. Stability tuning parameters must meet performance requirements that dictate the pole and zero locations in the root locus diagram.

In order to validate the performance of steady–state and dynamic flowsheets for the ammonia production process (based on the reference ammonia plant), the heat and mass balances were developed. The results of heat and mass balance of design production capacity (1360 t/day) of the reference ammonia plant are given in Appendix 1. The simulated results at a name plant capacity, show the difference of a maximum of 1,5% in comparison with the real process data of the main process parameters subject to with proposed control structure. The difference of only 1,5% justifies the validity of both balances.

The validated steady–state and dynamic models were used for placing the PID controllers included in the APC control system. Afterward, follows the determination of stability tuning parameters, testing, and validation. In order to achieve control of the ammonia production rate, it can be observed from Figures 12, 13, 16, and 18 that the same consists PID molar ratio controllers of the main process parameters (natural gas, steam for primary reformer, and air for secondary reformer) interlinked in the cascade structure with the feedforward characteristic. This will ensure a straightforward control strategy because the proposed advanced control system will combine all advantages of the following control methods – feedforward, feedback, ratio, and cascade. These control techniques can reduce the effect of specific types of process disturbances or feed flow rate changes during ammonia production.

5.1.1. Design and tuning of single closed–loop PID controllers for natural gas, steam and air process streams

The major process streams which define the production capacity and quality of the final product (liquid ammonia) are natural gas flow rate and steam mass flow rate for the primary SMR unit and the airflow rate for the secondary reformer. Their mutual interdependencies are shown in Figure 13, which describes the ideal stoichiometry molar ratios between ammonia–to–methane and air–to–methane during ammonia production. These ideal stoichiometry molar ratios are used as the premises for the molar ratio controllers' designing procedure. To control these major process streams, it is critical to design controllers which will adequately control the same. The PID controllers for the natural gas flow rate, steam mass rate, and airflow rate was labeled as 21FC108, 21FC109, and 21FC112 as in the reference ammonia plant, respectively.

Table 18. Stability tuning parameters for closed–loop single PID controllers 21FC108, 21FC109, and 21FC112.

Tuning parameter	Unit	21FC108		21FC109		21FC112	
		model	reference plant	model	reference plant	model	reference plant
K_c	-	0,180	0,250	0,0334	1,000	0,114	0,700
τ_i	minutes	0,0423	1,000	0,0438	3,000	0,043	0,800
τ_d	minutes	0,00941	0,000	0,00974	0,000	0,00955	0,000

From the values given in Table 18, it can be concluded that simulated stability tuning parameters differ significantly from the reference ammonia plant parameters. Besides that, all simulated stability tuning parameters are smaller in comparison with the values in the reference ammonia plant. One reason for this is that the current PID controllers are never tuned with any automated tuning techniques. According to the collected information, the same was adjusted according to the operator's experience to get as much as possible smaller overshoot percentage, settling time, and oscillation frequency. Also, in the current operational philosophy, these PID controllers operate as individual units without no mutual interlinks.

In order to get as much as possible better results for advanced control structure, all three controllers were additionally tuned in Control System Designer. The tuning procedure in Control System Designer needs adequate transfer functions. The closed–loop system step response input/output data for all three PID controllers were transferred in the System

Identification Tool and transfer functions were determined. The resulting plant model continuous transfer functions for all three PID controllers are shown in Table 19.

Plant model transfer functions corresponding to the estimated coefficients in the input/output plant model were estimated with the minimum fit to estimation data of 95%. With regard to achieving as much as a possible better response, final tuning of the PID controllers was performed according to the desired system performance requirements (stability of the process, disturbance rejections, and robustness) by location adjustments of the poles and zeros on the real and imaginary axes.

Table 19. Plant model transfer functions for closed-loop single PID controllers 21FC108, 21FC109, and 21FC112.

PID Controller	**Plant model transfer functions [GP(s)]**		
21FC108	$\frac{7{,}07s^2 + 1{,}076s + 0{,}0157}{s^3 + 22{,}32s^2 + 1{,}935s + 0{,}05177}$	-	-
21FC109	-	$\frac{11{,}29s^2 + 0{,}3015s + 0{,}009712}{s^3 + 11{,}19s^2 + 0{,}3062s + 0{,}009716}$	-
21FC112	-	-	$\frac{2392s^2 + 196{,}7s + 0{,}002576}{s^3 + 5296s^2 + 181{,}6s + 5{,}93e - 10}$

For all three PID controller's the following system performance requirements were set up:

1. percentage overshoot not higher than 10%;
2. rise time less than 1 second;
3. settling time less than 100 seconds;
4. oscillatory frequency as much as possible lower.

The impact of fine–tuning on the model PID controller's stability tuned parameters (Table 18) are shown in Table 20 and the values of the same were adjusted by changing the locations of poles and zeros in the root locus editor.

The root locus diagram for the PID controller 21FC108, with the location of the poles and zeros before and after adjustments according to the desired system performance requirements is shown in Figure 20. According to the location of the poles and zeros, it can be seen that before adjustments, the action of PID controller 21FC108 could not meet system performance

requirements. After moving the poles and zeros in an admissible area (white area) the action was improved and the PID controller could meet the same.

It can be seen that PID controller 21FC108 meets specified system performance requirements if the pole location is moved from the value of -50 to -300 at the real axis. This movement minimizes the gain of the PID controller and gives a better response regarding the rising time. The results of the closed-loop step test system response of the PID controller 21FC108 before and after adjustments of the poles and zeros location in the root locus diagram are shown in Figure 21.

Table 20. Stability tuning parameters for closed-loop single PID controllers 21FC108, 21 FC109, and 21FC112 before and after adjustments of poles and zeros.

Tuning parameter	Unit	21FC108		21FC109		21FC112	
		model	fine tuned	model	fine tuned	model	fine tuned
K_c	-	0,180	0,0412	0,0334	0,0300	0,114	0,050
τ_i	minutes	0,0423	0,00320	0,0438	0,0438	0,043	0,043
τ_d	minutes	0,00941	0,00320	0,00974	0,00974	0,00955	0,0090

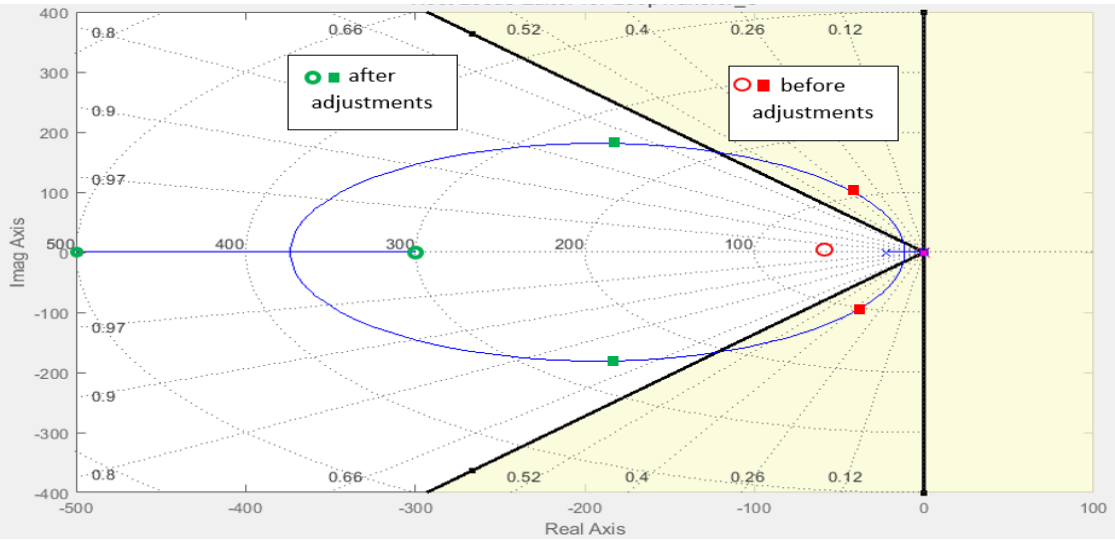

Figure 20. Root locus location of the poles and zeros of PID controller 21FC108 before and after adjustments.

From the presented results it can be noticed oscillation effect for the PID regulator designed and tuned by ATV technique during the rise time, after which the PID controller shows smooth response without overshooting. The settling time started after 150 seconds and the same does

not show any oscillation. However, after adjustment of poles and zeros location in the root locus editor, the gain of the PID controller was minimized and the step response shows better performance, which completely meets system performance requirements. The rise time shows no more oscillation effect while settling time is below the desired value of 100 seconds. According to this result, the PID controller 21FC108 could be used in the further design of the control system.

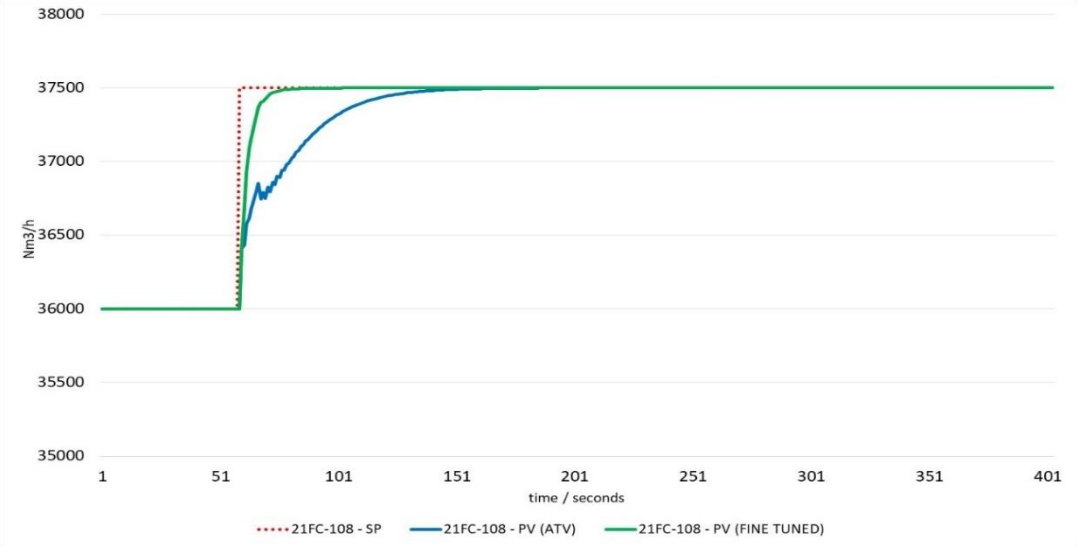

Figure 21. Closed-loop step test system response for the PID controller 21FC108 before and after adjustments of the poles and zeros location in root locus diagram.

The mass steam flow rate is controlled by the PID controller 21FC109. After determination of stability tuning parameters in the UniSim Design R470 the same procedure was repeated, as with PID controller 21FC108. The locations of the poles and zeros are shown in Figure 22. From obtained results, it can be observed that the location of poles and zeros meets desired system performance requirements and additional tuning is unnecessary. Because of simplicity, the gain was adjusted from the value of 0,0334 to 0,0300 and the closed—loop step system response was repeated. The results of the step system response to the PID controller 21FC109 are shown in Figure 23. From the results presented in Figure 23, it can be seen that the response of the PID controller 21FC109 is almost the same. It can be noticed an only negligible difference which is attributed to the changing of the controller gain. The PID controller shows excellent response and completely satisfies all desired system performance requirements. Regarding achieved results, the controller 21FC109 is used in the further development phase of the advanced control system.

The third PID controller in charge of controlling airflow rate (secondary reformer process air) must be able to ensure the adequate molar quantity of the nitrogen as one of the most important elements in the ammonia synthesis reaction. The location of the poles and zeros in the root locus editor for the PID controller 21FC112 obtained from the closed–loop step test system response before and after location adjustments is shown in Figure 24.

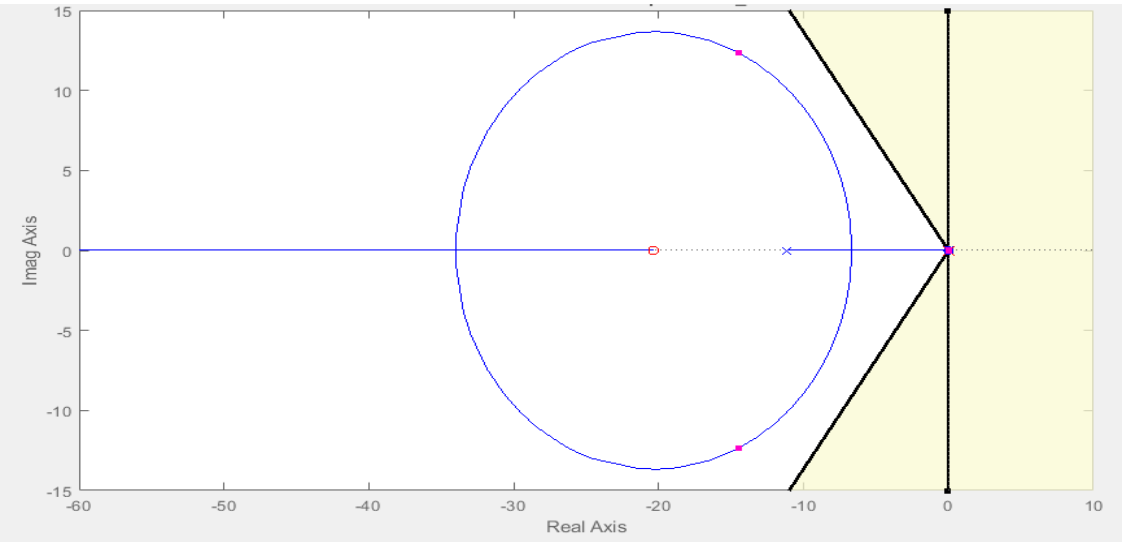

Figure 22. Root locus location of the poles and zeros of PID controller 21FC109.

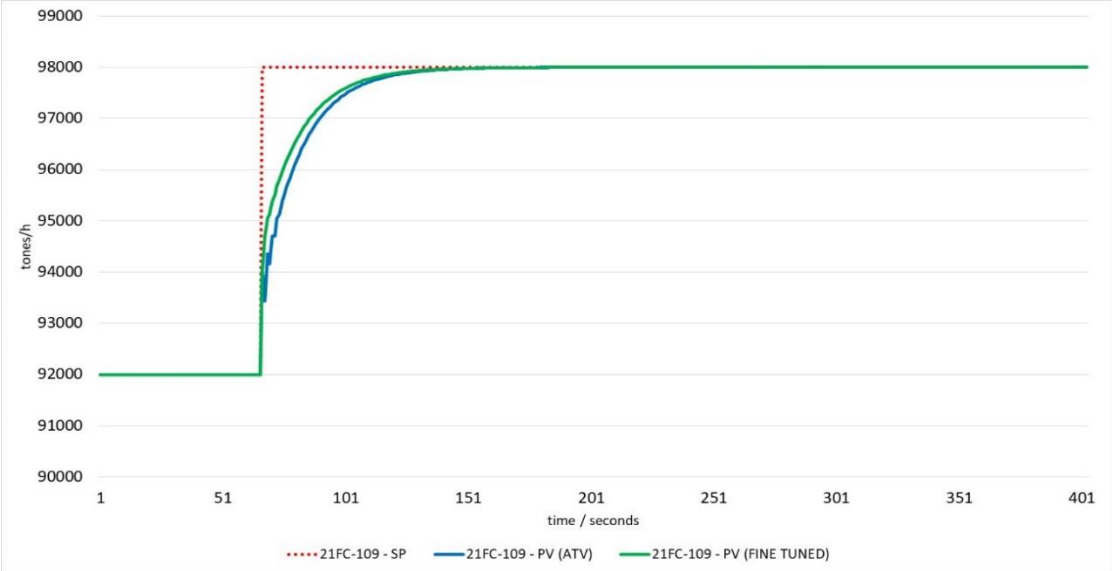

Figure 23. Closed-loop step test system response for the PID controller 21FC109.

From the locations of poles and zeros given in Figure 24, it can be observed that the PID controller designed and tuned in UniSim Deign R470 does not meet system performance requirements (locations are in an inadmissible yellow area). By moving the location of the real zeros in an admissible area, the gain of the PID controller was changed from the value of 0,114 to 0,050. After tuning, the closed–loop step response test gave an excellent response to rising time, which can be seen in Figure 25. Besides that, after adjustment of the real zero location, the settling time also meets the system performance requirement in a fewer period of less than 100 seconds.

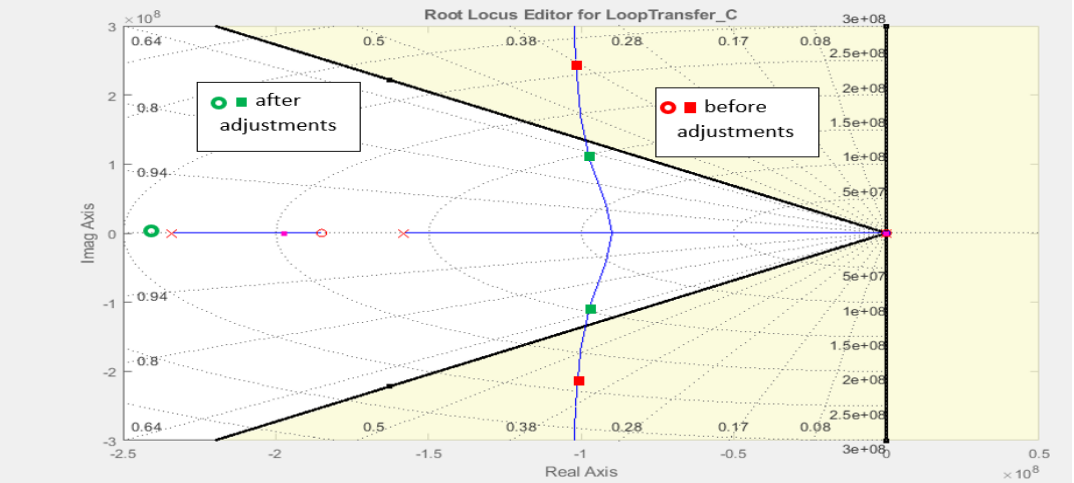

Figure 24. Root locus location of the poles and zeros of PID controller 21FC112 before and after adjustments.

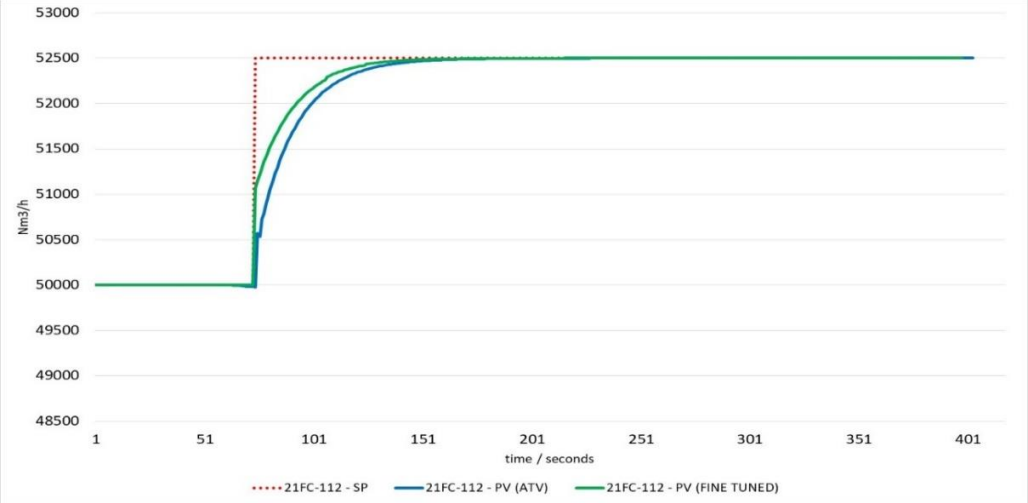

Figure 25. Closed-loop step test system response for the PID controller 21FC112 before and after adjustments of the poles and zeros location in root locus diagram.

According to performed tuning procedure, stability tuning parameters for all three main PID controllers were defined and it was used for further design steps. In the next designing step, the two PID ratio controllers in charge of control of S/N.G. and air–to–natural gas molar ratios were defined. This two molar ratio PID controllers present two inner or secondary/slave controllers in the overall control system.

5.1.2. Design and tuning of closed–loop steam–to–natural gas and air–to–natural gas molar ratio PID controllers

From Figure 13, it can be observed that the ideal molar ratio between CH_4 and steam is 1.0. However, as it was mentioned in the section of the steam–natural gas reforming unit, this molar ratio is not practicable because of technical limitations (*e.g.* carbon forming reactions, creep and rupture stress of reforming tubes, *etc*.). Due to the reason that the reference ammonia plant was designed for S/N.G. molar ratio between 3,5 and 3,6 the same was the starting point for designing the S/N.G. molar ratio PID controller.

The S/N.G. molar ratio influences process conditions in reforming tubes and related catalysts to bring the first step of hydrocarbon reforming reactions to the optimum level. The final objective of this molar ratio is a maximum hydrocarbon conversion with as much as possible lower molar concentration of the methane slip per dry basis at the outlet of the reformer tubes. Keeping the molar ratio at the optimum operating level and in stable conditions directly influences the lifetime of reforming tubes and related catalysts. Nevertheless, for ammonia operators, it is of utmost importance to keep the reforming tubes and related catalyst in the optimum temperature range which will ensure a prolonged lifetime. This is an important fact, because of reasons that reforming tubes present one of the highest maintenance costs in the ammonia production unit. Besides that, the catalyst charged in reforming tubes with the time loses their activity and selectivity with subsequent decrease of hydrocarbon conversion efficiency and higher molar concentration of the methane slip at the outlet of the reforming tubes. Both drawbacks directly influence the production cost (loss of valuable hydrogen and increased power cost for synthesis gas compression because of higher methane concentration in synthesis loop – higher content).

In case that an inappropriate S/N.G. molar ratio is applied during the operation of the ammonia plant, side effects become pronounced, which must be diminished by corrective measures of other process parameters. One of the most common corrective measures is increasing firing rate in the furnace box to compensate for the lower hydrocarbon efficiency

and reduce the methane slip. The intensive firing rate in the furnace box directly decreases the lifetime of the reformer tubes. The reason for this is that a prolonged increase of the reforming tube wall temperature of 20^{o}C over the design temperature decreases the reforming tube's lifetime by half [61-63]. On top of this, the more intensive firing rate will increase the more energy consumption and CO_2 emissions which consequently will have higher production costs.

All mentioned was the reason for the design of an adequate S/N.G. molar ratio PID controller, which will be able to keep the stable operation of the reforming tubes and related catalyst in a safe temperature range. The final goals are to sustain the maximum hydrocarbon conversion, minimum methane slip, and reduced firing rate in the furnace box. This molar ratio PID controller is one of the most important controllers of the advanced control system (inner or secondary/slave) with the main task to keep as much as possible ideal process conditions in the front-end of the ammonia plant. With respect to desired system performance requirements, the S/N.G. molar ratio PID controller was designed and tuned in UniSim Design R470 with an identical location as is in the reference ammonia plant. The stability tuning parameters for designing molar ratio PID controller 21RC110 in comparison with the molar ratio controller in the reference ammonia plant is presented in Table 21.

Table 21. Stability tuning parameters for closed–loop ratio PID controllers 21RC110 and 21RC111.

Tuning parameter	Unit	21RC110		21RC111	
		model	reference plant	model	reference plant
K_c	-	0,0572	0,250	2,150	n.a.
τ_i	minutes	0,0436	1,000	0,124	n.a.
τ_d	minutes	0,00969	0,000	0,0275	n.a.

It can be observed from the values given in Table 21 that model stability tuning parameters for the molar ratio controller 21RC110 differs significantly in comparison with the values from the reference ammonia plant. As was the case for the single PID controllers, the reason is the same. Namely, the stability tuning parameters for the molar ratio controller 21RC110 in the reference ammonia plant were estimated according to the operator's judgment. At the same time, any automated tuning techniques were never applied to this molar ratio controller.

In order to verify the values obtained by the ATV tuning technique, the closed–loop step system response was performed. According to the input/output response data, the plant model transfer function of the molar ratio PID controller 21RC110 was estimated with the minimum

fit to estimation data of 95%. The estimated plant model transfer function for this controller is given in Table 22.

Table 22. Plant model transfer functions for closed–loop molar ratio PID controllers 21RC110 and 21RC111.

PID Controller	Plant model transfer functions [GP(s)]
21RC110	$\frac{0{,}0004656s^4 + 4{,}756e-5s^3 + 5{,}003e-6s^2 + 2{,}181e-7s + 5{,}276e-9}{s^5 + 5{,}108s^4 + 0{,}5255s^3 + 0{,}05396s^2 + 0{,}0024s + 5{,}567e-5}$
21RC111	$\frac{-1{,}193e-6s^3 + 1{,}146e-7s^2 - 1{,}253e-8s + 3{,}006e-10}{s^4 + 0{,}1687s^3 + 0{,}0208s^2 + 0{,}001284s + 8{,}742e-5}$

Plant model transfer functions were analyzed by the Control System Designer. With respect to accomplish as much as a possible better response, final tuning of the molar ratio PID controller was performed according to the desired system performance requirements by zeros and pole location adjustment on the real and imaginary axes. System performance requirements were the same as was the case for closed–loop single PID controllers. The location of poles and zeros before and after adjustment is shown in Figure 26. According to the poles and zeros location, it can be concluded that the ATV technique cannot meet the stability tuning parameters regarding the defined system performance requirements. However, their location was very close to admissible area (white area). After a minor adjustment of the pole at -30 on the real axis toward the value of -20, the real zeros of molar ratio PID controller 21RC110 were moved from an inadmissible area (yellow area) to the admissible area (white area). This adjustment caused an increase of the controller gain value with a subsequent better response regarding the rising and settling time. The results of closed–loop step system response before and after adjustment of poles and zeros of a plant model transfer function are shown in Figure 27.

From Figure 27 it can be noticed that the molar ratio PID controller 21RC110 before adjustment of poles and zeros possess high oscillatory effect during the rising time, while after adjustment this behavior was diminished. At the same time, rising time was improved, while the settling time was almost the same before and after adjustment. The stability tuning parameters for molar ratio controller 21RC110 determined by ATV tuning technique and by adjustment of poles and zero locations are given in Table 23. From the results given in Table 23, it can be seen that the major change was in the value of the PID controller gain, which was

increased from 0.0572 to 0.110. This stability tuning parameter gave a satisfactory response, and it was used in designing the overall control system.

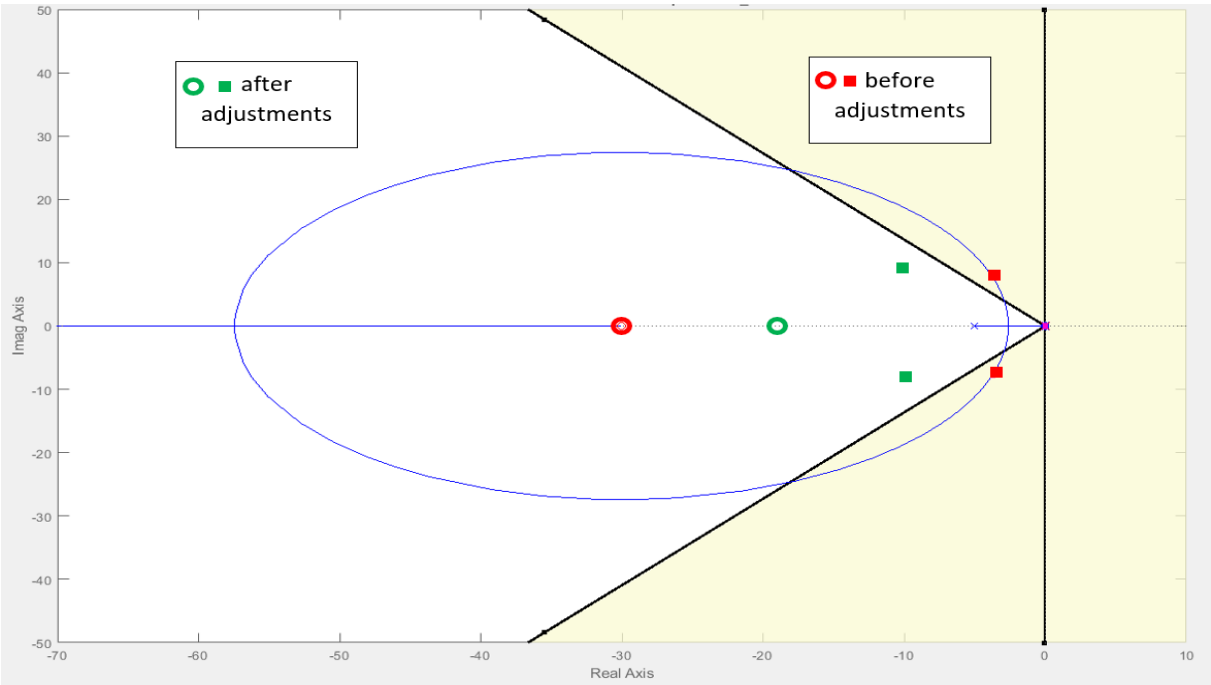

Figure 26. Root locus location of the poles and zeros of molar ratio PID controller 21FC110 before and after adjustments.

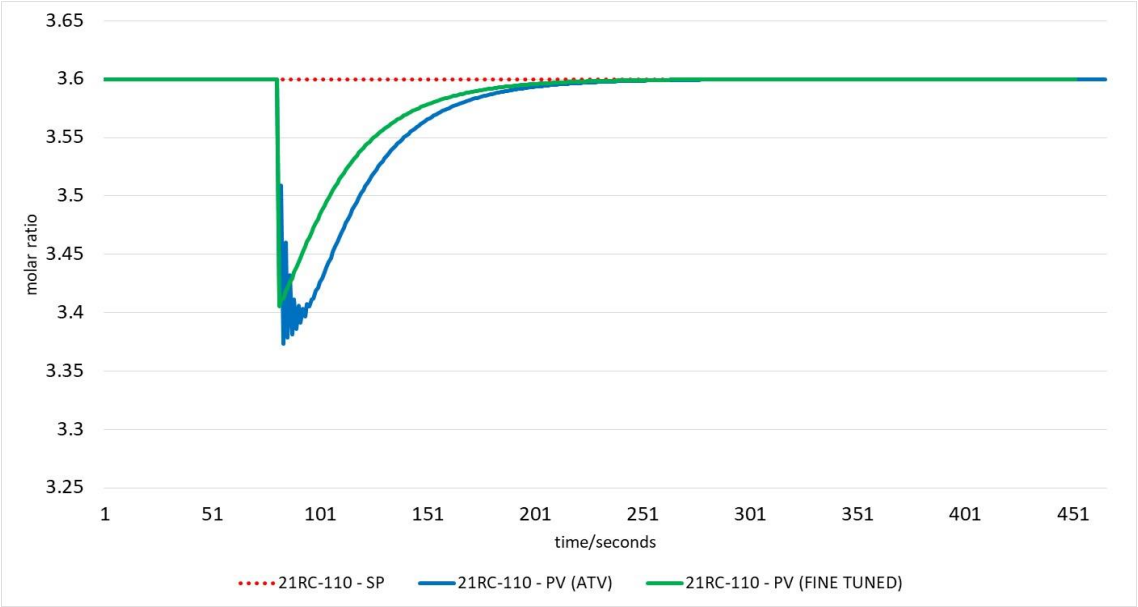

Figure 27. Closed–loop step test system response for the molar ratio PID controller 21RC110 before and after adjustments of the poles and zeros location in root locus diagram.

Table 23. Stability tuning parameters for closed–loop molar ratio PID controllers 21RC110 and 21RC111 before and after adjustments of poles and zeros.

Tuning parameter	Unit	21RC110		21RC111	
		model	fine tuned	model	fine tuned
K_c	-	0,0572	0,110	2,150	0,750
τ_i	minutes	0,0436	0,0444	0,124	0,050
τ_d	minutes	0,00969	0,0010	0,0275	0,025

The ammonia synthesis reaction is stoichiometrically determined by H_2–to–N_2 molar ratio of 3 to 1. In order to ensure this molar ratio in front of the ammonia synthesis compressor, it is necessary to bring an adequate molar quantity of air into the secondary reformer by an air compressor. According to Equation (47), the oxygen from the air reacts with the equivalent molar amount of methane and produces heat for the secondary reforming step. At the same time, the nitrogen takes part further as an inert gas in the rest of the ammonia flowsheet. Regarding ideal stoichiometry given in Figure 13, it can be noticed that the molar ratio between air and methane to satisfy the molar ratio between hydrogen and nitrogen in the synthesis loop (3 to 1) must be at the level of 1,709. However, with natural gas, which is the mixture of methane and higher hydrocarbons, this value is between 1,400 and 1,709 depending on the molar content of the different higher hydrocarbons and other constituents in the natural gas (CO_2, N_2, CO, *etc*.). Taking into consideration the reference ammonia plant and their design basis regarding the molar composition of the natural gas, the molar ratio of 1,429 gave the most satisfactory results during steady–state and dynamic simulations. The value of 1,429 gave the molar ratio between H_2–to–N_2 at the outlet of the secondary reformer at the level of 2,439. This molar ratio at the outlet of the secondary reformer ensures the final ideal molar ratio between H_2–to–N_2 (3 to 1) for ammonia synthesis reaction. Regarding this, the second inner molar ratio PID controller 21RC111 was designed. The primary task of this molar ratio PID controller is to sustain the stable molar ratio between air and natural gas and subsequently to keep the molar ratio between hydrogen and nitrogen at the outlet of the secondary reformer at the level of 2,439. Finally, the H_2–to–N_2 molar ratio of 3 to 1 in front of the ammonia synthesis loop was ensured. The value of 1,429 was the set point value for the inner ratio controller 21RC111 in the advanced control system.

The stability tuning parameters of the molar ratio PID controller 21RC111 determined by the ATV tuning technique is given in Table 21. The reference ammonia plant does not have this feature installed in the current control system and the same was never designed. This was why this data is not available for comparison with the model data. According to the closed–loop step

test system response performed in the dynamic flowsheet the input/output relationship for the molar ratio controller 21RC111 was determined. According to the same, the plant model transfer function was estimated by System Identification Tool with the minimum fit to estimation data of 95%. The plant model transfer function is given in Table 22. Regarding estimated plant model transfer function, final adjustment of poles and zero locations was performed and results of adjustment are shown in Figure 28.

After adjustment of the closed–loop poles and zeros along the locus the tuned controller loop gain was established. The final determined value of the closed-loop gain was 0,750. This new value was achieved by relocating the real zero from the value of -0,2 to -0,3 at the real axes. Afterward, the closed–loop step system response gave better results with the tuned molar ratio PID controller 21RC111 in comparison with the PID controller tuned in UniSim Design R470.

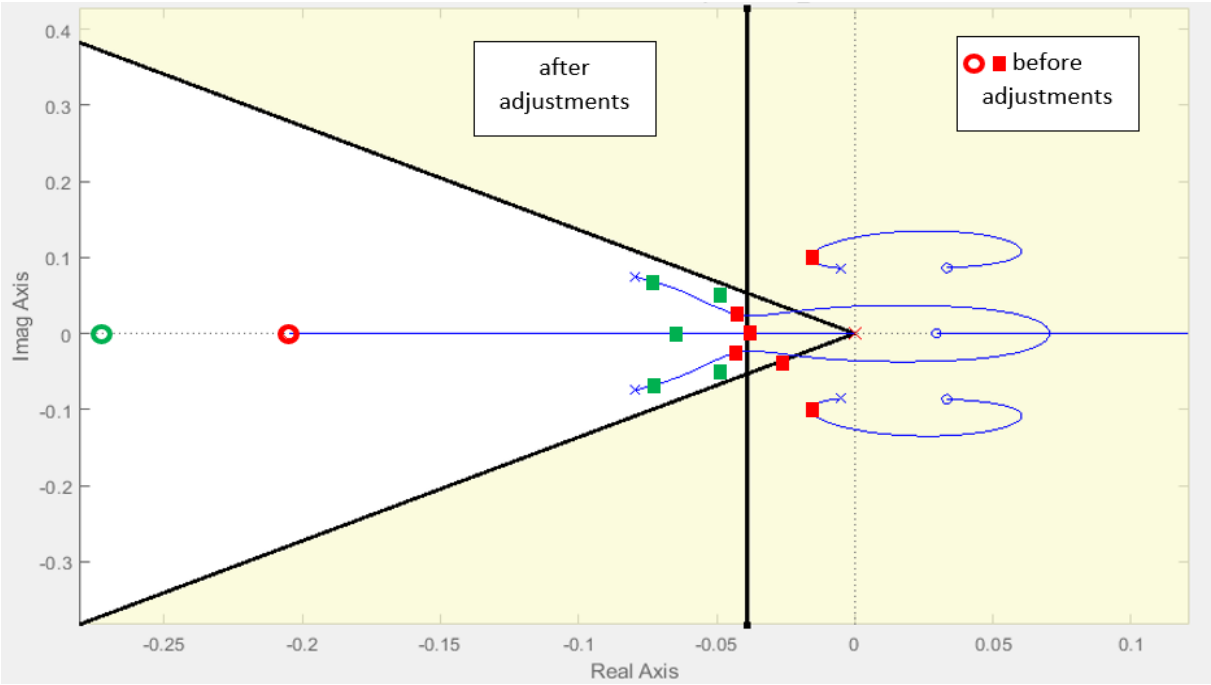

Figure 28. Root locus location of the poles and zeros of molar ratio PID controller 21RC111 before and after adjustments.

This adjustment caused the decrease of the PID controller gain value with a subsequent better response regarding the rising and settling time. The results of closed–loop step system response before and after adjustment of poles and zeros of a plant model transfer function are shown in Figure 29. From Figure 29, it can be noticed that the molar ratio PID controller 21RC111 before adjustment of poles and zeros possesses a slight oscillatory effect during the rising time. After

adjustment, this behavior was completely minimized. At the same time, rising time was improved, with the improvement of the settling time.

The final stability tuning parameters for molar ratio PID controller 21RC111 determined by adjustment of poles and zeros locations are given in Table 23. This adjusted value was used in the final designing phase of advanced ratio and cascade control system.

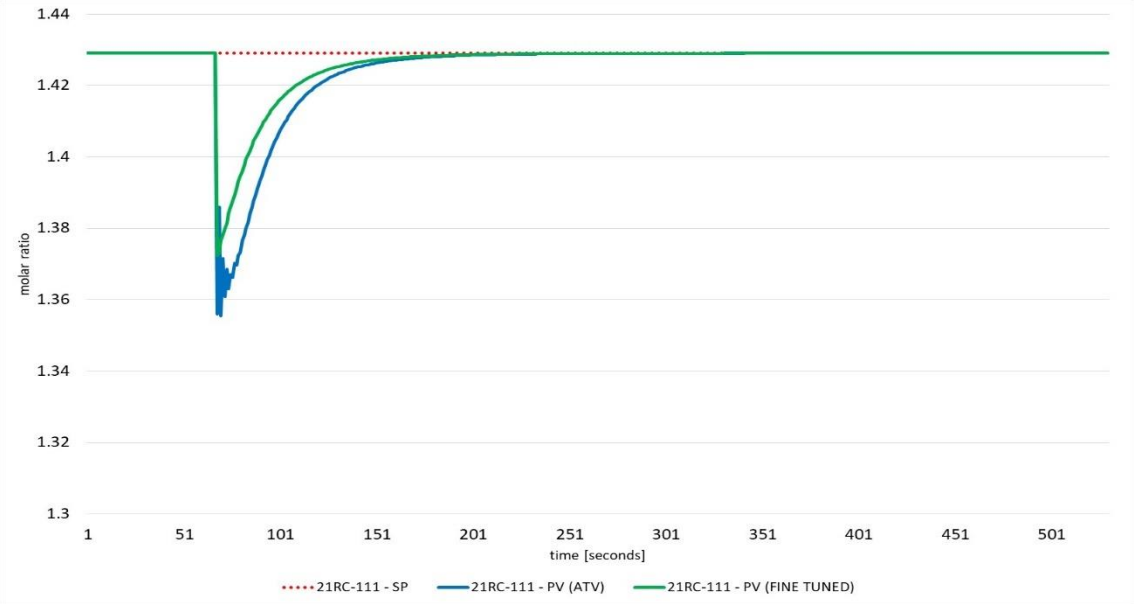

Figure 29. Closed-loop step test system response for the molar ratio PID controller 21RC111 before and after adjustments of the poles and zeros location in root locus diagram.

5.1.3. Design and tuning of master advanced ratio–cascade PID controller

From the perspective of the ammonia synthesis reaction defined by Equation (155), it can be concluded that the ammonia production process is simple and that the same can be performed with no serious difficulties. However, the complex nature of preparing the pure synthesis gas and subsequent ammonia synthesis reaction which involves recycling operation causes a high level of complexity. This complexity must be appropriately addressed and controlled to achieve as much as possible better economic performance, stable throughput and capacity, smooth operation, and to meet required quality specifications.

With regard to reconciling all the mentioned aspects during ammonia production, one pathway could be the implementation of the advanced control system which can to interlink and control the most influencing process parameters, such as natural gas volume flow rate,

steam mass rate, and air volume flow rate for the secondary reformer unit. As it was already mentioned, according to Equation (155) the stoichiometry molar ratio between hydrogen and nitrogen in ammonia synthesis reaction is 3 to 1. The hydrogen source is hydrocarbon feedstock (in this case natural gas) and steam, while the source of nitrogen is atmospheric air. So, the major process streams which define the molar composition of the synthesis gas are natural gas flow rate and steam mass rate for the primary SMR unit and the airflow rate for the secondary reformer. All other process steps in ammonia production after secondary reformer unit are consequently process operations in charge of additional hydrogen production by WGS reaction and afterward purification of the raw synthesis gas by the CO_2 washing unit and final removal of carbon oxides by methanation unit. All these process units bring the synthesis gas in front of the ammonia synthesis loop with the ideal molar composition between hydrogen and nitrogen as it was defined by Equation (155).

In the previous chapter, it was described how the advantages of the ratio control technique could be used in the control of the process streams which determine the behavior of the front–end of an ammonia plant (primary and secondary reforming units). Molar ratio control between steam and natural gas and then between air and natural gas directly determines the H_2–to–N_2 molar ratio at the outlet of the secondary reformer unit which is reflected to the H_2–to–N_2 molar ratio in front of the synthesis loop. Also, these molar ratios are under the direct influence of the volume flow rate of the natural gas as the leading process stream in ammonia production. Besides that, the natural gas volume flow rate directly determines the production capacity of an ammonia unit or the mass flow rate of liquid ammonia. These findings were used for designing the master PID controller, which will interlink the ammonia production rate and natural gas volume flow rate in the proposed control system.

Regarding the ideal stoichiometry relationship given in Figure 13, it could be concluded that the molar ratio between the ammonia production rate and methane is at the level of 2.667. So, if the master control can control the molar ratio between the ammonia production rate and natural gas volume flow rate, the plantwide control of the complete ammonia plant could be achieved. Subsequently, the natural gas volume flow rate controls the steam mass flow rate by inner/slave molar ratio controller in charge for S/N.G. molar ratio control and also air volume flow rate for the secondary reformer unit by second inner/slave molar ratio controller in charge for control of air–to–natural gas molar ratio (H_2–to–N_2 molar ratio at the outlet of the secondary reformer unit).

This premise was used in the final design stage of master PID controller 21RC156 for control of ammonia production rate regarding natural gas volume flow rate. According to Figures 16

and 19, the master PID ratio controller controls by feedforward and cascade control structure two inner ratio controllers and finally brings stability and smooth operation of an ammonia plant regarding production capacity and quality specification, keeping the economic performance indicators at the highest possible level.

Except for the cascade and ratio features, the master PID controller has additional benefits in terms of feedforward control. The major benefit of the feedforward characteristic is the possibility to compensate disturbances before the process is affected. The general overview of the feedforward characteristic is given in Figure 30. From Figure 30, it can be noticed that the feedforward controller requires information from two variables to determine the value of OP%. These two variables are the set point of the process variable and the disturbance affecting the process. To successfully implement a feedforward feature to the advanced control system, it is mandatory to consider that disturbance is measurable and that a fairly accurate plant model of the system exists.

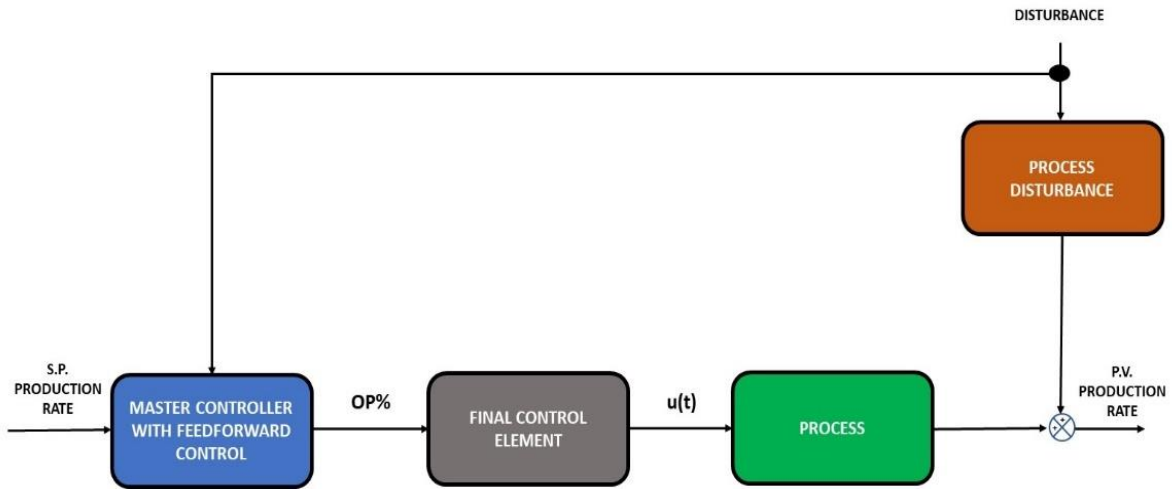

Figure 30. General overview of the feedforward control characteristic.

First, the design of the master PID ratio controller 21RC156 with feedforward characteristic was conducted in a developed dynamic flowsheet of ammonia plant by application of the ATV tuning technique. The stability tuning parameters for PID molar ratio controller 21RC156 determined by ATV tuning technique are given in Table 24.

Table 24. Stability tuning parameters for closed–loop ratio PID controller 21RC156.

Tuning parameter	Unit	21RC156	
		model	reference plant
K_c	-	0,357	n.a.
τ_i	minutes	23,8	n.a.
τ_d	minutes	5,29	n.a.

Such kind of controller is the novelty of this thesis and because of this reason, it cannot be compared to any other PID controllers, either from the reference ammonia plant or from the literature data. This is the reason why stability tuning parameters are not available in Table 24. According to performed closed–loop step test system response, input/output data was obtained for the control system. The input/ output data was served for estimation of the plant model transfer function, which was estimated with the minimum fit to estimation data of 95% and expression is given by the following relationship:

$$g(s) = \frac{-1{,}978s^2 + 0{,}01893s + 1{,}873e - 6}{s^3 + 21{,}77s^2 + 0{,}02163s + 1{,}872e - 6}$$

Because of the extremely complex nature of the ammonia production process, the system performance requirements were set with the longer rising and settling time taking a precaution that the overshoot must be only 1%. The rising time was chosen to be at the level of 10 minutes, while the settling time was chosen to be at the level of 30 minutes. These two system performance requirements were chosen according to observation from the reference ammonia plant and changing the production rate during normal operation. This approach takes into consideration the main recommendation from the heuristic's IFSH method.

In order to check the stability tuning parameters obtained by the ATV tuning technique, the plant model transfer function was analyzed by a root locus editor for further estimation of pole and zero locations regarding desired system performance requirements. The locations of the poles and zeros for the tuned PID controller are shown in Figure 31.

From the location of poles and zeros, it can be concluded that further adjustment is unnecessary and that the stability tuning parameters completely meet the desired system performance requirements. This is also confirmed by closed–loop step test system response, which results are presented in Figure 32. From Figure 32, it can be observed that the master controller performs almost perfectly with desired rise and settling time and without overshooting effect.

A summary of the controller tuning parameters for the primary/master and two secondary/slave controllers in the control system is given in Table 25. The parameters are determined using the ATV tuning technique and additionally analyzed by a root locus editor. The outstanding performance of the cascade control system implies that the time constants of the inner control loops must be significantly shorter in the comparison with the master control loop.

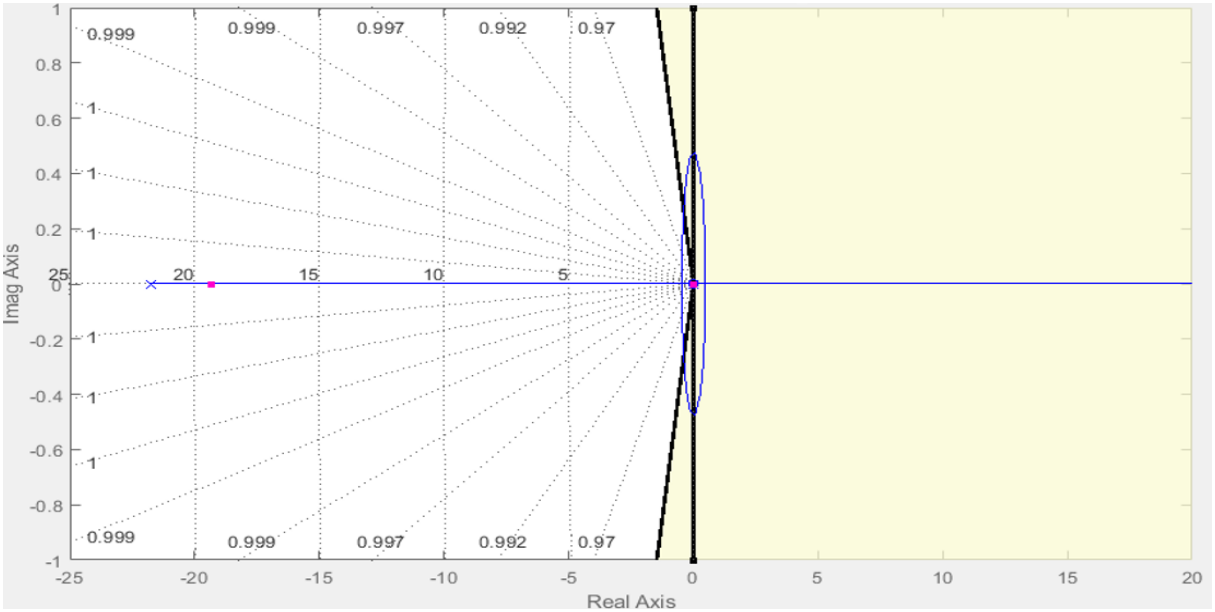

Figure 31. Root locus location of the poles and zeros of molar ratio PID controller 21RC156.

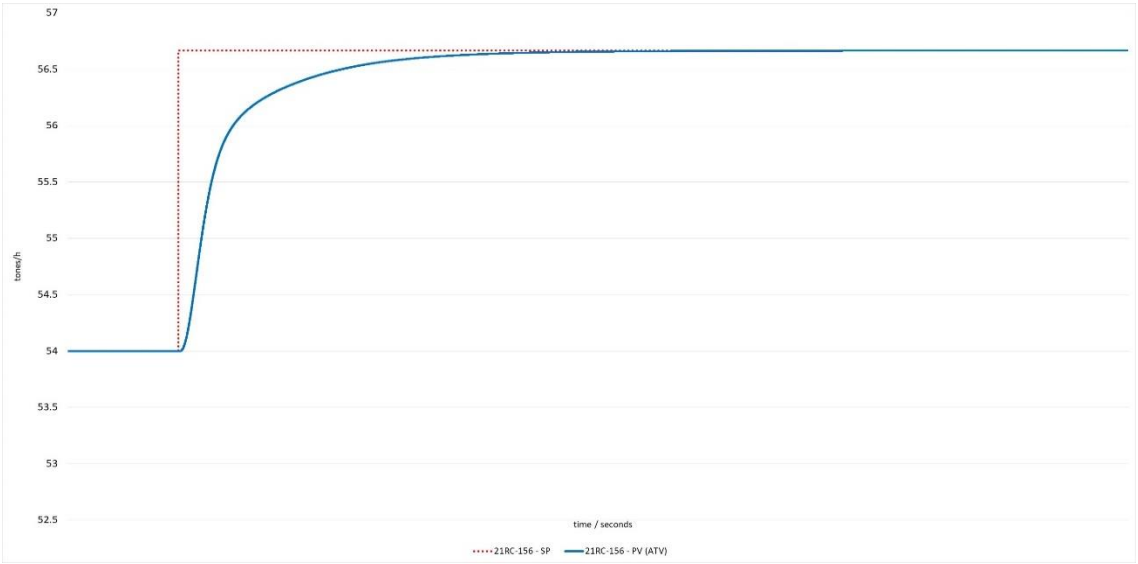

Figure 32. Closed–loop step test system response for the molar ratio PID controller 21RC156.

Table 25. Summary of stability tuning parameters for primary/master and two secondary/slave controllers in control system.

Tuning parameter	Unit	21RC110		21RC111	
		model	**fine tuned**	**model**	**fine tuned**
K_c	-	0,0572	0,110	2,150	0,750
τ_i	minutes	0,0436	0,0444	0,124	0,050
τ_d	minutes	0,00969	0,0010	0,0275	0,025
		21RC156			
		model		**fine tuned**	
K_c	-	0,357		0,357	
τ_i	minutes	23,8		23,8	
τ_d	minutes	5,29		5,29	

5.2.Testing and validation of the of the advanced ratio – cascade control system

The second objective of this thesis was the deployment of the plant model for testing the proposed control structure against main process disturbances during ammonia production. By placing these three molar ratio PID controllers in cascade structure with feedforward characteristic, it is obtained a more straightforward control strategy which combines all advantages of the following control methods – feedforward, feedback, ratio, and cascade. These control techniques can reduce the effect of specific types of disturbances or feed flow rate changes during ammonia production. In order to achieve stable and smooth operation of the ammonia production process, it is also necessary to test and validate developed advanced control structure against main measured process disturbances that affect the ammonia production rate.

To verify the reliability of the proposed advanced control structure which comprises feedforward, feedback, ratio, and cascade features, the first step was the identification of the most influencing process disturbances during ammonia production. After performing analysis, it was determined the most important process disturbances which affect the ammonia production process and the same are given in Table 26.

The effectiveness of the closed–loop system was tested by the introduction of a typical step–like disturbances for all five disturbances listed in Table 26. The results of performed closed–loop step test system response against measured process disturbances are shown in Figures 33 to 37.

Table 26. List of typical process disturbances (DVs) observed during ammonia production.

Name	Disturbance variables	Unit	Nominal value	Disturbance range	Disturbance change
DV1	Air flow (H_2/N_2 molar ratio)	-	2,439	2,317 to 2,561	0.122
DV2	Steam–to–natural gas molar ratio	-	3,50	2,9 to 3,5	0.3
DV3	Low heating value (LHV) of natural gas	kJ/m^3	34500	31050 to 34500	3450
DV4	Purge gas rate	m^3/h	8000	6800 to 9200	1200
DV5	Ammonia production rate	metric t/h	56,60	50,0 to 56,60	1,0

5.2.1. DV 1 – Air flow (H_2–to–N_2 molar ratio) disturbance case

Partially reformed synthesis gas at about 32 bars from the outlet of the reformer tubes is mixed with an amount of preheated air fixed by the nitrogen requirement for the ammonia synthesis reaction. This mixture burns above the catalyst bed in the secondary reformer unit, raising the temperature to approx. 1250^oC, which is enough high to complete reforming reaction to a very low methane content (less than 0,30 mol.% per dry basis).

According to the operational experience from the reference ammonia plant the best performance of this unit is achieved, if the H_2–to–N_2 molar ratio in the secondary reformer effluent is at the level of 2,439, which will bring the H_2–to–N_2 molar ratio in the make–up synthesis gas at the level of 3,0. In the current operation of the reference ammonia plant, the airflow is controlled only by the single airflow controller. The air volume flow rate is adjusted according to the H_2 and N_2 content in the effluent from the secondary reformer, which is continuously analyzed by the gas chromatograph.

However, with the variation of the ambient temperature, a significant influence on the air compressor performance is observed because of changes in air density. Besides that, a variation in the speed of the air compressor can influence the changes in the airflow rate, which can cause the deviation from the ideal H_2–to–N_2 molar ratio. These two disturbances can cause a significant influence on the single airflow controller and all control actions are only under the responsibility of the operators. To minimize the operator's judgment, the proposed control system will reject the air disturbance and keep H_2–to–N_2 molar ratio at the desired set point regarding nominal production rate.

The effectiveness of the control system at the nominal production rate of 56,666 metric t/h, under step disturbance of 5% from the ideal air volume flow rate, was tested. The control system response to this step disturbance is shown in Figure 33. In Figure 33 it can be seen that with a lower H_2–to–N_2 molar ratio the production capacity is decreased for a very short time with the amount of 0,3 metric tons/h because of the lower airflow rate (lower amount of N_2). However, the quick response of the PID controller system brings back the production capacity to the set point without offset. A similar reciprocal pattern is observed when a disturbance occurs in the opposite direction, with the overshooting effect from 0,25 to 0,45 metric t/h. It can be concluded that the control system responds excellent to the typical step disturbance, keeping the controlled variable close to the set point at the nominal production rate and subsequent reduction of operator interventions is expected. Regarding all mentioned it can be also concluded that any disturbances in airflow rate will be successfully compensated and subsequently ensure stable operation of the ammonia plant during temperature transition periods which mainly occur during the day/night and summer/winter operational periods.

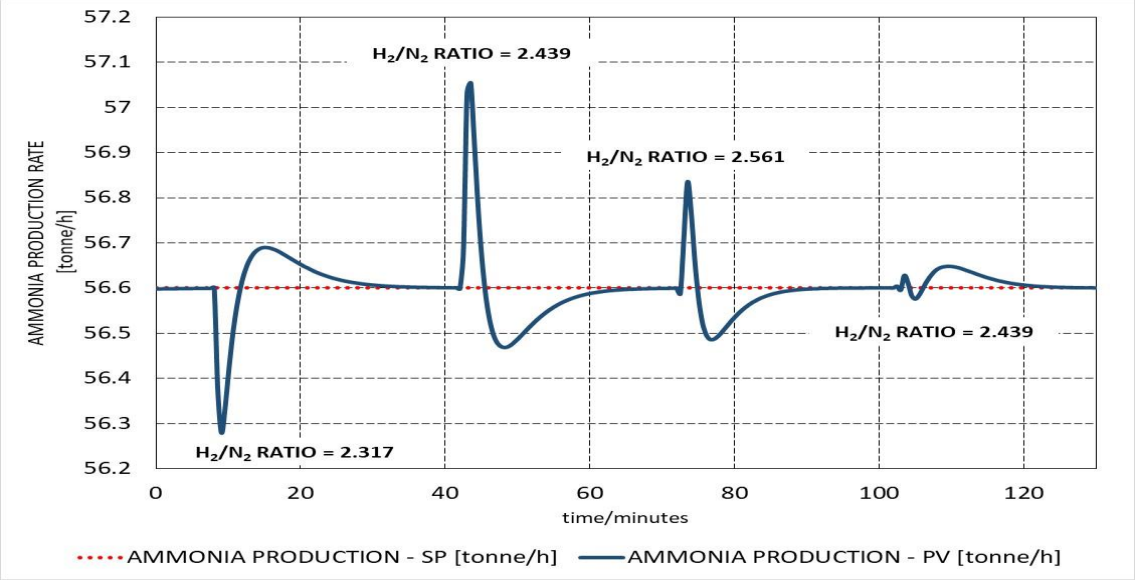

Figure 33. Master PID control variable response to the air (H_2–to–N_2 ratio) step disturbance.

5.2.2. DV 2 - Steam–to–natural gas molar ratio disturbance case

The S/N.G. molar ratio strongly affects the conversion of a hydrocarbon feedstock to hydrogen, energy demand in the overall ammonia plant, and finally determines the production capacity. Except this, the sufficient steam mass rate is of vital consideration to prevent catalyst

coking and keep the reforming tubes on the safe side against creep damage. Because of all mentioned, it is of utmost importance to keep the constant S/N.G. molar ratio at the designed level.

In the case of a lower S/N.G. molar ratio the overall energy demand of the ammonia unit is lowered down, but consequently, it can result in a catalyst shorter lifetime and reforming tubes because of a higher firing rate to compensate equilibrium reactions (Table 2), and to keep CH_4 outlet molar concentration at the designed level. At the S/N.G. molar ratio of 3,5, with the reforming tubes' outlet temperature of approx. 800^oC and at a pressure of 32 bar the primary reformer unit in the reference ammonia plant reforms natural gas to yield an effluent containing approx. 69,0 mol.% H_2 and 10,35 mol.% CH_4 per dry basis.

The control system is tested against S/N.G. molar ratio disturbance between 2,9 and 3,5 with the step change of 0,3. The value of 2,9 is the minimum level that is acceptable in the reference ammonia plant because of constraints in the WGS and CO_2 removal units. The efficiency of the control system in rejecting the disturbances in the S/N.G. molar ratio (range from 2,9 to 3,5 with the step change of 0,3) at the nominal production rate is shown in Figure 34. It can be seen that the control system responds extremely well throughout the tested range. Effect of lowering down the S/N.G. molar ratio causes a drop of the production rate based on lower natural gas and steam flow rates. Overshooting effect is almost negligible (± 0,03 metric tons/h) and after transient response, the production rate stabilizes at the set point with any offset. The opposite response can be observed with increasing the S/N.G. molar ratio, where the overshooting effect is reversed because of higher natural gas and steam flow rate. With this disturbance, it can be concluded that the control system response is excellent.

Besides that, the inner controller located inside the overall control structure possesses the gain–scheduled feature which can set programmatically three typical process conditions of S/N.G. molar ratios (3,0; 3,3 and 3,6). Regarding this feature, the inner PID controller can assure that the closed–loop methane slip values approach their set point more quickly than under the standard PID control approach because it accounts for the process model and bounds on the control action, while programmatically reject the disturbance and transient conditions. The production process can satisfy higher conversion of hydrogen and closely keep safety concerns related to the lifetime of the reforming tubes. The additional benefit can be achieved for older facilities with higher S/N.G. molar ratios to elevate safely energy efficiency.

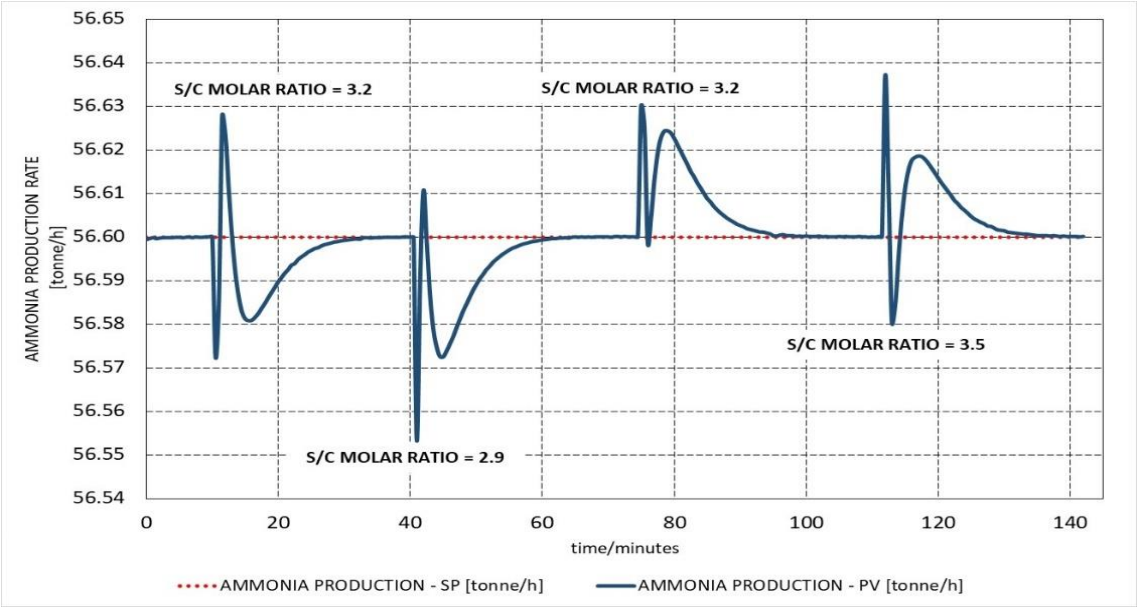

Figure 34. Master control variable response to the S/N.G. molar ratio step disturbance.

5.2.3. DV 3 – Low heating value of natural gas disturbance case

The reference ammonia plant uses natural gas (mainly CH_4) as the main feedstock and a source of hydrogen. According to the base design principles, the reference ammonia plant is designed for the lower heating value (LHV) of the natural gas of 34500 kJ/m^3, with an average sulfur content of 30 mg/m^3 (mainly H_2S). In the current operation, natural gas feedstock comes from the outside source according to the national gas quality standard [113]. Regarding the quality standard, the allowed deviation from the nominal value for CH_4 is a minimum 85 mol.%, while the LHV can be between 33300 and 41292 kJ/m^3. Based on the operational experience and historical data, the maximum deviation from the natural gas quality standard is in the range ± 5%. The reference ammonia plant possesses *in situ* on–line gas chromatograph which can automatically analyses the molar composition of the natural gas from the outside natural gas network. According to this analysis, the LHV value is automatically calculated and read on the DCS screen. In most cases, the operator of the natural gas distribution system does not provide information on natural gas molar composition changes, which can cause a significant disturbance during the operation of an ammonia plant. This is the reason why is important to predict any changes in LHV value and compensate for the same. Hence, this deviation has served as the starting point to test the control system rejection capability against LHV disturbance.

The control system response to the LHV step disturbance is shown in Figure 35.

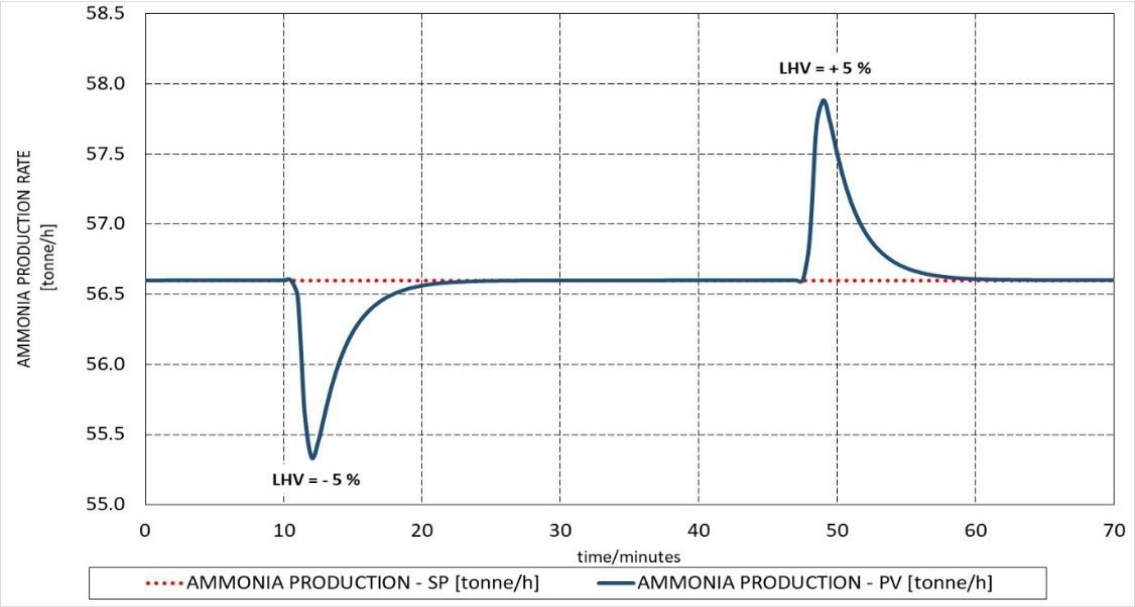

Figure 35. Master control variable response to the LHV step disturbance.

In the case of lowering down the LHV by 5%, the nominal production rate is decreasing. The overshooting effect is approx. 1,2 metric t/h, which is related to the lower volume flow rate of the natural gas, which brings down also the mass flow rate of the steam by the action of the S/N.G. molar ratio PID controller (21RC110). After the overshooting effect, the control system successfully brings the production rate to the nominal value with no offset. The opposite can be observed with increasing the natural gas LHV by 5%. The overshooting effect is the same, approx. 1,2 metric t/h.

As with previous disturbances, it can be noted satisfactorily behaviour of the control system where the master control loop successfully compensates significant step disturbances to the manipulated variable regarding the changes of LHV value.

5.2.4. DV 4 – Purge gas rate disturbance case

A portion of the recycled synthesis gas is always vented as a continuous purge to control the concentration of CH_4 and Ar inert gases in the synthesis loop. These components would otherwise build up in the ammonia synthesis loop, reducing the effective synthesis pressure that would be reflected in lower conversion and production per pass. Variation in the inert gas molar content of the circulating synthesis gas affects the main process parameters in the ammonia

converter – pressure, temperature and H_2–to–N_2 molar ratio. All the mentioned process variables significantly influence the ammonia production rate. In the reference ammonia plant, the ammonia converter performance withstands the molar concentration of the inert gases of approx. 13,50 mol.% per dry basis. To maintain this molar level of inert gases in the synthesis loop, it is necessary to bleed continuously 8000 m^3/h of the synthesis gas.

To determine the effectiveness of the designed control system against the change of inert molar content in the recycle gas the disturbance for 1200 m^3/h of purge gas was tested. The result of this effect is shown in Figure 36.

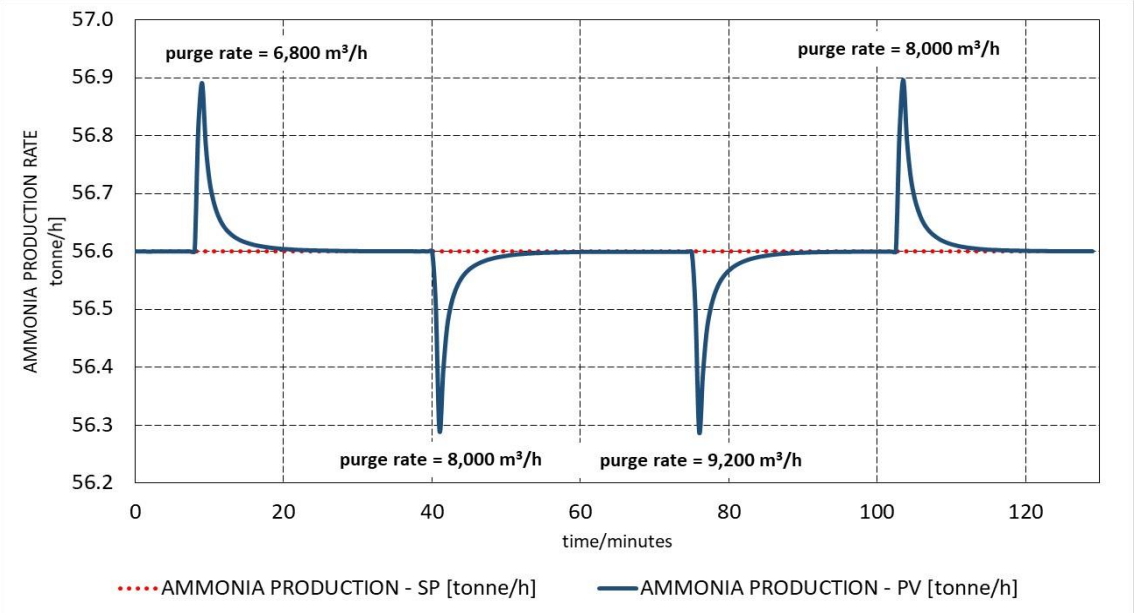

Figure 36. Master control variable response to the purge gas rate disturbance.

As it can be seen in Figure 36, the control system again satisfactorily responds to the disturbance and effectively rejects it. With lowering down the purge gas rate for the 1200 m^3/h, the production rate has an overshooting effect for approx. 0,3 metric t/h after which the control system successfully brings down the same to the steady–state without offset. The reason is the higher volume flow rate of the recycled gas in the synthesis loop (more H_2 and N_2). The negative consequence of this disturbance is higher pressure in the ammonia converter on the account of the higher molar content of the inert gas which was approx. 15,3 mol.% per dry basis and consequently higher duty at the synthesis gas compressor. By increasing the purge gas rate to 9200 m^3/h the production rate is decreased on the account of higher purge gas flow rate – the lower amount of synthesis gas in the synthesis loop (approx. 11,90 mol.% per dry basis). The overshooting effect is analogous to the case of a previous disturbance. The control system again

satisfactorily rejects the disturbance without offset. Here, the pressure in the synthesis loop is decreased on account of lower inert gas molar content, which brings positive effects to the compressor duty. However, there is a loss of valuable synthesis gas, which causes a higher amount of natural gas and steam to compensate for this loss to keep the production rate at the desired set point.

5.2.5. DV 5 – Ammonia production rate disturbance case

As it is mentioned in the introduction, the model is based on the M. W. Kellogg Inc. catalytic high–pressure reforming method for producing liquid ammonia with a production rate of 1360 metric tons per stream day using natural gas as the main feedstock. If all process parameters are not under control (*e.g.* operator subjective decisions, untuned control loops, inappropriate control system, *etc*.) the operation may not be optimal. Clearly, a well–conceived control design that generates alignment of all major process variables can give significantly optimized production.

According to the literature [114] a fundamental characteristic of an appropriately designed plant control system is effective management of the production rate. In order to control the whole ammonia production process, it was considered two main process paths, namely production of synthesis gas from the hydrocarbon feedstock, air, and steam and ammonia production from the mentioned synthesis gas.

As it was mentioned, one of the crucial links which can be controlled between these two process paths is the molar ratio between hydrocarbon feedstock (in this work natural gas) and ammonia production rate. Regarding elemental stoichiometry (Figure 13), it can be easily calculated that the ideal molar ratio between ammonia product and CH_4 is 2,667. Besides that, this molar ratio determines the ideal molar ratio between air to CH_4, which is 1,709. This molar ratio must be satisfied to keep the molar ratio between H_2–to–N_2 at the ideal molar level of 3 to 1. Subsequently, the last important molar ratio is S/N.G., which should be theoretically only slightly over 1,0 to avoid cracking, carbon formation, and reformer tubes overheating effect [60]. However, in practical applications, these molar ratios are different because of the different composition of the hydrocarbon feedstock, catalysts, and reforming tubes temperature limits [60]. The largest deviation in practical applications can be observed with the S/N.G. molar ratio.

If the ammonia production rate will be connected with the hydrocarbon feedstock volume flow rate through the molar ratio control, which will act to two other molar ratios (S/N.G. and

air–to–natural gas) by implementing feedforward and cascade control techniques, the total control of the ammonia process can be achieved.

Last, in order to prove the effectiveness of the control system, the set point of the production rate was changed between 50,00 and 56,66 metric t/h with different step increments. The results are shown in Figure 37.

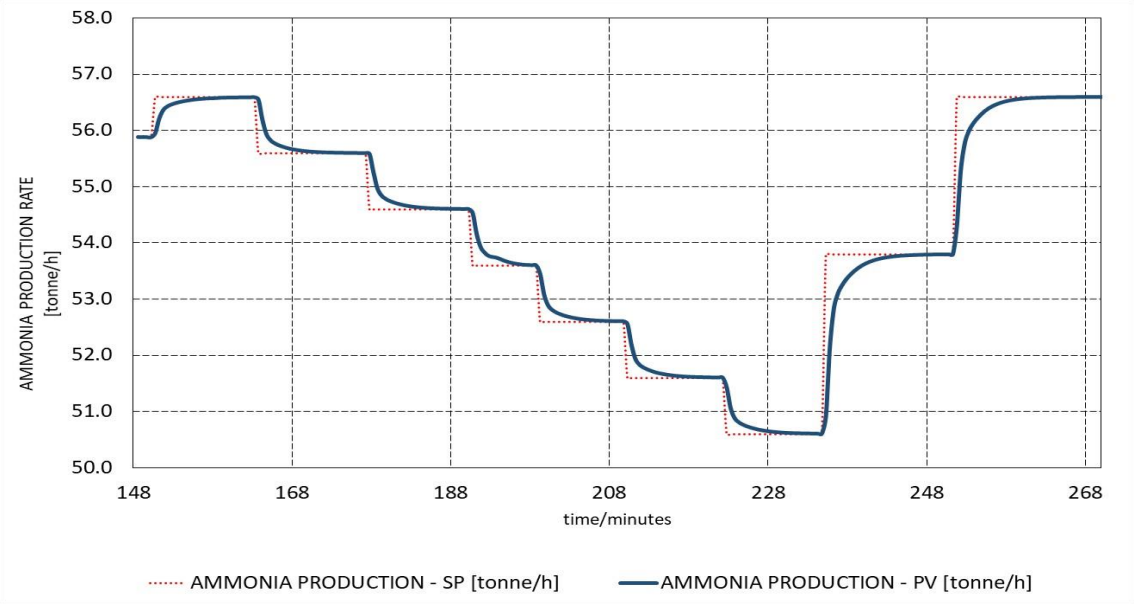

Figure 37. Response of the control system to the changes of the ammonia production rate.

It can be observed that there is no overshoot effect in the testing range of all set point step increments. The transient time to reach a new steady–state is between 20 and 40 minutes. In comparison with the reference ammonia plant, the time needed to achieve a new steady state for the same set point changes is between 15 and 45 minutes which, of course, depends on the production rate change.

Regarding all main process disturbances, it can be concluded that the proposed control system which combines different controlling techniques presents a promising solution for optimization and advanced control of the ammonia production plant.

5.3.Optimization analysis

5.3.1. Problem definition and description of the optimal approach

For the complete synthesis of anhydrous ammonia, based on steam reforming of natural gas, Appl provides a total cost of 172,50 USD/t for an 1800 metric t/day plant with total energy consumption of 27 MMBtu/t (29,541 GJ/t) in 1998 USD [1]. The cost estimate assumes the natural gas cost is 2,80 USD/MMBtu or 8,062 €/MWh. The breakdown of total costs comprises feedstock and energy cost of 75,6 USD/t, other cash costs of 28,5 USD/t, total cash cost of 104,6 USD/t, and capital–related cost of 68,4 USD/t. According to this literature data, it can be concluded that even with most modern ammonia facilities, the natural gas cost is over 70% of the total cash costs. From this information, it can be observed that any optimization in the ammonia production process will bring savings in natural gas consumption and subsequently have a positive influence on operational economic performance.

"Brown-field" ammonia plants could be optimized either with high or low CAPEX revamping options. Intensive CAPEX revamping options primarily include changes in current process equipment which is mainly related to the replacement of more efficient heat exchangers and/or rotating turbomachinery (steam turbines and/or compressors). However, due to the extremely volatile natural gas market (unpredictive escalation of natural gas prices), it is very hard to decide about high CAPEX revamping solutions. This is the reason why ammonia operators are looking for low CAPEX revamping solutions to achieve as much as possible better optimization of the ammonia production process. One of the low CAPEX scenarios could revamp existing DCS's with the possibility to optimize process parameters which mostly influence production costs. Regarding this, a properly designed control system with the possibility to reject process disturbances could be one of the possible technical solutions for optimization of the process parameters and maximizing the production profit.

Araújo and Skogestad [16] proposed in their work expression for calculation of the operating profit function (*P*) in the ammonia synthesis loop with the objective to be maximized:

$$P = \$_{\mathrm{prod}}\left(x_{\mathrm{NH_3}}F_{\mathrm{prod}}\right) + \$_{\mathrm{purge}}F_{\mathrm{purge}} + \$_{\mathrm{steam}}F_{\mathrm{steam}} - \$_{\mathrm{gas}}F_{\mathrm{gas}} - \$_{\mathrm{WS}}(W_{\mathrm{K-401}} + W_{\mathrm{K-402}}) - \$_{\mathrm{CW}}F_{\mathrm{CW}} \quad (210)$$

where x_{NH_3} is the product purity while F is the process stream flow in related units (kg/h or m^3/h).

The operating profit function (P) does not include other fixed costs or capital costs and the profit is expressed in USD/h.

However, Araújo and Skogestad [16] did not anticipate one very important parameter which is related to the CO_2 emissions which in the last decade present extremely high operating costs to all ammonia producers. Namely, according to Guidance Document no. 9 [115] ammonia is the benchmarked product regarding the ETS emission scheme and all CO_2 emission quantities which are not freely allocated are charged and presents additional operating cost. The current benchmark for ammonia production is 1,619 metric tons of CO_2 per ton of ammonia. In comparison with this benchmark value, the reference ammonia plant emits on average 1,952 metric tons of CO_2 per ton of ammonia. A difference of 0,333 metric tons present at the yearly basis additional cost of approximately 3 to 4 million €, depends on the open market price of EUA's units.

Figure 38 shows the energy inputs and emissions associated with ammonia production. The production process leads to direct CO_2 emissions and to CO_2 that is used as feedstock in the chemical production processes. Both emissions are included in the system boundaries. The CO_2 emissions because of the steam production are also included in the system boundaries.

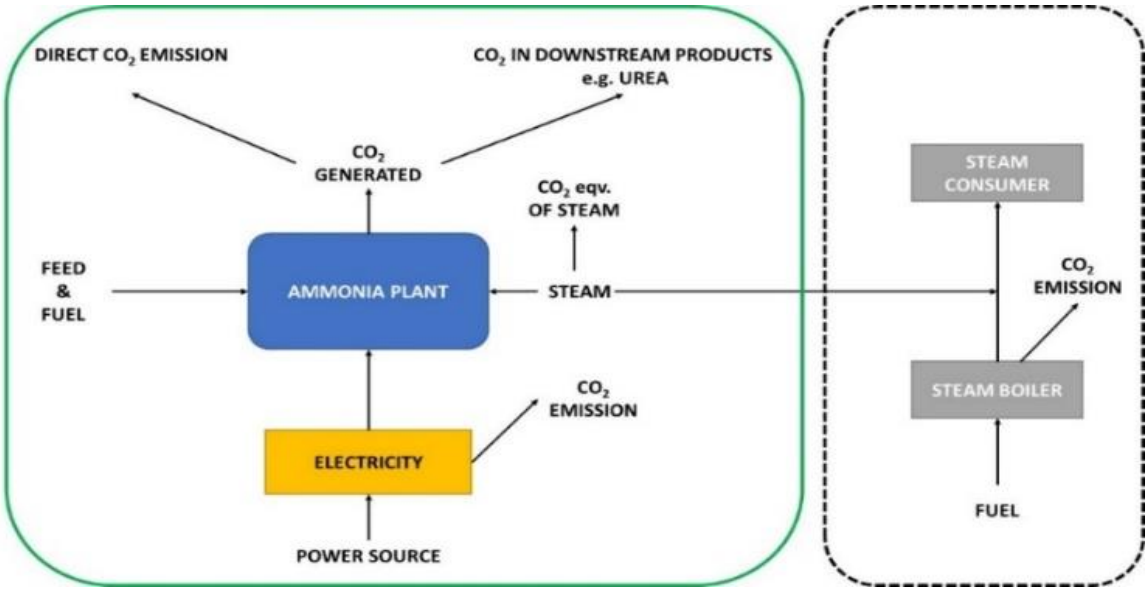

Figure 38. Energy inputs and emissions related to ammonia production.

The emissions related to electricity production and consumption are not eligible for free allocation [115].

The product benchmark for ammonia is based on total emissions since the energy produced from fuels is exchangeable for energy from electricity. The allocation should however be based on direct emissions only. In order to achieve consistency between the benchmarks and the allocation, the preliminary allocation is calculated using a ratio of direct and total emissions [115]:

$$F_{\mathrm{p,k}} = \frac{Em_{\mathrm{direct}} + Em_{\mathrm{NetHeatImport}}}{Em_{\mathrm{direct}} + Em_{\mathrm{NetHeatImport}} + Em_{\mathrm{inderct}}} \times BM_{\mathrm{p}} \times HAL_{\mathrm{p}} \times CLEF_{\mathrm{p,k}} \quad (211)$$

where

$F_{\mathrm{p,k}}$ – annual preliminary allocation for a product benchmark sub–installation producing ammonia in year k (expressed in EUAs);

BM_{p} – benchmark for ammonia (expressed in EUAs / unit of product);

HAL_{p} – historical activity level, i.e. the arithmetic mean of annual production in the baseline period as determined and verified in the baseline data collection (expressed in units of product);

$CLEF_{\mathrm{p,k}}$ – applicable Carbon Leakage Exposure Factor for product *p* in year *k*;

Em_{direct} – direct emissions within the system boundaries of the ammonia production in the baseline period. (Note: the direct emissions meant here do not correspond to the direct emissions in the figure above). The direct emissions further include the emissions due to the production of heat within the same ETS installation, which is consumed within the system boundaries of the ammonia production process. Direct emissions should (by definition) exclude any emissions from electricity generation or net heat export/import from other ETS installations or non–ETS entities;

$Em_{\mathrm{NetHeatImport}}$ – emissions from any net measurable heat import from other ETS installations and non–ETS entities over the baseline period by a sub–installation producing ammonia, irrespective of where and how the heat is produced;

Em_{inderct} - indirect emissions from electricity consumption within the system boundaries of the production of ammonia over the baseline period. Irrespective of where and how the electricity is produced, these emissions expressed in tonne CO_2 are calculated as follows:

$$Em_{\text{inderct}} = Elec.use \times 0{,}376 \tag{212}$$

$Elec.use$ – total electricity consumption within the system boundaries of the ammonia production over the baseline period, expressed in MWh.

From all mentioned it must be emphasized the importance of CO_2 emission cost during ammonia production due to reason that the same highly contributes to the ammonia production cost. This is the reason why it is necessary to include this cost in optimization analysis regarding the determination of the operating profit function (*P*). Regarding the relationship proposed by Araújo and Skogestad [16], the same must be corrected to achieve complete optimization of the ammonia production plant. The newly proposed operating profit function (*P*) has the following expression:

$$P = unit\ price_{\text{prod}} F_{\text{prod}} + unit\ price_{\text{purge}} F_{\text{purge}} + unit\ price_{\text{steam}} F_{\text{steam}} - unit\ price_{\text{natural gas}} F_{\text{natural gas}} - unit\ price_{\text{electricity}} F_{\text{electricity}} - unit\ price_{\text{CW}} F_{\text{CW}} - unit\ price_{CO_2} F_{\text{p,k}} \tag{213}$$

The final objective of the proposed control system is the ability to keep process parameters at such level, which will ensure that operating profit function (*P*) meets maximum profit, product yield, and heat recovery, while in parallel minimize the energy consumption and CO_2 emissions. In order to meet all mentioned targets, the operating profit function (*P*) of the optimization problem given in Equation (213) must be expressed in terms of the selected decision variables [116]:

$$Minimize\ or\ Maximize\ f(x,y,z) \qquad f: \mathbb{R}^{\text{p}} \to \mathbb{R} \tag{214}$$

subject to

$$h_{\text{i}}(x,y,z) = 0 \qquad h_{\text{i}}: \mathbb{R}^{\text{p}} \to \mathbb{R} \qquad with\ i = 1, 2, \dots, n \tag{215}$$

and

$$g_j(x,y,z) \leq 0 \qquad g_j : \mathbb{R}^p \to \mathbb{R} \qquad with\ j = 1,2,\dots,m \tag{216}$$

in the region of feasible solutions,

$$\Omega = \left\{(x,y,z) \in \mathbb{R}^p : h_i(x,y,z) = 0, i = 1,2,\dots,n; g_j(x,y,z) \leq 0, j = 1,2,\dots,m\right\} \tag{217}$$

where:

x is the set of the continuous real independent variables corresponding to design and operating parameters of the chemical plant components (mass flow, pressure, temperature, reaction rates, *etc*.);

y is the set of the discrete independent variables used in the design optimization (nominal capacities, geometric standardized dimensions, *etc*.). The sizing and design correlations for the different components and equipment can be given by simple algebraic equations (explicit or implicit functions in terms of the system parameters) or in the form of complex partial differential equations. In the later case, quadrature methods such as orthogonal collocation could be required.

z represents the set of the integer independent variables used to determine the structure of the optimal flowsheet (*i.e.* existance of selected components, interconnections, *etc*.) starting from a proposed structure. Thus, only one variable of this kind is assigned to a component of stream, indicating whether the component exists in the optimal configuration or not.

Furthermore, the search through the space of alternatives often requires to be subject to a set of equality or inequality constraints, imposed by the reliability, availability, maintenance, operability and environmental impact of the energy systems. Therefore,

$h_i(x)$ is the set of the equality restrictions, which contains the equations derived from the conservation laws (mass, energy, momentum, cost) and the constitutive equations of the plant model, variable connections, correlations for physical and chemical property, and

$g_j(x)$ is the set of inequality restrictions, which contains upper and lower bounds for mass and heat transfer rates, temperatures, pressures, concentrations as well as limits for the environmental and safety–related issues.

UniSim Design R470 offers an in–built feature of a multi–variable steady–state optimizer, which can find the operating conditions which minimize (or maximize) an objective function. For optimization analyses, it was used the Honeywell Sequential Quadratic Programming (SQP) approach. The Honeywell SQP method is a sequential quadratic programming (SQP) algorithm incorporating an L1–merit function and a BFGS approximation to the Hessian of the Lagrangian in which the objective function is locally approximated as a quadratic function, whereas the restrictions are suitably linearized, according to:

$$f(x) \approx f(x^{\mathrm{p}}) + \nabla f(x^{\mathrm{p}})^{\mathrm{T}}(x - x^{\mathrm{p}}) + \frac{1}{2}(x - x^{\mathrm{p}})^{\mathrm{T}}[H_{\mathrm{f}}(x^{p})](x - x^{\mathrm{p}}) \tag{218}$$

$$h(x) \approx h(x^{\mathrm{p}}) + \nabla h(x^{\mathrm{p}})(x - x^{\mathrm{p}}) \tag{219}$$

$$g(x) \approx g(x^{p}) + \nabla g(x^{\mathrm{p}})(x - x^{\mathrm{p}}) \tag{220}$$

In this way, the optimization problem takes the form of a quadratic programming problem, to be solved in each iteration by using, *e.g*. augmented Lagrangian methods. In case, if it were not for constraints, the SQP approach would resemble the application of the Newton method for the numerical solution of non-linear algebraic systems of equations. In more detailed shape the Equations (214) to (216) are following:

$$\min_{\mathrm{x}} \nabla f(x^{\mathrm{p}})(x - x^{\mathrm{p}}) + \frac{1}{2}(x - x^{\mathrm{p}})^{\mathrm{T}}[H_{\mathrm{f}}(x^{\mathrm{p}})](x - x^{\mathrm{p}}) \tag{221}$$

subject to

$$h(x^{\mathrm{p}}) + \nabla h(x^{\mathrm{p}})(x - x^{\mathrm{p}}) = 0 \tag{222}$$

$$g(x^{\mathrm{p}}) + \nabla g(x^{\mathrm{p}})(x - x^{\mathrm{p}}) \leq 0 \tag{223}$$

in the region of feasible solutions

$$x - x^{\mathrm{p}} \in \mathbb{R}^{\mathrm{p}} \tag{224}$$

The major algorithm features are step size restriction, the decision variable and objective function scaling, a basic watchdog method, and a problem–independent and scale–independent relative convergence test. The algorithm also ensures that the model is evaluated only at points feasible regarding the variable bounds.

With respect to determining optimized operating conditions (flow rates of natural gas, steam, air, and ammonia product) the proposed control system can keep the same in stable conditions and successfully reject process disturbances. On top of this, the master controller can adjust the production rate capacity at the level which is defined by the optimizer taking into consideration desired equality and inequality restrictions. Figure 39 shows the systematic relationship adopted for conducting a multi–variable steady–state optimization and control of process parameters in ammonia plant by the advanced control system. Control of the ammonia plant with the recursive evaluation of the operational profit function actually entails a feedback interaction between those steps.

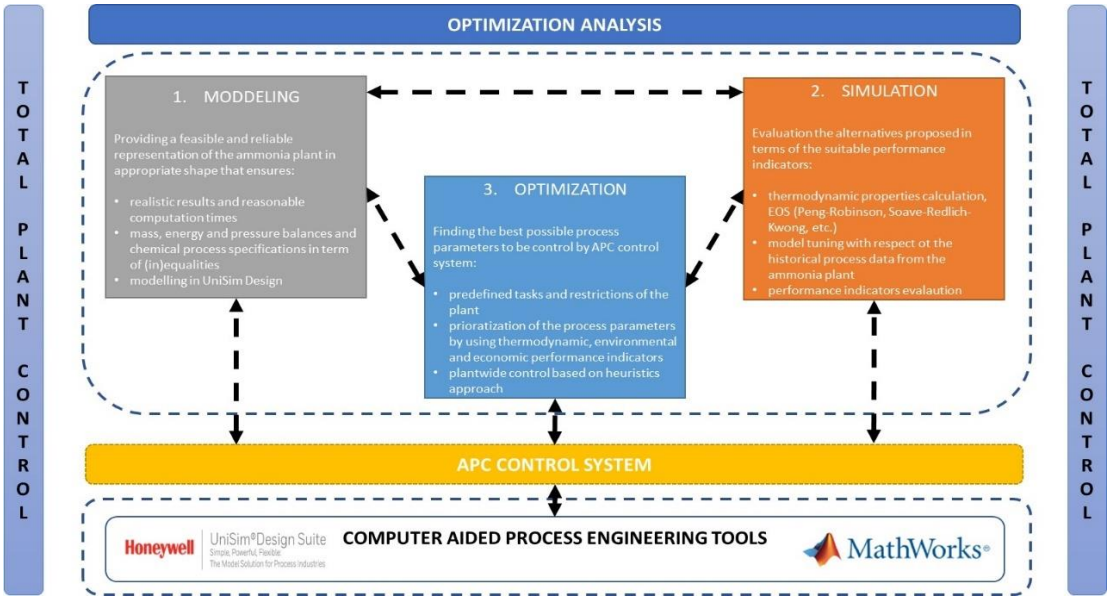

Figure 39. Systematic relationship between optimization and advanced control system.

5.3.2. Diagnostic of the reference ammonia plant performance

In order to conduct optimization analysis of the reference ammonia plant and to determine the process parameters values which could be controlled by the proposed control system, it is

necessary to address how the same influence on production costs. In optimization analysis, all process units described in more detail in the previous chapters are shown in the combined layout in Figure 40.

As it was mentioned, the reference ammonia plant is composed of integrated front–end syngas and back–end ammonia synthesis and refrigeration units with an intermediate raw syngas purification system that supplies required pure syngas for the ammonia synthesis loop. Besides this process part, in the ammonia plant exists also two other parts which handle the steam and cooling water network. A comprehensive steam network recovers the waste heat along the process part, allowing for the reduction of the fuel consumption in the utility system and the same is shown in Figure 41. The cooling water network ensures extracting of the unused heat energy, which cannot be appropriately used and must be stored in the cooling water. The cooling water network is shown in Figure 42. On top of this is coming the layer of CO_2 emissions, which arise from the combustion of natural gas in the reformer furnace, as well as from the reforming and WGS reactions in the front–end syngas production units. The CO_2 material balance of the reference ammonia plant is shown in Figure 43. All mentioned layers in the ammonia plant, together with the cost of electricity, bring all necessary parameters in Equation (213) which must be optimized against different constraints to deliver the best possible process parameter values which could be controlled by the proposed control system.

In conventional SMR process (as it is used in the reference ammonia plant), approximately 40% of the total supply of natural gas are burnt as fuel in a reformer furnace, whereas the balance (approx. 60%) is consumed as feedstock in the process of primary reforming of natural gas by steam. As it can be seen from Figure 40 the primary reformer is the most exergy–intensive process of the ammonia plant, requiring in the reference case a heat exergy duty of 164,0 MW at about 800^{o}C, provided by 198 arch burners at the top of the radiant box. More than half of this duty (92,49 MW) is used for reforming reaction, while the balance (71,51 MW) is used for further recovery in the heat recovery convection train (HRCT). In case that waste gases are not at the adequate exergy level, additional heat is ensured by 11 tunnel burners at the bottom of the radiant box. The waste gas is recovered against mixed feed preheater (natural gas + steam), air–steam preheater (air + steam for secondary reformer), hot and cold steam preheater, boiler feedwater preheater, and finally in the combustion air preheater. In order to bring the temperature of the steam to the level of 525^{o}C additional 21 superheater burners are located over the hot steam superheater coil. The auxiliary boiler is the part of the reformer furnace, with the task to produce additional steam, which is necessary to be ensured to close completely the steam balance of the ammonia plant.

The auxiliary boiler is equipped with 5 burners. The waste gas from the auxiliary boiler is joined with the waste gas from the convection section of the reformer furnace in the middle of the hot and cold steam superheater coils (exchanger coils). The balance between the total heat duty of the reformer furnace and heat duty ensured by arch burners are allocated to these three additional locations of the tunnel, superheater, and auxiliary burners (33,90 MW). According to this exergy balance, the total heat duty of the reformer furnace is 198,10 MW. The exergy balance of the reformer furnace from the waste gas side is shown in Table 27. From the data given in Table 27, it can be seen that the main liberation of the heat is coming from the arch burners which can liberate in total 164,0 MW from which 92,49 MW is used for reforming reaction inside the reformer tubes and the balance of 71,51 MW is recovered in the convection section of the reformer furnace.

Table 27. The exergy balance of the reformer furnace.

Item	**Module**	**Heat duty [MW]**
A1	Arch burners for heat recovery	71,51
A2	Tunnel burners	6,69
A3	Superheater burners	8,87
A4	Auxiliary burners	18,54
Total A		**+ 105,61**
B1	Mixed feed preheater	11,10
B2	Air steam preheater	6,08
B3	Hot steam preheater	27,385
B4	Cold steam preheater	27,385
B5	Boiler feed water preheater	5,21
B6	Combustion air preheater	21,43
Total B		**- 98,59**
Balance total A – B (waste gas in atmosphere)		**7,02**

The balance from the total heat duty of the reformer furnace (198,10 MW) which is necessary to implement in the convection section to recover the waste heat comes on account of the tunnel (6,69 MW), superheater (8,87 MW), and auxiliary burners (18,54 MW).

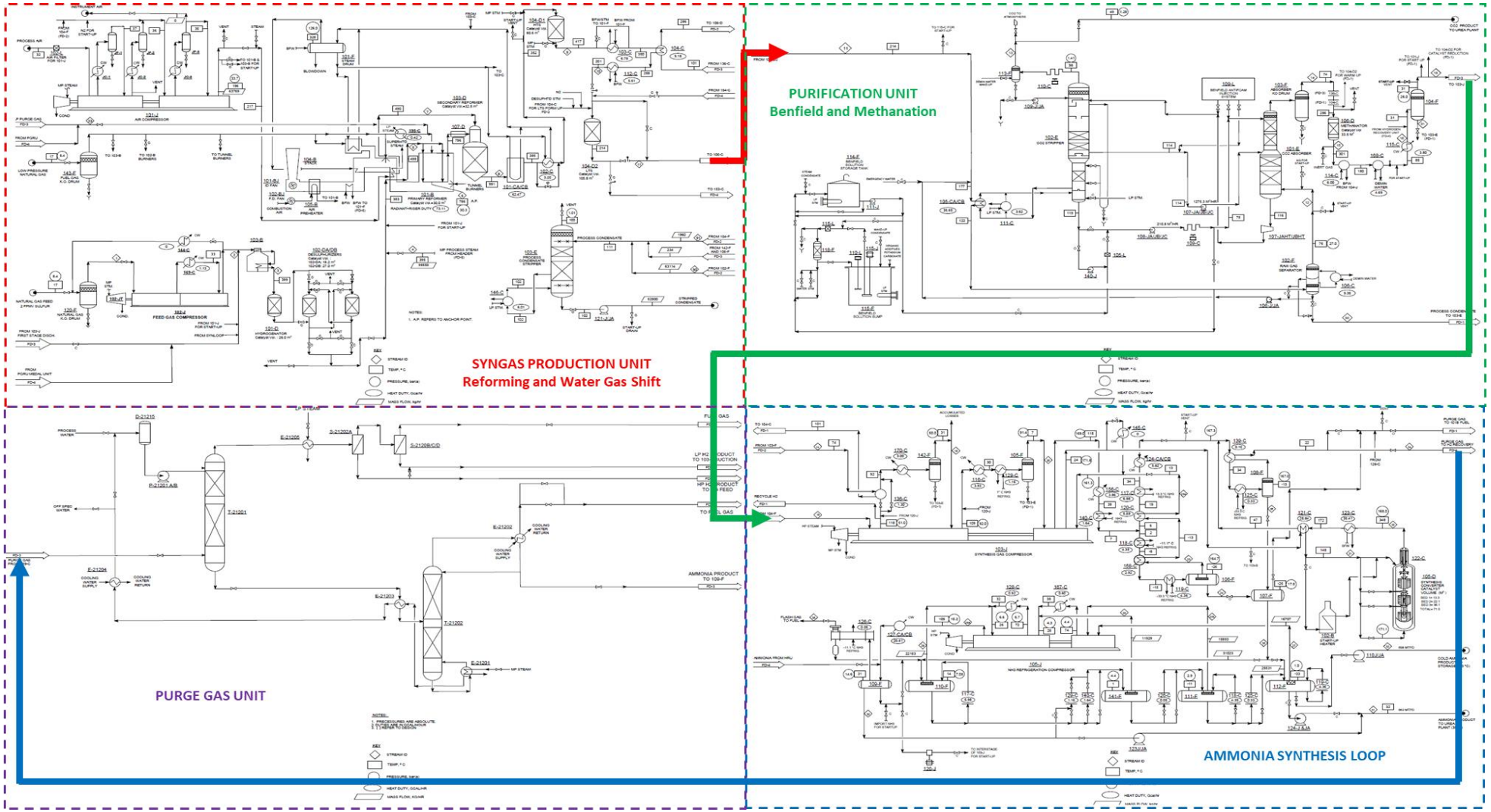

Figure 40. General overview of reference ammonia plant with all process units included in optimization analysis.

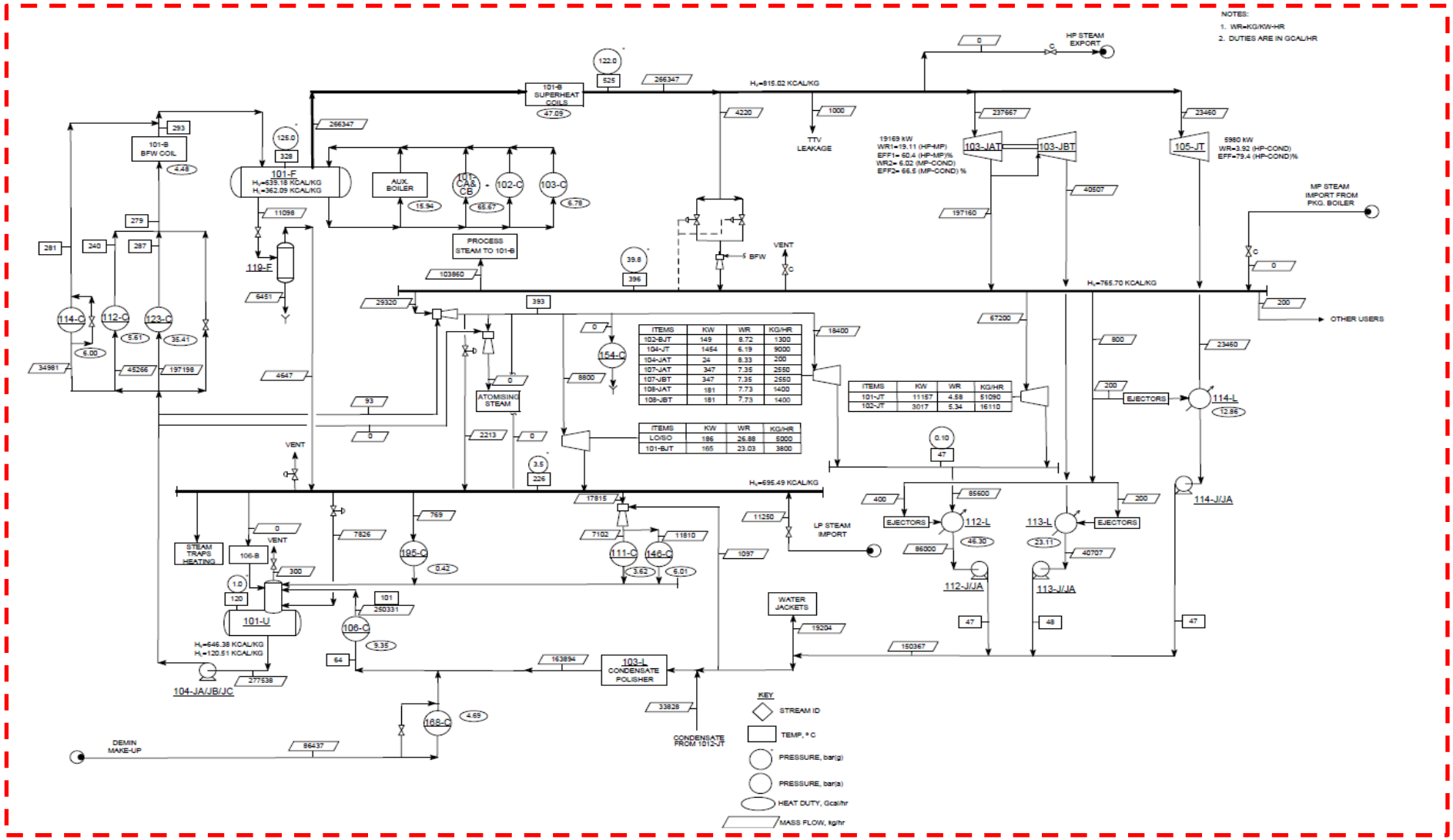

Figure 41. Steam network of the ammonia reference plant included in optimization analysis.

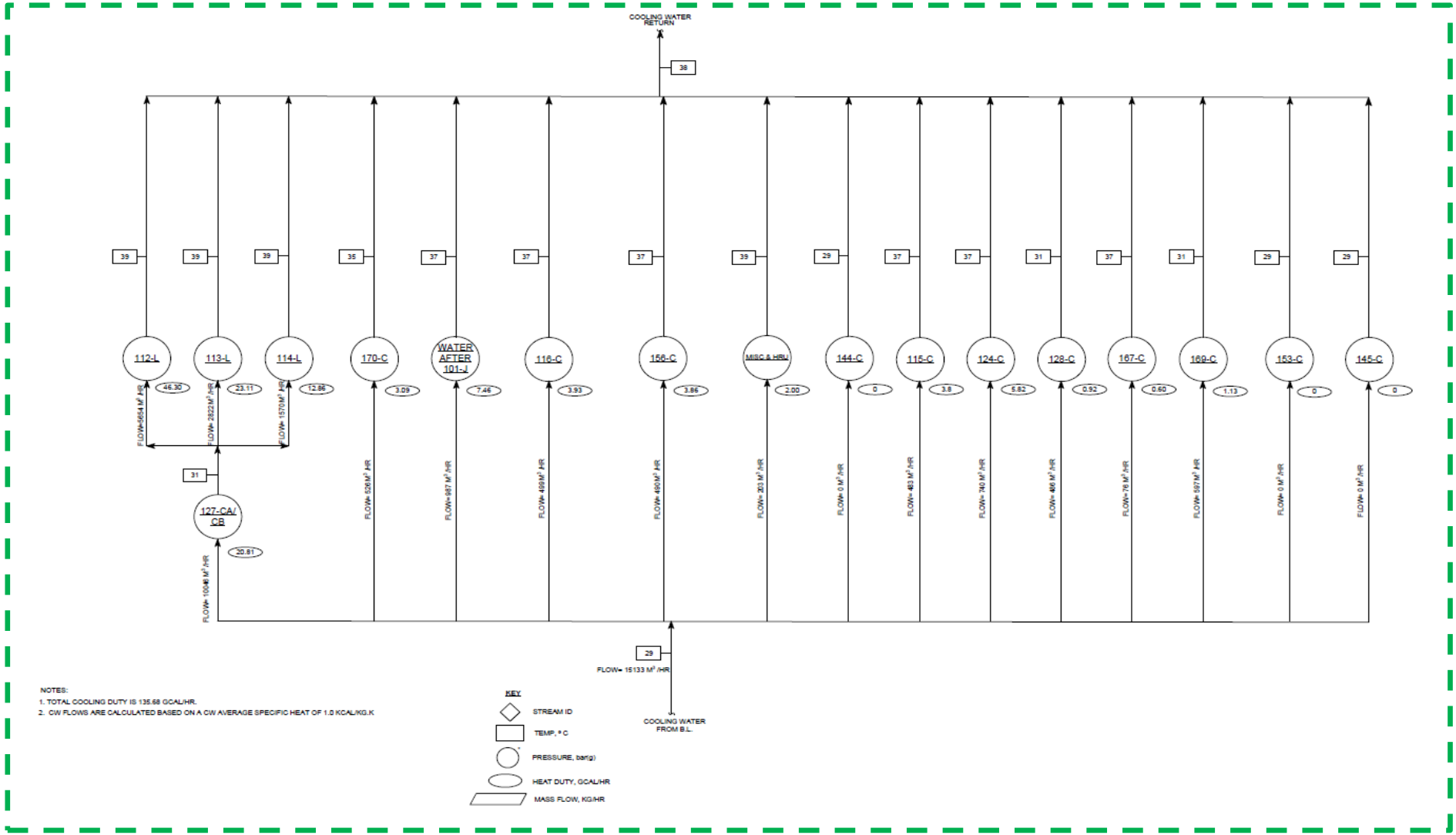

Figure 42. Cooling water network of the ammonia reference plant included in optimization analysis.

The last part of the heat in the amount of 7,02 MW is waste heat, which cannot be used in further process due to the low temperature of the waste gases (approx. 130°C).

Waste heat in the convection section is used for preheating of the process streams in the ammonia production process which are mixed feed of natural gas and steam, a mixture of air and steam, steam, boiler feed water, and finally combustion air used in reformer furnace. The major part is used for preheating of the steam (54,77 MW) and combustion air used in the reformer furnace (21,43 MW), while the balance is used for other mentioned process streams.

From the data presented in Table 28 and Figure 44 it can be seen that the main equipment in charge for the steam production is the waste heat boilers 101–CA/CB, 102–C, and 123–C (approx. 47,0%) which uses the waste heat coming out from the SMR reaction (primary and secondary SMR's) and ammonia synthesis reaction. Another part of the steam is produced on account of natural gas combustion in the reformer furnace, 101–B superheater coil, auxiliary boiler, and 101–B BFW coil (approx. 31,0%). The balance of approx. 22,0% belongs to the utilization of the LP steam, heat extracted from the Benfield system, and the reaction heat coming out from the WGS and methanation reaction. The main dissipation of the steam can be noticed at the steam condensers 112–L, 113–L, and 114–L (approx. 38,0%), while the second consumer of the steam is the SMR reaction in the reformer tubes (approx. 37,0%). The next consumer is back pressure and condensed steam turbines (approx. 19,0%), while the rest (approx. 6,0%) is related to the blowdown process of the steam drum and for heating of different process streams by heat exchangers.

The heat coming out of the primary and secondary SMR units is used for desorption of CO_2 chemically absorbed into Benfield solution for which it is required approx. 30000 kW per kmol of CO_2. Together, the CO_2 emissions of the stripper vent (approx. 69,0%) and the reformer furnace stack (approx. 21,0%) achieve 1,952 t_{CO2}/t_{NH3}. This is close to 1,87 t_{CO2}/t_{NH3} reported in [117], with CO_2 typically compressed and used for urea production. The benchmark value of ammonia production is at the level of 1,619 t_{CO2}/t_{NH3} [115].

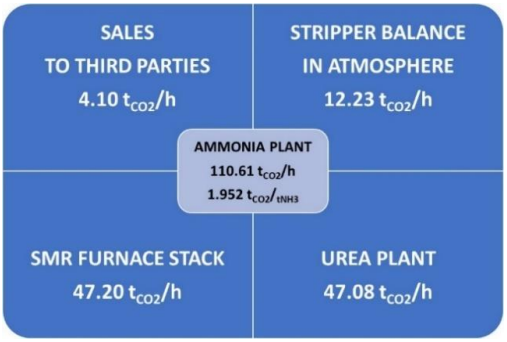

Figure 43. The CO_2 emission balance form the reference ammonia plant.

Table 28. The steam balance from production and consumption side.

Item	Module	Heat duty [MW]
STEAM PRODUCTION		
146-C	Condensate stripper	6,99
111-C	Benfield solution reboiler	4,21
195-C	Natural gas heater	0,49
LP steam	LP steam for deaerator	6,33
168-C	Demineralised water heater – methanator effluent	5,45
106-C	Demineralised water heater – synthesis gas before CO_2 absorber	10,87
114-C	BWF heater - methanator effluent	6,98
112-C	BWF heater - LTS effluent	6,52
123-C	BWF heater – ammonia convertor effluent	41,18
101-B BFW coil	BWF heater – waste heat from reformer furnace	5,21
101-B superheater coils	HP steam heater – waste heat from reformer furnace	54,77
Auxiliary boiler	HP steam production – natural gas firing	18,54
101-CA/CB + 102-C	HP steam production – waste heat from secondary reformer	76,37
103-C	HP steam production – waste heat from HTS effluent	7,88
TOTAL STEAM PRODUCTION		**+ 251,79**
STEAM CONSUMPTION		
103-JT	Synthesis gas compressor	25,13
105-JT	Refrigeration compressor	5,98
Leakages	HP system leakages	0,95
Steam reforming	MP steam for SMR reaction	92,49
102-BJT	Combustion air fan	0,150
104-JT/JAT	BFW pump	1,50
107-JAT/JBT	Semi-lean Benfield solution pump	0,70
108-JAT/JBT	Lean solution Benfield pump	0,360
101-BJT	Waste gas fan	0,360
101-JT	Secondary reformer air compressor	11,16
102-JT	Natural gas compressor	3,02
112-L	Steam condenser for MP steam turbines	53,85
113-L	Steam condenser for 103-JT steam turbine	26,88
114-L	Steam condenser for 105-JT steam turbine	14,96
146-C	Condensate stripper	6,99
111-C	Benfield solution reboiler	4,21
195-C	Natural gas heater	0,49
Blowdown	Blowdown of the steam system	8,57
TOTAL STEAM CONSUMPTION		**- 251,79**
BALANCE TOTAL STEAM PRODUCTION - CONSUMPTION		**0,0**

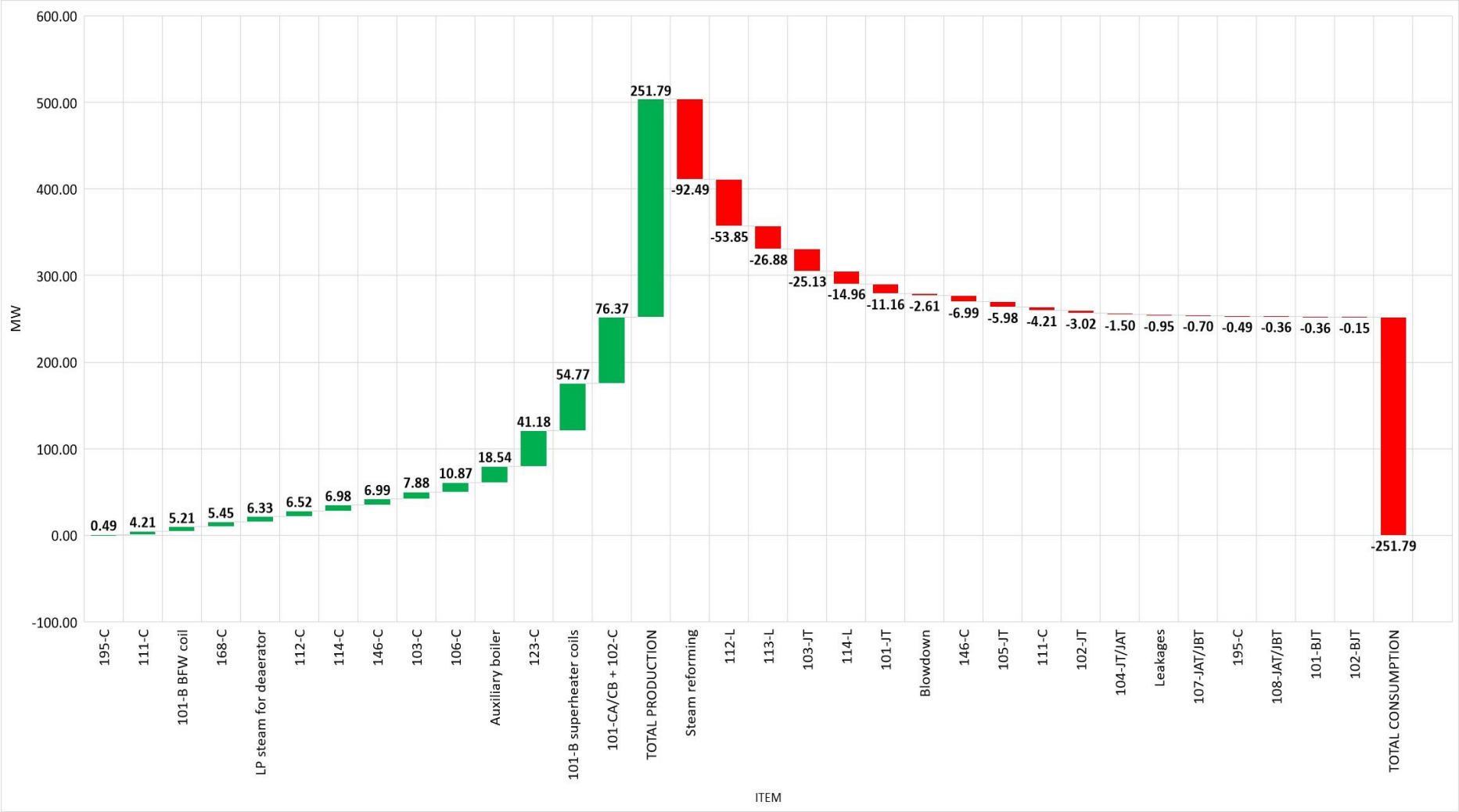

Figure 44. The steam balance from production and consumption side.

Regarding data given in Figure 42, the total cooling duty for an ammonia plant is 157,8 MW. The biggest part of the cooling duty is related to steam condensers, after steam turbines in the amount of 95,68 MW or approx. 60,0%. The balance of the cooling duty is used in the ammonia synthesis unit for cooling down synthesis gas in the inter–stage coolers of synthesis gas compressor and for ammonia cooler. The total cooling water consumption is 15133 m^3/h or 267 m^3/t_{NH3}.

Due to reason that a major part of the rotating equipment is driven by steam turbines, electricity consumption during ammonia production presents a minor part in the overall consumption scheme. At 100% of production capacity of the reference ammonia plant, the electricity consumption is at the level of 0,014 MWh/t_{NH3}.

In order to make the optimization of the reference ammonia plant, according to Equation (213), in Table 29 is given necessary data which were used as reference consumption values (without application of the proposed control system) in optimization analysis.

Table 29. Consumption and emission values for the reference ammonia plant.

Feedstock/utility/CO_2	**Unit**	**Value**
Natural gas for the process	MWh/t	6,25
Natural gas for combustion	MWh/t	3,61
Total natural gas	MWh/t	9,86
Steam	MW/t	4,44
Electricity	MWh/t	0,015
CO_2	t/t	1,952

5.3.3. Optimization cases

As discussed in the previous chapters, the ammonia production plant is designed in a highly integrated complex format where process streams are interlinked through a recycling loop and an extensive heat recovery network. In order to perform optimization analysis, it is necessary to define different realistic optimization problems, according to which objective function will define the optimal solutions. Optimized solutions will be the subject of the proposed control system, which primary task is keeping these optimal solutions in a steady state with the possibility to reject all process disturbances. Finally, the goal to make more ammonia at a reasonable cost, or the same quantity at less cost. In order to test the application of the proposed control system, selected optimization problems were following:

1. Case 1 – variation in steam–to–natural gas molar ratio;
2. Case 2 – variation in air–to–natural gas molar ratio;
3. Case 3 – variation in ammonia–to–natural gas molar ratio;
4. Case 4 – primary reformer catalyst and reforming tubes wall temperature optimization.

In order to perform optimization analysis, it is necessary to define the reference unit price of each indicator of net profit defined in Equation (213). The related values are given in Table 30 and the same are weighted averaged values surveyed on 31 ammonia plants in 2019 ordered by the Fertilizer Europe Association [118].

Table 30. The reference unit price of net profit indicators.

Profit index	Ammonia	Purge gas	Steam	Natural gas	Electricity	Cooling water	CO_2
The reference unit	€/ton	€/MWh	€/MWh	€/MWh	€/MWh	€/ton	€/ton
Price	187,31	12,93	18,76	18,47	57,22	0,01	20,00

The steady–state flowsheet of the reference ammonia plant with the systematic SQP approach is used to find an optimal solution object to the technical, thermodynamic, and operational constraints regarding design variables and constants.

Subject to constraints are:

- the plant is operated in self–sustaining mode between 88% and 106% of production capacity with possibility to export LP steam (4 bars; 192^{o}C);
- minimum energy requirements satisfied by the waste heat recovery in radiation and convection section of the reformer furnace;
- 3,0 to 4,0 mol.% per dry basis of O_2 excess in waste gas of reformer furnace to achieve appropriate combustion conditions;
- natural gas LHV between 32775 and 36225 kJ/m^3;
- minimum and maximum primary SMR catalyst temperature in reformer tubes between 700 and 815^{o}C to achieve reasonable catalyst activity, reformer tubes lifetime due to metallurgical limitations, and hydrogen production;
- minimum S/N.G. molar ratio of 2,8 to avoid hydrocarbon cracking and carbon deposition;
- maximum methane slip after reformer tubes of 10,60 mol.% per dry basis;

- maximum operating pressures of reformer tubes of 32 bar;
- maximum secondary SMR catalyst temperature of 1150^{o}C to achieve reasonable catalyst activity, refractory lining lifetime and hydrogen production;
- maximum methane slip after secondary reformer unit of 0,50 mol.% per dry basis;
- minimum steam–to–synthesis gas molar ratio for HT WGS of 0,40 and for LT WGS of 0,30;
- maximum CO slip after HT WGS converter of 2,50 mol.% per dry basis and of 0,25 mol.% per dry basis after LT WGS converter;
- maximum CO_2 content in the purified synthesis gas after CO_2 absorber of 500 ppm;
- no CO_2, CO and O_2 content in the purified synthesis gas after the methanator converter;
- maximum inert gas content (CH_4 + Ar) in the synthesis loop of 16,0 mol.% per dry basis;
- maximum ammonia content in the recycled synthesis gas after condensation of ammonia of 2,60 mol.% per dry basis;
- minimum temperature approach at the gas–gas heat exchangers of 30^{o}C;
- minimum temperature approach in the waste heat recovery exchanger of 30^{o}C to avoid temperature cross between the process gas and steam;
- convergence of the recycle stream in the ammonia synthesis loop;
- purge gas volume flow rate between 6800 and 9200 m^3/h;
- maximum temperature of the ammonia synthesis catalyst of 550^{o}C due to prevention of hydrogen embrittlement, catalyst activity and ammonia production;
- maximum approach to equilibrium for all catalysts in series of 10^{o}C;
- minimum H_2–to–N_2 molar ratio in the synthesis gas of 2,3.

Design variables are:

- S/N.G. molar ratio between 2,8 and 3,6;
- primary reformer outlet temperature between 700 and 815^{o}C;
- fuel to feedstock ratio of 60 to 40%;
- mixed feed preheating temperature of 498^{o}C;
- air + steam preheating temperature for the secondary SMR of 490^{o}C;
- steam preheating temperature of 525^{o}C;
- BFW preheating temperature of 293^{o}C;
- four level cascade steam system of 125, 40, 12 and 4 bars;

- energy consumption in the Benfield unit of 25789 kcal/kmol;
- steam–to–synthesis gas molar ratio for HT WGS between 0,4 and 0,6 and for LT WGS between 0,30 and 0,46;
- normal air molar rate for the secondary reformer of 2195,5 kmol/h;
- normal natural gas mass rate to feedstock of 25574 kg/h;
- normal natural gas mass rate to fuel of 14950 kg/h;
- preheating temperature to the 1st bed of ammonia synthesis catalyst of 340^{o}C;
- ammonia synthesis loop pressure between 150 and 200 bar;
- electrical power import with 30% efficiency of 1506 kWh/h.

Constants are:

- nominal ammonia production rate of 1360 metric tons/day or 56,666 metric t/h;
- compression efficiency of 85%;
- steam turbine efficiency of 75%;
- cooling water temperature of 28^{o}C inlet and 38^{o}C outlet;
- demineralised water temperature of 25^{o}C;
- steam condensate temperature of 48^{o}C;
- minimum temperature approach in the heat exchanger network of 20^{o}C;
- catalyst properties as were defined in the Chapter 4.1;
- "rich" Benfield solution mass concentration of 30,0 mas.%;
- all other assumptions and limitations as it were defined in Chapter 4.3.

5.3.3.1.Case 1 – variation in steam–to–natural gas molar ratio

The S/N.G. molar ratio has a significant influence during ammonia operation because of several reasons. This are a prevention of the carbon forming reactions under steam reforming conditions, promotion of the SMR and WGS reactions with subsequent production of more hydrogen, reduction of the methane content in the synthesis gas entering the ammonia synthesis loop, and ensuring the heat in the WGS and Benfield units. In practice, S/N.G. molar ratios between 3,0 and 3,5 are commonly used, however, there can be economic attractions in using lower S/N.G. molar ratios and there is a trend in this direction. In the case of higher S/N.G. molar ratio methane slip out of the primary and secondary reformer decrease which reflects the lower methane molar content (inert gas) in the ammonia synthesis loop and subsequently lower

compression costs. From another point of view, a higher S/N.G. molar ratio will also promote the WGS reaction giving a better conversion of carbon monoxide, creating more hydrogen, and increase ammonia production. The Benfield unit, which is a high consumer of heat, will also benefit from the higher S/N.G. molar ratio because a lower amount of steam will be used for the "rich" Benfield solution regeneration process. The higher amount of steam in the reformer tubes will also have beneficiary process conditions against reformer catalyst because of the prevention of the carbon forming reactions and it will positively influence the lower temperature of the reforming tubes alloy prolonging their lifetime. However, a higher S/N.G. molar ratio negatively influences the production costs due to the reason that the higher amount of steam must be produced which will cause the higher consumption of the natural gas and higher CO_2 emission.

A decrease in the S/N.G. molar ratio will increase the methane slip out of the primary and secondary reformer, which must be compensated with a higher firing rate in the radiation section of the reforming furnace. The higher firing rate will negatively influence the lifetime of the reforming tubes and potentially cause carbon forming reactions. Consequently, the smaller amount of steam will be available for WGS and Benfield units with the final negative impact on the ammonia synthesis loop which will suffer from the higher inert gas molar content and higher compression costs. The positive effect of a smaller S/N.G. molar ratio is a smaller amount of heat needed for steam generation and smaller CO_2 emissions.

Regarding all mentioned and to keep the SMR furnace operation in the safe regime with the final objective to achieve as much as possible lower energy consumption, the trade–off between these two extremes must be accomplished.

According to all given constraints, the trends from the optimization case for variation of the S/N.G. molar ratios and their influence on profit income can be seen in Figure 45. As it can be observed from the trend given in Figure 45, when the S/N.G. molar ratio was increased, the profit income also increased until it reached 3,3. After this point, the extra conversion of the natural gas and carbon monoxide did not give enough increase in the profit income to compensate for the additional steam quantity. In Table 31, it can be seen the influence of the S/N.G. molar ratios on the main process parameters for the three extremes, low, optimum, and reference case.

It can be observed from Table 31 that the steam consumption is lowered down with the decrease of S/N.G. molar ratio, which could positively affect profit income. However, at the same time, the methane slip is higher, which causes lower hydrogen yield and higher molar concentration of the inert gases in the synthesis loop. The higher molar concentration of the

inert gases in the synthesis loop causes higher ammonia synthesis converter pressure, which negatively influences the synthesis gas compressor power.

Figure 45. The relationship of profit income against steam – to – natural gas molar ratio.

All these drawbacks negatively reflect the profit income. Regarding the optimal case (S/N.G. = 3,3) in comparison with the reference case, the lower amount of steam compensates the higher costs caused by higher molar concentration of the inert gases in the synthesis loop, higher synthesis converter pressure, and higher synthesis gas compressor power. Lower steam to synthesis gas molar ratio after HT and LT WGS is high enough to bring hydrogen yield at a satisfactory level, while the heat input is good enough to regenerate successfully the "rich" Benfield solution without the additional import of LP steam.

In the reference ammonia plant, operational philosophy is to keep the S/N.G. molar ratio at the level of 3,6 which creates the loss at the given conditions in the amount of 2,78 million of € per year (the basis for calculation is 330 operating days). By implementation of the proposed control structure based on recommendations from optimization analysis, the profit income could be improved by 3,31% which presents an attractive opportunity for carrying out.

Table 31. Influence of the steam–to–natural gas molar ratios on the main process parameters for the three extremes, low, optimum and reference case.

Process parameter	Unit	Steam – to – natural gas molar ratio		
		minimum case	optimal case	reference case
		2,8	3,3	3,6
Methane slip after primary SMR	mol. %	10,89	10,52	10,39
Methane slip after secondary SMR	mol. %	0,39	0,35	0,31
Steam to synthesis gas molar ratio after HT WGS	kmol/kmol	0,371	0,420	0,458
Steam to synthesis gas molar ratio after LT WGS	kmol/kmol	0,331	0,393	0,429
Hydrogen yield	%	65,17	67,32	69,22
Ammonia synthesis converter pressure	bar	174,5	171,0	168,0
Synthesis gas compressor power	MW	27,45	26,24	25,13
Inert molar concentration in ammonia synthesis loop	mol. %	16,65	15,57	14,69
Ammonia molar concentration after ammonia synthesis converter	mol. %	14,68	15,32	15,68
Steam consumption	t/t	4,32	4,55	4,70

5.3.3.2.Case 2 – variation in air–to–natural gas molar ratio

By changing the air–to–natural gas molar ratio it is influenced directly to the H_2–to–N_2 molar ratio in the ammonia synthesis loop. The H_2–to–N_2 molar ratio is one of the more important process parameters in the operation of an ammonia facility. The rate–determining step in the ammonia synthesis reaction is the dissociative chemisorption of nitrogen on the activated catalyst surface, suggesting that the use of nitrogen “rich” synthesis gas would enhance the reaction rate [60]. In practice, within the limits imposed by overall optimization, a molar ratio between 2,4:1 to 3,0:1 gives the efficient operating point.

There are a couple of the main factors which individually or collectively could contribute to a change in the H_2–to–N_2 molar ratio of the recycling synthesis gas. This is a change in the synthesis’s gas composition from the reforming and purification units, a change in the synthesis feedstock gas rate, a change in the ammonia content of the recycling gas, and a change in the inert gas molar content. All these changes could be controlled by the proposed control system.

Figure 46 demonstrates the relationship of profit income against H_2–to–N_2 molar ratio, which was obtained by changing the air–to–natural gas molar ratio. The lower H_2–to–N_2 molar ratio has a negative influence on the air compressor shaft because it needs more power for the delivery of more air in the secondary reforming unit. At the same time, the molar content of methane leaving the secondary reformer was reduced, which is explained by the effect of additional oxygen and higher combustion temperature above the secondary reformer catalyst – a positive impact on SMR equilibrium. This effect on SMR equilibrium brings more hydrogen into the synthesis unit, but the quantity is not significant. At the same time, an additional amount of oxygen could react with hydrogen to produce water and in such a way to have a negative influence on the WGS reaction. In combination with the oxygen, it comes the additional amount of nitrogen which pushes the ammonia synthesis equilibrium towards the ammonia product and subsequently to increased ammonia production. All this leads to the direction that the ideal molar ratio of 3 to 1 is not attractive from the economic side, which can be observed in Figure 46.

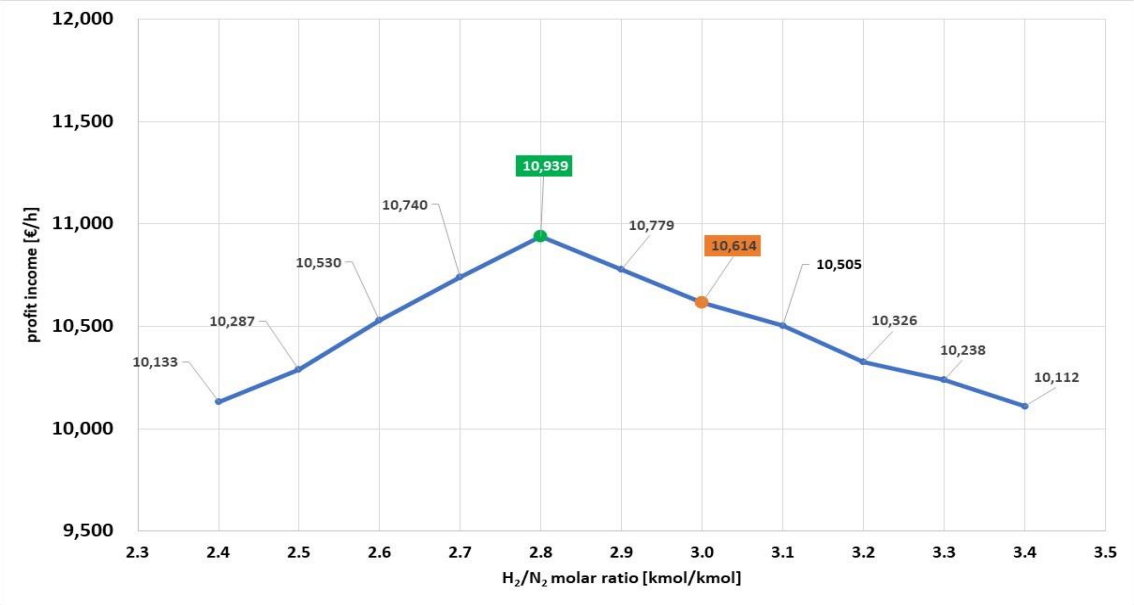

Figure 46. The relationship of profit income against H_2 – to – N_2 molar ratio.

It can be noticed from the optimization case that the highest profit income is achieved at the H_2–to–N_2 molar ratio of 2,8. It is also visible that an increase in the molar ratio in the direction of the ideal molar ratio and even higher was not profitable. This can be explained by the fact of less air in the secondary reformer (lower combustion temperature), higher methane molar

content leaving the secondary reformer (higher molar content of inert gases in ammonia synthesis loop negatively influence the power consumption on ammonia synthesis compressor because of higher synthesis pressure) and less nitrogen to react with hydrogen (lower ammonia production rate). Also, it can be noticed that further decrease of H_2–to–N_2 molar ratio below 2,8 decreases the profit income. Too much nitrogen in the ammonia synthesis loop acts similarly as inert gases (CH_4 + Ar), because the same will build–up the pressure in the ammonia synthesis converter if the molar concentration of the hydrogen is too low. In case of too much nitrogen in the synthesis loop, it can be created process conditions that can cause a drop in ammonia production and even in extreme cases cessation of the ammonia synthesis reaction over the catalyst.

In Table 32 it can be seen the influence of the H_2–to–N_2 molar ratios on the main process parameters for the three extremes, low, optimum, and ideal case.

Table 32. Influence of the H_2–to–N_2 molar ratios on the main process parameters for the three extremes, low, optimum and reference case.

		H_2–to–N_2 molar ratio		
Process parameter	**Unit**	**minimum case**	**optimal case**	**ideal case**
		2,4	**2,8**	**3,0**
Air gas compressor power	MW	13,45	12,34	11,16
Methane slip after secondary SMR	mol. %	0,26	0,28	0,31
Hydrogen yield	%	67,82	71,01	69,22
Ammonia synthesis converter pressure	bar	169,5	166,5	168,0
Synthesis gas compressor power	MW	26,45	24,34	25,13
Inert molar concentration in ammonia synthesis loop	mol. %	12,65	13,57	14,69
Ammonia molar concentration after ammonia synthesis converter	mol. %	15,01	16,75	15,68
Steam consumption	t/t	5,32	4,55	4,70

From the process parameters given in Table 32 it can be noticed that in the optimal case air gas compressor power increases, but at the same time synthesis gas compressor power decreases. This is explained because the synthesis pressure is lower on account of favourable ammonia conditions against ammonia synthesis reaction and lower inert gas molar content in

the recycle loop. This is also confirmed by the higher ammonia molar concentration after the ammonia synthesis converter.

As with S/N.G. molar ratio, the operational philosophy in the reference ammonia plant is to keep the H_2–to–N_2 molar ratio at the ideal conditions or 3 to 1. The difference in the profit income between ideal molar ratio (3 to 1) and optimized molar ratio (2,8 to 1) is 2,57 million € per year (330 operating days). Again, by control of process parameters which will keep a constant value of H_2–to–N_2 molar ratio at optimized level, it can be saved 2,97% of variable production cost which presents an attractive opportunity for implementation of the advanced control system.

5.3.3.3.Case 3 – variation in ammonia–to–natural gas molar ratio

The turn-down ratio (minimum production capacity) of the reference ammonia plant is 88% of the name plant capacity or 49,81 metric t/h. At this ratio, it is not possible to operate the ammonia plant in a self–sustaining mode so the import of HP and MP steam from the adjacent power generation facility is mandatory. At name plant capacity, the ammonia–to–natural gas molar ratio is 2,667. Regarding conducted technical adjustments, during the years, the facility can operate beyond name plant capacity and the maximum practical confirmed result is at the level of 106%. Between 88% and 106% of production capacity, the ammonia plant can export the LP steam. Regarding this, optimization case 3 was performed with the ammonia–to–natural gas molar ratio between 2,347 and 2,827. The results are shown in Figure 47.

From the simulated trend in Figure 47, it can be observed that the minimum profit income is achieved at the turn–down ratio, while the maximum profit income is at the level of 106%. This is supported mainly on account of the LP steam export (credit), which has a maximum value of 106% at no LP steam export at 88% of the name plant production capacity. However, it can be also noticed that over 100% of the name plant capacity, the positive effect is minor one due to reason that the cost of CO_2 diminishes the positive effect of the LP steam export. On account of the higher ammonia production rate, it can be achieved the positive effect of 0,840 million € which represents an overall gain of 1%. Nevertheless, control of constant ammonia–to–natural gas molar ratio has another important role, and this is control of the two inner PID controllers in the advanced control system in charge of controlling the S/N.G. and air–to–natural gas molar ratios. In the end, an additional 1% of savings presents the overall saving in the amount of 7,28% or in total 6,19 million € per year. In Table 33, it is shown the influence of ammonia–to– natural gas molar ratio variations on main process parameters.

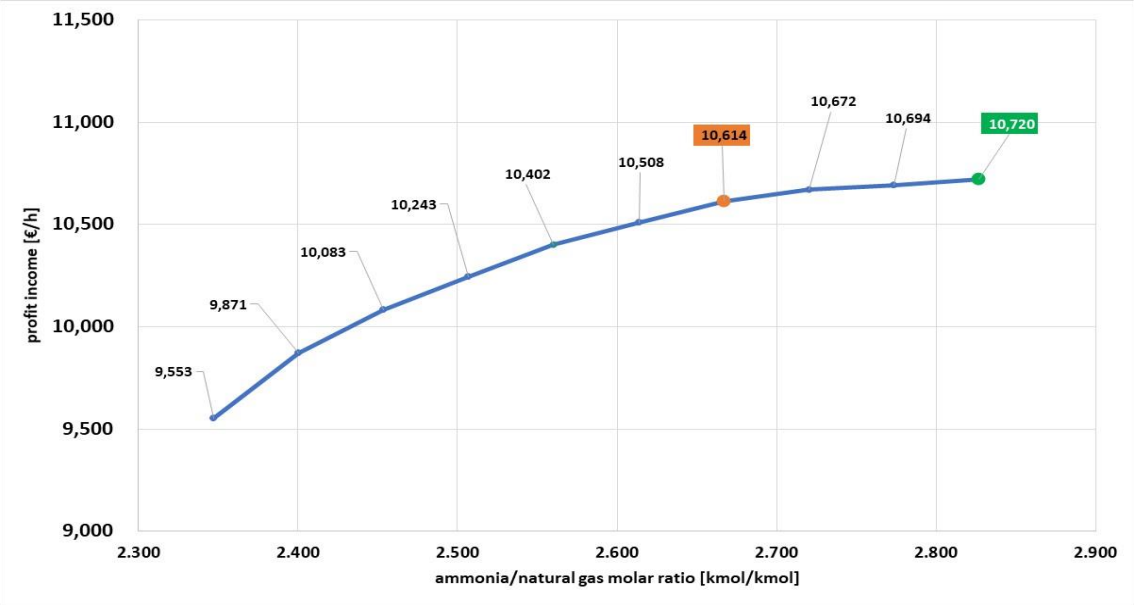

Figure 47. The relationship of profit income against ammonia–to–natural gas molar ratio.

The simulated results given in Table 33 show that at 106% of the name plant production capacity the net export of LP steam is the highest and this effect contributes to the highest profit income of the ammonia production facility. Besides that, the facility can deliver 3,34 metric t/h of liquid ammonia in surplus, which presents at yearly basis additional amount of approx. 26000 metric tons. This offers the possibility to be transferred to downstream consumers or to be sold on the open market.

Regarding all mentioned it can be concluded that the proposed control system shows an opportunity for implementation in an ammonia production facility not only from the economic point of view but also from the safety and environmental points of view. In order to follow optimization procedure and keep stable operation, it is necessary to have the plant model, appropriate advanced control system interlinked with the DCS, and economic optimization algorithm. A mutual relationship between these three elements with the general scheme of data collecting and processing is shown in Figure 48.

Table 33. Influence of the ammonia–to–natural gas molar ratios on the main process parameters for the three extremes, low, optimum and reference case.

Process parameter	Unit	ammonia–to–natural gas molar ratio		
		88% production 2,347	**100% production 2,667**	**106% production 2,827**
Methane slip after primary SMR	mol. %	9,89	10,39	10,68
Methane slip after secondary SMR	mol. %	0,29	0,31	0,36
Steam to synthesis gas molar ratio after HT WGS	kmol/kmol	0,458	0,458	0,458
Steam to synthesis gas molar ratio after LT WGS	kmol/kmol	0,429	0,429	0,429
Hydrogen yield	%	68,25	69,22	70,85
Ammonia synthesis converter pressure	bar	163,5	168,0	176,0
Synthesis gas compressor power	MW	23,45	25,13	27,13
Inert molar concentration in ammonia synthesis loop	mol. %	14,01	14,69	15,32
Ammonia molar concentration after ammonia synthesis converter	mol. %	15,32	15,68	17,01
Steam consumption	t/t	4,32	4,70	4,80
LP steam export	t/h	0,0	5,0	10,0
CO_2 emission	t/t	1,720	1,952	2,069

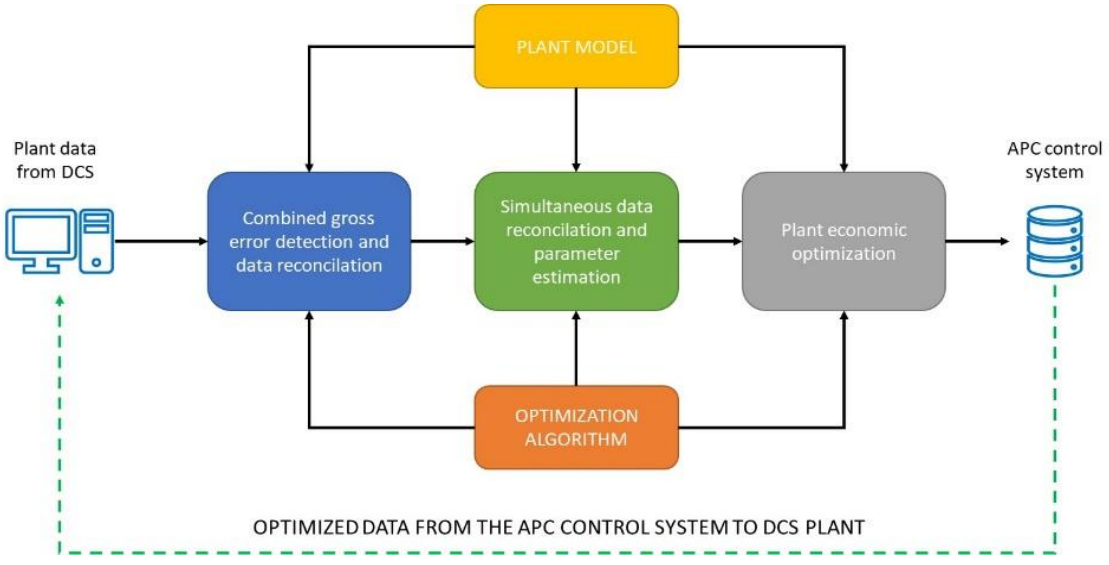

Figure 48. Key elements in optimization procedure of an ammonia plant.

Of course, the optimization economic procedure cannot be followed during transients and when disturbances are too big to be rejected by the proposed control system. However, during the online optimization of the process parameters operator must follow recommended procedure which interlinks the optimization objective function, a collection of the selected plant key process measurements, and execution of the advanced control system through DCS. In Figure 49 it is given a proposal of a flowchart with definitions of all necessary steps which must be taken to perform successful economic optimization of the ammonia production process.

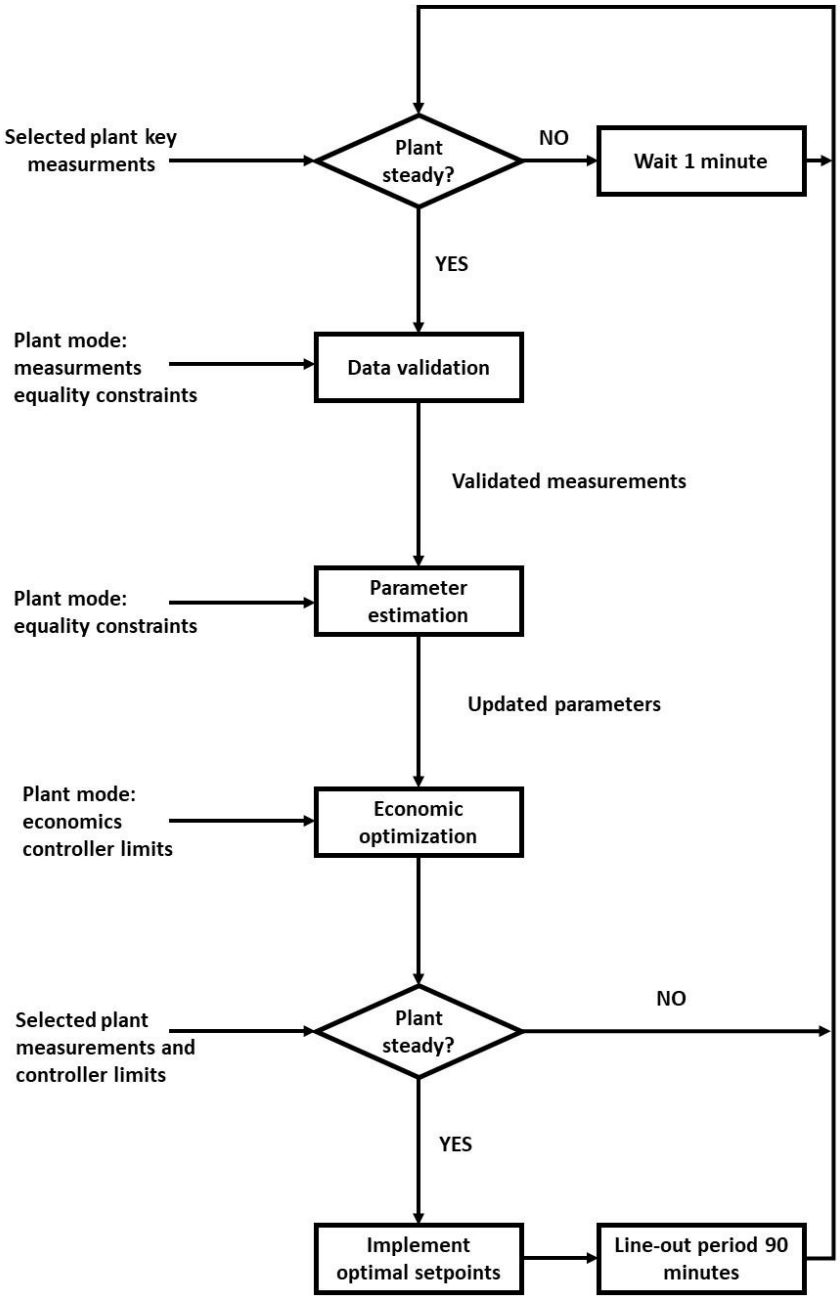

Figure 49. Flowchart for economic optimization procedure.

As it can be observed, the first and mandatory condition is that the plant must be in the steady–state condition when data are extracted from DCS and when set points are sent to the DSC. After that, follow the steps of data validation and parameter estimation. Herewith, it is emphasized again that the plant model for the economic optimization procedure must be in the steady–state regime. According to the practical operational experience, it is proposed that the optimization procedure is repeated every 90 minutes, which is enough time to get the most reliable process parameters. At the same time, this value complies with the transient time to reach a new steady–state of the proposed control system. As it was presented in the Figure 37, developed control system needs between 20 to 40 minutes to achieve steady–state conditions.

5.3.3.4. Case 4 – Primary reformer catalyst and reformer tubes wall temperature optimization

In order to address properly the evaluation of the catalyst performance in industrial conditions, the model determines the theoretical ATE_{CH4} at given process conditions and compares this value with the measured outlet CH_4 molar concentration. Properly designed reformers should, with the new catalyst, have ATE_{CH4} much lower than 5 to 10^oC. However, the ammonia plants which have desulphurization system often have reformer furnaces operating with ATE_{CH4} between 0 and 3^oC. When evaluation gives this level of ATE_{CH4}, the reformer catalyst is giving a satisfactory performance. The ATE_{CH4} levels above 10^oC would correspond to marginal performance and would become a factor in discharging the catalyst.

In any case, if the process parameters are not optimally adjusted, ATE_{CH4} regularly will be in the marginal range. Consequently, with appropriate adjustment of process parameters, the reformer catalyst performance can be brought to the satisfactory range below 10^oC. As it was mentioned, the temperature at which the exit gas composition would be at the equilibrium is determined in the model by calculating from the material balance the equilibrium constants and determining the corresponding temperature from the correlating equations.

According to data given in Table 3, it is visible that the SMR unit operates on the pressure of approx. 30 bars, exit temperature is at the level of 790^oC and S/N.G. molar ratio of 3,5 to 3,6. The reformer catalyst in the reference ammonia plant was delivered by Clariant and the same is in the operation for 1 year. All mentioned process parameters result in the outlet CH_4 molar concentration of 10,39 mol.% per dry basis. In order to evaluate the catalyst performance against the plant model, process data were fed from the DCS system to the model. The process data were used for the calculation of the theoretical equilibrium curve (the catalyst effectiveness

factor was additionally reconciled) and the plant model results were compared with the working point. The working point was at S/N.G. molar ratio between 3,5 and 3,6 and at the pressure level between 30 and 32 bars. The evaluation results are shown in Figure 50. According to the theoretical equilibrium curve at given process conditions, it can be seen that ATE_{CH4} is at the level of approximately 14^{o}C (790^{o}C minus 776^{o}C), which brings the marginal performance of the reforming catalyst in the operation. As it is stated, the reforming catalyst is only in operation for 1 year, and for the same, it is expected to have excellent activity and without carbon deposition because of a higher S/N.G. molar ratio of 3,5. Performed evaluation implies that with adjustments of process parameters, it can be improved the catalyst performance and the same brings in the satisfactory temperature range below 10^{o}C.

The model suggested that the heat load in the reformer furnace is not at the appropriate value to achieve theoretical equilibrium ATE_{CH4}. According to performed model evaluation, the main recommendation was to verify the firing conditions inside the reforming furnace. After examination of the flame patterns, tube wall temperatures, and distribution of the fuel volume flow rate through the arch and tunnel burners, it was concluded that there is space for improvement. By adjusting all mentioned parameters, the ATE_{CH4} was lowered down for 6^{o}C, which resulted in the final value of 8^{o}C.

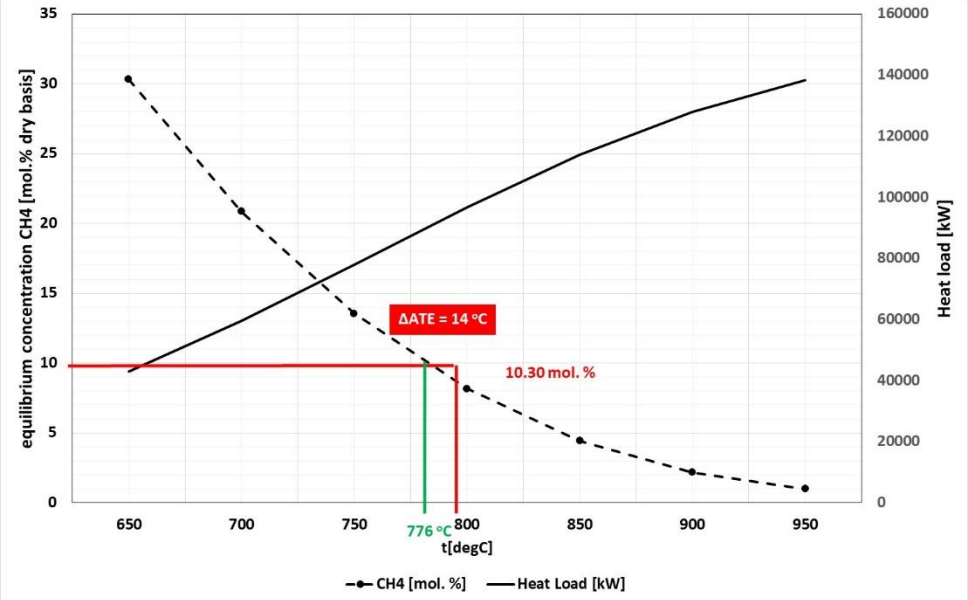

Figure 50. Evaluation of the reformer catalyst performance in operation of SMR unit.

In Figure 51 it is shown the catalyst outlet temperature readings regarding equilibrium temperature at three different outlet methane molar concentrations, namely 10,60, 10,40, and

10,20 mol.% per dry basis, respectively. In Figures 52 and 53 it is shown the tube wall temperature readings. In both cases, the results are shown before and after the implementation of recommendations given from the model in the period of 720 hours. From Figure 51 it can be seen that the ATE_{CH4} values before implementation of the recommendations from the model are at the level of approximately 14^{o}C. After following model recommendations (adjustments of the S/N.G. molar ratio and firing in the reformer furnace), the ATE_{CH4} values are approaching equilibrium temperature and the same are between 0 and 10^{o}C or precisely at 8^{o}C. The target value for outlet methane molar concentration was 10,40 mol.%.

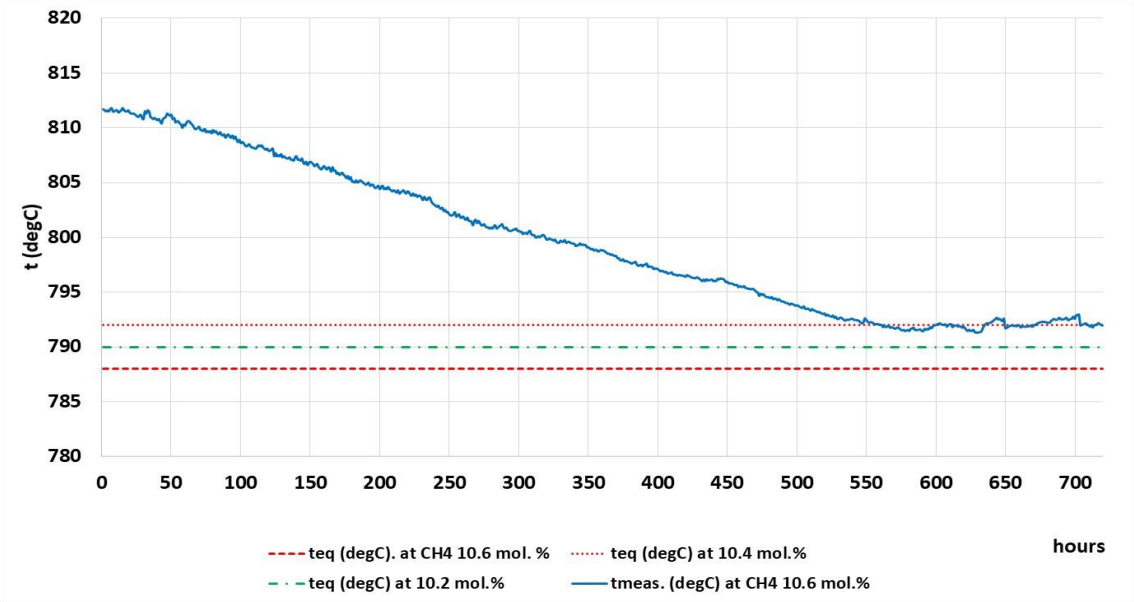

Figure 51. Catalyst outlet temperature readings regarding to equilibrium temperature at outlet methane molar concentrations of 10,6, 10,4 and 10,2 mol.%.

From Figure 52, it can be seen that the reforming tube wall temperatures are in the high–temperature range from 840 to 860^{o}C which reflects severe temperature conditions against reforming tube metal alloy. After following model recommendations by firing rate adjustment in the reformer furnace, the reforming tube wall temperature pattern is more uniform with the temperature range from 820 to 840^{o}C, which is shown in Figure 53. On average, this represents a 20^{o}C lower temperature, which is extremely favourable for the reforming tube performance, because a decrease of about 20^{o}C will significantly prolong the reforming tube lifetime.

During the test period, it was also measured the energy savings in the terms of lower natural gas consumption. Before applying the recommendations from the model, the natural gas

consumption was at the level of 1045 m^3/t of ammonia. Following model recommendations, it was observed that the natural gas consumption was lower for approximately 33 m^3/t of ammonia, which represents the savings in the amount of 3,15%. Achieved levels of savings present an extremely attractive savings scheme to be applied during the operation of top–fired SMR in ammonia production.

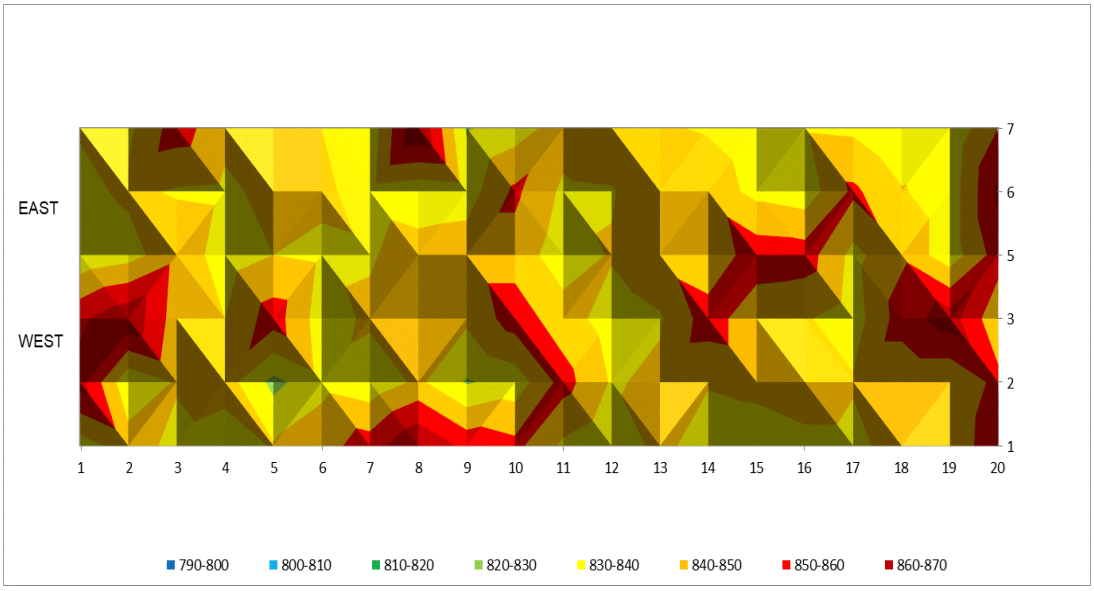

Figure 52. Tube wall temperature readings before implementation of recommendations from the model.

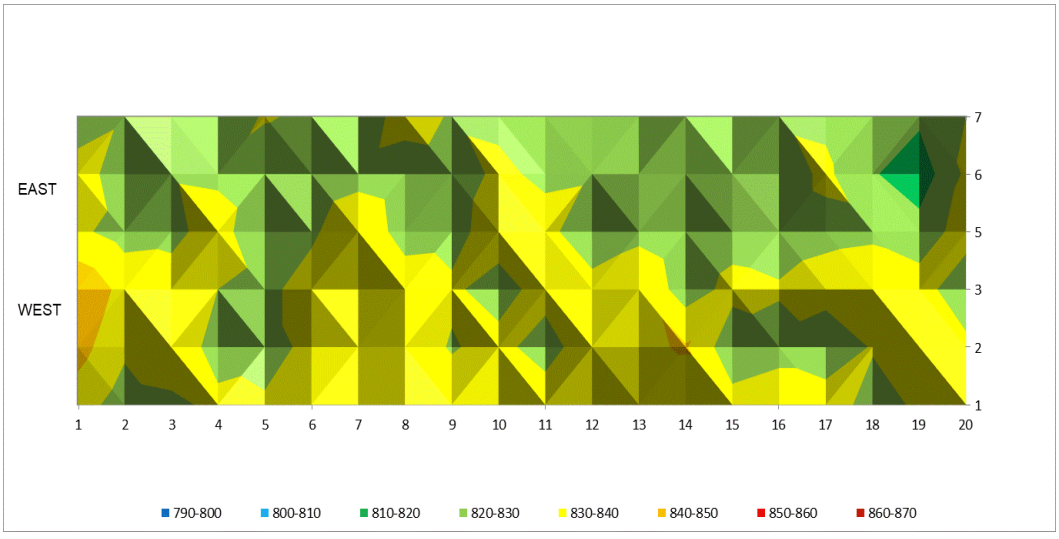

Figure 53. Tube wall temperature readings after implementation of recommendations from the model.

In total, it can be concluded that with the implementation of all investigated optimization cases the overall savings of approximately 10% could be achieved in the ammonia's operation production facility.

Last, the advanced control system could have a positive effect on the catalyst and reformer tube performance. The positive effect will reflect on catalyst activity, prolong the reforming tube lifetime, decreasing the maintenance costs, and reduce CO_2 emissions.

6. CONCLUSION

6.1.Achieved scientific contribution

Advancement of the process control system in ammonia production, which comprises steady–state and dynamic model, advanced ratio–cascade control system and optimization profit function have been studied in this dissertation. The major contributions and conclusions of this study are:

1. A critical review of the various APC methodologies with the accent to the PWC control theory together with their approach has been studied and presented. The combination of the theoretical approach based on heuristics and the operational experience was served for the development of an adequate steady–state and dynamic models of an ammonia plant.

2. Steady–state and dynamic simulation model of an ammonia plant as a test bed has been developed in UniSim Design R470 (Honeywell). The concept of the APC and the PWC control methodologies based on operational experience and actual process data from the reference ammonia plant have been applied to the plant models to develop centralized advanced control structure. The advanced control structure coupled all benefits of following independent control techniques, feedforward, feedback, ratio, and cascade control. The integration of these control techniques offered a new opportunity for a ratio–cascade advanced process control scheme with remarkable advantages against disturbance rejection. To achieve an optimal economic level and make a complex process simple, ammonia production rate set point acts as the primary/master while keeping the S/N.G. and air–to–natural gas molar ratios as secondary/slave controllers.

3. The dynamic performance of these control structures has been evaluated regarding actual process conditions, and it was found after the reconciliation of the tuning stability parameters, that a proposed control system yields superior performances which are robust and stable.

4. It has been proposed a new profit objective function which covers all process units in ammonia production plant, and also includes the cost minimization of the CO_2 emissions as the extra burden in the operating cost of the final ammonia product.

5. Regarding economic optimization objective function and control of all main process parameters with the new proposed control system, it could be achieved savings in the amount of approximately 10% or 6,19 million € per year in comparison with the reference ammonia plant at given feedstock and energy prices.

6. A model could be used for online monitoring activity and optimization of the catalyst's performance, prolonging lifetime of the reforming tubes, and minimizing maintenance costs.

7. Achieved results indicate that the developed model could be used for the application of the developed advanced control system on existing DCS ("brownfield" solution) or to be implemented as an additional feature during the development of the new projects ("greenfield" solution).

6.2.Recommendations for future work

Regardless to achieved theoretical contribution and indications that developed advanced control system could offer significant financial savings to the ammonia operators, there is still space for future work. The following items have been identified to be further developed:

1. In order to confirm theoretical results of the advanced control system, the same must be implemented in the real operation and tested against actual process parameters to confirm finally the economic benefits of the same.

2. Based on this approach it could be developed additional control system for the second layer in the ammonia production process which will consider the steam production system as the second important process during ammonia production.

3. It must be studied the development of the specific related control system which will be related to the further minimization of the CO_2 emissions from the ammonia plant with the major goal to approach as much as possible to the free allocated CO_2 emission quotas.

4. Regarding the achievement of even more savings during ammonia production, it must be further investigated a combination of other different optimization cases with the objective to find an absolute optimum.

5. Due to the reason that the ammonia plant is the starting raw material for fertilizer production it can be opened a new research area that can cover the development of the super–structured advanced control system for all other production units which are located inside of common fertilizer production complex, *e.g.* nitric acid plant, ammonium–nitrate plant, and urea plant. The main direction is the development of a master controller which will control the complete fertilizer production complex and minimize the overall production costs.

6. Implementation of “green” hydrogen source in ammonia production, and control with the advanced control system is the final recommendation for the future research to cover a new emerging industrial and scientific area in ammonia production with the major objective to deliver “green” ammonia as a raw material for fertilizers production, and energy carrier.

7. REFERENCES

[1] M. Appl, Ammonia principles and industrial practice, Wiley-VCH, Weinheim, 1999, pp. 1-5.

[2] D. A. Latham, K. B. McAuley, B. A. Peppley, T. M. Raybold, Mathematical modelling of an industrial steam-methane reformer for online deployment, Fuel Process. Technol. 92 (2011) 1574-1586.

[3] J. S. Lee, J. Seo, H. Y. Kim, J. T. Chung, S. S. Yoon, Effects of combustion parameters on reforming performance of a steam–methane reformer, Fuel 111 (2013) 461-471.

[4] J. E. Holt, J. Kreusser, A. Herritsch, M. Watson, Numerical modelling of a steam methane reformer, ANZIAM J. 59 (2018) C112-C127.

[5] L. Lao, A. Aguirre, A. Tran, Z. Wu, H. Durand, P. D. Christofides, CFD modelling and control of a steam methane reforming reactor, Chem. Eng. Sci. 148 (2016) 78-92.

[6] URL: https://openarchive.usn.no/usnxmlui/bitstream/handle/11250/2438478/2016Jinasena%2cLie%2cGlemmestad.pdf?sequence=2&isAllowed=y (accessed 15.01.2020.)

[7] I. I. Cheema, U. Krewer, Operating envelope of Haber-Bosch process design for power-to-ammonia, RCS Adv. 8 (2018) 34926-34936.

[8] M. J. Bland, Optimization of an Ammonia Synthesis Loop, Investigation of a Novel Approach for Optimization of Integrated plants, master thesis, Norwegian University of Science and Technology, Trondheim, 2015.

[9] D. Dilip, S. Raagaars, L. Chawes, L. Olesen, Energy Savings and Capacity Utilization of Advanced Control System, in Safety in Ammonia Plants & Related Facilities Symposium, 37th Annual Safety in Ammonia Plants and Related Facilities Symposium, San Antonio, TX-USA, Omnipress, New York, 1992, str. 278-289.

[10] A. Ishikawy, T. Baba, T. Miki, H. Ochi, Large-Scale Multivariable Controllers for Ammonia Plant, in Ammonia Plants & Related Facilities Symposium, 40th Annual Safety in Ammonia Plants and Related Facilities Symposium, Tuson, AZ-USA, Omnipress, New York, 1995, str. 313-320.

[11] K. Grasdal, P. Barone, W. A. Poe, Benefits of Advanced Control to Ammonia Plant Operations, in Ammonia Plants & Related Facilities Symposium, 38th Annual Safety in Ammonia Plants and Related Facilities Symposium, San Francisco, CA-USA, Omnipress, New York, 1997, str. 286-295.

[12] B. Frahm, R. Lin, W. A. Poe, Advanced Process Control Systems Improve Ammonia Plant Safety, in Ammonia Plants & Related Facilities Symposium, 41th Annual Safety in Ammonia Plants and Related Facilities Symposium, Tucson, AZ-USA, Omnipress, New York, 2000, str. 1-8.
[13] D. Seepersad, J. H. Ghouse, T. A. Adams, Dynamic simulation and control of an integrated gasifier/reformer system. Part II: Discrete and model predictive control, Chem. Eng. Res. Des., 100 (2015) 497-508.
[14] W. L. Luyben, B. D. Tyreus, M. L. Luyben, Plantwide Process Control, McGraw-Hill, New York, 1998, str. 45-48.
[15] W. L. Luyben, Plantwide control of a coupled reformer/ammonia process, Chem. Eng. Res. and Des. 134 (2018) 518-527.
[16] A. Araújo, S. Skogestad, Control structure design for the ammonia synthesis process, Comput. Chem. Eng. 32 (2008) 2920-2932.
[17] C. Zhang, S. Vasudevan, G. Rangaiah, Plantwide control system design and performance evaluation for ammonia synthesis process, Ind. Eng. Chem. Res. 49 (2010) 12538-12547.
[18] A. J. Groenendijk, A. C. Dimian, P. D. Iedema, Systems approach for evaluating dynamics and plantwide control of complex plants, AIChE J. 46 (2000) 133-145.
[19] N. V. S. N. M. Konda, G. P. Rangaiah, P. R. Krishnaswamy, Plantwide control of industrial processes: An integrated framework of simulation and heuristics, Ind. Eng. Chem. Res. 44 (2005) 8300-8313.
[20] L. C. Daigre, G. R. Nieman, Computer control of ammonia plants, in Ammonia Plants & Related Facilities Symposium, 18th Annual Safety in Ammonia Plants and Related Facilities Symposium, Vancouver, Canada, Omnipress, New York, 1973, str. 45-49.
[21] P. Tijssen, Optimizing ammonia plant operation by computer, in Ammonia Plants & Related Facilities Symposium, 21st Annual Safety in Ammonia Plants and Related Facilities Symposium, Atlantic City, USA, Omnipress, New York, 1976, str. 155-159.
[22] P. G. Friedman, Evaluating computer control of ammonia plant, in Ammonia Plants & Related Facilities Symposium, 22nd Annual Safety in Ammonia Plants and Related Facilities Symposium, Denver, USA, Omnipress, New York, 1977, str. 85-88.
[23] C. C. Yost, C. R. Curtis, C. J. Ryskamp, Advanced control at Wycon's ammonia plant, in Ammonia Plants & Related Facilities Symposium, 24th Annual Safety in Ammonia Plants and Related Facilities Symposium, San Francisco, CA-USA, Omnipress, New York, 1979, str. 200-205.

[24] R. W. Parish, Microcomputers for off-line evaluation of ammonia plant operation, in Ammonia Plants & Related Facilities Symposium, 25th Annual Safety in Ammonia Plants and Related Facilities Symposium, Portland, USA, Omnipress, New York, 1980, str. 108-115.
[25] R. L. Allen, G. A. Moser, Advanced control and optimization applications in ammonia plants, in Ammonia Plants & Related Facilities Symposium, 36th Annual Safety in Ammonia Plants and Related Facilities Symposium, Los Angeles, CA-USA, Omnipress, New York, 1991, str. 170-176.
[26] D. Deshmukh, S. Raagaard, L. Chawes, L. Olesen, Energy savings and capacity utilization of advanced control system, in Ammonia Plants & Related Facilities Symposium, 37th Annual Safety in Ammonia Plants and Related Facilities Symposium, San Antonio, TX-USA, Omnipress, New York, 1992, str. 278-289.
[27] E. Kharbat, S. A. Matthews, Adaptive technologies economic optimization and process control, in Ammonia Plants & Related Facilities Symposium, 41st Annual Safety in Ammonia Plants and Related Facilities Symposium, Boston, USA, Omnipress, New York, 1996, str. 320-329.
[28] P. S. Buckley, Techniques of Process control. Chap. 13. John Wiley & Sons. 1964, pp 156-168.
[29] A. S. Foss, Critique of Chemical process control theory, AIChE J. 19 (1973) 209-214.
[30] A. Papadourakis, M. F. Doherty, J. M. Douglas, Relative gain array for units in plants with recycle, Ind. Eng. Chem. Res. 26 (1987), 1259–1262.
[31] E. A. Wolff, S. Skogestad, M. Hovd, Controllability of integrated plants, AIChE Spring National Meeting Paper 67a, 1992.
[32] R. M. Price, P. R. Lyman, C. Georgakis, Selection of throughput manipulators for plant-wide control structures. ECC ’93, pp. 1060–1066 (1993).
[33] W. L. Luyben, Snowball effect in reactor/separator processes with recycle. Ind. Eng. Chem. Res. 33 (1994), 299–305.
[34] W. L. Luyben, C. A. Floudas, Analyzing the interaction of design and control. 2. reactor separator recycle system. Comp. Chem. Eng. 18 (1994), 971–994.
[35] P. Mizsey, I. Kalmar, Effects of recycle on control of chemical processes. ESCAPE- 6, 26–29 May 1996, Rhodes, Greece; Supplement to Computers & Chemical Engineering, pp. S883–S888.
[36] K. L. Wu, C. C. Yu, Reactor/separator process with recycle-1. candidate control structure for operability. Comp. Chem. Eng. 20 (1996), 1291–1316.

[37] J. E. Hansen, Plant wide dynamic simulation and control of chemical processes. PhD thesis. Danmarks Tekniske Universitet, 1998.

[38] C. Ng, G. Stephanopoulos, Plant-wide control structures and strategies. To be published in Process System Engineering Series of Academic press, 1998.

[39] S. Skogestad, Control structure design for complete chemical plants. Computers and Chemical Engineering. 28 (2004) 219-234.

[40] S. Skogestad, Plantwide control: The search for the self-optimizing control structure. Journal of Process Control. 10 (2000) 487-507.

[41] J. C. Morud, S. Skogestad, Analysis of instability in an industrial ammonia reactor. AIChe Journal. 44 (1998) 888-895.

[42] M. van Wuck, Apparatus and method for controlling and ammonia production system. World Intellectual Property Organization, International Bureau, WO 2008/112621 A1, (2008).

[43] S. Vasudevan, Plant-wide control: methodologies, applications and performance assessment. A thesis submitted for the degree of doctor philosophy, Department of chemical and biomolecular engineering, National university of Singapore, (2010) pp. 167-171.

[44] E. Holter, Feedforward for stabilization of an ammonia synthesis reactor. A thesis submitted for the degree of master of science in engineering cybernetics, Norwegian university of science and technology, Department of engineering cybernetics (2010) pp. 167-171.

[45] Z. Chi, Studies on design and plant-wide control of chemical processes. A thesis submitted for the degree of master of engineering department of chemical and biomolecular engineering, National university of Singapore, (2011) pp. 40-65.

[46] M. Vinatoru, Modelling and control of the ammonia synthesis column. Seria Inginerie Electrica. 27 (2003) 71-78.

[47] A. Desai, S. Shah, S. Goyal, Simulation and energy optimization of ammonia synthesis loop. Int. J. Chem. Eng. Res. 5 (2018) 6-13.

[48] A. J. Gunorubon, R. N. Raphael, Simulation of an ammonia synthesis converter. Can. J. of Pure and Appl. Sci. 8 (2014) 2913-2923.

[49] C. P. Upaka, T. Izonowei, Model prediction on the reliability of fixed bed reactor for ammonia production. Chem. Int. 3 (2017) 46-57.

[50] F. T. Dastjerd, J. Sadeghi, The simulation and control of ammonia unit of Shiraz Petrochemical Complex, Iran. J. Chem. Petr. Eng. 52 (2018) 107-122.

[51] K. V. Reddy, A. Husaln, Modelling and simulation of an ammonia synthesis loop. Ind. Eng. Chem. Proc. Des. Dev. 21 (1982) 359-367.

[52] M. N. Pedernera, D. O. Borio, N.S. Schbib, Steady state analysis and optimization of a radial-flow ammonia synthesis reactor, Comp. Chem. Eng. 23 (1999) 783-786.

[53] M. R. Rahimpour, A. Z. Kashkooli, Modelling and simulation of industrial carbon dioxide absorber using amine-promoted potash solution. Iranian Journal of Science and Technology, 28 (2004) 656-666.

[54] J. G. Akpa, N. Raphael, Optimization of an ammonia synthesis convertor. World Journal of Engineering and Technology, 2 (2014) 305-313.

[55] UniSim Design, version R470; Software for Process Design and Simulation; Honeywell International Inc. US, https://www.honeywellprocess.com/en- US/online campaigns/unisim-design/Pages/index.html

[56] MATLAB (Matrix Laboratory), Version 2019b; Software for Numerical Computing; MathWorks: The MathWorks, Inc., 1994-2020 US. Available online: https://www.mathworks.com/products/matlab.html

[57] J. Rostrup-Nielsen, L. J. Christiansen, Concepts in Syngas Manufacture, Catalytic Science Series – Vol.10, Imperial College Press: London, 2011.

[58] J. Xu, G. F. Froment, Methane steam reforming, methanation and water-gas shift: I. Intrinsic kinetics. AIChE J. 35 (1989) 88−96.

[59] J. Xu, G. F. Froment, Methane steam reforming: diffusional limitations and reactor simulation. *AIChE J.* AIChE J. 35 (1989) 97-103.

[60] M. W. Twigg, Catalyst Handbook, Second Edition, Wolfe Publishing Ltd: London, 1989.

[61] C. M. Schillmoller, U. W. van den Bruck, Furnace Alloy Update**.** Hydrocarb. Process. 63 (1984) 55.

[62] D. Latham, Mathematical Modelling of An Industrial Steam Methane Reformer. Master's Thesis, Queen's University, 2008.

[63] G. Pantoleontos, G. Skevis, G. Karagiannakis, A. G. Konstandopoulos, A Heterogenous Multiscale Dynamic Model for Simulation for Catalytic Reforming Reactors. Int. J. Chem. Kin. 48 (2016) 239-252.

[64] Z. Wu, A. Aguirre, A. Tran, H. Durand, P. D. Christofides, Model Predictive Control of a Steam Methane Reforming Reactor Described by a Computational Fluid Dynamics Model. Ind. Eng. Chem. Res. 56 (2017) 6002-6011.
[65] L. Sun, Modelling and MPC for a Primary Gas Reformer, A thesis submitted to the Faculty of Graduate Studies and Research in partial fulfillment of the requirements for the degree of Master of Science in Process Control, Department of Chemical and Materials Engineering, 2013.
[66] A. M. Meziou, P. B. Deshpande, I. M. Alatiqi, Dynamic matrix control of an industrial steam gas reformer. J. Hydrogen Energy. 20 (1995) 187- 192.
[67] I. M. Alatiqi, A. M. Meziou, Dynamic simulation and adaptive control of an industrial steam gas reformer. Computers Chem. Eng. 15 (1991) 147-155.
[68] A. Tran, A. Aguirre, M. Crose, H. Durand, P. D. Christofides, Temperature balancing in steam methane reforming furnace via an integrated CFD/data-based optimization approach, Comp. & Chem. Eng. 104 (2017) 185-200.
[69] R. Pupo, Adiabatic Flame Temperature for Combustion of Methane. Undergraduate Journal of Mathematical Modelling: One+Two. 3 (2011) 2-10.
[70] S. Elnashaie, F. Uhlig, Numerical Techniques for Chemical and Biological Engineers Using MATLAB, A Simple Bifurcation Approach, Springer: New York, 2007.
[71] A. Olivieri, F. Veglio, Process simulation of natural gas steam reforming: Fuel distribution optimization in the furnace. Fuel Processing Technology. 89 (2008) 622-631.
[72] R. Rennhack, R. Heinisch, Kinetische Untersuchung der Reaktion Zwischen Methan und Wasserdampf an Nickel-Oberfächen. Erdöl und Kohle-Erdgas-Petrochemie Verinigt mit Brennstoff-Chemie. 1 (1972) 22.
[73] S. Z. Abas, V. Dupont, T. Mahmud, Kinetics study and modelling of steam methane reforming process over a Ni/Al_2O_3 catalyst in an adiabatic packed bed reactor. International Journal of Hydrogen Energy. 42 (2017) 2889-2903.
[74] F. M. Alhabadan, M. A. Abashar, S. S. Elnashaie, A Flexible Computer Software Package for Industrial Steam Reformers and Methanators Based on Rigorous Heterogeneous Mathematical Model. Math.Comput.Modelling. 16 (1992) 77-86.
[75] S. S. Elnashaie, S. S. Elshishini, Modelling, Simulation and Optimization of Industrial Fixed Bed Catalytic Reactors, Topics in Chemical Engineering. Gordon and Breach Science Publisher: London, 1993.
[76] M. Leva, M. Winstraub, M. Grummer, M. Pollchik, H. H. Storch, Fluid flow through packed and fluidized systems. U.S.Bur. Mines Bull. (1951), 504.

[77] E. L. Cussler, Diffusion: Mass Transfer in Fluid Systems (2nd ed.), Cambridge University Press: New York, 1997.
[78] E. Nauman, Chemical Reactor Design, Optimization, and Scaleup. John Wiley and Sons Inc.: Hoboken, 2008.
[79] D. Wolf, M. Höhenberger, M. Baerns, External Mass and Heat Transfer Limitations of the Partial Oxidation of Methane over Pt/MgO Catalyst-Consequences for Adiabatic Reactor Operation. Ind. Eng. Chem. Res. 36 (1997) 3345.
[80] A. A: Al-Dhfeery, A. A. Jassem, Modelling and simulation of an industrial secondary reformer reactor in the fertilizer plant. IJIC, 3 (2012) 1-8.
[81] W. H. Chen, T. C. Hsieh, An experimental study on carbon monoxide conversion and hydrogen generation from water gas shift reaction. Energy Conversion and Management, 49 (2008) 2801-2808.
[82] B. Smith, L. Muruganandam, A review of the water gas shift reaction kinetics. International Journal of Chemical Reactor Engineering, 8 (2010), Review R4, 1-31.
[83] D. S. Newsome, The water-gas shift reaction. Catal. Rev. Sci. Eng., 21 (1980) 275-318.
[84] R. L. Keiski, S. Tapio, J. P. Veikko, Development and verification of a simulation model for a nonisothermal water-gas shift reactor. The Chemical Engineering Journal, 48 (1992) 17-29.
[85] Y. Choi, H. G. Stenger, Water gas shift reaction kinetics and reactor modelling for fuel cell grade hydrogen. Journal of Power Sources, 124 (2003) 432–439.
[86] G. F. Froment, K. B. Bischoff, Chemical reactor analysis and design. John Wiley and Sons, London, 2nd edition, (1990) pp. 403-404.
[87] T. J. Edwards, G. Maurer, J. Newman, J.M. Prausnitz, Vapor-liquid equilibria in multicomponent aqueous solution of volatile week electrolytes. AIChE J., 24 (1978) 966-976.
[88] M. Ahmadi, V. G. Gomes, K. Ngian, K. Advanced modelling in performance optimization for reactive separation in industrial CO_2 removal. Sep. Purif. Tech., 63 (2008) 107-115.
[89] G. Astarita, D. W. Savage, J. M. Longo, Promotion of CO_2 mass transfer in carbonate solutions. Chem. Eng. Sci., 36 (1981) 581-588.
[90] P.V. Danckwertz, Gas-Liquid Reactions. Mc Graw-Hill Book Company (1970).
[91] H. Thee, Y. A. Suryaputradinata, K.A. Mumford, K. H. Smith, G. Silva, S. E. Kentish, G. W. Stevens, A kinetic and process modelling study of CO_2 capture with MEA-promoted potassium carbonate solutions. Chem. Eng. J. 210 (2012) 271-279.
[92] P. C. Tseng, W. S. Ho, D. W. Savage, Carbon dioxide absorption into promoted carbonate solutions. AIChE J., 34 (1988) 922-931.

[93] N. K. Aroua, A. Benamor, M. Z. Haji Sulaiman, Temperature dependence of the equilibrium constant for the formation of carbamate from DEA. J. Chem. Eng. Data, 42 (1997) 692-696

[94] M. Z. Haji-Sulaiman, M. K. Aroua, A. Benamor, Analysis of equilibrium data of CO_2 in Aqueous solution of DEA, MDEA and their mixture using the Modified Kent Eisenberg Model. Trans. IChemE., 76 (1998) 961-968.

[95] F. Yi, Z.H. Kui, C. G. Wen, L. Shao, C. J. Feng, Modelling and experimental studies on absorption of CO_2 by Benfield solution in rotating packed bed. Chem. Eng. J., 145 (2009) 377-384.

[96] S. Weisenberger, A. Schumpe, Estimation of gas solubility in salt solutions at temperatures from 273 K to 363 K. AIChE J., 42 (1996) 298-300.

[97] K. Onda, E. Sada, M. Saito, Gas-Side Mass Transfer Coefficients in Packed Towers. Chem. Eng. Sci. J., 25 (1982) 820-829.

[98] R. Taylor, R. Krishna, Multicomponent Mass Transfer; John Wiley & Sons, Inc.: USA, (1993).

[99] E. N. Fuller, P. D. Schettler, J. C. Giddings, New Method for Predicting of Binary Gas-Phase Diffusion Coefficients. Ind. Eng. Chem J., 58 (1966) 18-27.

[100] R. H. Perry, D. W. Green, Perry's Chemical Engineers' Handbook. 7th Edition, Mc Graw-Hill (1997).

[101] J. Kopyscinski, Production of synthetic natural gas in a fluidized bed reactor: Understanding the hydrodynamic, mass transfer, and kinetic effects. Thesis for the degree of Doctor of Sciences, Paul Scherrer institute, Villigen, Switzerland (2010).

[102] E. Filippi, F. Di Muzio, E. Strepparola, The Casale plate-cooled design, redefining chemical reactors. Presentation at Defining the future, Munich, Germany, (2007). https://pdfs.semanticscholar.org/dc15/2d59f2bf8fc41a3cfa1de675b9d0bd4b1534.pdf

[103] M. Temkin,V. Pyzhev, Kinetics of the synthesis of ammonia on promoted iron catalyst. J. Phys. Chem. 13 (1940) 851-867.

[104] D. C. Dyson, J. M. Simon, A kinetic expression with diffusion correction for ammonia synthesis on industrial catalyst. Ind. Eng. Chem. Fundamental. 7 (1986) 605-615.

[105] A. Dashti, K. Khorsand, M.A. Marvast, M. Kakavand, Modelling and simulation of ammonia synthesis reactor. Journal of Petroleum & Coal, 48 (2006)15-23.

[106] A. J. Gunorubon, R. N. Raphael, Simulation of an ammonia synthesis converter. Canadian Journal of Pure and Applied Sciences, 8(2), (2014) 2913–2923.

[107] C. P. Ukpaka, T. Izonowei, T. Model prediction on the reliability of fixed bed reactor for ammonia production. Chemistry International, 3 (2017) 46-57.
[108] B. Elverse, D. Hawkins, G. Russey, G. Schulz, Ullman's Encyclopaedia of Industrial Chemistry, 5th Edition, 85-98 (1993).
[109] A. T. Mahfouz, S. S. Elshishini, S. S. Elnshaie, Steady state modelling and simulation of an industrial ammonia synthesis reactor, ASME press. 10 (1987) 1-12.
[110] T. S. Mogaji, Simulation and comparison of the performance of refrigerant fluids in single stage vapour compression refrigeration system. British Journal of Applied Science & Technology, 8 (2015) 583-594.
[111] UniSim Design Operations Guide R470 Release, Honeywell International Sarl (2019).
[112] K. Ogata, Modern Control Engineering, Fifth Edition, Prentice Hall: London, (2010).
[113] General terms of gas supply, "Official Gazette" no.158/13, 2013.
[114] R. M. Price, P. R. Lyman, C, Georgakis, Throughput Manipulation in Plantwide Control Structures. Ind. Eng. Chem. Res. 33 (1994), 1197 - 1203.
[115] Guidance Document n°9 on the harmonised free allocation methodology for the EU-ETS post 2020, Sector – specific guidance, European Commission, Directorate – General, Climate Action, Directorate B - European and International Carbon Markets, (2019).
[116] C. Frangopoulos, M. Spakovsky, M. Sciubba, A brief review of methods for the design and synthesis optimization of energy systems. Int. J. Applied Thermodynamics, 5, (2002), 151-160.
[117] R. Strait, M. Nagvekar, Carbon dioxide capture and storage in the nitrogen and syngas industries. Nitrogen and Syngas, 303, (2010).
[118] Arco Association Management, Fertilizer production cost survey 2019. Zurich, Switzerland, (2020).
[119] D. E. Seborg, T. F. Edgar, D.A. Mellichamp, Process Dynamics, Modelling, and Control, Oxford University Press: New York, (1994).

8. APPENDIX

8.1.Appendix 1 Material balance – 1360 t/day base case operation

Stream ID	**1**	**2**	**3**	**4**	**5**	**6**	**7**	**8**	**9**	**10**	**11**	**12**	**13**
Description	NATURAL GAS FEED	RECYCLE H_2	NATURAL GAS FEED&RECYCLE H_2	PROCESS STEAM	PRIMARY REFORMER FEED	PRIMARY REFORMER EFFLUENT	AIR/STEAM FEED	SECONDARY REFORMER EFFLUENT	HTS EFFLUENT	LTS FEED	LTS EFFLUENT	CO2 ABSORBER FEED	CO_2 PRODUCT
Phase	VAPOR	VAPOR	VAPOR	VAPOR	VAPOR	VAPOR	VAPOR	VAPOR	VAPOR	VAPOR	VAPOR	VAPOR	VAPOR
Composition dry mole %													
H_2	0,00	93,60	2,25		2,25	69,22	0,00	56,04	60,00	60,00	60,81	60,83	0,83
N_2	1,45	2,77	1,48		1,48	0,44	78,08	22,97	20,90	20,90	20,48	20,49	0,15
CH_4	92,97	1,43	90,77		90,77	10,39	0,00	0,31	0,28	0,28	0,27	0,27	0,00
Ar	0,00	2,20	0,05		0,05	0,02	0,94	0,28	0,26	0,26	0,25	0,25	0,00
NH_3	0,00	0,00	0,00		0,00	0,00	0,00	0,00	0,00	0,00	0,00	0,00	0,00
CO	0,00	0,00	0,00		0,00	9,12	0,00	12,36	2,23	2,23	0,16	0,16	0,00
CO_2	0,19	0,00	0,19		0,19	10,83	0,03	8,04	16,32	16,32	18,02	18,02	99,00
C_2H_6	4,53	0,00	4,42		4,42	0,00	0,00	0,00	0,00	0,00	0,00	0,00	0,00
C_3H_8	0,66	0,00	0,64		0,64	0,00	0,00	0,00	0,00	0,00	0,00	0,00	0,00
i-C_4	0,08	0,00	0,08		0,08	0,00	0,00	0,00	0,00	0,00	0,00	0,00	0,00
n-C_4	0,07	0,00	0,07		0,07	0,00	0,00	0,00	0,00	0,00	0,00	0,00	0,00
i-C_5	0,03	0,00	0,03		0,03	0,00	0,00	0,00	0,00	0,00	0,00	0,00	0,00
n-C_5	0,02	0,00	0,02		0,02	0,00	0,00	0,00	0,00	0,00	0,00	0,00	0,00
C_6	0,00	0,00	0,00		0,00	0,00	0,00	0,00	0,00	0,00	0,00	0,00	0,00
O_2	0,00	0,00	0,00		0,00	0,00	20.95	0,00	0,00	0,00	0,00	0,00	0,00
Dry flow, kmol/h	1488,5	36,7	1525,2		1525,2	5157,7	2,195.5	7559,7	8308,5	8308,5	8480,2	8476,6	1543,3
Dry flow, kg/h	25574,0	138,0	25712,0		25712,0	54198,0	63,593.0	111328,0	124817,0	124817,0	127910,0	127791,0	67184,0
H_2O, kmol/h	0,0	0,0	0,0	5470,4	5470,4	3889,2	304.5	4552,4	3803,7	3803,7	3632,0	135,2	141,2
Total flow kmol/h	1488,5	36,7	1525,2	5470,4	6,995.5	9046,9	2,500.0	12112,1	12112,1	12112,1	12112,1	8611,9	1684,5
kg/h	25574,0	138,0	25712,0	98550,0	124262,0	124262,0	69,079.0	193341,0	193341,0	193341,0	193341,0	130227,0	69728,0
t [ºC]	16,4	37,8	399,0	395,0	498,4	786,2	489.6	981,1	416,9	201,0	214,3	75,6	48,8
p [barabs.]	8,4	43,0	42,9	40,4	31,6	30,3	32.4	29,7	28,2	27,5	27,2	27,0	1,3
Vapor fraction	1,000	1,000	1,000	1,000	1,000	1,000	1.000	1,000	1,000	1,000	1,000	1,000	1,000
MW, kmol/kg	17,181	3,771	16,859	18,015	17,763	13,735	27.631	15,963	15,963	15,963	15,963	15,122	41,270
Density, kg/m^3	6,13	6,14	12,78	13,89	8,85	4,70	13.97	4,53	7,83	11,19	10,77	13,99	1,98
Vapor viscosity, cP	0,0110	0,0114	0,0215	0,0245	0,0278	0,0382	0.0357	0,0465	0,0281	0,0204	0,0209	0,0173	0,0158

Stream ID	14	15	16	18	19	20	21	22	23	23A	24	25	26
Description	CO2 ABSORBER OVERHEAD	METHANATOR EFFLUENT	104-F INLET	MAKE-UP SYN GAS	103-J 2ND STAGE SUCTION	103-J 3RD STAGE SUCTION	AMMONIA CONVERTER FEED	CONVERTER EFFLUENT	106-F VAPOR	RECYCLE GAS TO 103-J	106-F LIQUID	108-F LIQUID	LETDOWN DRUM LIQUID
Phase	VAPOR	VAPOR	MIXED	VAPOR	VAPOR	VAPOR	VAPOR	VAPOR	VAPOR	VAPOR	LIQUID	LIQUID	LIQUID
Composition dry mole %													
H_2	74,15	73,95	73,95	74,19	74,19	74,19	62,85	50,94	62,85	62,85	0,33	0,41	0,03
N_2	24,97	25,17	25,17	24,71	24,71	24,71	20,69	16,69	20,69	20,69	0,13	0,16	0,01
CH_4	0,33	0,58	0,58	0,67	0,67	0,67	8,79	9,99	8,79	8,79	0,15	0,26	0,03
Ar	0,31	0,31	0,31	0,43	0,43	0,63	5,90	6,70	5,90	5,90	0,06	0,09	0,01
NH_3	0,00	0,00	0,00	0,00	0,00	0,00	1,77	15,68	1,77	1,77	99,33	99,08	99,92
CO	0,20	0,00	0,00	0,00	0,00	0,00	0,00	0,00	0,00	0,00	0,00	0,00	0,00
CO_2	0,04	0,00	0,00	0,00	0,00	0,00	0,00	0,00	0,00	0,00	0,00	0,00	0,00
C_2H_6	0,00	0,00	0,00	0,00	0,00	0,00	0,00	0,00	0,00	0,00	0,00	0,00	0,00
C_3H_8	0,00	0,00	0,00	0,00	0,00	0,00	0,00	0,00	0,00	0,00	0,00	0,00	0,00
i-C_4	0,00	0,00	0,00	0,00	0,00	0,00	0,00	0,00	0,00	0,00	0,00	0,00	0,00
n-C_4	0,00	0,00	0,00	0,00	0,00	0,00	0,00	0,00	0,00	0,00	0,00	0,00	0,00
i-C_5	0,00	0,00	0,00	0,00	0,00	0,00	0,00	0,00	0,00	0,00	0,00	0,00	0,00
n-C_5	0,00	0,00	0,00	0,00	0,00	0,00	0,00	0,00	0,00	0,00	0,00	0,00	0,00
C_6	0,00	0,00	0,00	0,00	0,00	0,00	0,00	0,00	0,00	0,00	0,00	0,00	0,00
O_2	0,00	0,00	0,00	0,00	0,00	0,00	0,00	0,00	0,00	0,00	0,00	0,00	0,00
Dry flow, kmol/h	6933,3	6880,0	6880,2	7064,1	7037,3	7037,3	27701,2	24370,2	27701,2	27701,2	3287,0	55,5	3332,0
Dry flow, kg/h	60606,0	60251,0	60251,0	61430,0	61197,0	61197,0	61197,0	308,331,0	308331,0	308331,0	55901,0	944,0	56554,0
H_2O, kmol/h	102,0	121,7	121,7	13,0	0,00	0,00	0,00	0,00	0,00	0,00	0,00	0,00	0,00
Total flow kmol/h	7035,4	7002,0	7002,0	7077,1	7037,3	7037,3	27701,2	24370,2	27701,2	27701,2	3287,0	55,5	3321,0
kg/h	62444,0	62444,0	62444,0	61664,0	61197,0	61197,0	308331,0	308331,0	308331,0	308331,0	55901,0	944,0	56554,0
t [ºC]	74,3	300,9	30,6	30,8	31,3	7,2	147,5	347,8	-26,2	12,9	-26,2	-12,7	-25,2
p [barabs.]	26,9	26,4	26,0	26,0	50,0	91,4	171,1	168,0	164,7	164,1	164,7	167,0	17,5
Vapor fraction	1,000	1,000	0,984	1,000	1,000	1,000	1,000	1,000	1,000	1,000	0,000	0,000	0,000
MW, kmol/kg	8,876	8,918	8,918	8,713	8,696	8,696	11,131	12,652	11,131	11,131	17,006	17,004	17,029
Density, kg/m^3	8,16	4,89	9,21	8,85	16,75	32,50	50,,61	39,07	83,74	71,47	680,86	664,53	672,56
Vapor viscosity, cP	0,0161	0,0229	0,0146	0,0146	0,0148	0,0143	0,0203	0,0261	0,0151	0,0162			

Stream ID	27	27A	28	28A	29	30	31	32	33	34	35	90	91
Description	112-F VAPOR TO 105-J	111-F VAPOR TO 105-J	141-F VAPOR TO 105-J	FROM 105-J TO 127-C	110-F VAPOR TO 105-J	WARM AMMONIA FROM 109-F	WARM PRODUCT	COLD PRODUCT	PURGE GAS TO 101-B FUEL	PURGE GAS TO H2 RECOVERY	FLASH GAS TO FUEL	PROCESS CONDENSATE FROM 102-F	PROCESS CONDENSATE FROM 104-F
Phase	VAPOR	VAPOR	VAPOR	VAPOR	VAPOR	LIQUID	LIQUID	LIQUID	VAPOR	VAPOR	MIXED	LIQUID	LIQUID
Composition dry mole %													
H_2	0,04	0,00	0,00	0,03	0,06	0,01	0,01	0,00	23,29	58,64	23,29	21,83	77,83
N_2	0,02	0,00	0,00	0,01	0,03	0,01	0,01	0,00	37,32	19,20	11,46	4,44	20,31
CH_4	0,05	0,00	0,00	0,05	0,10	0,03	0,03	0,00	24,27	11,48	20,34	0,09	1,13
Ar	0,01	0,00	0,00	0,01	0,02	0,00	0,00	0,00	12,82	7,71	20,34	0,09	0,74
NH_3	99,87	100,0	100,0	99,90	99,79	99,95	99,95	100,0	2,29	2,97	5,65	0,00	0,00
CO	0,00	0,00	0,00	0,00	0,00	0,00	0,00	0,00	0,00	0,00	39,26	0,05	0,00
CO_2	0,00	0,00	0,00	0,00	0,00	0,00	0,00	0,00	0,00	0,00	0,00	73,51	0,00
C_2H_6	0,00	0,00	0,00	0,00	0,00	0,00	0,00	0,00	0,00	0,00	0,00	0,00	0,00
C_3H_8	0,00	0,00	0,00	0,00	0,00	0,00	0,00	0,00	0,00	0,00	0,00	0,00	0,00
i-C_4	0,00	0,00	0,00	0,00	0,00	0,00	0,00	0,00	0,00	0,00	0,00	0,00	0,00
n-C_4	0,00	0,00	0,00	0,00	0,00	0,00	0,00	0,00	0,00	0,00	0,00	0,00	0,00
i-C_5	0,00	0,00	0,00	0,00	0,00	0,00	0,00	0,00	0,00	0,00	0,00	0,00	0,00
n-C_5	0,00	0,00	0,00	0,00	0,00	0,00	0,00	0,00	0,00	0,00	0,00	0,00	0,00
C_6	0,00	0,00	0,00	0,00	0,00	0,00	0,00	0,00	0,00	0,00	0,00	0,00	0,00
O_2	0,00	0,00	0,00	0,00	0,00	0,00	0,00	0,00	0,00	0,00	0,00	0,00	0,00
Dry flow, kmol/h	981,1	933,2	700,5	3915,8	1301,0	1619,5	1619,5	1708,7	158,3	364,5	3,2	3,5	0,0
Dry flow, kg/h	16707,0	15893,0	11929,0	66682,0	22,53,0	27580,0	27580,0	29099,0	3218,0	4369,0	51,0	120,0	0,0
H_2O, kmol/h	0,0	0,0	0,0	0,0	0,0	0,0	0,0	0,0	0,0	0,0	0,0	3496,7	108,8
Total flow kmol/h	981,1	933,2	700,5	3915,8	1301,0	1619,5	1619,5	1708,7	158,3	364,5	3,2	3500,3	108,8
kg/h	16707,0	15893,0	11929,0	66682,0	22153,0	27580,0	27580,0	29099,0	3218,	4369,0	51,0	63114,0	1960,0
t [ºC]	-33,2	-10,5	0,9	109,0	14,1	30,9	31,8	-33,0	41,4	22,2	6,0	113,7	30,8
p [barabs.]	1,0	2,9	4,4	15,2	7,1	14,6	24,5	6,8	4,7	166,9	14,6	27,0	26,0
Vapor fraction	1,000	1,000	1,000	1,000	1,000	0,000	0,000	0,000	1,000	1,000	1,000	0,000	0,000
MW, kmol/kg	17,028	17,030	17,030	17,029	17,028	17,030	17,030	17,030	20,331	11,989	15,887	18,031	18,012
Density, kg/m^3	0,89	2,29	3,46	8,64	5,36	592,50	591,12	682,63	3,62	76,30	10,41	949,81	995,16
Vapor viscosity, cP	0,0080	0,0089	0,0093	0,0134	0,0099				0,0169	0,0168	0,0127		

Curriculum vitae of the doctoral candidate

Surname, Name: Zečević Nenad

[redacted]

[redacted] Received B. Sc. degree at the Faculty of Natural Science in Chemistry, the University of Zagreb in 1999. Since 1999 employed in Petrokemija Plc. Kutina, in different positions, starting from production engineer to production manager up to higher management positions such as COO and CEO. From 2018 to 2019 employed in SIEMENS as an expert for automation systems in the chemical industry with the accent to fertilizer production in charge for centre of competence in the fertilizer industry at the global level. In 2019 joined again in Petrokemija Plc. as Director for the Production and Maintenance department. In 2019 started with the Ph. D. research at the Faculty of Chemical Engineering and Technology, Chemical Engineering and Applied Chemistry, the University of Zagreb. His research is related to the development of advanced process control for ammonia production and the name of the thesis is "Advancement of process control system in ammonia production". His primary field of expertise is ammonia production and syngas generation systems with the accent to the development of the advanced process control systems through modelling and simulation approaches. Additional interest is directed to the field of "green" hydrogen and ammonia production as the main fundamental change in the ammonia industry. His list of publications comprises over 25 original scientific and professional papers mainly concentrated on the chemical industry and related fertilizer production. He is a member of the Croatian Academy of Sciences and Arts, Section for the petrochemical industry, and a member of Croatian Society of Chemical Engineers.

Doctoral candidate bibliography

1. **N. Zečević**, **Discrete** Simulation Model of Industrial Natural Gas Primary Reformer in Ammonia Production and Related Evaluation of the Catalyst Performance, Johnson Matthey Technology Review (2021), https://doi.org/10.1595/205651322X16221965765527
2. **N. Zečević** and N. Bolf, Advanced Operation and Monitoring the Economic Performance of Ammonia Production Based on Natural Gas Steam Reforming by Using Programmed Feedforward – Ratio – Cascade Controllers, Chem. Eng. Comm. (2021), DOI: 10.1080/00986445.2021.1919651
3. **N. Zečević**, Energy intensification of steam methane reformer furnace in ammonia production by application of digital twin concept, Int. J. Sustain. Energ. (2021) DOI: https://doi.org/10.1080/14786451.2021.1893727
4. **N. Zečević**, and N. Bolf, N. Integrated Method of Monitoring and Optimization of Steam Methane Reformer Process, Processes, 8 (2020), 4; 408-427 DOI:10.3390/pr8040408
5. **N. Zečević**, and N. Bolf, Digitalni model primarnog parnog reforminga prirodnog plina u proizvodnji sinteznog plina // XIII. Susret mladih kemijskih inženjera Zagreb, Hrvatska, 2020 (Znanstveni skupovi i radionice, Usmeno izlaganje)
6. **N. Zečević** and N. Bolf, Advanced operation of the steam methane reformer by using gain-scheduled model predictive control, Ind. Eng. Chem. Res. (2020), 59,8,3458-3474, DOI: https://pubs.acs.org/doi/abs/10.1021/acs.iecr.9b06260
7. **N. Zečević**, M. Ljubičić, J. Bjelić, H. Lisac i S. Valkov Proizvodnja jednostavnog mineralnog dušičnog gnojiva u obliku dvostruke soli amonijeva sulfonitrata, Kem. Ind. **66** (9-10) (2017) 457–466, DOI: https://doi.org/10.15255/KUI.2016.041
8. **N. Zečević**, M. Ljubičić, J. Bjelić, H. Lisac i S. Valkov Proizvodnja sintetičkog granuliranog amonijeva sulfata, Kem. Ind. **65** (1-2) (2016) 51−58, DOI: https://doi.org/10.15255/KUI.2015.032
9. **N. Zečević**, R. Kamenski, T. Hajba, D. Mudrić i S. Sabljak Redukcija i praćenje rada heterogenog katalizatora niskotemperaturne pretvorbe vodenog plina u proizvodnji amonijaka, Kem. Ind. **62** (9-10) (2013) 299–305, DOI: https://doi.org/10.15255/KUI.2012.028

10. **N. Zečević** i L. Ćosić Primjena primarnih tehnologija smanjenja emisije N2O u proizvodnji dušične kiseline Petrokemije d. d., Kem. Ind. **62** (1-2) (2013) 13–18, DOI: https://doi.org/10.15255/KUI.2012.012
11. **Nenad Zečević**, Tihomir Hajba, Renato Kamenski, Dejan Mudrić Poboljšanje učinkovitosti heterogenih katalizatora pri industrijskoj proizvodnji amonijaka, 23. Hrvatski skup Kemičara i kemijskih inženjera, Osijek, Hrvatska, 2013 (Znanstveni skupovi i radionice, Usmeno izlaganje)
12. **Nenad Zečević**, Renato Kamenski, Tihomir Hajba, Dejan Mudrić and Slavko Sabljak Reduction and Optimization of low temperature shift catalyst for water gas reaction in ammonia production, 14th Ružička Days, Vukovar, Hrvatska, 2012 (Scientific and Professional Conference, Poster presentation)
13. **N. Zečević** i M. Ljubičić Postupak destruktivne kemijske oporabe plemenitih metala u proizvodnji dušične kiseline, Kem. Ind. **61** (7-8) (2012) 335–340, DOI: https://doi.org/10.15255/KUI.2011.031
14. **N. Zečević**, I. Hoško i S. Pavlaković Poboljšanje i nadogradnja uzbunjujuće-sigurnosno-blokirajućeg sustava u proizvodnji dušične kiseline Petrokemije d. d., Kem. Ind. **61** (4) (2012) 205–214, DOI: https://doi.org/10.15255/KUI.2011.014
15. **N. Zečević**, M. Ljubičić, D. Vdović, K. Mikoč, I. Herjavec i Ž. Kabljanac Niskotemperaturna selektivna katalitička redukcija dušikovih oksida u proizvodnji dušične kiseline primjenom tekućeg amonijaka, Kem. Ind. **60** (11) (2011) 543–549, DOI: https://doi.org/10.15255/KUI.2011.006
16. **N. Zečević** Poboljšanje rada sustava bistrenja sirove vode akumulacijskog jezera Pakra, Kem. Ind. **60** (10) (2011) 497–503, DOI: https://doi.org/10.15255/KUI.2010.023
17. **N. Zečević**, V. Panjkret i S. Miletić Obrada otpadnih voda nastalih ispiranjem pješčanih filtara, Kem. Ind. **60** (10) (2011) 491–496, DOI: https://doi.org/10.15255/KUI.2010.020
18. **N. Zečević**, D. Barta i Z. Bosak Iskorištenje topline otpadnih procesnih plinova u reaktoru za proizvodnju uljno-pećnih čađa, Kem. Ind. **60** (2) (2011) 51–59, DOI: https://doi.org/10.15255/KUI.2010.006
19. **N. Zečević** Poboljšanje rada rotirajućih sušionika za sušenje mokro granuliranih uljno-pećnih čađa, Kem. Ind. **59** (5) (2010) 215–226, DOI: https://doi.org/10.15255/KUI.2009.024
20. **N. Zečević**, D. Barta, Z. Bosak, D. Čuzela i I. Puh Filtriranje čestica prašine uljno-pećnih čađa iz otpadnih procesnih plinova pomoću filtar-vreća s PTFE-membranom, Kem. Ind. **59** (1) (2010) 1–9, DOI: https://doi.org/10.15255/KUI.2009.012

21. **N. Zečević**, D. Barta, Z. Bosak, G. Avirović i S. Šiklušić Spaljivanje otpadnih procesnih plinova u proizvodnji uljno-pećne čađe, Kem. Ind. **58** (1) (2009) 11–23, DOI: https://doi.org/10.15255/KUI.2008.010
22. **N. Zečević** Automatska metoda kontrole jodnog adsorpcijskog broja u industrijskim pećima za proizvodnju uljno-pećne čađe, Kem. Ind. **57** (12) (2008) 541–548, DOI: https://doi.org/10.15255/KUI.2008.002
23. **N. Zečević** Uporaba deemulgatora za odvajanje vode od antracenskog ulja, Kem. Ind. **57** (3) (2008) 101–108, DOI: https://doi.org/10.15255/KUI.2007.002
24. **N. Zečević** Selektivna oksidacija "mekih" tipova uljno-pećnih čađa amonijevim nitratom, Kem. Ind. **56** (12) (2007) 633–642, DOI: https://doi.org/10.15255/KUI.2006.010
25. Ž.Grahek, **N.Zečević**, S.Lulić Possibility of rapid determination of low-level 90Sr activity by combination of extraction chromatography separation and Cherenkov counting, Analytica Chimica Acta, **399** (3) (1999) 237-247, DOI: https://doi.org/10.1016/S0003-2670(99)00469-9

In addition, during Ph. D. research, Nenad Zečević has participated in two (2) international and domestic scientific conferences, presenting the lectures:

1. XIII Meeting of Young Chemical Engineers 2020., oral presentation (in Croatian) „Digital twin model of primary steam reformer of natural gas in syngas production"
2. 18th Ružička days 2020, oral presentation (in Croatian) „Waste as a feedstock and energy source for green ammonia production